Mineralogical, gemmological and petrological study of the Mogok Stone Tract in Myanmar with a special focus on gem-quality ruby and spinel

Inauguraldissertation

zur

Erlangung der Würde eines Doktors der Philosophie

vorgelegt der

Philosophisch-Naturwissenschaftlichen Fakultät

der Universität Basel

von

Myint Myat Phyo

aus Myanmar

Basel, 2019

Genehmigt von der Philosophisch-Naturwissenschaftlichen Fakultät

auf Antrag von

Prof. Dr. Christian de Capitani, PD Dr. Michael S. Krzemnicki, Prof. Dr. Leander Franz

(Members of the dissertation committee: Faculty representative, dissertation supervisor, and co-examiner)

Basel, 25. June. 2019

(Date of approval by the Faculty)

Signature of the Faculty representative

_____

The Dean of Faculty
Prof. Dr. Martin Spiess
Dekan der Philosophisch-
Naturwissenschaftlichen Fakultät

Abstract

This thesis mainly focuses on the gemstones (marble-hosted ruby and spinel) from world famous ruby deposits in the Mogok area, Myanmar. This dissertation consists of three main sections (one published paper and two drafts for publications to be submitted): (1) Spinel from Mogok, Myanmar - a detalied inclusion study by Raman microspectroscopy and scanning electron microscopy, (2) Petrology, geothermobarometry and geochemistry of granulite facies gneisses in the vicinity of gemstone deposits from Mogok area (Myanmar) and (3) U-Pb age dating of zircon and zirconolite inclusions in marble hosted gem-quality ruby and spinel from Mogok, Myanmar.

During the last few years, spinel became one of the most popular gemstones and currently is highly demanded in the international gem market. Therefore, it was my intention to carry out a detailed inclusion study on Mogok spinel which might become in the future an essential tool for gem laboratories to enable conclusive origin determination analyses of spinel. For this research, Raman microspectroscopy and scanning electron microscopy (SEM) analyses were carried out to identify the inclusions in Mogok spinel. Based on my research, I was able to document 16 mineral inclusions in Mogok spinel so far not known in literature. Furthermore, these studies confirmed that most solid inclusions in Mogok spinel are in fact multi-phase inclusions which may contain both, primary and secondary mineral phases (such as dolomite, apatite, anhydrite, phlogopite, and halite in calcite).

Three garnet-quartz gneisses, three peculiar garnet-clinopyroxene-nepheline gneisses and one clinopyroxene-clinoamphibole gneiss were selected for geothermobarometric studies. Conventional geothermobarometry of the garnet-quartz gneisses revealed granulite facies PT-conditions of 758-798°C at 7.2-7.6 kbar. The nepheline-gneisses and the clinopyroxene-clinoamphibole gneiss were also metamorphosed at such high-grade metamorphic conditions. Equilibrium phase diagram calculations with the Theriak-Domino program reproduced these PT-estimates and pointed at water activities of 0.34-0.4. Whole rocks geochemistry, trace elements analyses and isotope studies were carried out on the garnet-clinopyroxene-nepheline gneisses and the clinopyroxene-clinoamphibole gneiss. The geochemical investigations highlighted the high-K calcalkaline and shoshonitic character of these foid-bearing rocks pointing to a strong fractionation and to a subduction-related generation of their magmatic protoliths.

For the geochronology (U-Pb age dating) study, I analysed a selected number of zircon and zirconolite inclusions from ruby and spinel samples, and from ruby-and spinel-bearing marble as well as from gneisses (two garnet-quartz gneisses), all from the Mogok area. Two different setups of Laser Ablation Inductively Coupled Plasma Mass Spectrometers were used, (a) Time-Of-Flight and (b) Sector-Field mass spectrometer to detect the U-Pb isotopes in these inclusions. The calculated U-Pb ages in zircon inclusions from gemstones as well as from gneisses indicate that the Mogok area experienced several magmatic and metamorphic events. Specifically, the U-Pb ages of zircon from gem-quality corundum, spinel and marble revealed maximum ages of Late Cretaceous in their cores and minimum ages of Late Oligocene to Early Miocene in the rim of zircon grains.

Garnet-quartz gneiss from the western part of the area revealed significant lead loss conditions and U-Pb ages ranging from Precambrian to Jurassic age in the core, whereas the rim again revealed Oligocene ages. The garnet-quartz gneiss from central Mogok showed Middle Jurassic to Early Cretaceous ages in the zircon core and Oligocene ages in the rim of zircon grains. I assume that the Precambrian age of zircon in gneiss is probably representing the so-called Mogok gneiss of Iyer (1953).

Preface

This dissertation is an independent and original effort of Myint Myat Phyo, with the supervision of PD Dr. Michael S. Krzemnicki, Prof. Dr. Leander Franz, Dr. Walter A. Balmer, Prof. Dr. Christian de Capitani and with the collaboration of Eva Bieler, Dr. Alfons Berger, Dr. Marcel Guillong, Dr. Rolf L. Romer and Dr. Hao A. O. Wang.

List of Tables

List of Figures

Acknowledgements

First of all, I would like to thank my PhD supervisor's PD Dr Michael S. Krzemnicki, Prof Dr Leander Franz, Dr Walter A. Balmer and Prof Dr Christian de Capitani for their kind and continuous support, guidance, and for all their suggestions and discussions during our field trip as well as during my analytical work and the writing of publications and my final thesis. Specifically, I have learned a lot from PD Dr Michael S. Krzemnicki about scientific laboratory techniques on gemstones (spinel & corundum) that are not accessible in my home country Myanmar. I also have learnt so much from Prof Dr Leander Franz about mineralogy and petrology and geothermobarometry and from Prof Dr de Capitani about electron microprobe analysis and mineral chemistry of host rocks as well as the use of the Domino-Theriak software. And finally, I thank Dr Walter A. Balmer for his kind support and suggestions for my thesis.

I am truly thankful for the three years scholarship from Kanton Basel (Stipendienkommission für Nachwuchskräfte aus Entwicklungsländern), a research grant from FAG (Freiwillige Akademische Gesellschaft Basel) and financial and logistic support from the Swiss Gemmological Institute SSEF.

Furthermore, I would like to thank the external expert Dr Myo Min from the Department of Geology, Mandalay University, Upper Myanmar for his special guidance, advice, review and discussion on my thesis.

Also, I am really thankful to all participants in my field trip to Mogok, January 2016. In person, I would like to thank Sebastian Hänsel, Dr Walter A. Balmer, U Aung Kyaw Htoon, Ko Ja Mu, Ko Kyaw Swar and Ko Nay for their grateful help and logistic support during the field trip.

I also appreciate and thank the local miners who helped me a lot, providing and donating gem-quality gemstone samples for my PhD research project. Particularly, thanks to Ma Mie Mie (Silken East Ltd., Bangkok), Dr Takahito Mori (Mori's Inc., Japan), Ko Chu (Kyauksaung mine, Mogok), and mine managers and workers from Bawlongyi and Kyauksin mine, and all other mines within the research area. Thanks also to the local people who are living in Mogok area, Myanmar. Special thanks to Ah Ba, Anty Phyu and their sons for giving me their helping hands and providing me a place to stay whenever I was in Mogok for sample collection.

Many Thanks to Dr Alfons Berger (Geoscience, University of Bern), Eva Bieler (Nano Imaging Lab, University of Basel), Dr Marcel Guillong (ETH, Zurich), Dr Hao A.O Wang (SSEF), and Judith Braun (SSEF) for their help, guidance, support and discussions on both their specific technical knowledge as well as giving suggestion for my thesis. And also, many thanks to Pascal Tschudin for his perfect preparation for the thin-section slides. Moreover, I really appreciate the assistance of Dr Tashia J. Dzikowski and Dr Laurent E. Cartier (both SSEF) for their grateful help, advice and for fruitful discussions. I am very thanks to Victoria de La Soujeole (SSEF) for her grateful logistic support, planning for everything, starting from the beginning of my PhD until the end of my studies in Switzerland. Furthermore, I am really thanks to all of my colleges from the SSEF and Department of Mineralogy and Geology, University of Basel for their kind encouragement and friendship. Because of them, I could enjoy my stay in Switzerland so much far away from my home country for such a long time.

Last but not least, I am thankful to my family. My parents, Aye Kyaw and May May Win for letting me go abroad and study four years for my PhD in far distance from them. I am likewise thankful to my mom and younger sister Aye for travelling to Switzerland for a short visit. I also thank my sister Pyae and my younger brother Zin for their support and praise. And finally, I would like to thank my beloved husband, Nyi Nyi Win for his encouragement whenever I needed his support and advice in the past few years.

Dedication

To my beloved parents and husband

CHAPTER I

Introduction

Ruby (chromium-bearing red variety of corundum Al_2O_3) and spinel are two of the most valued coloured gemstones known in the market. They are found in a range of colours—from deep red to pink in various shades. They are found in several specific localities worldwide such as Tanzania (East-Africa), Mozambique (East-Africa), Madagascar, Sri Lanka, and along the Himalayan mountain range in Myanmar, Pakistan, Tajikistan, and Vietnam. Among these localities, the Mogok area in Myanmar is the most eminent source of exceptional quality rubies and spinel. They are found there in marbles (as primary deposits) and in eluvial and alluvial placers (secondary deposits). A simplified world map of gemstones deposits is shown in Figure 1.1.

The Mogok area is located in Mandalay region, upper Myanmar, approximately 700km north of Yangon and 200km NE of the city Mandalay. It is located in a mountainous region, covered with tropical forest and exposed to heavy seasonal rain (Monsoon). Historically, the Mogok area is always a region of high interest for the former rulers of Myanmar, but also other countries (e.g. England in the 19-20th century) governing Myanmar for certain time. This interest was and still is linked to the wealth in resources of valuable minerals and gems in that area (Brown & Judd 1896; Themelis 2008). Specifically, this area is known and especially famous for high-quality rubies since historic times (see Hughes 1997; Themelis 2008). Until today, Mogok is one of the most significant sources for rubies in the gem market. Although, there are numerous studies about the Mogok area focussing on different aspects, there is still only limited knowledge about the specific conditions for gemstone formation within the Mogok area. It is the aim of this research study to develop a better understanding of the geology and metamorphic conditions in the Mogok area which ultimately led to the formation of gemstones - especially of marble-hosted corundum (red and pink varieties) and spinel. Furthermore, we would like to develop our understanding and criteria to distinguish these gemstones from the Mogok area from those of other marble hosted deposits worldwide.

1.1 Location and Accessibility

The Mogok area is located in the Pyin-Oo-Lwin district, Mandalay division, Myanmar. Myanmar (also known as Burma) is located in Southeast Asia and is surrounded by China in the North and Northeast, Laos and Thailand in the East, and India and Bangladesh in the West. Myanmar has a long N-S stretching coastal line (1,930 km) formed by the Bay of Bengal and the Adaman Sea. It is 676,578 km^2 wide and currently has a population of approximately 54 million. In recent years, travel restrictions have been lifted and thus it is nowadays easy to visit Myanmar. However, to visit the Mogok gemstone area, still there is a special permit needed. For travellers, the normal points of entry to Myanmar are either Yangon or Mandalay International airports. From Mandalay to the Mogok area it takes about 7 hours using a car. The Mogok area is located approximately 190 km NE of the city of Mandalay. A map of Mogok area is shown in Figure 1.2. There are various ethnic groups living together in Mogok area, such as Lisus, Burmas, Palaungs, Shans, Nepali-Gurkhas and Sino-Shan. The estimated population of the Mogok area is around 150,000 people.

1.2 Physiography

The Mogok area is a highly mountainous region with steep slopes covered by dense forest (Bernardmyo, Ongaing, Kyatpyin and Shwe U Daung natural reserves). The highest peak in the study area is around 2000 m, and the lowest location is around 300 m above sea level. In Mogok area, numerous rivers and streams are shaping the landscape, such as Kinn Chaung, Chaunggyi Chaung, Yeni Chaung, Nampeik Chaung, Pandaw Chaung, etc. Most of the rivers and streams are the result of a dendritic drainage pattern and in some area, radial drainage pattern can be found. A physiogeographic map is shown in Figure 1.3. Moreover, numerous valleys are crossing the Mogok area such as Shwenyaungbin valley and Kin valley, Inngyauk valley, Mogok valley, Painpyit valley, etc., which are shown in the 3D topographical model map Figure 1.4.

1.3 Climate and Vegetation

Due to its location in a highly mountainous region as well as the presence of large natural reserve areas with forests in the Mogok area, the climate it is rather moderate compared to the other parts of country with hot subtropic climate. In Mogok there are commonly three seasons, i.e.

summer, winter and raining seasons, similar to the rest of Myanmar and the neighbouring countries. The average maximum temperature in the year is around 26 °C and minimum temperature is around 14°C and the maximum rain fall is around 2690 mm per year (Aung et al. 2017). Due to the rather cold weather and the mountainous topography, there are numerous types of vegetation found in the Mogok area, including zones with orange and grapefruit trees, strawberries, raspberries, tea plantations, cabbages, radish, and many more. In some places of the Mogok area we find also rice and wheat plantations using terrace cultivation techniques known in mountain ranges.

1.4 Geology of the Mogok area

The Mogok area or so-called Mogok Stone Tract (Iyer 1953; La Touche 1913) is a segment of the Mogok Metamorphic Belt (MMB) (Searle & Haq 1964), which is a sickle-shaped belt of high-grade metamorphic rocks and younger intrusive rocks. The Mogok Metamorphic Belt is approximately 1500 km long and extends from the China frontier in the north to the Tenesserim Penisular in the south (Bertrand et al. 2001; Chhibber 1934; Searle et al. 2017). The Mogok area is situated in the western part of the Sibumasu block and lies in the northwestern part of Shan plateau. This area also is bounded by the E-W trending Momeik dextral fault in the north and the major Sagaing fault, a N-S trending lateral strike slip fault in the west. The Mogok area is mainly composed of high-grade metamorphic rocks such as marbles, schists and gneisses of upper amphibolite to granulite facies, found together with igneous rocks such as biotite microgranites, leucogranite, gabbro and syenite. A geological map of the Mogok area is shown in Figure 1.5. Two third of the Mogok area is occupied by various gneisses and the rest is covered by Late Phanerozoic granitic intrusions. Small outcrops of marbles are interbedded within calc-silicate rocks in the Mogok area. In addition, small outcrops of basic and ultrabasic igneous rocks occur in the northern part of the Mogok area.

The gem-bearing marbles, the schists and the gneisses of the Mogok Stone Tract were formed within originally Precambrian sediments, which were transformed by complex multiple tectonic and metamorphic events and by granitic to syenitic igneous intrusions between the Mesozoic and Early Cenozoic. All these Late Phanerozoic events correspond to the major Southeast Asian tectonic evolution, i.e. the result of the Gondwana supercontinent break-up into continental fragments in the Jurassic to Early Cretaceous period (approximately 200 Ma - 150 Ma) and the

subsequent collision of the Indian plate with the Eurasian plate in the Eocene (approx. 50 Ma) (Harlow et al. 2007; Stern et al. 2013).

1.5 Previous Studies

The Mogok area - also known as Mogok Stones Tract (Iyer 1953; La Touche 1913) - is very famous for its gemstone occurrences. As such, it has been in the focus of many geologists, mineralogists, and gemmologists and consequently there were numerous research studies, publications and books published about this world famous gemstone area in the last 150 years. A selection of these studies is presented here:

Brown and Judd 1896) suggested that the Mogok limestone (later named marble) originated from igneous rocks by means of complicated chemical reactions.

La Touche (1913) pointed out that the principal rock type in the Mogok area are gneisses, which in his account of the northern Shan State he grouped under the term “Mogok gneiss”.

Chhibber (1934) described that the Mogok marble is homotaxial (similar geologic strata) of Permo-Carboniferous limestone occurring near Namyazeik in the Kachin State.

Iyer mapped the Mogok Stone Tract in a four-nches to one-mile scale and described the geological succession of this area under the term “Mogok series” instead of “Mogok gneiss” in 1953.

Halford-Watkins (1932) described the ruby mines in Mogok and about the mining methods applied in Mogok in separate publications in ‘The Gemmologists’ journal.

Clegg (1941) described the Mogok series as metamorphosed sedimentary rocks of Pre-Cambrian to Cretaceous age. He also reported about the similarity of the Mogok crystalline limestone with the Cretaceous limestone exposed at the first (close to Myitkyina) and second (close to Bhamo) defiles of the Irrawaddy.

Searle and Haq (1964) recognized the relationship of the Mogok Metamorphic Belt with the Himalayan orogeny. They suggested that the metamorphism of the Mogok Stone Tract took place in the middle Tertiary and separated the rocks in the area into two main groups: (1) intrusive rocks, such as the Kabaing granite, pegmatites and aplites, mafic and ultramafic rocks, and Alaskite suites, and (2) the Mogok series, consisting of marbles and calcsilicate, metamorphics, gneisses and migmatites.

Gübelin (1965) wrote about the ruby mines in Mogok in Burma. Moreover, Gübelin and Koivula published three volumes of their 'Photoatlas of Inclusions in Gemstones' in 1986, 2005, 2008 in which they presented in great detail inclusions observed in gemstones, including rubies and sapphires from the Mogok area.

Thein (1973) studied in detail the distribution of the rocks of the Mogok belt, including a stratigraphic classification, and described the relation of these rocks with tectonic events and the nature of mineralizations. He considered the Mogok Belt to be a part of the Shan block that was cratonized during Paleozoic and Mesozoic. He further postulated that the belt represents the southern continuation of the South-China shield. Moreover, he described the primary formation of ruby, sapphire and spinel (2008).

M. L. Thein et al. (1990) described ´Geology and stratigraphy of the metamorphosed Early Paleozoic rocks of the Mogok–Thabeikkyin–Singu–Madaya Areas´ in unpublished staff report of Applied Geology Department, University of Yangon.

Thu (2007) described the igneous rocks of the Mogok Stone Tract; their distributions, petrography, petrochemistry, sequences, geochronology and economic geology in his unpublished PhD thesis.

Giuliani et al. (2005) compared oxygen isotopes of rubies and sapphires from 106 deposits worldwide. In 2015, Giuliani and co-workers postulated genetic implications based on an extensive fluid inclusion study on marble hosted rubies from central and Southeast Asia, including samples from Mogok area. In two further studies, Giuliani and co-workers investigated trace element concentrations and oxygen isotopes of marble hosted spinel (2017), with a special focus on the formation of gems and the role of evaporates (2018).

The above list of studies over the past 150 years is only a personal selection. Moreover, there are several unpublished reports and research theses about the Mogok area which were done by students of various universities in Myanmar.

1.6 Objectives

The following objectives are carried out for the research.

1. To make a detailed list of inclusions found in spinel from Mogok area.
2. To estimate the formation pressure (*P*) and temperature (*T*) of host-rock gneisses from the Mogok area.
3. To study U-Pb geochronology of radioactive mineral inclusions (e.g. zircons) that are observed especially in corundum and spinel as well as in host rocks from Mogok area.
4. Finally, to postulate a conclusive synthesis to describe the formation of marble-hosted gemstones (corundum and spinel) based on our analysed data.

1.7 Research Approach

First, I made a field trip to Mogok from January to February 2016. During this field trip, I collected numerous gemstone and host rocks samples from several gemstone mining sites. In addition, I also visited the local gemstone markets in the Mogok area and selected a number of additional gems from the markets for my study. After my return from the field trip, I carried out sample preparation (for rough gemstones: one side of the sample was polished to be able to observe and analyse interal features; for host-rock samples: thin-sections were made from selected samples (kindly realised by Pascal Tschudin, university Basel) as well as polished block sections. These gem and rock samples were then used for the following study.

1.7.1 Detailed Inclusion Study of Spinel

Inclusions in gems have been studied since decades as they provide not only an understanding of the geological environment resulting in the formation of gemstones, but also as they are widely used by gemmological experts in commercial gemmological laboratories for gemstone identification, treatment detection and origin determination. My focus in this part of the thesis was to compile a detailed overview of inclusions in spinel from Mogok, especially as there is not much literature so far about inclusions in spinel and because this gemstone has become very popular in the last few years in the jewellery market.

For that purposes, I used a gemmological microscope to observe and describe the inclusions, and combined these observations with Raman microspectroscopy to identify the nature of these inclusions. In addition, I used a scanning electron microscope (SEM) equipped with an energy-dispersive spectrometer to further characterise the observed inclusions. This study was published recently in the Journal of Gemmology (Myint et al. 2019), an international peer-reviewed scientific journal.

1.7.2 *P-T* Conditions of Host Rocks in the Mogok Area

Petrographic studies of host rocks were performed on polished thin sections using polarization microscopy. Selected samples were analysed by electron microprobe (EPMA). The calculation of mineral formulas and the estimate of ferric iron by stoichiometry were executed with respective computer programs. The temperatures (*T*) and pressures (*P*) of different rock types were calculated based on the chemical composition of their minerals. Mineral isopleths and water activity were calculated by Theriak-Domino program of De Capitani and Petrakakis (2010). Furthermore, geochemistry, trace elements and isotopes studies were carried out on selected rock samples.

1.7.3 U-Pb Geochronology Study of Gemstones and Host-Rocks

In this study, I selected a number of inclusions containing traces of radioactivity which were observed in gemstones (corundum and spinel) as well as from host rocks collected in the Mogok area. These inclusions (e.g. zircon and zirconolite) were documented using scanning electron microscopy (SEM) in back-scattered electron mode (BSE), and using variable pressure secondary electron (VPSE) imaging. In addition, these inclusions were chemically analysed using energy dispersive X-ray spectroscopy (EDS). A selected number of these mineral inclusions were further analysed using LA-ICP-Time-Of-Flight Mass Spectrometry and LA-ICP-Sector-Field Mass Spectrometry to quantify U-Pb isotopes for age dating. The results are presented in this thesis as a paper draft, which will be submitted in the near future to an international journal in geosciences.

Figure 1.1 World map of gemstone deposits (modified after world gemstones map (www.realgems.org), on kodomo world maphttps://maprepublic.com/wp-content/uploads/2017/05/kanawa-world-map-large.jpg

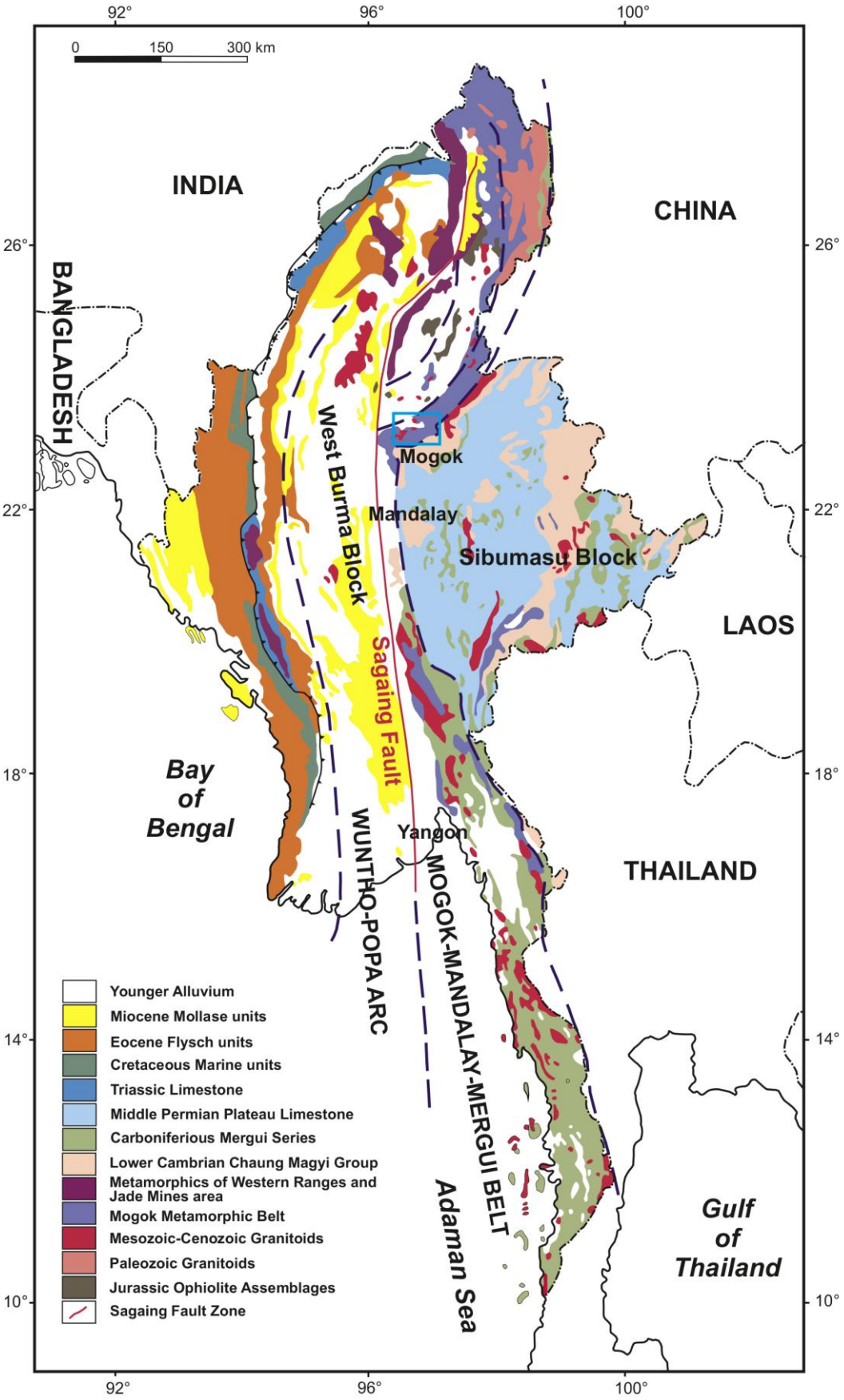

Figure 1.2 Geological map of Myanmar (modified after Sone and Metcalfe 2008). The research area in Mogok is highlighted by a blue frame.

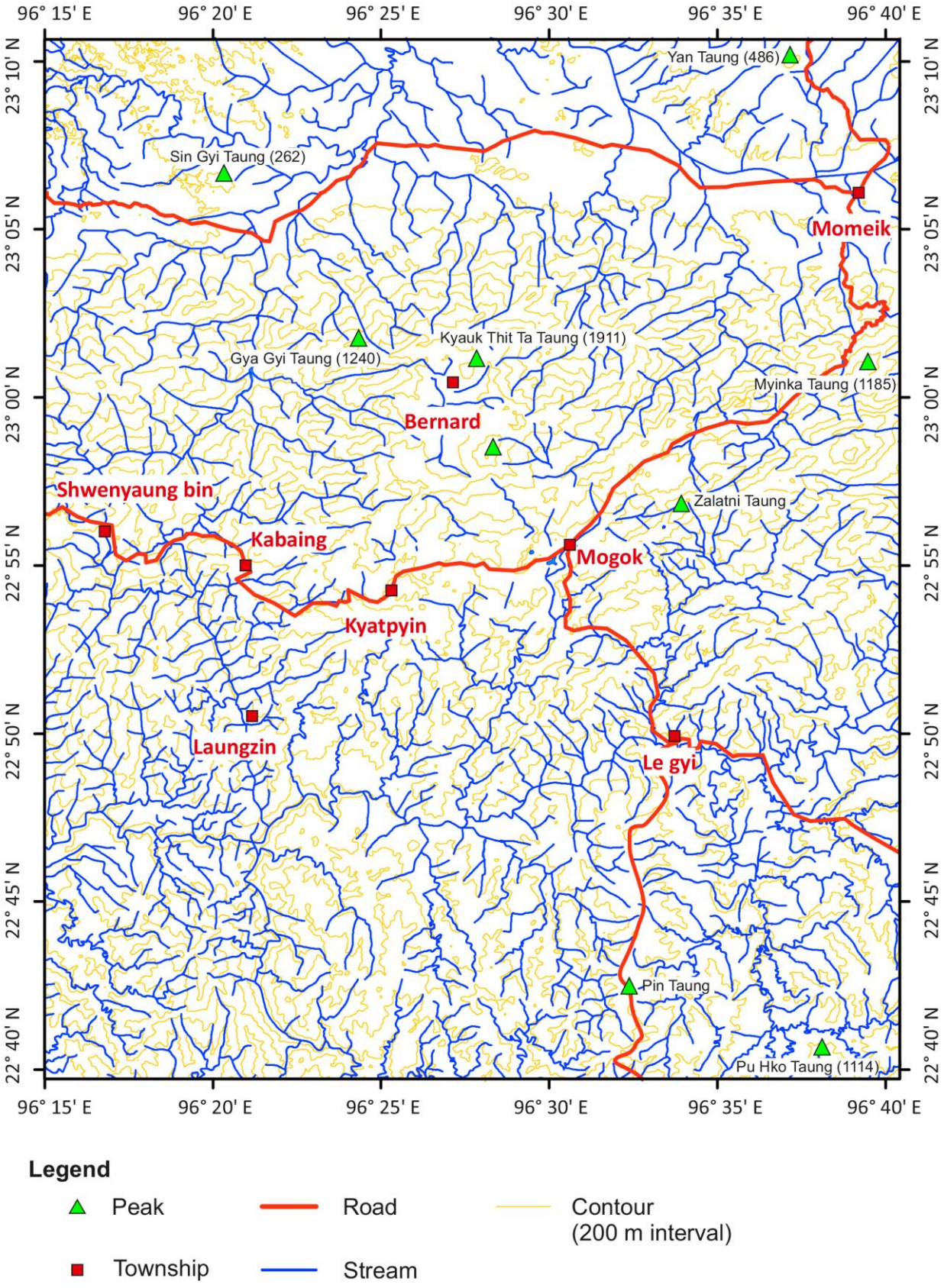

Figure 1.3 Physiogeographic map showing the drainage pattern of the Mogok area (based onone inch topographic maps 93 B/5, B/9)

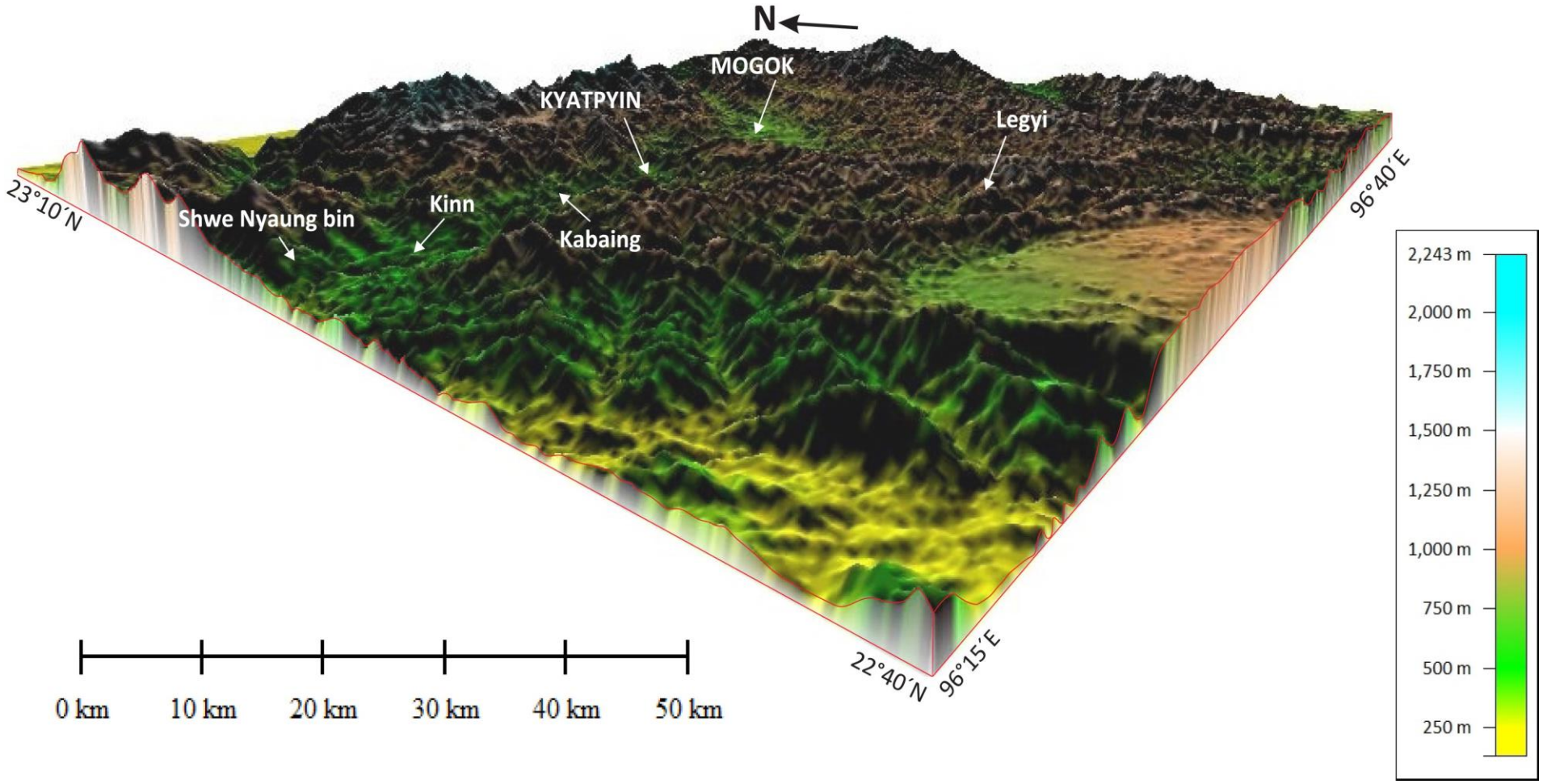

Figure 1.4 3D modelling map of the Mogok area (based on one-inch topographic maps 93 B/5, B/9)

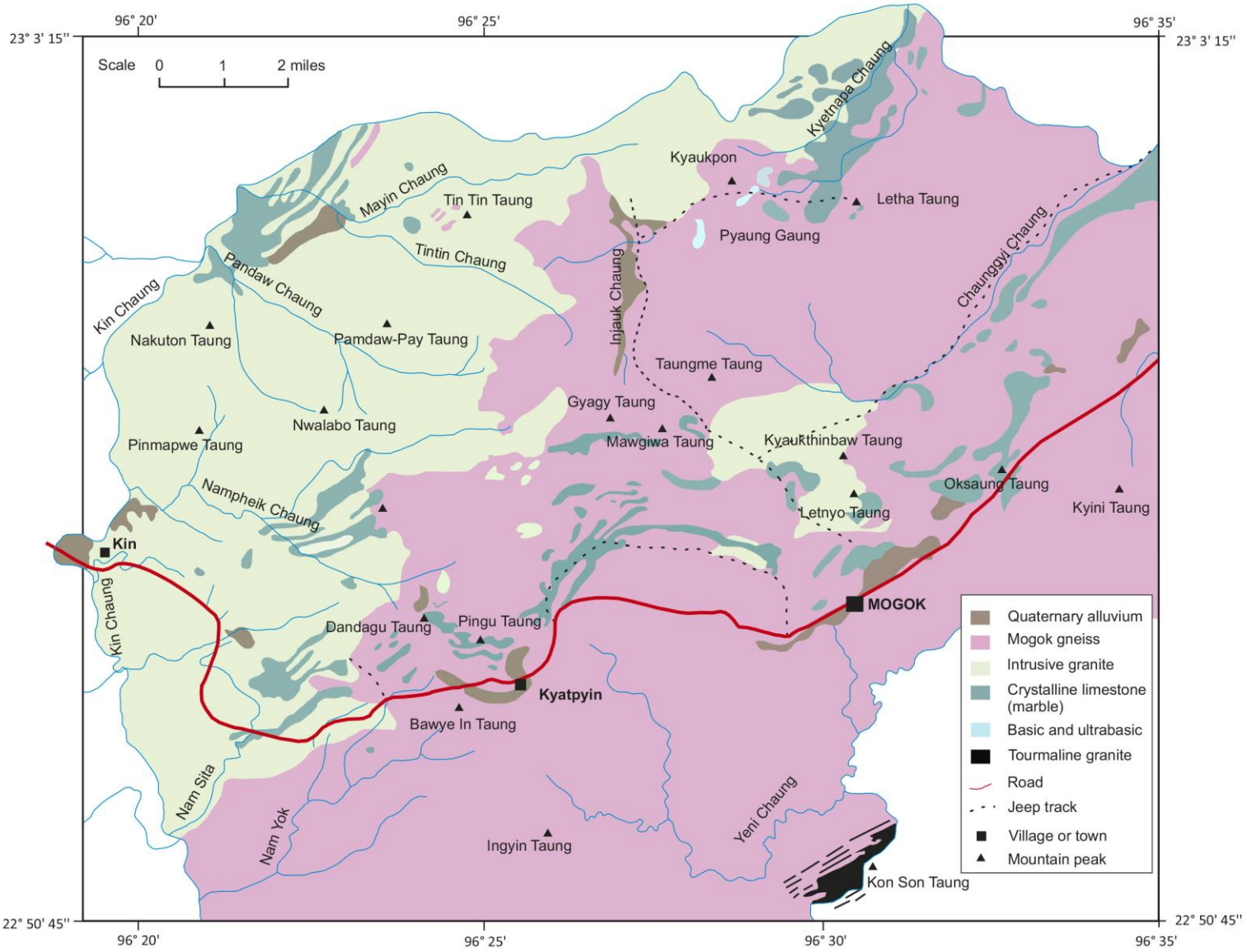

Figure 1.5 Simplified geological map of the Mogok area (after Iyer, 1953).

References

Ahmad, T., Harris, N., Bickle, M., Chapman, H., Bunbury, J., & Prince, C. (2000). Isotopic constraints on the structural relationships between the lesser Himalayan series and the high Himalayan crystalline series, Garhwal Himalaya. *Geological Society of America Bulletin*, *112*, 467–477.

Arculus, R. J., & Powell, R. (1986). Source component mixing in the regions of arc magma generation. *Journal of Geophysical Research*, *91*(B6), 5913. doi:10.1029/JB091iB06p05913

Aung, L. L., Zin, E. E., Theingi, P., Elvera, N., Aung, P. P., Han, T. T., et al. (2017). Myanmar Climate Report. *MET report*, (9).

Bader, T., Franz, L., de Capitani, C., & Zhang, L. (2014). The effect of water activity on calculated phase equilibria and garnet isopleth thermobarometry of granulites, with particular reference to Tongbai (east-central China). *European Journal of Mineralogy*, *26*, 5–23.

Bader, T., Franz, L., De Capitani, C., & Zhang, L. (2014). The effect of water activity on calculated phase equilibria and garnet isopleth thermobarometry of granulites, with particular reference to Tongbai (east-central China). *European Journal of Mineralogy*, *26*, 5–23.

Barley, M. E., Pickard, A. L., Zaw, K., Rak, P., & Doyle, M. G. (2003). Jurassic to Miocene magmatism and metamorphism in the Mogok metamorphic belt and the India-Eurasia collision in Myanmar. *Tectonics*, *22*(3), 1–11. doi:10.1029/2002TC001398

BAS, M. J. L., MAITRE, R. W. L., STRECKEISEN, A., & ZANETTIN, B. (1986). A Chemical Classification of Volcanic Rocks Based on the Total Alkali-Silica Diagram. *Journal of Petrology*, *27*(3), 745–750. doi:10.1093/petrology/27.3.745

Bayliss, P., Mazzi, F., Munno, R., & White, T. J. (1989). Mineral nomenclature : zirconolite. *Mineralogical Magazine*, *53*, 565–569.

Bender, F. (1983). *Geology of Burma*.

Bertrand, G., Rangin, C., Maluski, H., & Bellon, H. (2001). Diachronous cooling along the Mogok Metamorphic Belt (Shan Scarp , Myanmar): the trace of the northward migration of India-Indochina oblique convergence since the Oligocene. *Journal of Asian Earth Sciences*, *19*, 649–659. doi:10.1016/S1367-9120(00)00061-4

Bertrand, G., Rangin, C., Maluski, H., Han, T. A., Thein, M., Myint, O., et al. (1999). Cenozoic metamorphism along the Shan scarp (Myanmar): evidences for ductile shear along the Sagaing fault or the northward migration of the eastern Himalayan syntaxis? *Geophysical Research Letters*, *26*(7), 915–918.

Bhadra, S., & Bhattacharya, A. (2007). The barometer tremolite + tschermakite + 2 albite = 2 pargasite + 8 quartz: Constraints from experimental data at unit silica activity, with application to garnet-free natural assemblages. *American Mineralogist*, *92*, 491–502.

Bieri, W., Grobety, B., Peretti, A., Hametner, K., & Gunther, D. (2010). Chemical composition of apatite inclusions in corundum and spinel determined by LA-ICP-MS and its potential for authentication and provenance determination. *Geochimica et Cosmochimica Acta*, *74*(12), A89–A89.

Black, L. P., Kamo, S. L., Allen, C. M., Aleinikoff, J. N., Davis, D. W., Korsch, R. J., & Foudoulis, C. (2003). TEMORA 1: a new zircon standard for phanerozoic U–Pb geochronology. *Chemical Geology*, *200*, 155–170.

Brey, G. P., & Köhler, T. (1990). Geothermobarometry in four-phase lherzolites. I. New thermobarometers and practical assessment of existing thermobarometers. *Journal of Petrology*, *31*, 1353–1378.

Brook, M., & Snelling, N. J. (1976). K/Ar and Rb/Sr age determinations on rocks and minerals from Burma. *Institute of Geological Sciences, Keyworth, Nottingham, UK, Isotope Geology Unit Report*, *76*(12).

Brown, B., & Judd, J. W. (1896). The Rubies of Burma and Associated Minerals : Their Mode of Occurrence , Origin , and Metamorphoses . A Contribution to the History of Corundum. In *Philosophical Transactions of the Royal Society of London. Series A, Containing Papers of a Mathematical or Physical Character* (Vol. 187, pp. 151–228).

Campbell, I. H., Aleksandr, S., Stepanov, A. S., Liang, H.-Y., Allen, C. M., Norman, M. D., et al. (2013). The origin of shoshonites: new insights from the Tertiary high-potassium intrusions of eastern Tibet. *Contributions to Mineralogy and Petrology*, *167*, 983–1005.

Campbell, I. H., Stepanov, A. S., Liang, H. Y., Allen, C. M., Norman, M. D., Zhang, Y. Q., & Xie, Y. W.

(2014). The origin of shoshonites: New insights from the Tertiary high-potassium intrusions of eastern Tibet. *Contributions to Mineralogy and Petrology*, *167*(3), 1–22. doi:10.1007/s00410-014-0983-9

Chhibber, H. L. (1934). *The Geology of Burma*. *Macmillan and Co.,Ltd, St.Martin's Street, London*.

Clegg, E. L. G. (1941). The Cretaceous and associated rocks of Burma. *Memoirs of the Geological Survey of India*, *74*(1), 1–102.

Coenraads, R. R., Lin Sutherland, F., & Kinny, P. D. (1990). The origin of sapphires: U–Pb dating of zircon inclusions sheds new light. *Mineralogical Magazine*, *54*, 113–122. doi:10.1180/minmag.1990.054.374.13

Colombi, A. (1988). *Métamorphisme et géochimie des roches mafiques des Alpes ouest-centrales (Géoprofil Viège-Domodossola-Locarno).*

Conte, A. M., Dolfi, D., Gaeta, M., Misiti, V., Mollo, S., & Perinelli, C. (2009). Experimental constraints on evolution of leucite-basanite magma at 1 and 10− 4 GPa: implications for parental compositions of Roman high-potassium magmas. *European Journal of Mineralogy*, *21*, 763–782.

De Capitani, C., & Petrakakis, K. (2010). The computation of equilibrium assemblage diagrams with Theriak/Domino software. *American Mineralogist*, *95*, 1006–1016.

Deer, W. A., Howie, R. A., & Zussman, M. A. (1992). *An introduction to the rock forming minerals.* Longman, London.

Dewey, J. F., Cande, S., & Pitman, W. C. (1989). Tectonic evolution of the India/Eurasia Collision Zone. *Eclogae Geologicae Helvetiae*, *82*(3), 717–734. doi:10.1177/053331647600900219

Dewey, J. F., Shackleton, R. M., Chengfa., C., & Sun, Y. (1988). The tectonic evolution of the Tibetan Plateau. *Phil. Trans. Roy. Soc. Lond*, *327*, 379–413.

Downs, R. T. (2006). The RRUFF Project: an integrated study of the chemistry, crystallography, Raman and infrared spectroscopy of minerals. In *Program and Abstracts of the 19th General Meeting of the International Mineralogical Association in Kobe, Japan.* (pp. O03-13).

Dzikowski, T. J. (2013). *A Comparative study of the origin of carbonate-hosted gem corundum*

deposits in Canada. *unpublished thesis*. Retrieved from http://ir.obihiro.ac.jp/dspace/handle/10322/3933

Dzikowski, T. J., Dipple, G. M., Groat, L. A., Giuliani, G., & Cempírek, J. (2014). Origin of gem corundum in calcite marble: The Revelstoke occurrence in the Canadian Cordillera of British Columbia. *Lithos*, *198–199*, 281–297. doi:10.1016/j.lithos.2014.03.030

Eby, N., Woolley, A. R., Din, V., & Platt, G. (1998). Geochemistry and petrogenesis of nepheline syenites: Kaungu-Chipala, Iloba, and Ulindi nepheline syenites intrusions, North Nyasa alkaline Province, Malawi. *Journal of Petrology*, *39*, 1405–1424.

Elitok, Ö. (2019). Geology and petrology of the potassic and ultrapotassic rocks from the northern part of Senirkent (Isparta-SW Turkey): evidence of magma–carbonate wall-rock interactions. Arabian. *Journal of Geosciences*, *12*, 289–312.

Elmaleh, E., Schmidt, S. T., Karampelas, S., Link, K., Kiefert, L., Süssenberger, A., & Paul, A. (2019). U-Pb ages of zircon inclusions in Sapphires from Ratnapura and Balangoda (Sri Lanka) and Implications for Geographic origin, (May). doi:10.5741/GEMS.55.1.18

Faure, G. (2001). Alkalic Igneous Rocks on the Continents. In H. Springer, Berlin (Ed.), *Origin of Igneous Rocks* (pp. 281–350). Berlin, Heidelberg: Springer Berlin Heidelberg. doi:10.1007/978-3-662-04474-2_6

Fermor, L. L. (1930). *General report for the Geological Survey of India*. *Records of the Geological Survey, India*.

Gardiner, N. J., Robb, L. J., Morley, C. K., Searle, M. P., Cawood, P. A., Whitehouse, M. J., et al. (2016). The tectonic and metallogenic framework of Myanmar: A Tethyan mineral system. *Ore Geology Reviews*, *79*, 26–45. doi:10.1016/j.oregeorev.2016.04.024

Gardiner, N. J., Searle, M. P., Morley, C. K., Whitehouse, M. P., Spencer, C. J., & Robb, L. J. (2016). The closure of Palaeo-Tethys in Eastern Myanmar and Northern Thailand: New insights from zircon U–Pb and Hf isotope data. *Gondwana Research*, *39*, 401–422. doi:10.1016/j.gr.2015.03.001

Garnier, V., Long, P. Van, Fallick, A. E., Maluski, H., Lhomme, T., Giuliani, G., et al. (2008). Marble-hosted ruby deposits from Central and Southeast Asia: Towards a new genetic model. *Ore*

Geology Reviews, *34*(1–2), 169–191. doi:10.1016/j.oregeorev.2008.03.003

Garnier, V., Maluski, H., Ohnenstetter, D., Giuliani, G., & Schwarz, D. (2006). Ar-Ar and U-Pb ages of marble-hosted ruby deposits from central and southeast Asia. *Canadian Journal of Earth Sciences*, *43*(4), 509–532. doi:10.1139/e06-005

Garnier, V., Ohnenstetter, D., Giuliani, G., Blanc, P., & Schwarz, D. (2002). Trace-element contents and cathodoluminescence of “trapiche” rubies from Mong Hsu, Myanmar (Burma): Geological significance. *Mineralogy and Petrology*, *76*(3–4), 179–193. doi:10.1007/s007100200040

Garnier, V., Ohnenstetter, D., Giuliani, G., Maluski, H., Deloule, E., Trong, T. P., et al. (2005). Age and significance of ruby-bearing marble from the Red River Shear Zone, Northern Vietnam. *The Canadian Mineralogist*, *43*, 1315–1329.

Gellatly, D. C., & Hornung, G. (1968). Metasomatic nepheline-bearing gneisses from Darkainle Somali Republic. *The Journal of Geology*, *76*, 678–691.

GIAC. (1999). *The Tectonic of Myanmar: Final report GIAC project 1996-1999*.

Giuliani, G., Dubessy, J., Ohnenstetter, D., Banks, D., Branquet, Y., Feneyrol, J., et al. (2018). The role of evaporites in the formation of gems during metamorphism of carbonate platforms: a review. *Mineralium Deposita*, *53*(1). doi:10.1007/s00126-017-0738-4

Giuliani, G., Fallick, A. E., Boyce, A. J., Pardieu, V., & Pham, V. L. (2017). Pink and red spinels in marble: Trace elements, oxygen isotopes, and sources. *The Canadian Mineralogist*, *55*, 743–761. doi:10.3749/canmin.1700009

Giuliani, G., Fallick, A. E., Garnier, V., France-Lanord, C., Ohnenstetter, D., & Schwarz, D. (2005). Oxygen isotope composition as a tracer for the origins of rubies and sapphires. *Geology*, *33*(4), 249–252. doi:10.1130/G21261.1

Giuliani, G., Lhomme, T., Dubessy, J., Ohnenstetter, D., & Banks, D. A. (2015). Fluid inclusions in ruby from Asian marble deposits: genetic implications. *European Journal of Mineralogy*, *27*, 393–404. doi:10.1127/ejm/2015/0027-2442

Goldsmith, J. R., & Newton, R. C. (1977). Scapolite-plagioclase stability relations at high pressures and temperatures in the system NaAlSi3O8-CaAl2Si2O8-CaCO3-CaSO4. *American*

Mineralogist, *62*, 1063–1081.

Gübelin, E. J. (1965). The Ruby Mines in Mogok in Burma. *Journal of Gemmology*, *9*(12), 411–426.

Gübelin, E. J., & Koivula, J. I. (1986). *Photoatlas of Inclusions in Gemstones, ABC Edition*.

Gübelin, E. J., & Koivula, J. I. (2005). *Photoatlas of Inclusions in Gemstones, Vol. 2*.

Gübelin, E. J., & Koivula, J. I. (2008). *Photolas of Inclusions in Gemstones, Vol. 3*.

Halford-Watkins, J. F. (1932a). The Ruby Mines of Upper Burma: A Short History of their Working,. *The Gemmologist*, *1*(9), 263–272.

Halford-Watkins, J. F. (1932b). Methods of Ruby Mining in Burma. *The Gemmologist*, *1*(11), 335–342.

Halford-Watkins, J. F. (1932c). Methods of Ruby Mining in Burma. *The Gemmologist*, *1*(12), 367–373.

Harlow, G. E., Sorensen, S. S., & Sisson, V. B. (2007). Jade, in Groat, L.A., ed., The Geology of Gem Deposits: Quebec. *Mineralogical Association of Canada, Short Course Series, 37*, 207–254.

Hawthorne, F. C., Oberti, R., Harlow, G. E., Maresch, W. V., Martin, R. F., Schumacher, J. C., & Welch, M. D. (2012). Nomenclature of the amphibole supergroup. *American Mineralogist*, *97*, 2031–2048.

Henry, D. J., Guidotti, C. V., & Thomson, J. (2005). The Ti-saturation surface for low-to-medium pressure metapelitic biotites: Implications for geothermometry and Ti-substitution mechanisms. *American Mineralogist*, *90*, 316–328.

Hofmann, A. W. (1988). Chemical differentiation of the Earth: the relationship between mantle, continental crust, and oceanic crust. Earth and. *Planetary Science Letters*, *90*, 297–314.

Holdaway, M. J. (2000). Application of new experimental and garnet Margules data to the garnet-biotite geothermometer. *American Mineralogist*, *85*, 881–892.

Holland, T., & Blundy, J. (1994). Non-ideal interactions in calcic amphiboles and their bearing on amphibole-plagioclase thermometry. *Contributions to Mineralogy and Petrology*, *116*, 433–447.

Horz, K. H., Worthington, T. J., Winn, K., & Stoffers, P. (2004). Late Quaternary tephra in the New Ireland Basin, Papua New Guinea. *Journal of Volcanology and Geothermal Research*, *132*(1), 73–95. doi:10.1016/S0377-0273(03)00421-9

Htay, K. N., Aung, L. T., Tajcmanova, L., & Heinrich, C. A. (2017). The Evidances of High Temperature-Medium Pressure, Granulite grade metamorphism in Momeik Area, Mogok Metamorphic Belt, Myanmar. In *Conference Abstract of 1st Myanmar Applied Earth Sciences Associtation*.

Hughes, R. W. (1997). *Ruby & Sapphire*.

Hughes, R. W. (2014). *Ruby & Sapphire—A Collector's Guide*.

Hughes, R. W. (2016). *Ruby & Sapphire: A Gemologists Guide*.

Hynes, A. (1980). Carbonatization and mobility of Ti, Y, and Zr in Ascot Formation metabasalts, SE Quebec. *Contributions to Mineralogy and Petrology*, *75*, 79–87.

Iyer, L. A. N. (1953). *The Geology and Gemstones of the Mogok Stone Tract, Burma*.

Jackson, S. E., Longerich, H. P., Dunning, G. R., & Freyer, B. J. (1992). The application of laser-ablation microprobe; inductively coupled plasma-mass spectrometry (LAM-ICP-MS) to in situ trace-element determinations in minerals. *The Canadian Mineralogist*, *30*(4), 1049–1064. https://doi.org/

Jackson, S. E., Pearson, N. J., Griffin, W. L., & Belousova, E. A. (2004). The application of laser ablation-inductively coupled plasma-mass spectrometry to in situ U-Pb zircon geochronology. *Chemical Geology*, *211*(1–2), 47–69. doi:10.1016/j.chemgeo.2004.06.017

Keller, P. C. (1985). Gemstones and Their Origins. *Terra*, *23*(3–12). doi:10.1007/978-1-4684-6674-4

Koziol, A. M., & Newton, R. C. (1988). Redetermination of the anorthite breakdown reaction and improvement of the plagioclase-garnet-Al2SiO5-quartz geobarometer. *American Mineralogist*, *73*, 216–223.

La Touche, T. H. D. (1913). *Geology of the Northern Shan State*. *Office of the Geological Survey of India, Calcutta, India*.

Lal, R. K. (1993). Internally consistent recalibrations of mineral equilibria for geothermobarometry involving garnet-orthopyroxene-plagioclase-quartz assemblages and their application to the South Indian granulites. *Journal of Metamorphic Geology*, *11*, 855–866.

Leake, B. W., Wooley, A. R., Arps, C. E. S., Birch, W. D., Gilbert, M. C., Grice, J. D., et al. (1997). Nomenclature of amphiboles. Report of the subcommittee on amphiboles of the International Mineralogical Association Commission on new minerals and mineral names. *European Journal of Mineralogy*, *9*, 623–651.

Lee, H.-Y., Sun-Lin Chung, S.-L., & H.-M., H.-M. Y. (2016). Late Cenozoic volcanism in central Myanmar: Geochemical characteristics and geodynamic significance. *Lithos*, *245*, 174–190.

Lee, H. Y., Chung, S. L., & Yang, H. M. (2016). Late Cenozoic volcanism in central Myanmar: Geochemical characteristics and geodynamic significance. *Lithos*, *245*, 174–190. doi:10.1016/j.lithos.2015.09.018

Licht, A., France-Lanord, C., Reisberg, L., Fontaine, C., Soe, A. N., & Jaeger, J.-J. (2013). A paleo Tibet-Myanmar connection? Reconstructing the Later Eocene drainage systems of Central Myanmar using a multi-proxy approach. *J. Geol. Soc. London*, *170*, 929–939.

Link, K. (2015). Age determination of zircon inclusions in faceted sapphires. *J. Gemmol.*, *34*, 692–700.

Link, K. (2016). New age data for blue sapphire from Mogok, Myanmar. *J. Gemmol.*, *35*, 107–109.

Lustrino, M., Fedele, L., Agostini, S., Prelević, D., & Salari, G. (2019). Leucitites within and around the Mediterranean area. *Lithos*, *324–325*, 216–233.

Meschede, M. (1986). A method of discrimination between different types of mid-ocean ridge basalts and continental tholeiites with the Nb–Zr–Y diagram. *Chemical Geology*, *56*, 207–218.

Miller, C., Thoni, M., Frank, W., Grasemann, B., Klotzli, U., Guntli, P., & Draganits, E. (2001). The early Palaeozoic magmatic event in the Northwest Himalaya, India: source, tectonic setting and age of emplacement. *Geol. Mag.*, *138*, 237–251.

Min, M. (2007a). *Chapter 5. Exhumation of the Mogok Belt in central Myanmar:a geochronologic study. In: thermochronology applied to strike-slip zones Central Ameria and Myanmar.*

Min, M. (2007b). *Chapter 5 Exhumation of the Mogok belt in central Myanmar : a geochronologic study*.

Mitchell, A. H. G. (1993). Cretaceous-Cenozoic tectonic events in the western Myanmar (Burma)-Assam region. *Journal of the Geological Society*, *150*, 1089–1102.

Mitchell, A. H. G., Marshall, T. R., Skinner, A. C., Baker, A. D., Amos, B. J., & Bateson, J. H. (1977). Geology and exploration geochemistry of the Yadanartheingi anf Kyaukme-Longtawkno areas, Northern Shan States, Burma. *Overseas Geology and Mineral Resources*, *51*(35).

Mitchell, A. H. G., Oo, T., Win, M. N., Hlaing, T., Htun, K. M., & Htay, M. T. (2006). Rock relationships in the Mogok metamorphic belt, Tatkon to Mandalay, central Myanmar. *Journal of Asian Earth Sciences*, *29*(5–6), 891–910. doi:10.1016/j.jseaes.2006.05.009

Mitchell, A., Oo, T., Lin, T.-H., Hung, C.-H., & Chung, S.-L. (2012). Zircon U–Pb ages in Myanmar: Magmatic–metamorphic events and the closure of a neo-Tethys ocean? *Journal of Asian Earth Sciences*, *56*, 1–23. doi:10.1016/j.jseaes.2012.04.019

Morimoto, N., Fabries, J., Ferguson, A. K., Ginzburg, I. V., Ross, M., Seifert, F. A., et al. (1988). Nomenclature of amphiboles. *Mineralogy and Petrology*, *39*, 55–76.

Moyd, L. (1949). Petrology of the nepheline and corundum rocks of southeastern Ontario. *American Mineralogist*, *34*, 736–750.

Mullen, E. D. (1983). MnO/TiO2/P2O5: a major element discriminant for basaltic rocks of oceanic environments and its implications for petrogenesis. *Earth Planet. Sci. Lett.*, *62*, 53–62.

Newton, R. C., Aranovich, L. Y., Hansen, E. C., & Vandenheuvel, B. A. (1998). Hypersaline fluids in Precambrian deep-crustal metamorphism. *Precambrian Res.*, *91*, 41–63.

Norman, M. D., & Nemchin, A. A. (2014). A 4.2 billion year old impact basin on the Moon: U-Pb dating of zirconolite and apatite in lunar melt rock 67955. *Earth and Planetary Science Letters*, *388*, 387–398. doi:10.1016/j.epsl.2013.11.040

Pearce, J. A., & Cann, J. R. (1973). Tectonic setting of basic volcanic rocks using Ti, Zr and Y. *Earth and Planetary Sciences and Letters*, *19*, 290–300.

Pearce, J. A., & Parkinson, I. J. (1993). Trace element models for mantle melting: application to

volcanic arc petrogenesis; in Prichard, H.M., Alabaster, T., Harris, N.B.W., and Neary, C.R., eds., Magmatic Processes and Plate Tectonics,. *Geological Society Special Publications*, *76*, 373–403.

Peretti, A., Peretti, A. K., & Günther, D. (2015). World of Magnificent Spinels Provenance and Identification. *Contributions to Gemology*, *11*(May).

Phyo, M. M., Franz, L., Bieler, E., Balmer, W., & Krzemnicki, M. S. (2019). Spinel from Mogok, Myanmar—A Detailed Inclusion Study by Raman Microspectroscopy and Scanning Electron Microscopy. *The Journal of Gemmology*, *36*(5), 418–435. doi:10.15506/JoG.2019.36.5.418

Powell, M. & Powell, R. (1977). A nepheline-alkali feldspar geothermometer. *Contributions to Mineralogy and Petrology*, *62*, 193–204.

Powell, R. (1985). Regression diagnostics and robust regression in geothermometer/geobarometer calibration: the garnet-clinopyroxene geothermometer revisited. *Journal of Metamorphic Geology*, *3*, 231–243.

Prelević, D., Akal, C., Romer, R. L., Mertz-Kraus, R., & Helvacı, C. (2015). Magmatic response to slab tearing: constraints from the Afyon Alkaline Volcanic Complex, Western Turkey. *Journal of Petrology*, *56*, 527–562.

Prelević, D., Foley, S. F., Romer, R., & Conticelli, S. (2008). Mediterranean Tertiary lamproites derived from multiple source components in postcollisional geodynamics. *Geochimica et Cosmochimica Acta*, *72*, 2125–2156.

Reiners, P. W., Carlson, R. W., Renne, P. R., Coo per, K. M., Granger, D. E., M c Lean, N. M., & Schoene, B. (2018). *Geochronology and Thermochronology.* (J. W. & Sons, Ed.).

RICHARDS, A., ARGLES, T., HARRIS, N., PARRISH, R., AHMAD, T., DARBYSHIRE, F., & DRAGANITS, E. (2005). Himalayan architecture constrained by isotopic tracers from clastic sediments. *Earth and Planetary Science Letters*, *236*(3–4), 773–796. doi:10.1016/j.epsl.2005.05.034

Rickwood, P. C. (1989). Boundary lines within petrologic diagrams which use oxides of major and minor elements. *Lithos*, *22*(4), 247–263. doi:10.1016/0024-4937(89)90028-5

Romer, R. L., & Hahne, K. (2010). Life of the Rheic Ocean: Scrolling through the shale record.

Gondwana Res., *17*, 236–253.

Ryburn, R. J., Raheim, A., & Green, D. H. (1976). Determination of P,T paths of natural eclogites; a correction. *Lithos*, *9*, 161–164.

Santosh, M., & Omori, S. (2008). CO2 flushing: a plate tectonic perspective. *Gondwana Res.*, *13*, 86–102.

Schaltegger, U., Schmitt, A. K., & Horstwood, M. S. A. (2015). U-Th-Pb zircon geochronology by ID-TIMS, SIMS, and laser ablation ICP-MS: Recipes, interpretations, and opportunities. *Chemical Geology*, *402*(March), 89–110. doi:10.1016/j.chemgeo.2015.02.028

Searle, D. L., & Haq, B. T. (1964). The Mogok belt of Burma and its relationship to the Himalayan orogeny. In *The international geological congress 22* (pp. 132–161).

Searle, M. P., Noble, S. R., Cottle, J. M., Waters, D. J., Mitchell, A. H. G., Hlaing, T., & Horstwood, M. S. A. (2007). Tectonic evolution of the Mogok metamorphic belt, Burma (Myanmar) constrained by U-Th-Pb dating of metamorphic and magmatic rocks. *Tectonics*, *26*(3). doi:10.1029/2006TC002083

Searle, M. P., Waters, D. J., Morley, C. K., Gardiner, N. J., Htun, U. K., Nu, T. T., & Robb, L. J. (2017). *Chapter 12 Tectonic evolution of the Mogok metamorphic and Jade mines belts and ophiolitic terranes of Burma (Myanmar)*. *Myanmar: Geology, Resources and Tectonics* (Vol. 48). Geological Society Memoir48. doi:10.1029/2006TC002083

Sláma, J., Košler, J., Condon, D. J., Crowley, J. L., Gerdes, A., Hanchar, J. M., et al. (2008). Plešovice zircon — A new natural reference material for U–Pb and Hf isotopic microanalysis. *Chemical Geology*, *249*, 1–35.

Sone, M., & Metcalfe, I. (2008). Parallel Tethyab sutures in mainland Southeast Asia: new insights for Palaeo-Tethys closure and implications for the Indosinian Orogeny. *Comptes Rendus Geoscience*, *340*, 166–179.

Stern, R. J., Tsujimori, T., Harlow, G., & Groat, L. A. (2013). Plate tectonic gemstones. *Geology*, *41*(7), 723–726. doi:10.1130/G34204.1

Stucki, A., Trommsdorff, V., & Gunther, D. (2001). Zirconolite in metarodingites of Penninic

Mesozoic ophiolites, Central Alps. *Schweizerische Mineralogische Und Petrographische Mitteilungen*, *81*(2), 257–265.

Sutherland, F. ., Coenraads, R. ., Hoskin, P. W. ., Bosshart, G., & Fanning, C. . (2002). Sapphire crystallization, age and origin, Ban Huai Sai, Laos: age based on zircon inclusions. *Journal of Asian Earth Sciences*, *20*(7), 841–849. doi:10.1016/s1367-9120(01)00067-0

Sutherland, F. L., Duroc-Danner, J. M., & Meffre, S. (2008). Age and origin of gem corundum and zircon megacrysts from the Mercaderes-Rio Mayo area, South-west Colombia, South America. *Ore Geology Reviews*, *34*(1–2), 155–168. doi:10.1016/j.oregeorev.2008.01.004

Sutherland, F. L., Piilonen, P. C., Zaw, K., Meffre, S., & Thompson, J. (2015). Sapphire within zircon-rich gem deposits , Bo Loei , Ratanakiri Province , Cambodia : trace elements , inclusions , U – Pb dating and genesis. *Australian Journal of Earth Sciences*, *62*, 761–773. doi:10.1080/08120099.2015.1101015

Sutherland, F. L., Zaw, K., Meffre, S., Thompson, J., Goemann, K., Thu, K., et al. (2018). Diversity In Ruby Geochemistry And Its Inclusions, Intra- And Inter Comparisons From Myanmar And East Australia. In *Meeting of the international mineralogical association* (p. 329).

Sutherland, F. L., Zaw, K., Meffre, S., Thompson, J., Goemann, K., Thu, K., et al. (2019). Diversity in Ruby Geochemistry and Its Inclusions: Intra- and Inter- Continental Comparisons from Myanmar and Eastern Australia. *Minerals*, *9*(1), 28. doi:10.3390/min9010028

Sylvester, P. J., & Ghaderi, M. (1997). Trace element analysis of scheelite by excimer laser ablation-inductively coupled plasma-mass spectrometry (ELA-ICP-MS) using a synthetic silicate glass standard. *Chemical Geology*, *141*(1–2), 49–65. doi:10.1016/S0009-2541(97)00057-0

Tajčmanová, L., Konopasek, J., & Schulmann, K. (2006). Thermal evolution of the orogenic lower crust during exhumation within a thickened Moldanubian root of the Variscan belt of central Europe. *Journal of Metamorphic Geol.*, *24*, 119–134.

Thein, M. (1973). A preliminary synthesis of the geological evolution of Burma with reference to the tectonic development of Southeast Asia. *Geological Society of Malaysia*, *6*, 87–116.

Thein, M. (2008). Modes of occurrence and origin of precious gemstone deposits of the Mogok Stone Tract. *Journal of the Myanmar Geosciences Society*, *1*, 75–84.

Thein, M. L., Myint, O., Kyi, S., & P. N. Win. (1990). *Geology and stratigraphy of the metamorphosed Early Paleozoic rocks of the Mogok–Thabeikkyin–Singu–Madaya Areas. Unpublished staff report* (Vol. 98).

Themelis, T. (2008). *Gems and Mines of Mogok*.

Thu, K. (2007). *The Igneous Rocks of the Mogok Stone Tract: Their Distribution, Petrography, Petrochemistry, Sequence, Geochronology and Economic Geology. Ph.D. Thesis, University of Yangon, Yangon, Myanmar*.

Thu, Y. K., Enami, M., Kato, T., & Tsuboi, M. (2017). Granulite facies paragneisses from the middle segment of the Mogok metamorphic belt, central Myanmar. *Journal of Mineralogical and Petrological Sciences*, *112*(1), 1–19. doi:10.2465/jmps.160526

Thu, Y. K., Win, M. M., Enami, M., & Tsuboi, M. (2016). Ti-rich biotite in spinel and quartz-bearing paragneiss and related rocks from the Mogok metamorphic belt, central Myanmar. Journal of Mineralogical and. *Petrological Sciences*, *111*, 270–282.

Touret, J. L. R. (1971). Le faciés granulite en Norvège Méridionale. II: les inclusions fluides. *Lithos*, *4*, 423–436.

Touret, J. L. R., & Huizenga, J. M. (2012). Fluid-assisted granulite metamorphism: a continental journey. *Gondwana Res.*, *21*, 224–235.

Ulianov, A., Müntener, O., Schaltegger, U., & Bussy, F. (2012). The data treatment dependent variability of U-Pb zircon ages obtained using mono-collector, sector field, laser ablation ICPMS. *Journal of Analytical Atomic Spectrometry*, *27*(4), 663–676. doi:10.1039/c2ja10358c

Vermeesch, P. (2018). IsoplotR: A free and open toolbox for geochronology. *Geoscience Frontiers*, *9*(5), 1479–1493. doi:10.1016/j.gsf.2018.04.001

Waltham, T. (1999). The ruby mines of Mogok. *Geology Today*, *15*, 143–149.

Wang, Y., Sieh, K., Thura, A., Soe, M., Saw, N. K., & Soe, T. T. (2011). Earthquakes and Slip rate of the sounthern Sagaing-fault: insights from an offset ancient fort wall, lower Burma (Myanmar). *Geophysical Journal International*, *185*, 49–64.

Wiedenbeck, M., Alle, P., Corfu, F., Griffin, W. L., Meier, M., F., O., et al. (1995). Three natural

zircon standards for U–Th–Pb, Lu–Hf, trace element and REE analyses. *Geostandards Newsletter*, *19*, 1–23.

Win, M. M., Enami, M., & Kato, T. (2016). Metamorphic conditions and CHIME monazite ages of Late Eocene to Late Oligocene high-temperature Mogok metamorphic rocks in central Myanmar. *Journal of Asian Earth Sciences*, *117*, 304–316. doi:10.1016/j.jseaes.2015.11.023

Wu, C.-M., Zhang, J., & Ren, L. D. (2004). Empirical garnet-biotite-plagioclase-quartz (GBPQ) geobarometry in medium-to high-grade metapelites. *Journal of Petrology*, *45*, 1907–1921.

Wu, F. Y., Yang, Y. H., Mitchell, R. H., Bellatreccia, F., Li, Q. L., & Zhao, Z. F. (2010). In situ U-Pb and Nd-Hf-(Sr) isotopic investigations of zirconolite and calzirtite. *Chemical Geology*, *277*(1–2), 178–195. doi:10.1016/j.chemgeo.2010.08.007

Wuhrer, R., Beattie, R., Coenraads, R. R., Abduriyim, A., Giuliani, G., Hoskin, P. W. O., et al. (2015). Corundum (sapphire) and zircon relationships, Lava Plains gem fields, NE Australia: Integrated mineralogy, geochemistry, age determination, genesis and geographical typing. *Mineralogical Magazine*, *79*(03), 545–581. doi:10.1180/minmag.2015.079.3.04

Xiang, H., Zhang, L., Zhong, Z.-Q., Santosh, M., Zhou, H.-W., Zhang, H.-F., et al. (2012). Ultrahigh-temperature metamorphism and anticlockwise P-T-t path of Paleozoic granulites from north Qinling-Tongbai orogen, Central China. *Gondwana Res.*, *21*, 559–576.

Yang, W. Bin, Niu, H. C., Shan, Q., Sun, W. D., Zhang, H., Li, N. B., et al. (2014). Geochemistry of magmatic and hydrothermal zircon from the highly evolved Baerzhe alkaline granite: Implications for Zr-REE-Nb mineralization. *Mineralium Deposita*, *49*(4), 451–470. doi:10.1007/s00126-013-0504-1

Yonemura, K., Osanail, Y., Zaw, T. N., Nakano, N., Charusiri, P., & Adachi, T. (2013). EPMA U-Th-Pb monazite dating of metamorphic rocks from the Mogok Metamorphic Belt, central Myanmar. *Journal of Mineralogical and Petrological Sciences*, *108*(3), 184–188. doi:10.2465/jmps.121019a

Yui, T. F., Zaw, K., & Wu, C. M. (2008). A preliminary stable isotope study on Mogok Ruby, Myanmar. *Ore Geology Reviews*, *34*(1–2), 192–199. doi:10.1016/j.oregeorev.2008.05.001

Zartman, R. E., & Doe, B. R. (1981). Plumbotectonics - the model. *Tectonophysics*, *75*, 135–162.

Zaw, K. (1989). Comments on transcurrent movements in the Myanmar-Andaman sea region. *Geology*, *17*, 93–95.

Zaw, K. (1990). Geological, petrological and geochemical characteristics of granitoid rocks in Burma: with special reference to the associated W-Sn mineralization and their tectonic setting. *Journal of Southeast Asian Earth Sciences*, *4*, 293–335.

Zaw, K. (1998). Geological evolution of selected granitic pegmatites in myanmar (burma): Constraints from regional setting, lithology, and fluid-inclusion studies. *International Geology Review*, *40*(7), 647–662. doi:10.1080/00206819809465229

Zaw, K. (2017). *Overview of mineralization styles and tectonic-metallogenic setting in Myanmar. In Myanmar: Geology, Resources and Tectonics; Chapter 24; Barber, A.J., Zaw, K., Crow, M.J., Eds.; Geological Society London Memoirs*.

Zaw, K., Sutherland, F. L., Graham, I., Meffre, S., & Thu, K. (2010). Dating zircon inclusions in gem corundum deposits and genetic implications, 7.

Zaw, K., Sutherland, L., Yui, T. F., Meffre, S., & Thu, K. (2014). Vanadium-rich ruby and sapphire within Mogok Gemfield, Myanmar: implications for gem color and genesis. *Mineralium Deposita*, *50*(1), 25–39. doi:10.1007/s00126-014-0545-0

Zaw, K., Thu, K., Meffre, S., Yui, T. F., & Sutherland, F. L. (2015). Vanadium-rich ruby and sapphire within Mogok Gemfield, Myanmar: implications for gem color and genesis. *Mineralium Deposita*, *50*(1), 25–39. doi:10.1007/s00126-014-0545-0

Zuleger, E., & Erzinger, J. (1988). Determination of the REE and Y in silicate materials with ICP-AES. *Fresenius' Zeitschrift für Analytische Chemie*, *332*(2), 140–143. doi:10.1007/BF00470631

CHAPTER II

Spinel from Mogok, Myanmar—A Detailed Inclusion Study by Raman Microspectroscopy and Scanning Electron Microscopy

Myint Myat Phyo, Eva Bieler, Leander Franz, Walter A. Balmer and Michael S. Krzemnicki

Published 2019 in the Journal of Gemmology, 36 (5), 418-435

Figure 2.1 Cut and rough spinel from Mogok, Myanmar. (Size of cut stone: ranging from approximately 7ct to 35 ct.

2.1 Abstract

Mineral inclusions in 100 gem-quality spinels from both primary marble and alluvial mining sites within the Mogok area of Myanmar were analysed using Raman microspectroscopy and scanning electron microscopy (including backscattered electron imaging and energy-dispersive spectroscopy). The samples ranged from pink to red, orangey pink to orangey red and grey to

purplish grey. We identified a number of inclusions that are reported here for the first time in Mogok spinel: amphibole (presumably pargasite), anatase, baddeleyite, boehmite, brucite, chlorite, clinohumite, clinopyroxene, diaspore, geikielite, goethite, halite, marcasite, molybdenite, periclase and pyrrhotite. Furthermore, we found anhydrite, apatite, carbonates (calcite, dolomite and magnesite), chondrodite, elemental sulphur, graphite, iron oxides or iron hydroxides, phlogopite and zircon, which were previously known as mineral inclusions in Mogok spinel. We further differentiated the inclusions in spinel from different mining sites in Mogok to assess whether these mineral assemblages can enhance our understanding of the geological origin of these gems and whether the inclusions can help separate Mogok spinels from those of other marble-related deposits worldwide.

2.2 Introduction

Since ancient times, gem-quality spinel ($MgAl_2O_4$) has been appreciated for its range of colour and often exceptional clarity, and today spinel is the second most significant and popular red gemstone after ruby (Cesbron *et al.* 2002 & Pardieu *et al.* 2008). Spinel's significance is well illustrated by the famed 'Balas rubies'—which are actually spinels from historic mines in Badakhshan (i.e. Kuh-i-Lal, in what is today Tajikistan)—that were described and praised by the Persian scholar Al-Biruni (973–1048 AD). Exceptional pinkish red spinels were part of the Moghul imperial jewels and later were partly integrated into the British crown jewels (the so-called Black Prince Ruby and the Timur Ruby; see also Pardieu & Hughes 2008; Yavorskyy & Hughes 2010; Truong 2017).

Spinel may form by high-grade metamorphism in calc-silicate rocks and marbles (Balmer *et al.* 2017) or in skarns (contact zones between Ca-rocks and magmatic intrusions; cf. Gorghinian *et al.* 2013), and is also found in secondary deposits (Thein 2008). It shows a wide variety of colours, mainly red to pink and purple, orange, violet to blue, green and even black. Although sometimes showing greyish or brownish hues, it may also display strong colour saturation, especially in the pink to red range. Moreover, the demand for and value of spinel have increased sharply in the recent years. Although known from deposits throughout the world (Myanmar, Sri Lanka, Tanzania, Madagascar and Vietnam, to name a few), some of the finest spinels are found in the Mogok area in Myanmar (e.g. Figure 2.1), which is one of the world's most eminent gem sources that is renowned for producing exceptional rubies, sapphires and other stones, as well as rarities such as

hibonite, jeremejevite, johachidolite, poudretteite and painite (Iyer 1953; Hughes 1997 & 2017b; Themelis 2008).

Although the literature contains some information on inclusions in Burmese spinel (see, e.g., Gübelin & Koivula 1986; Hughes 1997, 2018; Themelis 2008; Malsy & Klemm 2010; Zhu & Yu 2018), most publications to date describe Burmese spinel in general (Themelis 2008; Peretti *et al.* 2015), or focus on specific gemmological features (Pardieu 2014; Vertriest & Raynaud 2017) or the oxygen isotopic composition of these spinels (Giuliani *et al*. 2017). Moreover, several more publications deal with inclusions in spinel from worldwide localities (Gübelin & Koivula 1986, 2005, Cooper & Ziyin 2014; Hughes 2017a).

In this study, we describe in detail the solid inclusions found in pink to red, orangey pink to orangey red and grey to purplish grey gem-quality spinels collected from various localities (and local gem markets) in the Mogok area. We found systematic variations in the inclusions related to the different mining sites, suggesting that such inclusion research may be applied to the origin determination of spinels and to separating them from their synthetic flux-grown counterparts (Krzemnicki 2008).

2.3 Geological Setting and Mining Methods

Since the 15th century, the Mogok area of Myanmar has been known as a major source of rubies and other gems (Iyer 1953). Often referred to as the 'Mogok Stone Tract' (La Touche 1913; Fermor 1931; Chhibber 1934; Iyer 1953), this gem-rich area is located within the central part of the Mogok Metamorphic Belt (MMB). The MMB is composed of Palaeozoic and Mesozoic high-grade metasediments and intrusive rocks (Searle & Haq 1964; Barley *et al*. 2003; Searle *et al.* 2007; Thu *et al.* 2016; Phyo *et al.* 2017) and forms part of the Mogok-Mandalay-Mergui Belt (Figure 2.2), which extends for more than 2,000 km, north to south, along the western margin of Shan-Thai (or Sibumasu) terrane, from the Himalayan syntaxis to the Andaman Sea (Bender 1983; Zaw 1990, 2017; Zaw *et al.* 2015). The Mogok Stone Tract is mainly underlain by gneiss, marble, calc-silicate rocks and quartzite, which were intruded by various felsic to mafic igneous rocks (Iyer 1953).

Ruby, sapphire, spinel and other gems are mined from primary deposits (calc-silicate rocks and marbles, with spinel only forming in the latter) and from secondary deposits like alluvial and eluvial placers, as well as karstic sinkholes and caverns (Thein 2008). To extract the gems from the primary rocks and associated karstic deposits, an extensive network of tunnels (e.g. Figure 2.4) has

been excavated by drilling and blasting. For the secondary deposits, traditional mining methods are used such as *twinlon* (digging shafts in the soil/gravel with a maximum depth of 30 m), *myawdwin* (hydraulic mining along hillsides; Figure 2.5) and *ludwin* (mainly used in sinkhole and cavern excavations). In the alluvial plains of the Mogok area, the gem-bearing gravel is usually reached at approximately 6–7 m below the surface (Iyer 1953). Detailed descriptions of the traditional mining methods used in the Mogok area are given in numerous reports (e.g. Gordon 1888; Halford-Watkins 1932a, b, c; Ehrmann 1957; Gübelin 1965; Keller 1983).

2.4 Materials and Methods

For this study, we collected and analysed 87 pink to red, orangey pink to orangey red and grey to purplish grey gem-quality spinel samples from six mining sites in the Mogok area (Yadanar Kaday Kadar, Bawlongyi, Kyauksaung, Kyauksin, Pyaungpyin and Mansin; see Figures 2.3 and 2.18) and 13 samples bought in local gem markets. A list of the samples is shown in Table 2.1.

We polished the surface of each spinel to provide a clear view of the interior, and then used a standard gemmological microscope (Cambridge Instruments) at 10×–70× magnification to observe mineral inclusions in the samples. Photomicrographs of the inclusions were taken with a Nikon D7000 digital camera attached to a System Eickhorst GemMaster microscope using 16×–80× magnification.

Raman microspectroscopy was performed on every inclusion, and the analyses were carried out with two different setups: a Renishaw inVia Raman system coupled with a Leica DM2500 M microscope, using an argon-ion laser at 514.5 nm wavelength; and a Bruker Senterra Raman spectrometer coupled with an Olympus microscope, using a frequency doubled Nd-YAG laser at 532 nm or a direct diode laser at 785 nm. The Raman spectra were mostly collected in the range of 100–1400 cm^{-1}, except for graphite (100–1600 cm^{-1}) and apatite (100–4000 cm^{-1}, to detect water peaks). Maximum exposure time per scan was 10 seconds and 10–50 scan accumulations were collected. Remarkably, there was only minor interference with the fluorescence of spinel. However, we were not able to identify very tiny inclusions with Raman microspectroscopy due to their small size. In addition, some inclusions produced Raman spectra of superposed combinations of two or more minerals, while others did not reveal a conclusive spectrum (probably because their weak Raman signal was dominated by the signal from the host spinel).

Scanning electron microscopy (SEM) was used to gain more information about selected mineral inclusions by visualising their shape and paragenetic intergrowths. In addition, SEM with energy-dispersive X-ray spectroscopy (EDS) was used to analyse their chemical composition. To accomplish this, the samples were carefully polished to expose the inclusions at the surface, and were then analysed at the Nano Imaging Lab of the University of Basel using a REM-FEI Nova Nano SEM 230 unit equipped with an energy-dispersive spectrometer, a secondary-electron (SE) and a backscattered electron (BSE) detectors. This system employed an in-lens detector for secondary electron images and an Octane Elite detector for EDS analysis. With this setup, we were able (in principle) to detect elements ranging from carbon to uranium as long as they were above the instrumental detection limit. We used an accelerating voltage of 15 kV, with magnifications of 50×–2500× and a working distance of 4.0–12.5 mm.

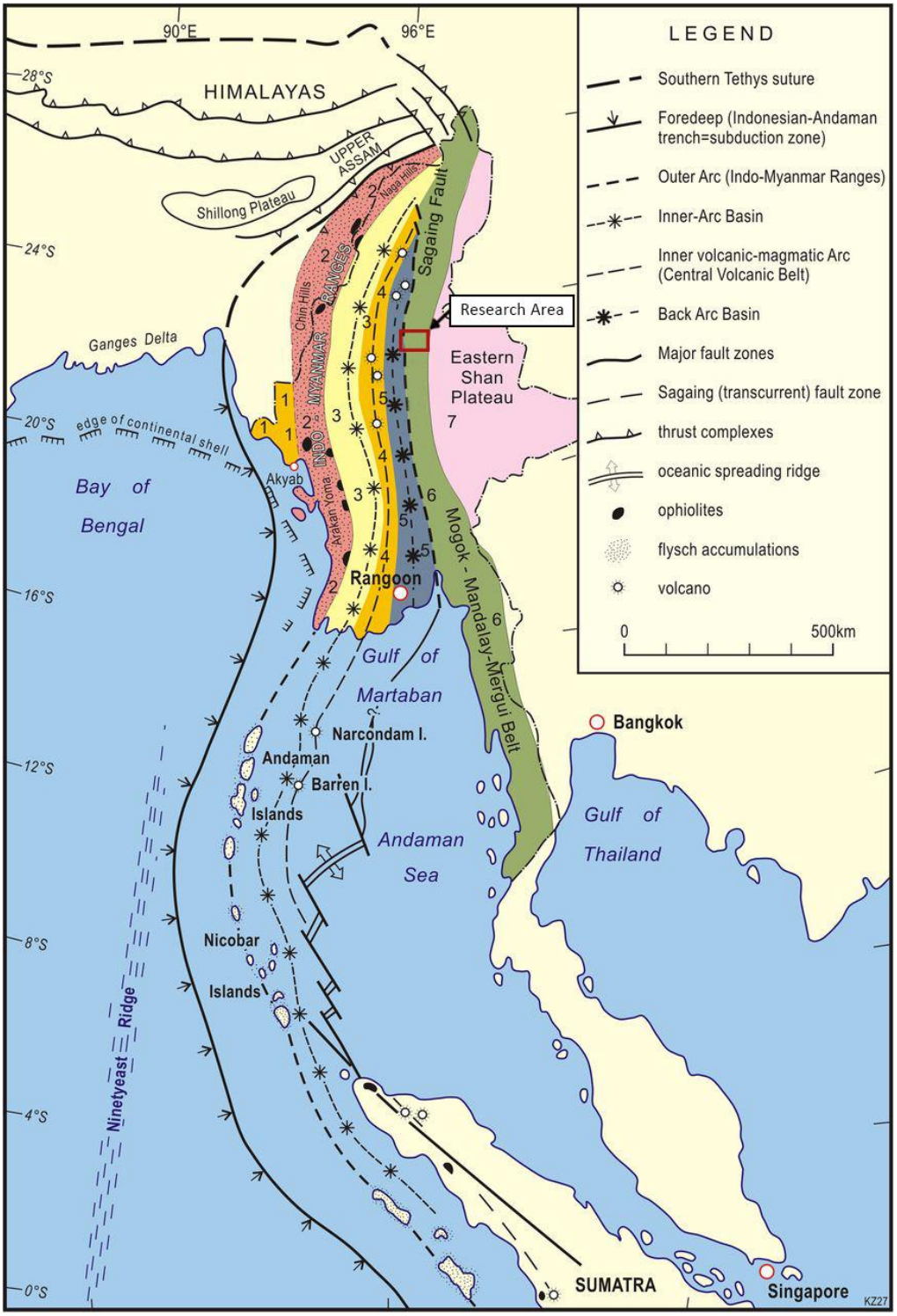

Figure 2.2 The Mogok research area is indicated on this regional map of Myanmar, which shows the main tectonic domains (numbered 1–7 from west to east) and fault structures (after Bender 1983; Zaw *et al.* 1989, 2015; Zaw 1990). The domains are: (1) Arakan (Rakhine) coastal strip, (2) Indo-Myanmar ranges, (3) western Inner-Burman Tertiary basin, (4) central volcanic belt (or central volcanic line), (5) eastern Inner-Burman Tertiary basin, (6) Mogok-Mandalay-Mergui belt and (7) eastern Shan Highlands.

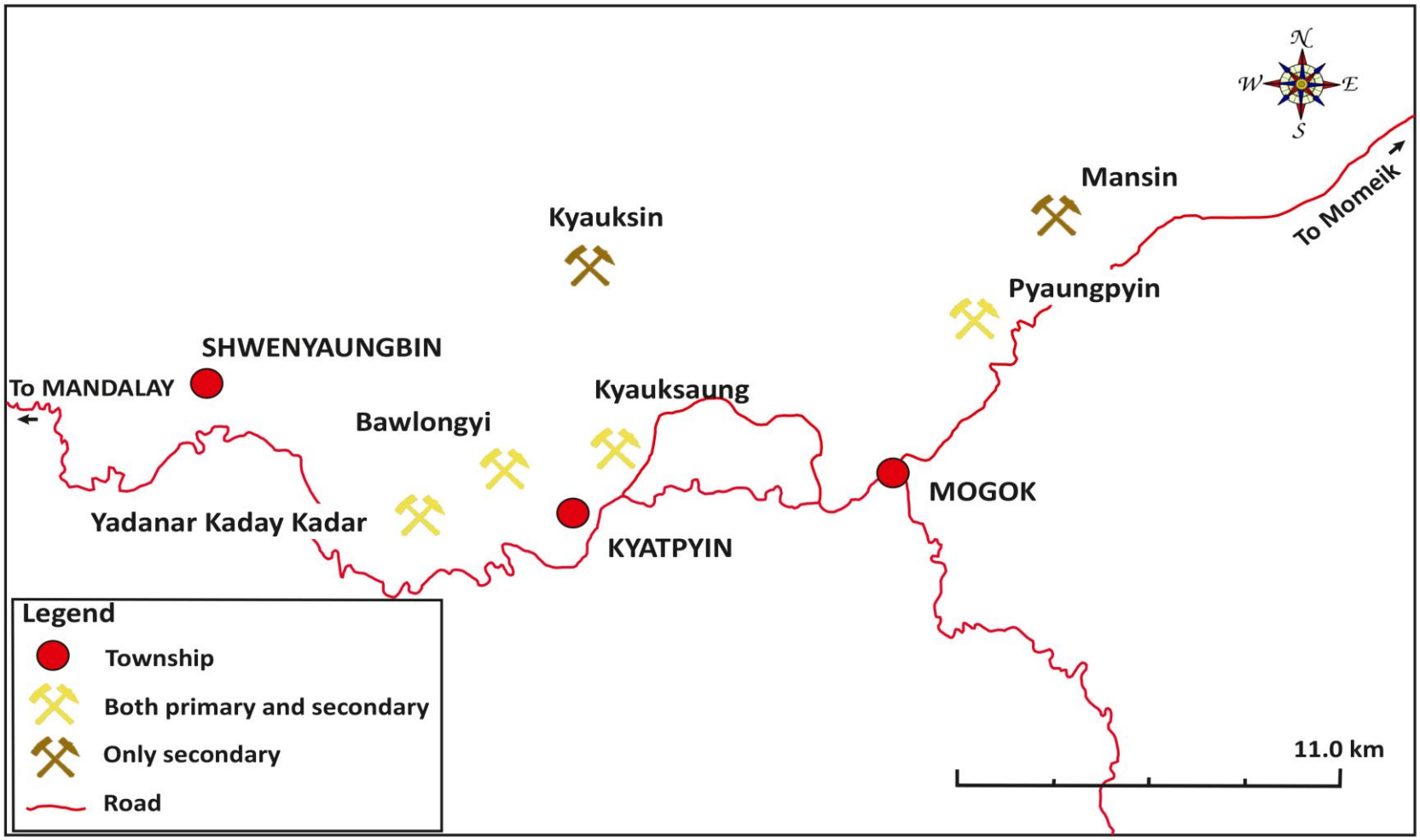

Figure 2.3 The mining locations from which spinel samples were obtained for this study (the 'research area' in Figure 2.2) are plotted on this map of the Mogok area.

Figure 2.4 The main tunnel of the Kyauksaung mine in central Mogok provides an example of extraction from primary (marble) host rocks.

Figure 2.5 Hydraulic mining of gem-bearing gravels at the Mansin pit in north-eastern Mogok demonstrates how spinels are obtained from secondary deposits.

Table 2.1 Spinel samples from Mogok investigated for this study.

Location*	Coordinates	No. samples	Weight range	Colour	Photo
Yadanar Kaday Kadar	22°54'18.54"N 96°22'38.18"E	5	0.18–0.35 ct	Orangey pink, light pink to red	
Bawlongyi	22°54'53.59"N 96°23'53.09"E	19	0.16–2.21 ct	Light pink to red, dark red, orange to orangey red, grey, purplish grey	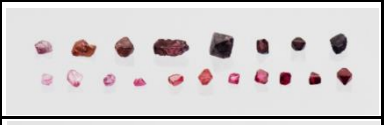
Kyauksin	22°57'26.51"N 96°25'31.63"E	17	0.45–1.24 ct	Light orange to orange, purplish grey	
Kyauksaung	22°55'20.08"N 96°25'55.44"E	10	0.10–0.62 ct	Light orange to orange, grey to purplish grey	
Pyaungpyin	22°57'13.53"N 96°31'10.63"E	6	0.45–0.67 ct	Intense red	
Mansin	22°58'28.64"N 96°32'23.57"E	30	0.05–2.59 ct	Light pink to strong pink, red to dark red	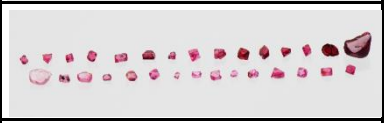
Market	_	13	0.54–8.65 ct	Light pink to dark red, grey	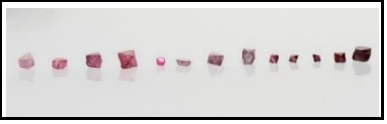

* Sample locations (top to bottom) are arranged from west to east

2.5 Results

The solid inclusions that we identified in the Mogok spinels are listed in Table II, along with those identified by other researchers in the published literature for spinels from Mogok and various deposits worldwide. Raman spectra of representative inclusions that we identified are given in Figures 2.6 to 2.8, and photomicrographs and BSE images are shown in subsequent figures. Mineral abbreviations in the images are from Whitney & Evans (2010).

In general, most of the inclusions formed anhedral grains, although some of them (such as amphibole and phlogopite) showed subhedral to euhedral shapes. Inclusion sizes commonly ranged from 1 µm to several millimetres. Their wide range of composition is reflected in the presence of several mineral groups (silicate, oxide, hydroxide, carbonate, phosphate, sulfate, sulfide and native element).

2.5.1 Optical Microscopy and Raman Analysis

Since Mogok spinels formed in marbles, it was not surprising to find abundant carbonates (i.e. calcite, dolomite and magnesite; e.g. Figure 2.9a) in most of the samples. They were typically present as colourless, irregularly shaped (partially resorbed) inclusions. Raman microspectrometry further revealed that carbonates sometimes also occurred as filling substances in octahedral negative crystals (similar to calcite and dolomite found by Zhu & Yu 2018).

Ca- and Mg-bearing silicate inclusions were found in the investigated spinels. The humite-group minerals chondrodite, $(Mg,Fe^{2+})_5(SiO_4)_2(F,OH)_2$, and clinohumite, $Mg_9(SiO_4)_4F_2$, were the most abundant Mg-silicates in our samples (Figures 2.9b and 2.10a). Colourless, short-prismatic Ca-Mg amphibole (presumably pargasite; Figure 2.10b) and clinopyroxenes (diopside and augite) were found in spinels from both Kyauksin (northern Mogok) and Mansin (eastern Mogok). Figure 2.11a reveals a colourless clinopyroxene inclusion with distinct cleavage that is associated with minute yellow elemental sulphur and black marcasite grains in a spinel from Mansin. In accordance with Gübelin & Koivula (2005), we also found forsterite, the Mg end member of the olivine group, as colourless rounded crystals (Figure 2.11b) in a few Mogok spinels. However, we did not find titanite and feldspar in our samples, both of which were mentioned by Gübelin & Koivula (2005) in spinel from Mogok. Zircon, although a common inclusion in sapphires and rubies from Mogok, was found only as tiny accessory inclusions in a few spinels from Kyauksin and Kyauksaung.

Oxides were commonly present as accessory phases in the studied spinels. We found yellow, rounded anatase (TiO_2) and bright yellow, prismatic baddeleyite (ZrO_2) inclusions, both surrounded by tension cracks (Figures 2.12a and b). Interestingly, using SEM-EDS we identified geikielite ($MgTiO_3$) as tiny needles/lamellae in spinel from Yadanar Kaday Kadar (western Mogok; Figure 2.13a). They were oriented along {111} lattice planes and presumably formed by epigenetic exsolution, similar to geikielite-rich ilmenite exsolution lamellae seen in chromite-chrome spinel from metacarbonates of the Oetztal-Stubai complex in Austria (Mogessie *et al.* 1988). To our knowledge, this is the first time such geikielite exsolution lamellae have been reported in gem-quality spinel.

We also found in our spinels several hydroxides, including diaspore [α-AlO(OH)], boehmite [γ-AlO(OH)], brucite [$Mg(OH)_2$] and goethite [α-$Fe^{3+}O(OH)$], mostly as retrograde phases in secondary inclusion trails.

Additional accessory inclusions in our spinels included anhydrite ($CaSO_4$, known also from Mogok rubies; Smith & Dunaigre 2001), apatite [$Ca_5(PO_4)_3(F,Cl,OH)$], sulphides (marcasite, molybdenite and pyrrhotite) and native graphite (C) and elemental sulphur (S_8). The apatite was seen as transparent to semi-transparent, anhedral to subhedral crystals (Figure 2.13b). As for the elemental sulphur, its presence within fluid inclusions and as solid inclusions (Figure 2.14) seems to be highly characteristic for spinels from Mansin (eastern Mogok; Pardieu *et al.* 2016 and Peretti *et al.* 2017). Less commonly, we also found elemental sulphur in the spinels from Kyauksaung (central Mogok) and Pyaungpyin (eastern Mogok).

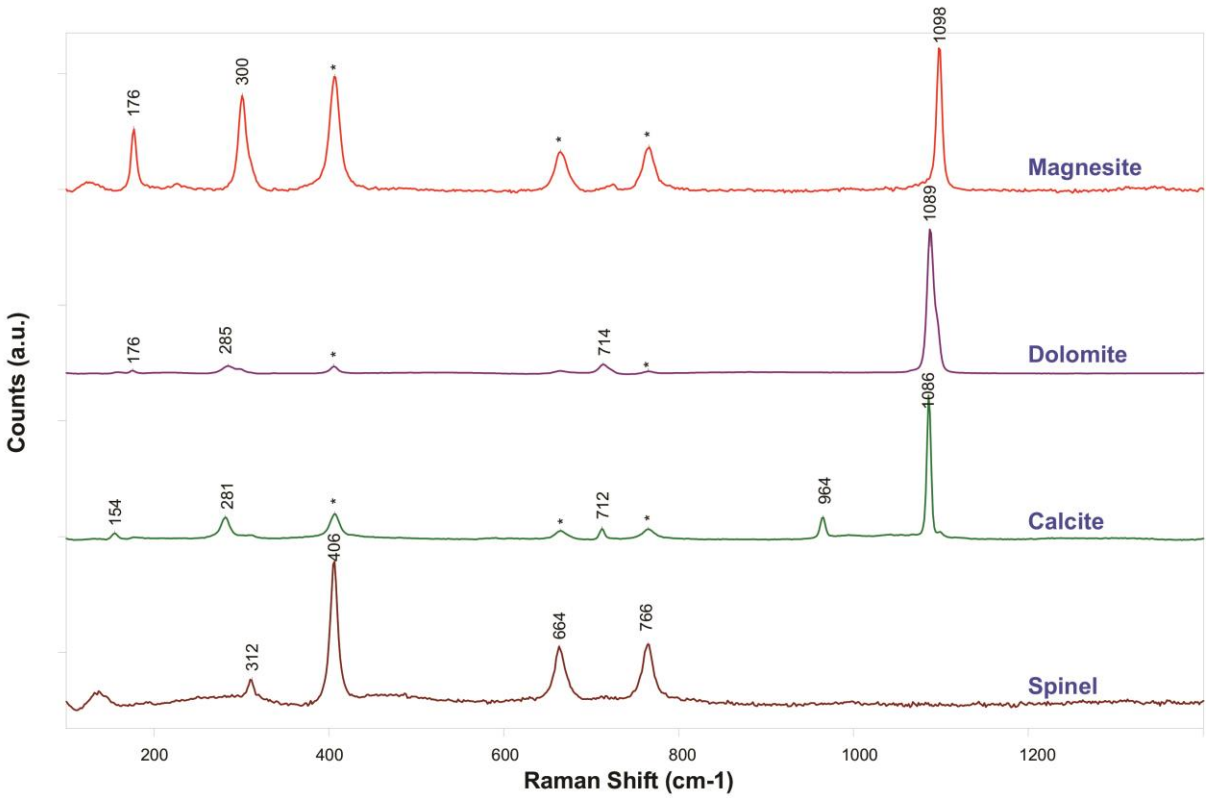

Figure 2.6 Representative Raman spectra are shown for carbonate mineral inclusions analysed in our samples from Mogok, together with a spectrum of the host spinel. Peaks in the inclusion spectra that are marked with an asterisk (*) are from the host spinel.

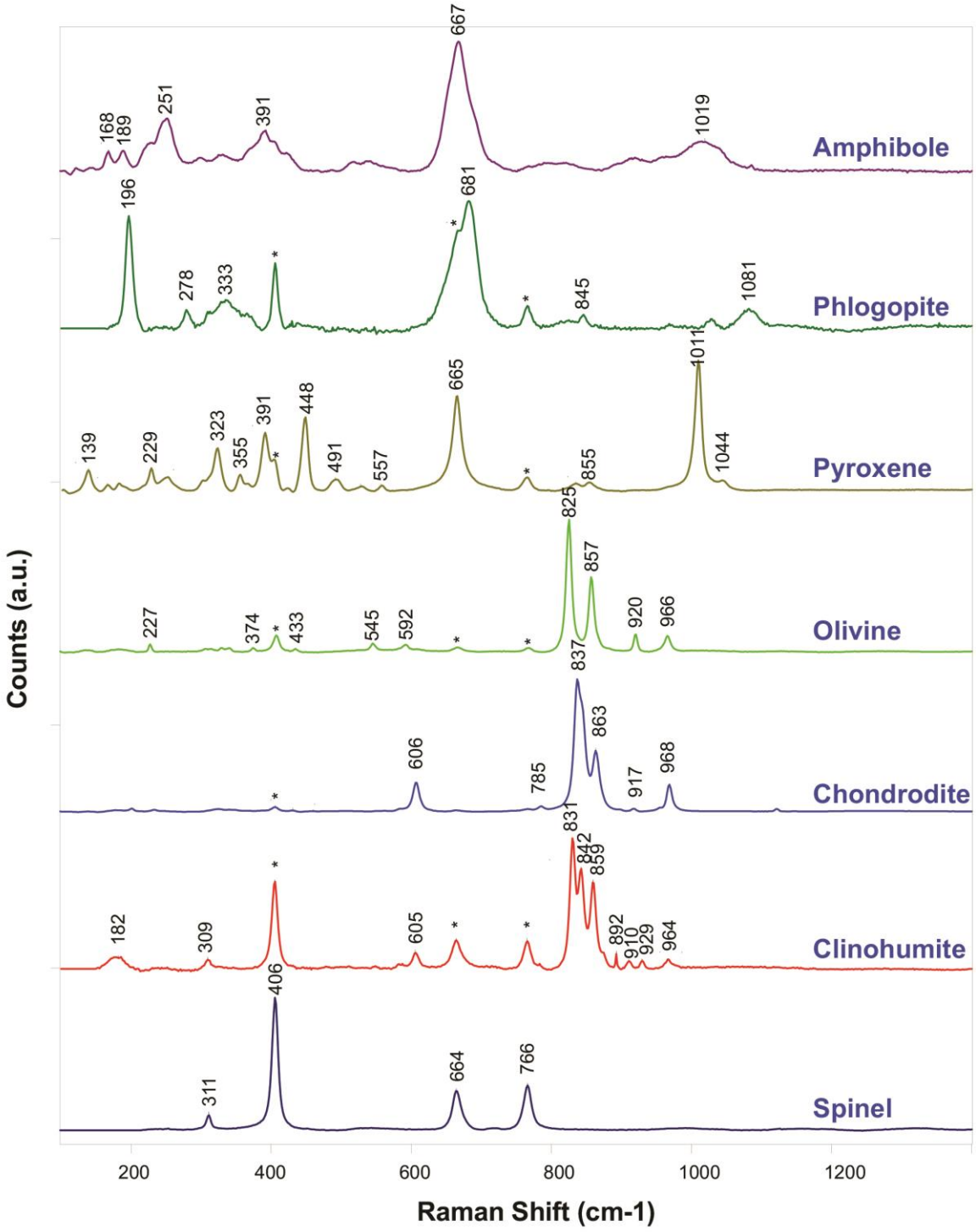

Figure 2.7 Representative Raman spectra are shown for various silicate mineral inclusions analysed in our samples from Mogok, together with a spectrum of the host spinel. Peaks in the inclusion spectra that are marked with an asterisk (*) are from the host spinel.

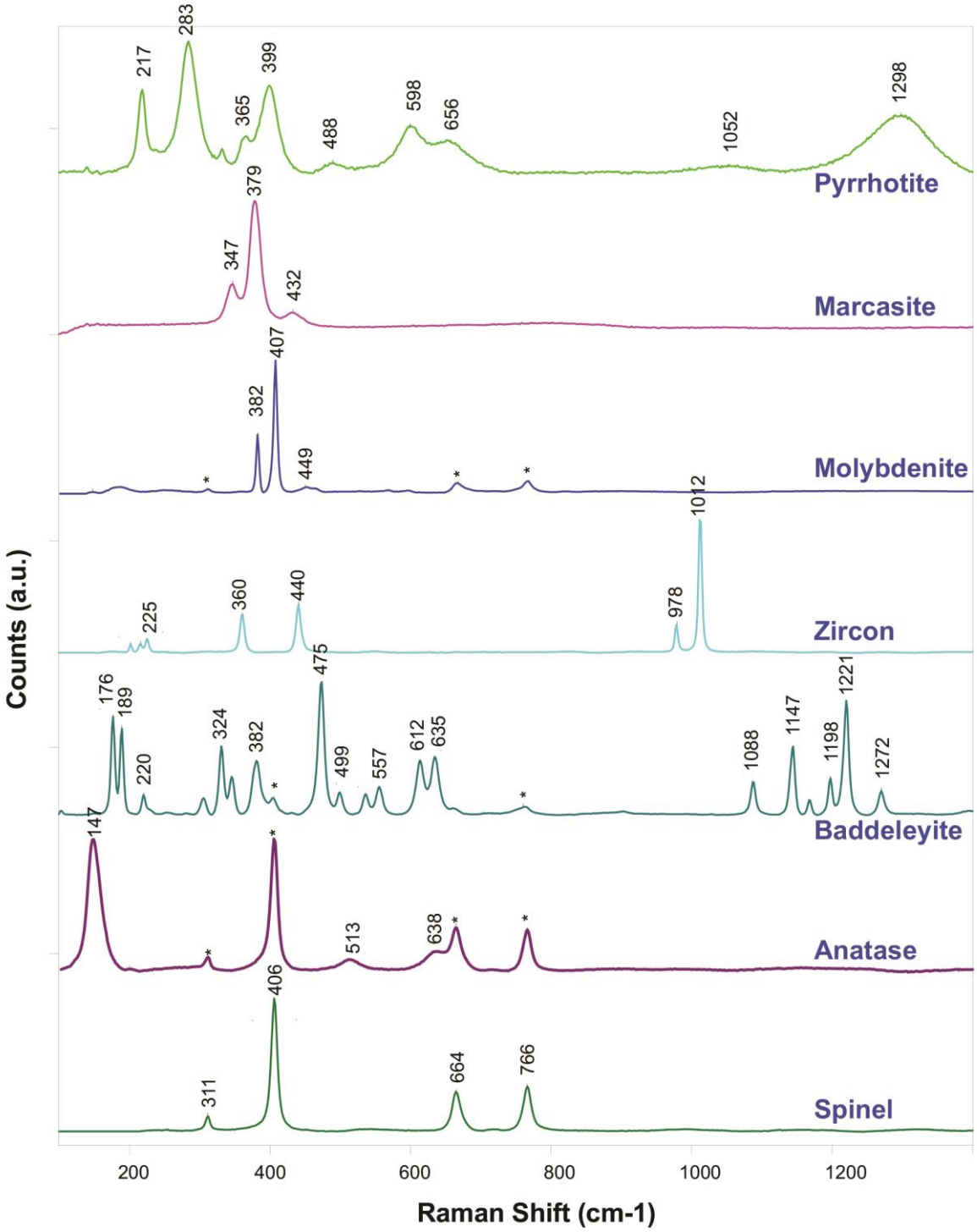

Figure 2.8 Representative Raman spectra are shown for various accessory mineral inclusions analysed in our samples from Mogok, together with a spectrum of the host spinel. Peaks in the inclusion spectra that are marked with an asterisk (*) are from the host spinel.

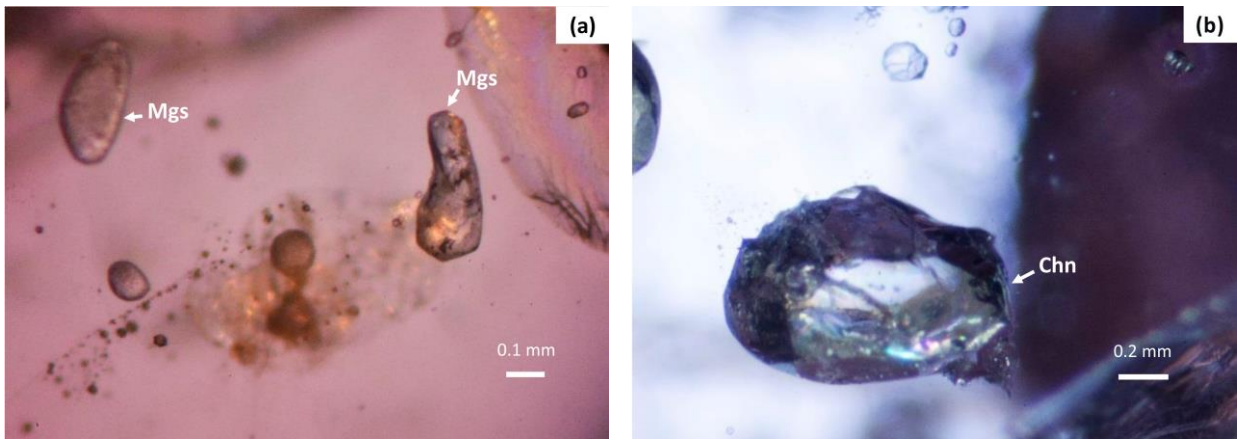

Figure 2.9 (a) An example of carbonate inclusions observed in the Mogok spinel samples is shown here by magnesite (Mgs). (b) Anhedral chondrodite (Chn) crystal.

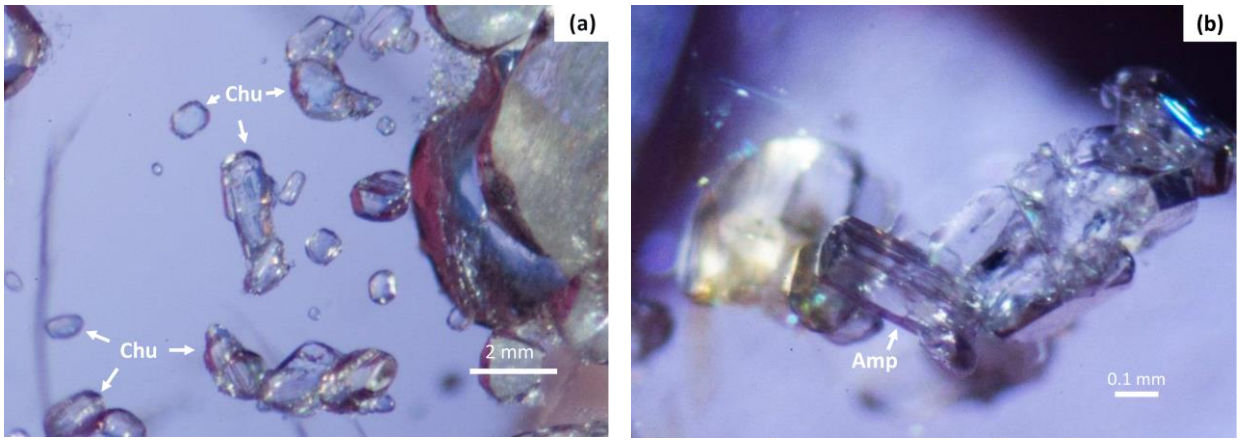

Figure 2.10 (a) common minerals (humite group), a cluster of subhedral clinohumite (Chu) crystals. (b) Ca- and Mg-bearing silicate inclusions -Euhedral colourless amphibole (presumably pargasite) form clusters in Kyauksin spinel.

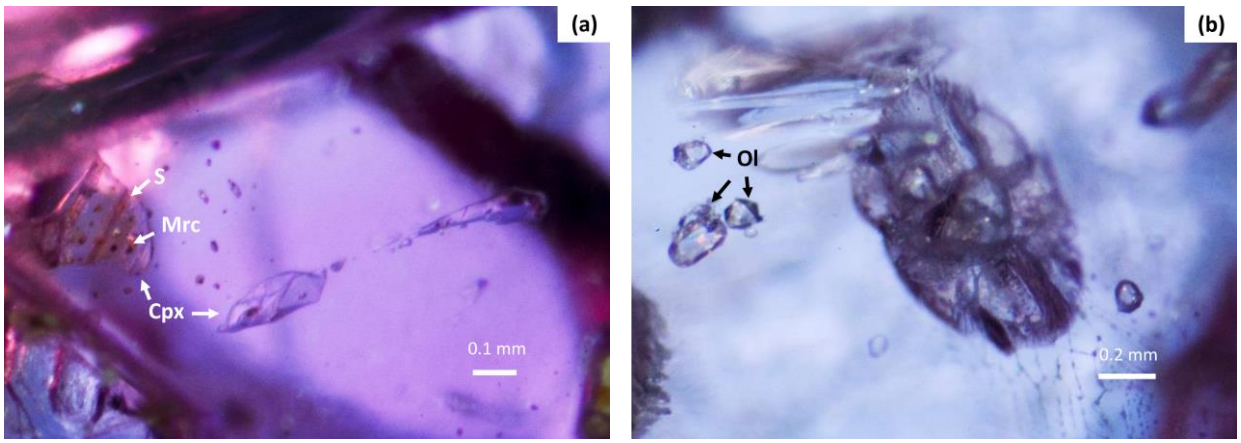

Figure 2.11 (a) Anhedral clinopyroxene (Cpx) showing a distinct set of cleavage planes is associated with tiny yellow sulphur (S) and black marcasite (Mrc) spots in a spinel from Mansin. (b) Anhedral olivine (Ol) crystals are seen here next to a larger clinohumite inclusion.

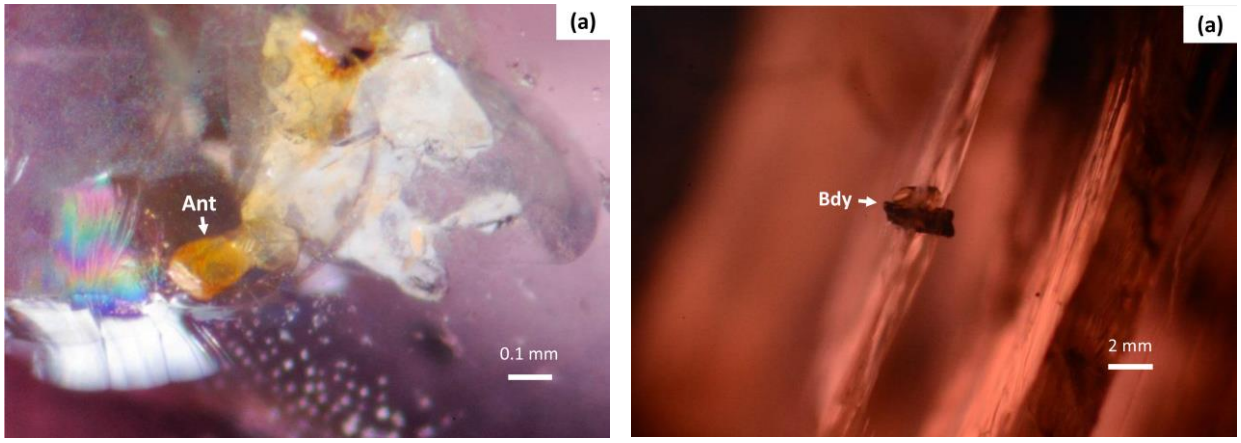

Figure 2.12 Oxide minerals identified in the spinels include (a) yellow anatase (Ant) that is surrounded here by negative crystals and tension cracks, (b) baddeleyite (Bdy) crystals that are also often associated with tension cracks.

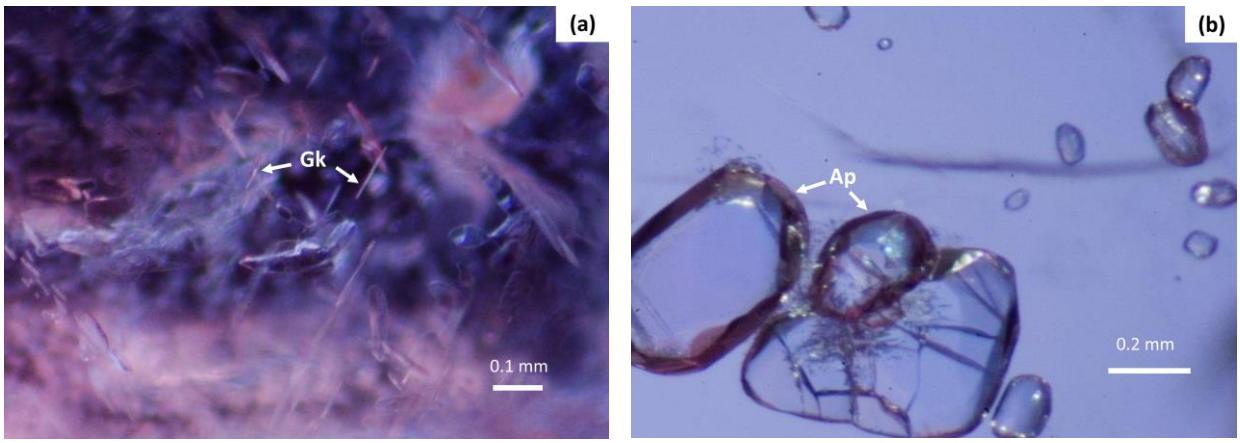

Figure 2.13 (a) Tiny flake-like colourless geikielite (Gk) crystals along {111} orientations in spinel from Yadanar Kaday Kadar (b) Rounded anhedral apatite (Ap) inclusions also present in this Mogok spinel.

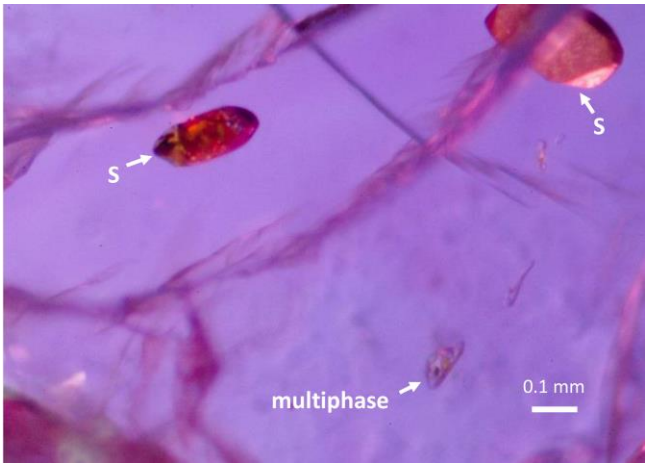

Figure 2.14 Single solid sulfur(S) inclusion and multiple phase (two phase) sulfur inclusions from Mansin spinel.

2.5.2 SEM Imaging and EDS Analysis

Using SEM-EDS, it was possible to visualise and identify for the first time the complex intergrowth of multiphase inclusions (some containing small fluid cavities) within spinel from Mogok. These assemblages consisted of various minerals such as calcite ($CaCO_3$), dolomite [$CaMg(CO_3)_2$], halite (NaCl), phlogopite [$KMg_3(AlSi_3O_{10})(F,OH)_2$], apatite and/or anhydrite of sugary texture (Figures 2.15a and b). They were similar to the inclusions containing residues of molten salts described by Giuliani *et al*. 2015 in rubies from Mogok.

SEM-EDS also revealed other inclusion features in the spinels. A euhedral amphibole inclusion contained clinopyroxene and phlogopite domains in a spinel from Kyauksin (northern Mogok; Figure 2.15c). We also imaged some phases that presumably exsolved from their hosts: calcite blebs in certain dolomite inclusions (Figure 2.15d) and the geikielite lamellae in spinel (Figure 2.16a) that were mentioned above. Furthermore, rare accessory inclusions of baddeleyite (also mentioned above) were easily visible in the SEM (Figure 2.16b).

Various secondary mineral inclusions were identified with SEM-EDS, such as chlorite and brucite, together with a phlogopite inclusion (Figure 2.16c), and a red powder-like substance that proved to be an iron compound, an iron oxide or iron hydroxide, probably goethite that formed an epigenetic encrustation along the cleavages and boundaries of a phlogopite inclusion (Figure 2.16d).

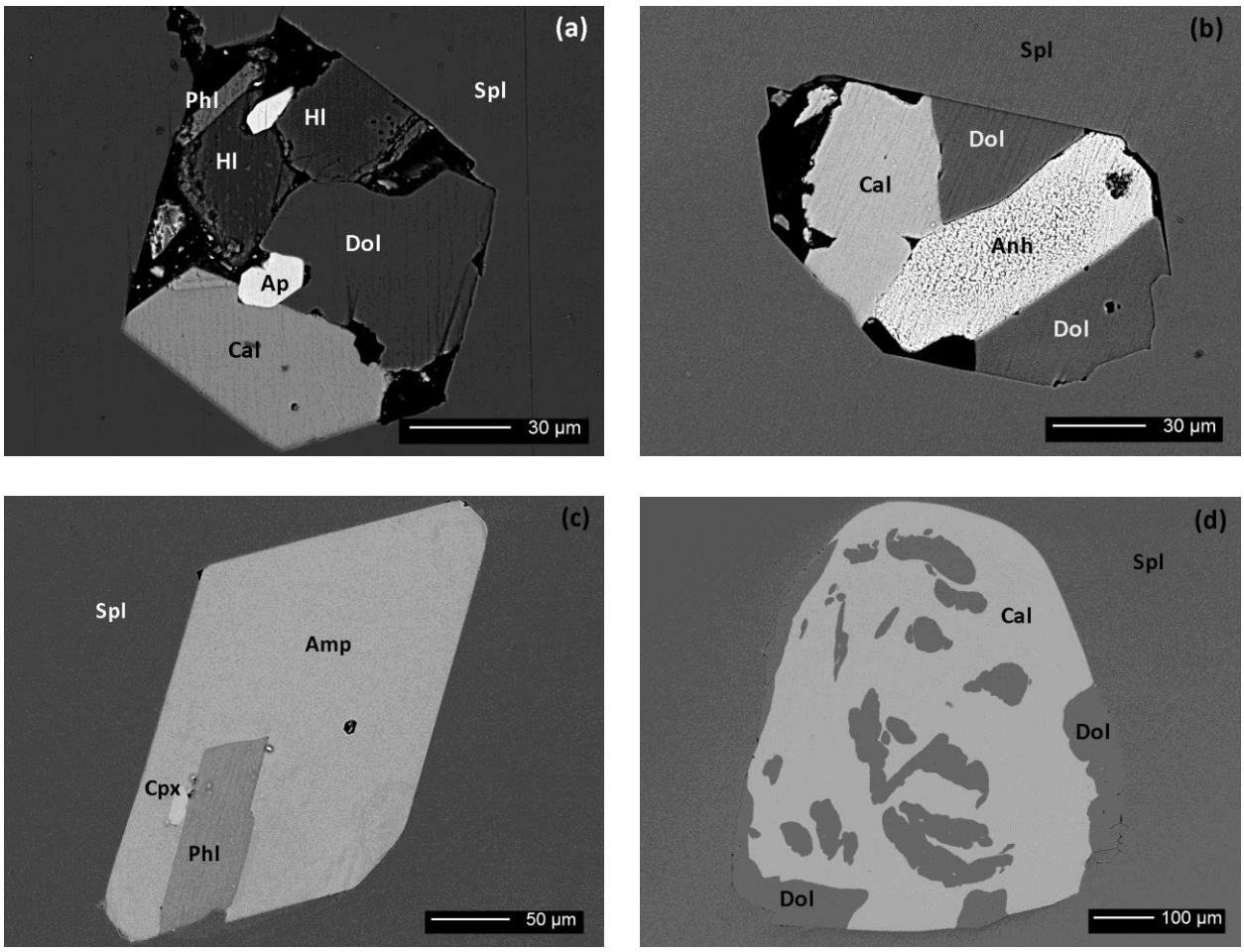

Figure 2.15 BSE images reveal the contents of multiphase inclusions: (a) calcite (Cal), dolomite (Dol), halite (Hl), phlogopite (Phl) and apatite (Ap), and (b) calcite (Cal), anhydrite (Anh) in a dolomite (Dol) multiphase inclusion (c) BSE imaging shows that a euhedral amphibole inclusion in a spinel from Kyauksin contains inclusions of phlogopite (Phl) and clinopyroxene (Cpx) (d) Evidence of exsolved mineral phases in Mogok spinels is seen in these BSE images of dolomite blebs in a calcite inclusion.

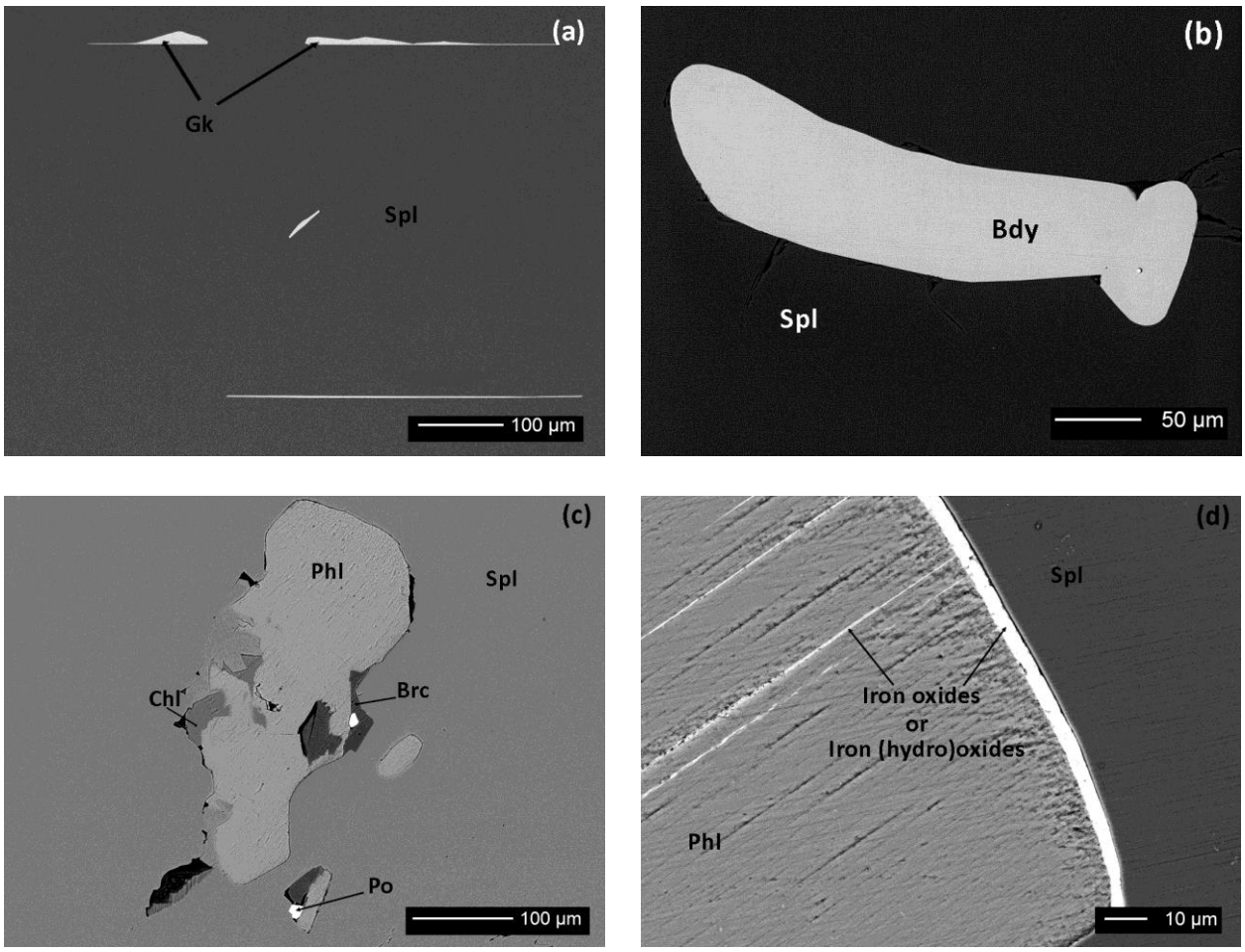

Figure 2.16 (a) oriented geikielite (Gk) lamellae (b) A baddeleyite (Bdy) inclusion with tension cracks shows high contrast against the host spinel in this BSE image (c) various secondary mineral assemblages associated with phlogopite (Phl) in Mogok spinel, tiny pyrrhotite (Po) grains are intergrown with the secondary minerals brucite (Brc) and chlorite (Chl) (d) Secondary iron oxides or iron hydroxides are seen as bright areas along the rim and within cleavages in this phlogopite.

2.6 Discussion

In the present study, we not only confirmed the presence of most inclusions previously described in the literature for Burmese spinel, but also identified for the first time 16 new solid inclusions in our samples from Mogok: amphibole (presumably pargasite), anatase, baddeleyite, boehmite, brucite, chlorite, clinohumite, clinopyroxene, diaspore, geikielite, goethite, halite, marcasite, molybdenite, periclase and pyrrhotite (see Table 2.2).

Interestingly, we did not observe in our study any 'belly button' apatite inclusions that are considered typical for spinel from Mogok (Gübelin & Koivula 1986, 2005). These inclusions are characterized by a tiny black graphite or ilmenite platelet attached to rounded apatite. As described by Malsy & Klemm (2010), we observed in our samples only subhedral to anhedral colourless apatite crystals as individual crystals or clusters.

We also documented for the first time in gem-quality spinel multiphase inclusions (Figures 2.15a and b) with small fluid cavities that may be interpreted as residues of molten salts (Giuliani *et al.* 2003, 2015, 2018 and Peretti *et al.* 2017, 2018). Their assemblages are reflective of paragenetic relationships within the host rock (e.g. calcite-dolomite-phlogopite-apatite). Some of the spinel inclusions also demonstrate mineral exsolution (e.g. oriented geikielite in Figures 2.13a and 2.16a) and retrograde transformations after spinel formation (e.g. the breakdown of phlogopite to chlorite, brucite and Fe-oxides/hydroxides; see Figure 16c &d; Yau *et al.* 1984).

We observed carbonate inclusions in our spinels from all mining locations sampled in the Mogok area. Some of these carbonate inclusions did not occur as a single mineral phase but were present within multiphase inclusions (Figures 2.15a and b) and possibly as exsolved assemblages (Figure 2.15d). In a few cases, such carbonates were also found in negative-crystal cavities. Moreover, the presence of various silicates such as amphibole (presumably pargasite), chondrodite, clinohumite, zircon etc. in spinel—similar to the carbonate inclusions—reflects the compositional range of the marbles and interlayered calc-silicate host rocks in which these spinels from the Mogok area were formed.

The complex metamorphic evolution of the Mogok Stone Tract during the Himalayan orogeny is connected to and influenced by several magmatic events (Barley *et al.* 2003; Searle *et al.* 2007). Geographically and geologically, all of the spinel localities that were sampled for this study (primary marbles and secondary deposits) were found in close proximity to granite intrusions (Thu 2007). Mineral inclusions such as anatase, olivine, clinopyroxene, periclase and chondrodite could

have formed either during granulite-facies regional metamorphism (Thu 2007; Thu & Zaw 2017; Phyo *et al.* 2017) or by contact metamorphism from the nearby intrusions. Remarkable is the prevalence of elemental sulphur and graphite in spinel from Mansin (Gübelin & Koivula 2005; Pardieu 2014; Vertriest & Raynaud 2017), which points to highly reducing conditions. Moreover, the multiphase inclusions with small fluid cavities that we observed in our Mogok spinels showed similarities to hypersaline fluid inclusions in Mansin spinel (Peretti *et al.* 2017, 2018) and to the residues of molten salts found in Mogok ruby (Giuliani *et al.* 2015).

We also sought to investigate if it is possible to separate spinels from different locations within the Mogok Stone Tract based on their inclusions (see Figure 2.17; also see sample locations in Figures 2.5 and 2.18). Although the number of samples (87, not including those obtained from local markets) and inclusions analysed (about 400) might not be sufficient, we can still draw some conclusions. Similar to Themelis (2008) and Malsy & Klemm (2010), and as expected for marble-related spinels, we observed an abundance of carbonate inclusions in spinels from all of the studied localities. Closely related are impurities in the marble host rock—graphite, apatite and phlogopite—which were present in spinels from nearly all of the localities, although in distinctly smaller quantities. Additional inclusion phases were observed in spinel from a few localities, such as native sulphur (most prominently from Mansin but also from Pyaungpyin and Kyauksaung), anatase (Yadanar Kaday Kadar, Kyauksin and Kyauksaung) and chondrodite (Bawlongyi, Kyauksaung and Mansin). In contrast, a number of inclusions were found only in samples from one locality, such as amphibole (presumably pargasite), goethite and pyrrhotite (Kyauksin); anhydrite (Pyaungpyin); and geikielite lamellae (Yadanar Kaday Kadar). Whether these findings are truly specific to these locations or just the result of the limited sampling is unknown. 'Nevertheless, the assemblages documented in spinel from Mogok and elsewhere are clearly different from the inclusions seen in synthetic flux-grown spinel (Krzemnicki 2008), and therefore are useful for separating natural spinels from their synthetic counterparts.'

Table 2.2. Alphabetical list and abundance of solid inclusions in Mogok spinels documented in the present study and compared with previously published work and other localities.

Mineral	Mogok area		Other localities				
	Present study[1]	Previous studies[2]	Vietnam	Tajikistan	Tanzania	Madagascar	Sri Lanka
Amphibole (presumably pargasite)	xxx	—	—	—	—	—	—
Anatase	x	—	—	—	—	—	—
Anhydrite	x	3	—	—	—	—	—
Apatite	xxx	1, 2, 3, 6, 7	1, 3	—	1	1	1, 6
Baddeleyite	x	—	—	—	—	—	—
Boehmite	x	—	—	—	—	—	1
Brucite	x	—	—	—	—	—	—
Calcite	xxxxx	3, 6, 7	3	—	—	—	1
Chlorite	x	—	—	—	—	—	—
Chondrodite	xxxxx	3	—	—	—	—	—
Clinohumite	x	—	—	—	—	—	—
Clinopyroxene	xxx	—	—	—	—	1	—
Diaspore	x	—	—	—	—	—	1
Dolomite	xxxxx	1, 3, 7	3	—	—	—	1
Geikielite	xxx	—	—	—	—	—	—
Goethite	x	—	1	—	—	—	—
Graphite	x	1, 3	3	—	—	—	1
Halite	x	—	—	—	—	—	—
Ilmenite	—	1	—	—	1	—	—
Magnesite	xxx	3	3	—	—	—	—
Marcasite	x	—	—	—	—	—	—
Molybdenite	x	—	—	—	—	—	—
Olivine/ forsterite	x	1	—	—	1	—	1
Periclase	x	—	—	—	—	—	—
Phlogopite	xxx	1	—	—	1	—	1
Potassium feldspar	—	3	3	—	—	—	1
Pyrite	—	1	—	—	—	—	1
Pyrrhotite	x	—	—	—	—	—	1
Quartz	—	1	—	—	—	—	1
Rutile	—	1	—	—	1	1	1
Sulfur (Elemental)	xxxxx	4, 5, 6	—	—	—	—	—
Titanite	—	1	3	—	—	—	1
Uraninite	—	1	—	—	1	—	1
Zircon	x	2	3	3	—	—	1

[1] Inclusion abundance documented in this study: xxxxx = frequently seen; xxx = sometimes encountered; x = rarely found.

[2] References: 1 = Gübelin & Koivula (1986, 2005); 2 = Themelis (2008); 3 = Malsy & Klemm (2010); 4 = Pardieu *et al.* (2016); 5 = Peretti et al. (2017); 6 = www.lotusgemology.com (accessed June 2018); 7 = Zhu & Yu (2018).

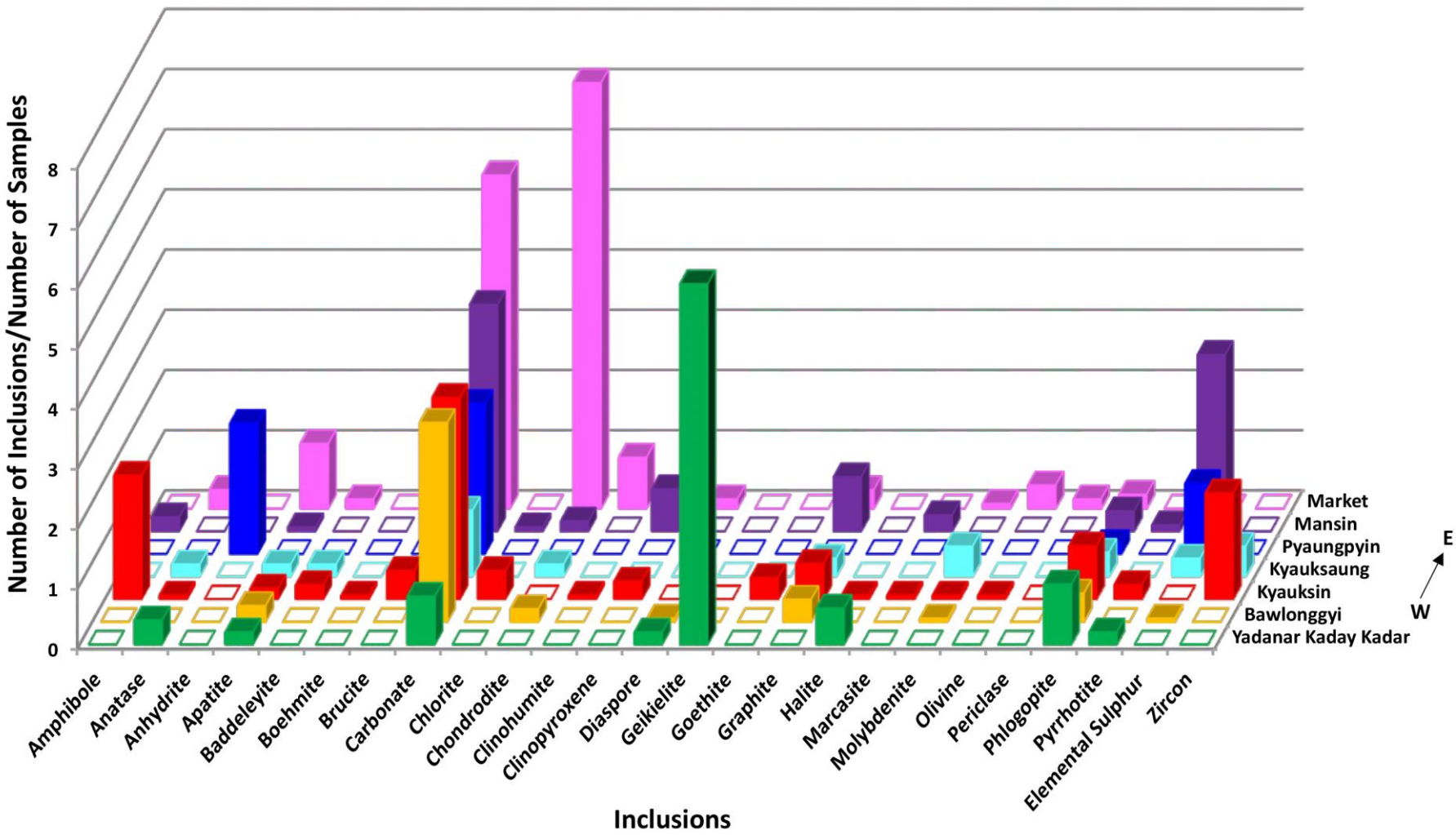

Figure 2.17 The distribution of different inclusions found in spinels from the various spinel mining sites (and local markets) in the Mogok region of Myanmar suggests that, with further research, it might be possible to distinguish spinels from certain localities.

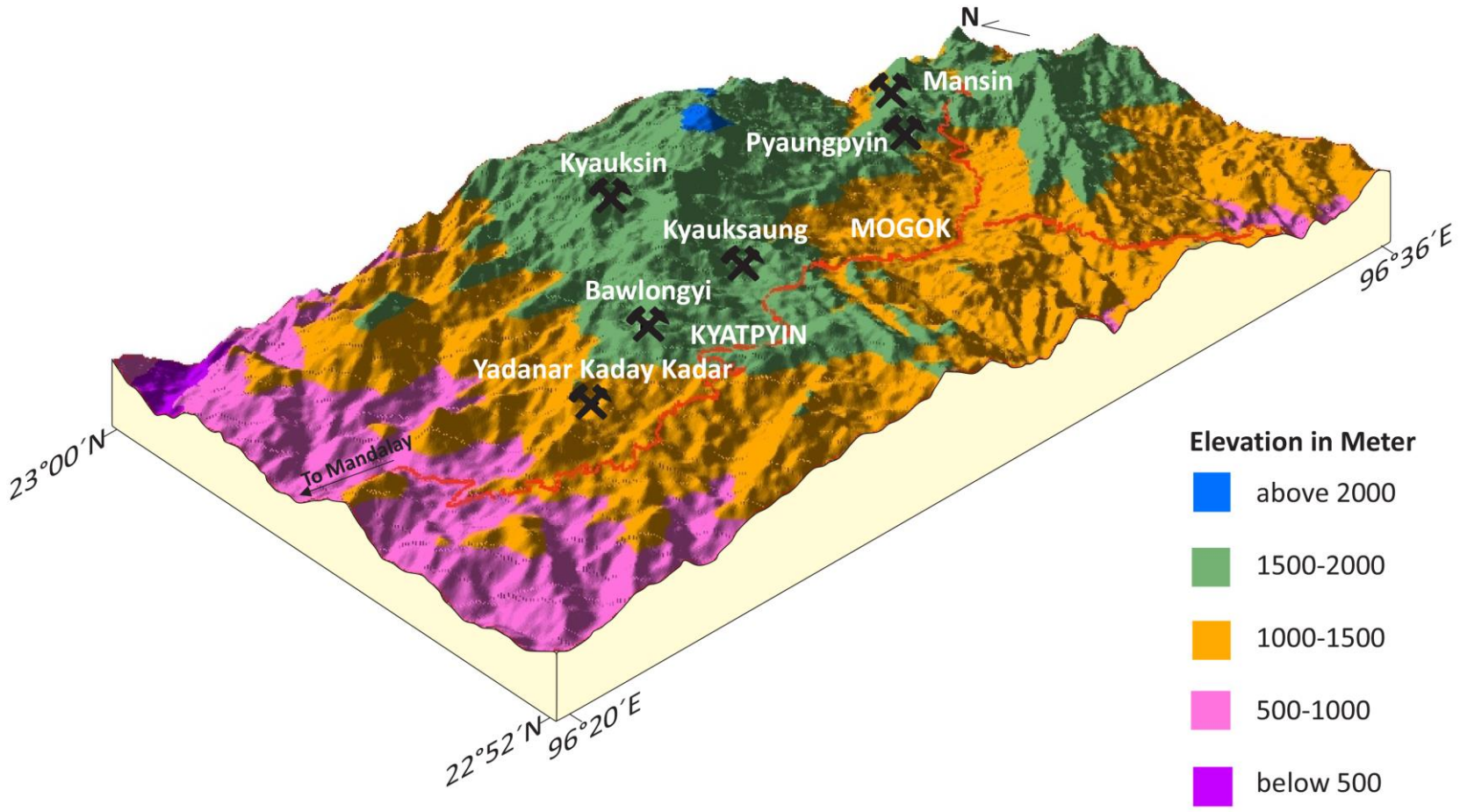

Figure 2.18 This three-dimensional map of the Mogok area shows that most of the mine sites sampled for this study are situated at elevations ranging from 1,500 to 2,000 m. Spatial data is based on topographic maps (map number: 93 B-5 & 93 B-9, scale 1'' = 1 mile.)

2.7 Conclusions

This study presents the first detailed description of inclusions in spinel from Mogok, Myanmar. It documents several solid inclusions for the first time in these spinels, as well as multiphase assemblages (some containing small fluid cavities) that add to their complexity. All of the mineral inclusions are related to the local geology and geochemistry of the host rocks in the Mogok area. Spinel and its associated minerals such as ruby, diopside, olivine, chondrodite and clinohumite testify to granulite-facies metamorphic conditions in the Mogok Metamorphic Belt (Thu *et al*. 2016, Phyo *et al.* 2017). Elemental sulphur and graphite inclusions furthermore indicate highly reducing conditions during the formation of these spinels. The generation of gem-quality spinel by skarn-forming processes can be excluded due to the absence of typical skarn mineral inclusions (e.g. vesuvianite, pectolite or nephrite) in our samples.

Based on the data presented in this article, we feel that such inclusion studies can help distinguish Mogok spinels from those of other sources worldwide and therefore contribute to the origin determination of spinels in gemmological laboratories. We expect that further studies of spinel inclusions in the future will add to this knowledge. U-Pb age dating of zircon inclusions in spinel was carried out in the research, see in Chapter 4.

2.8 Acknowledgements

We would like to thank many people for their valuable help, support and encouragement, and for providing samples. In particular, we thank Ma Mie Mie, Ko Chu (Kyauksaung mine), Dr Mori, Ko Kyaw Swar and Ko Nay for all their support and for providing gem-quality spinel samples and rock samples. Further thanks to Sebastian Hänsel, U Aung Kyaw Htoon and Ko Ja Mu for their help during the field trip. Special thanks to Ah Ba, Aunty Phyu and the local people and miners of the Mogok area, Myanmar, for their kind encouragement during the field trip. Many thanks to Judith Braun, Dr Tashia Dzikowsk, Dr Laurent E. Cartier (all of the Swiss Gemmological Institute SSEF, Basel) for their help, advice and fruitful discussions on this paper.

References

Balmer, W.A., Hauzenberger, C.A., Fritz, H. & Sutthirat, C. 2017. Marble-hosted ruby deposits of the Morogoro region, Tanzania. *Journal of African Earth Sciences*, **134**, 626–643.

Barley, M.E., Pickard, A.L., Zaw, K., Rak, P. & Doyle, M.G. 2003. Jurassic to Miocene magmatism and metamorphism in the Mogok Metamorphic Belt and the India-Eurasia collision in Myanmar. *Tectonics*, **22**(3), article no. 1019, 11 pp., http://doi.org/10.1029/2002tc001398.

Bender, F. 1983. *Geology of Burma*. Gebrüder Borntraeger, Berlin, Germany, 295 pp.

Cesbron, F., Lebrun, P. *et al.* (2002) Corindon et spinelles. *Minéraux & Fossiles*, Hors-Série No. 15, 105 pp.

Chhibber, H.L. 1934. *The Geology of Burma*. Macmillan and Co. Ltd, London, 538 pp.

Cooper, A. & Ziyin, S. 2014. Lab Notes: Spinel inclusion in spinel. *Gems & Gemology*, **50**(4), 293–301.

Ehrmann, M. 1957. Gem mining in Burma. *Gems & Gemology*, **9**(1), 2–30.

Fermor, L.L. 1931. General report for the Geological Survey of India, 1930. *Records of the Geological Survey India*, **65**, 445–456.

Gordon, R. 1888. On the ruby mines near Mogok, Burma. *Proceedings of the Royal Geographical Society and Monthly Record of Geography*, **10**(5), 261–275, http://doi.org/10.2307/1801309.

Gorghinian, A., Mottana, A., Rossi, A., Oltean, F.M., Esposito, A. & Marcelli, A. 2013. Investigating the colour of spinel: 1. Red gem-quality spinels (“balas”) from Ratnapura (Sri Lanka). *Rendiconti Lincei*, **24**, 127–140.

Giuliani, G., Dubessy, J., Banks, D., Hoàng Quang Vinh, Lhomme, T., Pironon, J., Garnier, V., Phan Trong Trinh, Pham Van Long, Ohnenstetter, D. & Schwarz, D. 2003. CO_2–H_2S–COS–S_8–AlO(OH)-bearing fluid inclusions in ruby from marble-hosted deposits in Luc Yen area, North Vietnam. *Chemical Geology*, **194**(1–3), 167–185, http://doi.org/10.1016/s0009-2541(02)00276-0.

Giuliani, G., Dubessy, J., Banks, D.A., Lhomme, T. & Ohnenstetter, D. 2015. Fluid inclusions in ruby from Asian marble deposits: Genetic implications. *European Journal of Mineralogy*, **27**(3), 393–404, http://doi.org/10.1127/ejm/2015/0027-2442.

Giuliani, G., Fallick, A.E., Boyce, A.J., Pardieu, V. & Pham, V.L. 2017. Pink and red spinels in marble: Trace elements, oxygen isotopes, and sources. *Canadian Mineralogist*, **55**(4), 743–761, https://doi.org/10.3749/canmin.1700009.

Giuliani, G., Dubessy, J., Ohnenstetter, D., Banks, D., Branquet, Y., Feneyrol, J., Fallick, A.E. & Martelat, J.-E. 2018. The role of evaporites in the formation of gems during metamorphism of carbonate platforms: A review. *Mineralium Deposita*, **53**(1), 1–20, http://doi.org/10.1007/s00126-017-0738-4.

Gübelin, E. 1965. The ruby mines in Mogok in Burma. *Journal of Gemmology*, **9**(12), 411–425, http://doi.org/10.15506/JoG.1965.9.12.411.

Gübelin, E.J. & Koivula, J.I. 1986. *Photoatlas of Inclusions in Gemstones*. ABC Edition, Zurich, Switzerland, 532 pp.

Gübelin, E.J. & Koivula, J.I. 2005. *Photoatlas of Inclusions in Gemstones, Vol. 2*. Opinio Publishers, Basel, Switzerland, 829 pp.

Halford-Watkins, J.F. 1932a. The ruby mines of upper Burma: A short history of their working. *The Gemmologist*, **1**(9), 263–272.

Halford-Watkins, J.F. 1932b. Methods of ruby mining in Burma. *The Gemmologist*, **1**(11), 335–342.

Halford-Watkins, J.F. 1932c. Methods of ruby mining in Burma: Washing, grading and selling the stones. *The Gemmologist*, **1**(12), 367–373.

Hughes, E.B. 2017a. Beyond octahedra: Inclusions in spinel. *Journal of the Gemmological Association of Hong Kong*, **38**, 41–44,

www.gahk.org/journal/GAHK_Journal_2017_v5.pdf.

Hughes, R.W. 1997. *Ruby & Sapphire*. RWH Publishing, Bangkok, Thailand, 511 pp.

Hughes, R.W. 2017b. *Ruby & Sapphire: A Gemologist's Guide*. RWH Publishing, Bangkok, Thailand, 816 pp.

Hughes, R.W. 2018. Hyperion: The Lotus Gemology inclusion search engine (natural spinel, Myanmar, enhancement). Lotus Gemology,

www.lotusgemology.com/index.php/library/inclusion-gallery.

Iyer, L.A.N. 1953. *The Geology and Gem-stones of the Mogok Stone Tract, Burma*. Office of the Geological Survey of India, Calcutta, India, 100 pp.

Keller, P.C. 1983. The rubies of Burma: A review of the Mogok Stone Tract. *Gems & Gemology*, **19**(4), 209–219, http://doi.org/10.5741/gems.19.4.209.

Krzemnicki, M.S. 2008. Trade Alert: Flux-grown synthetic red spinels on the market. *SSEF Newsletter*, No. 14, October, 1–3,

La Touche, T.H.D. 1913. *Geology of the Northern Shan States*. Office of the Geological Survey of India, Calcutta, India, 379 pp.

Malsy, A. & Klemm, L. 2010. Distinction of gem spinels from the Himalayan mountain belt. *CHIMIA International Journal for Chemistry*, **64**(10), 741–746, http://doi.org/10.2533/chimia.2010.741.

Mogessie, A., Purtscheller, F. & Tessadri, R. 1988. Chromite and chrome spinel occurrences from metacarbonates of the Oetztal–Stubai complex (northern Tyrol, Austria). *Mineralogical Magazine*, **52**(365), 229–236, http://doi.org/10.1180/minmag.1988.052.365.09.

Pardieu, V. 2014. Hunting for "Jedi" spinels in Mogok. *Gems & Gemology*, **50**(1), 46–57, http://doi.org/10.5741/gems.50.1.46.

Pardieu, V. & Hughes, R.W. 2008. Spinel: Resurrection of a classic. *InColor*, No. 2, 10–18.

Pardieu, V., Sangsawong, S., Vertriest, W. & Raynaud, V. 2016. Gem News International: "Star of David" spinel twin crystal with multiphase inclusions from Mogok. *Gems & Gemology*, **52**(1), 100–101.

Peretti, A., Kanpraphai-Peretti, A. & Günther, D. 2015. World of magnificent spinel: Provenance and identification. *Contributions to Gemmology*, **11**, 293 pp.

Peretti, A., Mullis, J., Franz, L. & Günther, D. 2017. Spinel formation by sulphur-rich saline brines from Mansin (Mogok area, Myanmar). *15th Swiss Geoscience Meeting*, Davos, Switzerland, 17–18 November, 149–150.

Peretti, A., Mullis, J., Franz, L. & Günther, D. 2018. Spinel formation by sulphur-rich saline brines from Mansin (Mogok area, Myanmar). GRS GemResearch Swisslab AG, http://gemresearch.ch/spinel-formation-mansin.

Phyo, M.M., Franz, L., de Capitani, C., Balmer W. & Krzemnicki, M. 2017. Petrology and PT-conditions of quartz- and nepheline-bearing gneisses from Mogok Stone Tract, Myanmar. *15th Swiss Geoscience Meeting*, Davos, Switzerland, 17–18 November, 88–89.

Searle, D.L. & Haq, B.T. 1964. The Mogok belt of Burma and its relationship to the Himalayan orogeny. *22nd International Geological Congress*, New Delhi, India, 14–22 December, 132–161.

Searle, M.P., Noble, S.R., Cottle, J.M., Waters, D.J., Mitchell, A.H.G., Hlaing, T. & Horstwood, M.S.A. 2007. Tectonic evolution of the Mogok metamorphic belt, Burma (Myanmar) constrained by U-Th-Pb dating of metamorphic and magmatic rocks. *Tectonics*, **26**(3), article no. TC3014, 24 pp, https://doi.org/10.1029/2006tc002083.

Smith, C.P. & Dunaigre, C. 2001. Gem News: Anhydrite inclusion in a ruby from Myanmar. *Gems & Gemology*, **37**(3), 236.

Thein, M. 2008. Modes of occurrence and origin of precious gemstone deposits of the Mogok Stone Tract. *Journal of the Myanmar Geosciences Society*, **1**(1), 75–84.

Themelis, T. 2008. *Gems & Mines of Mogok*. Self-published, 352 pp.

Thu, K. 2007. *The Igneous Rocks of the Mogok Stone Tract: Their Distributions, Petrography, Petrochemistry, Sequence, Geochronology and Economic Geology.* PhD thesis, Department of Geology, University of Yangon, Myanmar, http://m.palaminerals.com/mogok.

Thu, K. & Zaw, K. 2017. Gem deposits of Myanmar. *Geological Society, London, Memoirs*, **48**(1), 497–529, http://doi.org/10.1144/m48.23.

Thu, Y.K., Win, M.M., Enami, M. & Tsuboi, M. 2016. Ti-rich biotite in spinel and quartz-bearing paragneiss and related rocks from the Mogok metamorphic belt, central Myanmar. *Journal of Mineralogical and Petrological Sciences*, **111**(4), 270–282, http://doi.org/10.2465/jmps.151020.

Truong, A.R. 2017. A highly-important imperial Mughal spinel, India, dated 1024 AH/1615 AD and 1070 AH/1659 AD. www.alaintruong.com/archives/2017/03/23/35086977.html, accessed 24 December 2018.

Vertriest, W. & Reynaud, V. 2017. G&G Micro-World: Complex yellow fluid inclusions in red Burmese spinel. *Gems & Gemology*, **53**(4), 468.

Whitney, D.L. & Evans, B.W. 2010. Abbreviations for names of rock-forming minerals. *American Mineralogist*, **95**(1), 185–187, http://doi.org/10.2138/am.2010.3371.

Yau, Y.C., Anovitz, L.M., Essene, E.J. & Peacor, D.R. 1984. Phlogopite-chlorite reaction mechanisms and physical conditions during retrograde reactions in the Marble Formation, Franklin, New Jersey. *Contributions to Mineralogy and Petrology*, **88**(3), 299–306, http://doi.org/10.1007/bf00380175.

Yavorskyy, V.Y. & Hughes, R.W. 2010. *Terra Spinel: Terra Firma*. Ivy, New York, New York, USA, 203 pp.

Zaw, K. 1990. Geological, petrological and geochemical characteristics of granitoid rocks in Burma: With special reference to the associated W-Sn mineralization and their tectonic setting. *Journal of Southeast Asian Earth Sciences*, **4**(4), 293–335, http://doi.org/10.1016/0743-9547(90)90004-w.

Zaw, K. 2017. Overview of mineralization styles and tectonic–metallogenic setting in Myanmar. *Geological Society, London, Memoirs*, **48**(1), 531–556, https://doi.org/10.1144/m48.24.

Zaw, K., Acharyya, S.K. & Maung, H. 1989. Comments and reply on "Transcurrent movements in the Burma-Andaman Sea region". *Geology*, **17**(1), 93–98, http://doi.org/10.1130/0091-7613(1989)017<0093:carotm>2.3.co;2.

Zaw, K., Sutherland, L., Yui, T.-F., Meffre, S. & Thu, K. 2015. Vanadium-rich ruby and sapphire within Mogok gemfield, Myanmar: Implications for gem color and genesis. *Mineralium Deposita*, **50**(1), 25–39, http://doi.org/10.1007/s00126-014-0545-0.

Zhu, J. & Yu, X. 2018. Inclusions of spinel from Burma. *Journal of Gems and Gemmology*, **20**(Sup.), 18–23.

CHAPTER III

Petrology, geothermobarometry and geochemistry of granulite facies gneisses in the vicinity of gemstone deposits from Mogok area (Myanmar)

Myint Myat Phyo[1], Leander Franz[1], Rolf L. Romer[2], Christian de Capatini[1],
Walter A. Balmer[3] and Michael S. Krzemnicki [3]

[1]Institute of Mineralogy and Petrography, Department of Geosciences, University of Basel,
[2]GFZ German Research Centre for Geosciences, Helmholtz Center Potsdam,
[3]Swiss Gemmological Institute SSEF, Basel.

3.1 Abstract

The Mogok Metamorphic Belt (MMB) of Myanmar, which formed in Paleogene due to the collision of the West Burma Block and the Shan Tai Block, is mainly composed of high-grade metamorphic rocks such as marbles, calc-silicate rocks, gneisses, quartzites, peridotites and igneous rocks such as granites, syenites and gabbros. The Mogok area in the central part of this belt is well-known for its magnificent quality rubies and other precious gemstones such as spinel, sapphire, peridot, etc and rare gemstones such as hibonite, jeremejevite, johachidolite, etc. In the framework of a study on the genesis of spinel and ruby from the Mogok area, an investigation of the host rocks was performed to unravel the metamorphic conditions, which were also responsible for the generation of these gemstones. For this reason, three high-grade quartz-garnet gneisses from the adjacent neighbourhood of the examined gemstone mines were investigated by electron microprobe. Conventional geothermobarometry reveals granulite facies PT-conditions of 756-792°C at 7.4-7.6 kbar, which is reproduced with the Theriak-Domino program within the error of both methods at water activities of 0.34-0.4. Within the marbles and calcsilicate rocks hosting the ruby and spinel deposits, garnet-nepheline and clinopyroxene-clinoamphibole gneisses were discovered. Petrographic investigations and field relations indicate that these rocks intruded the carbonatic host rocks as dykes prior or during the Paleogene metamorphism. Equilibrium phase diagram calculations and conventional geothermobarometry prove that these melanocratic gneisses also

formed under high-grade metamorphic conditions of 700-800°C. Geochemical investigation identifies the garnet-nepheline gneisses as high-K calcalkaline and shoshonitic foidite, phonotephrite and thephriphonolite while the clinopyroxene-clinoamphibole gneiss is a picrobasalt. Discrimination diagrams, trace element patterns and isotopic data point to a generation of these rocks during subduction-related magmatic processes. Especially the magmatic protoliths of the garnet-nepheline gneisses are assumed to be genetically linked to foid-bearing syenites, which intruded the Mogok Metamorphic Belt 35-23 Ma ago.

Keywords: Mogok Metamorphic Belt (MMB), granulite facies metamorphism, quartz-garnet gneisses, garnet-nepheline gneisses, clinopyroxene-clinoamphibole gneiss, geochemistry, high-K calcalkaline and shoshonitic magmatites, subduction-related magmatism.

3.2 Introduction

The Mogok area, also known as Mogok Stone Tract (Iyer 1953) is situated in upper Myanmar and lies within the Mogok metamorphic belt (MMB; cf. Chhibber 1934; Fermor 1930; La Touche 1913). This area is since the 15th century a major source of finest quality rubies, spinels and numerous other gemstones (Iyer, 1953). The MMB is mainly composed of medium to high-grade metamorphic rocks such as marbles, calc-silicate rocks, gneisses, peridotites, and igneous rocks such as granites, syenites and gabbros. The formation of the Mogok area is commonly related to the collision of the Indian plate with the Eurasia about 45 Ma ago (Dewey et al. 1988, 1989).

The Mogok area has been studied by numerous geoscientists who mainly focused on gemmology, mineralogy, geology, geochemistry, geochronology and geothermobarometry along the MMB. Their research include gemmological and mineralogical studies (Brown & Judd 1896; Giuliani et al. 2005, 2015, 2017, Gübelin & Koivula 1986, 2005, Themelis 2008, Hughes 2014, 2016) as well as geochronological investigations (Bertrand et al. 1999, 2001; Garnier et al. 2005, 2006, 2008; Mitchell 1993; Sutherland et al. 2019; Zaw et al. 2010). Furthermore, numerous investigations on the formation of gemstones and the rocks hosting the gem deposits in the Mogok and nearby area were carried out in the past decades (Chhibber 1934; Fermor 1930; Htay et al. 2017; Iyer 1953; Searle et al. 2007; Thu 2007; Thu et al. 2017; Win et al. 2016; Yonemura et al. 2013).

The present study concentrates on the petrology, geochemistry and the PT-conditions of the formation of gneisses, which were collected in the vicinity of gem deposits of the central and western part of the Mogok area. The high-grade metamorphic rocks analysed in this study originate

from the locations of Aunglan Taung, Bawpadan, Yadanar Kadae Kadar and Kinn. It is the aim of this petrologic and geothermobarometric study to provide detailed information about the physiochemical conditions during the formation of the gemstones and their host-rocks in the Mogok area.

3.3 General Geology

The Mogok area is located within the central part of the Mogok Metamorphic Belt (MMB) that extends over 1500 km from N to S and over 40 km from E to W. It formed due to the Paleogene collision of the West Burma block with the Sibumasu terrane (also referred to as Shan-Thai block) and ranges from the Himalayan Syntaxis to the Andaman Sea (Searle & Haq 1964; Searle et al. 2007; 2017, cf. Fig. 3.1). It is part of one of the main tectonic domains of Myanmar, the so called Mogok-Mandalay-Mergui Belt (MMMB; see Fig. 3.2), which is composed of Palaeozoic and Mesozoic sediments and magmatic intrusive rocks (Bender 1983; Zaw 1989, 1990; Zaw 2017; Zaw et al. 2015). The Mogok area is mainly composed of gneiss, marble, calc-silicate rocks, peridotites and quartzites, intruded by various acid to basic igneous rocks (Iyer 1953). The Mogok gneisses cropping out in the southern part of the Mogok area (La Touche 1913) are regarded to constitute the oldest rock unit in Myanmar (Chhibber 1934). Biotite granite intrusions also known as Kabaing granites are widely distributed in the western part of Mogok area (Kinn, Kabaing area) and also extend to the Thabeikkyin area in the West (Themelis 2008; K. Thu 2007; Waltham 1999; K. Zaw 1990; Khin Zaw 1998).

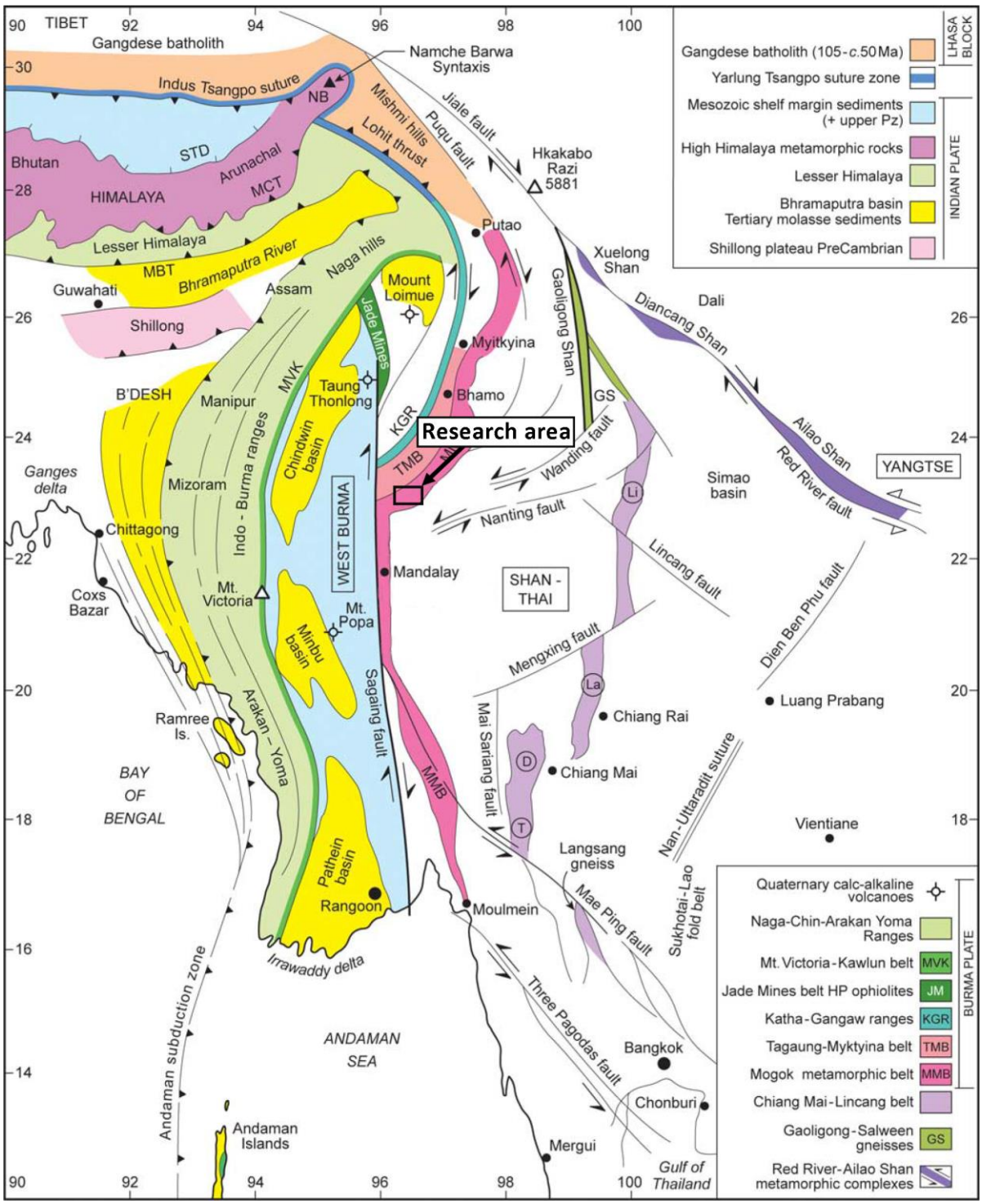

Figure 3.1 Geological map of SE Asia, Myanmar, and the Andaman Sea region showing the major structural features and terrane boundaries (modified after Searle et al. 2007).

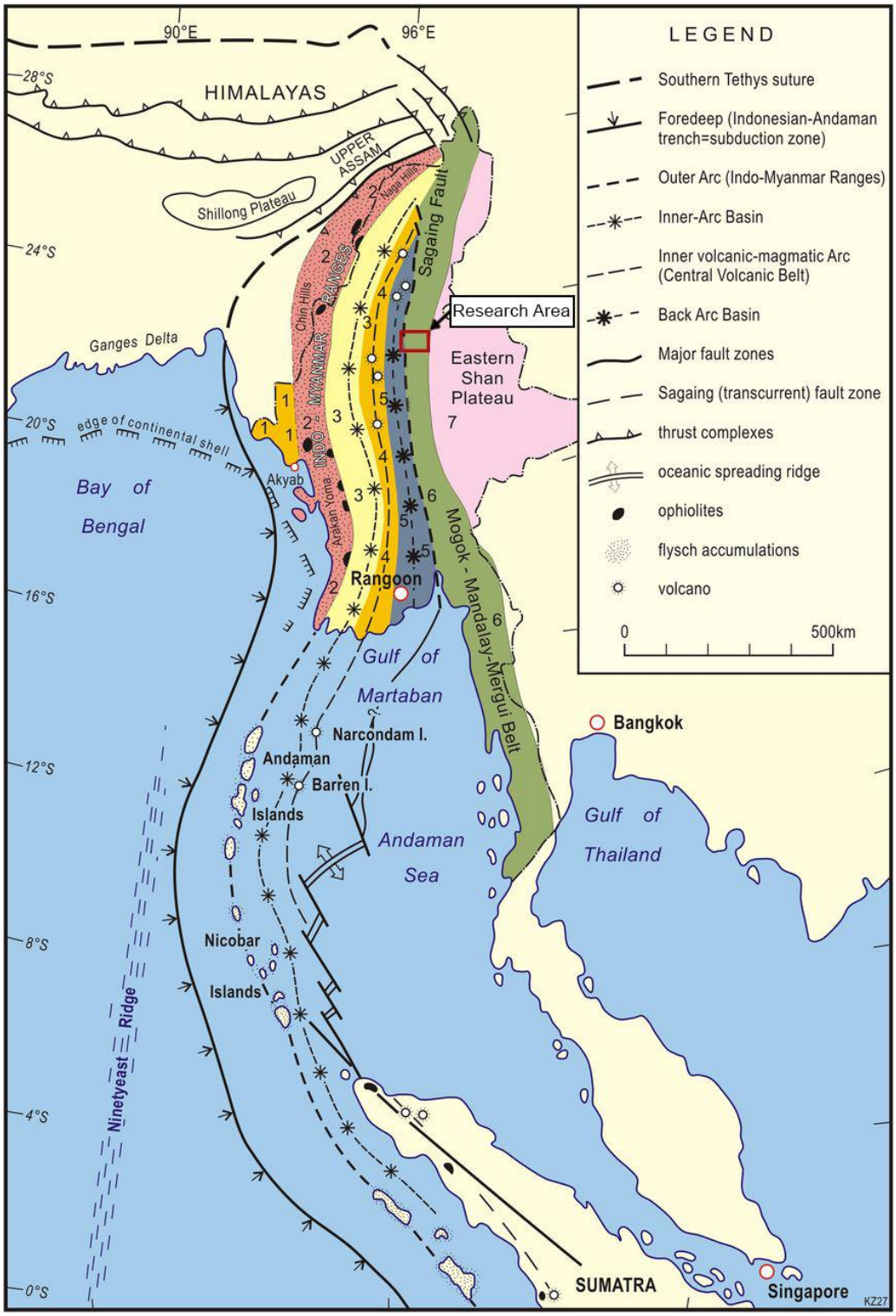

Figure 3.2 Research area plotted on the regional tectonic map of Myanmar showing the main tectonic domains (numbered 1-7 from west to east) and fault structures of Myanmar (modified after Bender 1983; Khin Zaw 1989, 1990; Khin Zaw *et al*. 2015). 1) Arakan (Rakhine) Coastal Strip; 2) Indo-Myanmar Ranges; 3) Western Inner-Burman Tertiary Basin; 4) Central Volcanic Belt (Central Volcanic Line); 5) Eastern Inner-Burman Tertiary Basin; 6) Mogok-Mandalay-Mergui Belt (MMMB); 7) Eastern Shan Highlands.

Thu et al. (2017) showed that the metamorphic conditions of MMB vary from the lower amphibolite to granulite facies with the metamorphic grade increasing from East to West based on thermobarometry of garnet-biotite paragneisses from the Ozone and the Thabeikkyin area west of Mogok. They estimated maximum PT- conditions of 780-860°C at 6.0-8.4 kbar, which is close to investigations of Yonemura et al. (2013), who determined 800-950°C at 6.5-7.8 kbar on a garnet-orthopyroxene granulite from the Mogok area. Win et al. (2016) yielded similar PT-conditions of 780-850°C at 6.0-10.0 kbar on a granulite facies paragneiss from the Sagaing area. Searle et al. (2007) depicted upper amphibolite facies PT-conditions of 680°C at 4.5±1.7 kbar for a granitic gneiss from Kyanigan quarry. Htay et al. (2017) reported PT-conditions of >840°C at >3.5 kbar for a sillimanite-garnet gneiss and 770-840°C at 2.2-3.5 kbar for a migmatite from the Momeik area. Furthermore, they also described that area is implied by polymetamorphism in these high-temperature and low- to medium-pressure granulites.

3.4 Analytical Methods

Polished thin sections of all samples were used for petrographic and electron microprobe investigations. Mineral identification was performed by polarization microscopy (Leica DMRD with a DFC450 digital camera) and by a confocal Bruker Senterra Raman micro-spectroscope. Raman analyse were carried out using a solid-state Nd-YAG laser at 532 nm and a direct diode laser at 785 nm. For spectral matching purposes the RRUFF database was applied as a reference (Downs 2006). Electron electron microprobe analyses were carried out using a JEOL JXA-8600 instrument equipped with an UltraDry silicon energy-dispersive X-ray detector (EDS) with Noran System 7 spectral imaging system by Thermo Scientific and wavelength dispersive X-ray spectroscopy (WDS). An acceleration voltage of 15kV and a beam current of 10nA were used. Measuring times were 30-60 s depending on the elements. EDS analyses with enlarged electron microbeam were applied to map the composition of feldspar with exsolution lamellae and of nepheline crystals. For WDS measurements, integrated natural and synthetic standards of the electron microprobe were used. Data correction was performed using the Proza ($\phi\rho Z$) method.

Whole rock major element oxides (SiO_2, Al_2O_3, Fe_2O_3, MnO, CaO, K_2O, TiO_2, Na_2O, P_2O_5) and some trace elements (V, Cr, Ni, Zn, Ga, Y, Zr, Nb, and Ba) were analysed on fused glass disks making use of a PANalytical® AXIOS Advanced X-ray fluorescence (XRF) spectrometer. This spectrometer is equipped with a rhodium anode end-window X-ray tube operating at 2.7 kW. Whole rock samples

were crushed and ground to powder in an agate disc mill, and afterwards sieved to < 63 µm grain size. The powdered samples were dried overnight in an oven at 105 °C. After that 1.0 g of the powdered sample were mixed with 6.0 g of lithium tetraborate as fluxing agent and 0.5 – 0.7 g ammonium nitrate as oxidizer in platinum vessels. Then, heated in several steps of 400 °C – 1150 °C to produce fused lithium tetraborate discs (for further more analytical details cf. Romer & Hahne 2010 and references therein).

For rare earth element analysis, samples were digested and performed by the Na_2O_2 sinter digestion method Zuleger and Erzinger (1988). 1.0 g of rock powder (<63 µm) was mixed with 3.0 g Na_2O_2 in a platinum crucible, covered with 1.0 g Na_2O_2 and then placed in a muffle furnace at 480 °C for one hour. The sinter cake was filled into tubes and centrifuged twice with distilled water to clear the cake of sodium hydroxide and soluble silica salts. Afterwards, the remaining sinter cake was dissolved in ~100 ml 1mol/l HCl. Rare earth element separation and concentration was performed by ion exchange columns with a diameter of 20 mm, using 31.5 cm^3 Dowex® 50-WX-8 (200–400 mesh) resin. After washing and conditioning, major and trace elements were washed out using 500 ml 1.7 mol/l HCl. Then, rare earth elements and Y were eluted quantitatively with 500 ml 4 mol/l HCl. After filtering and drying, the residue was dissolved in 10 ml 10% HCl. Analytics were executed with an Agilent Technologies® 5110 ICP-OES.

To perform the determination of trace elements, 125 mg of rock powder (<63 µm) were digested with 2 ml concentrated HF and 2 ml aqua regia in closed Savillex vials on a heating plate at 160 °C for several hours. Further digestion steps involved addition of 1 ml concentrated $HClO_4$ followed by another evaporation step, addition of 2 ml H_2O and 1 ml concentrated HNO_3. After further drying, an addition of 1 ml concentrated HNO_3 and 5 ml H_2O was done. Beakers were then put on the heating plate for another 10 hours at 100 °C. Finally, the solution was diluted 1:2000 with 2% HNO_3 for trace element determination using a Thermo Fisher® Element 2XR.

3.5 Petrography and mineral chemistry

Petrologic and thermobarometric investigations were performed on a garnet-orthopyroxene gneiss (ALT-03), a sillimanite-garnet gneiss (BPD-02), a garnet-biotite gneiss (K-01), two garnet-clinopyroxene-nepheline gneisses (YKK-1a; YKK-1c; M-25) and one clinopyroxene-amphibole gneiss (YKK-2a) from the central and the Western part of the Mogok area (Figure 3.3). Selected electron

microprobe mineral analyses of the minerals are listed in Tables 3.1-3.8. Mineral assemblages of rock samples are shown in Table 3.9.

Sample ALT-03 is a fine-grained biotite-garnet-orthopyroxene gneiss, which shows cm-sized, alternating leucocratic layers rich in quartz and feldspar and layers enriched in biotite, orthopyroxene and garnet (Figure 3.4a). Both layers display a granoblastic texture with a slight foliation by aligned biotite flakes. Main minerals are quartz, perthitic K-feldspar, plagioclase, biotite, orthopyroxene, garnet and accessory ilmenite, zircon and apatite. Garnet has a pinkish colour and often shows elongate and irregular shapes with inclusions of quartz, orthopyroxene and plagioclase (Figures 3.5a & b). Electron microprobe analyses reveal a slight increase of almandine at the expense of grossular from core ($Alm_{71.6}Prp_{11.2}Sps_{5.3}UGA_{12.0}$) to rim ($Alm_{74.1}Prp_{11.4}Sps_{5.5}$ $UGA_{9.1}$). Orthopyroxene forms granoblastic and irregular grains with a faintly brownish colour and have a rather constant composition of $En_{33.5\text{-}34.6}Fs_{64.4\text{-}65.2}Wo_{1.0\text{-}1.3}$. Reddish brown biotite has elevated TiO_2 contents of 5.8-6.3 wt.-% and an X_{Mg} of 0.396-0.412. Plagioclase is unzoned with an average composition of $Ab_{72.2}An_{25.6}Or_{2.2}$ whereas perthitic K-feldspar shows a somewhat variable composition of $Or_{66\text{-}71.7}Ab_{027.3\text{-}34}An_{0\text{-}2.6}$.

Sample BPD-02 is a small- to medium-grained sillimanite-bearing biotite garnet gneiss, showing several cm-wide, more and less leucocratic layers with homogeneously interspersed red garnet porphyroblasts (Figure 3.4b). Under the microscope, a weak main foliation is visible formed by elongate quartz and feldspar grains and by biotite flakes aligned parallel to the layering. Main minerals are quartz, perthitic K-feldspar, plagioclase, garnet and subordinate biotite. Sillimanite almost only occurs as inclusions in garnet (Figures 3.5c & d) and rarely in the matrix while ilmenite, apatite and zircon are accessory. Remarkable are numerous myrmekites at plagioclase-K-feldspar grain boundaries. Pale red garnet porphyroblasts show a flat zonation profile with slight, irregular variations of the composition ($Alm_{55.1\text{-}65.0}Prp_{38.1\text{-}38.9}Sps_{2.1\text{-}2.8}UGA_{3.1\text{-}3.8}$). Orangey red biotite flakes reveal high TiO_2-contents of 7.3-8.3 wt.-% and X_{Mg}-values of 0.58-0.62. Plagioclase is virtually unzoned with an average composition of $Ab_{76.6}An_{21.9}Or_{1.5}$ while perthitic K-feldspar has an average composition of $Or_{66.9}Ab_{30.52}An_{2.4}Cs_{0.2}$.

Sample K-01 is a porphyroblastic biotite-garnet gneiss from the westernmost part of the Mogok Metamorphic belt and shows cm-sized, irregular microfolds (Figure 3.4c). Under the microscope, a small grained matrix made up of aligned biotite flakes and elongate quartz and feldspar grains with porphyroblastic garnet crystals is visible. Main minerals are quartz, K-feldspar, plagioclase, biotite, garnet and accessory apatite, zircon and pyrite. Poikiloblastic, pale red garnet

has diameters up to 7 mm and often yields numerous rounded quartz inclusions (Figures 3.5e & f). Electron microprobe analyses reveal an absence of zonation with rather constant compositions of $Alm_{59.1-61.9}Prp_{29.5-32.4}Sps_{1.8-2.9}UGA_{6.1-7.2}$ in all investigated garnet grains. Biotite shows TiO_2-contents of 4.4-4.8 wt.-% and X_{Mg}-values of 0.59-0.60. Plagioclase shows slight irregular variations in composition from grain to grain ($Ab_{55.9-58.3}An_{39.9-41.9}Or_{1.3-2.3}$) which is also the case for K-feldspar ($Or_{87.4-87.9}Ab_{11.2-13.3}An_{07-1.4}Cs_{0-1.6}$).

Sample M-25, which originates from the vicinity of sample K-01, is part of a mafic layer within a calcsilicate marble. The medium grained rock shows a somewhat inhomogeneous texture with mafic and felsic mineral accumulations (Figure 3.4d). Under the microscope, the carbonate-garnet-K-feldspar-clinopyroxene-nepheline gneiss reveals a granoblastic texture with randomly oriented minerals. In the mafic sections, aggregates of green clinopyroxene and poikiloblastic garnet are found while felsic sections show granular K-feldspar and nepheline (Figures 3.6a & b). Subordinately, accumulations of carbonate occur and further accessories are apatite, titanite and magnetite. Electron microprobe analyses of yellowish brown garnet reveal elevated Ca- and Fe-contents with a composition of $Alm_{7.6-10.6}Prp_{0.9-1.2}Sps_{0.9-1.8}Uv_{0-0.3}Grs_{51.9-58.9}Adr_{28.0-37.0}$. Conspicuous are elevated TiO_2 contents of 1.4-1.8 wt.-%. These compositional variations occur from grain to grain whereas zoning is not present. Clinopyroxene is identified by electron microprobe analyses as aegirine-rich augite following the classification after (Morimoto et al. 1988) with a composition of $Q(=En+Fs+Wol)_{81.5-86.7}Aeg_{12.7-16.6}Jd_{0.5-2.3}$, which somewhat varies from grain to grain. Nepheline was calculated on a base of 32 oxygens (cf. Deer et al. 1992), which revealed a typical Si-oversaturation with Si contents of 8.283-8.508 p.f.u. An elevated K-content is indicated by X_K-values (=K/(K+Na+Ca)) of 0.168-0.183. K-feldspar shows a variable composition from grain to grain with ($Or_{73.3-75.4}Ab_{22.4-24.6}An_{1.3-1.8}Cs_{0.5-1.1}$). Carbonate is almost pure calcite with a $CaCO_3$-content of >99 mole-%.

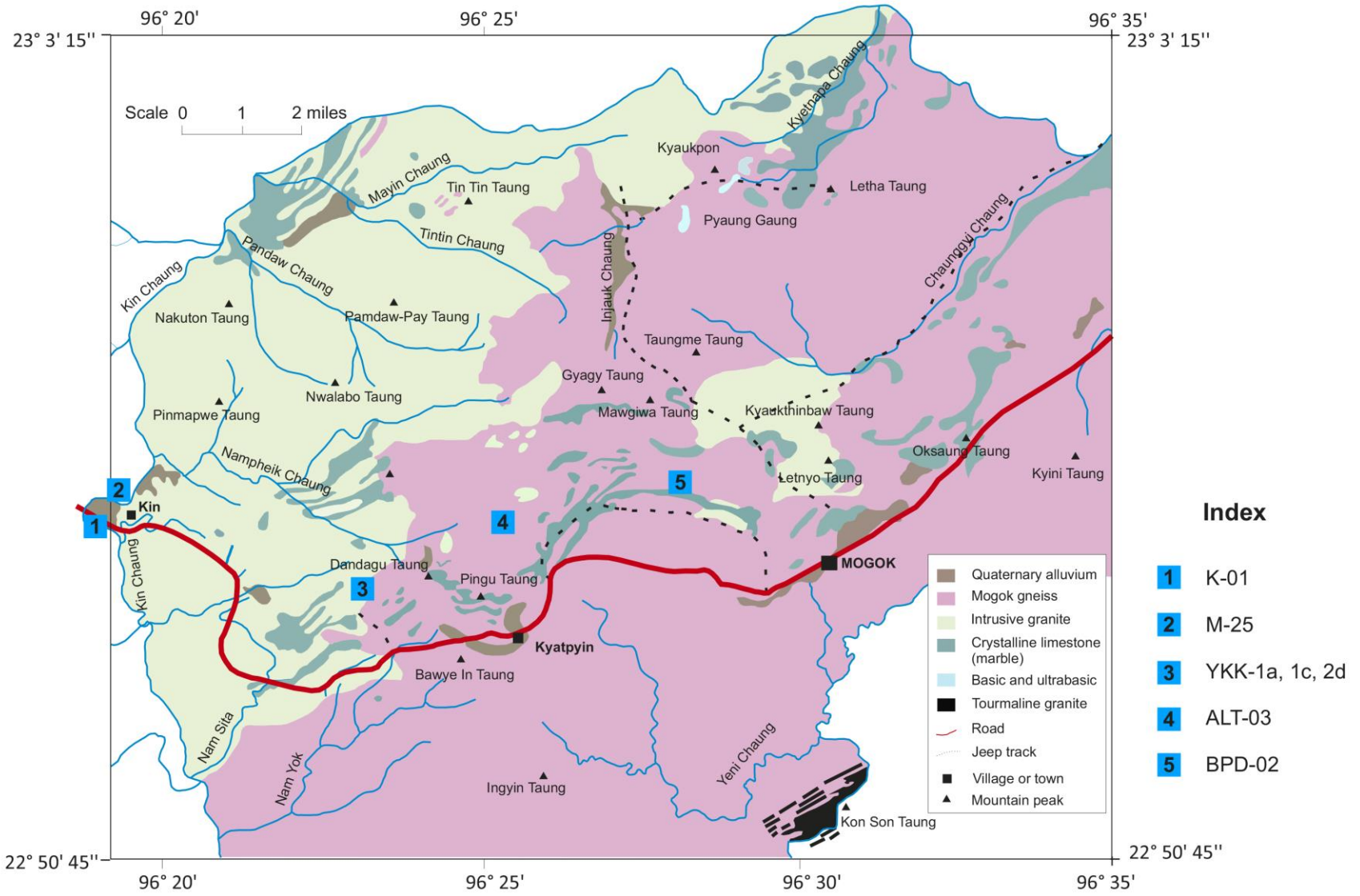

Figure 3.3 Sample locations of the investigated gneisses plotted on the geological map of the Mogok area (modified after Iyer, 1953).

Table 3.1 Selected microprobe analyses of garnet. Ferric iron estimate according to them method of Franz & Harlov (1998).

Garnet	ALT-03	ALT-03	ALT-03	BPD-02	BPD-02	BPD-02	K-1	K-1	K-1	M-25	M-25	M-25	YKK-1a	YKK-1a	YKK-1a	YKK-1c	YKK-1c	YKK-1c
	F8 8	F8 11	F8 13	F2 8	F2 11	F2 14	F1 1	F1 6	F1 9	F1 17	F4 2-1	F4 3-1	F2 9	F1 1	F5 25	F2 Grt	F2 5	F2 7
	core	intermediate	rim	core	intermediate	rim	rim	intermediate	core	core	core	core	core	core	rim	core	intermediate	rim
SiO_2	37.37	37.36	37.25	39.14	39.41	39.41	39.14	39.05	39.01	38.48	37.89	37.69	37.15	37.33	35.83	37.79	38.54	38.63
TiO_2	0.00	0.00	0.00	0.00	0.00	0.00	0.00	0.00	0.00	1.70	1.38	1.64	2.32	2.30	3.10	1.31	1.33	1.30
Al_2O_3	20.29	20.30	20.44	21.49	21.46	21.69	21.30	21.39	21.28	15.32	15.07	14.62	11.04	10.67	8.21	15.78	16.06	16.14
Cr_2O_3	0.00	0.00	0.00	0.01	0.00	0.04	0.03	0.03	0.15	0.04	0.09	0.00	0.04	0.00	0.06	0.00	0.00	0.00
Fe_2O_3	1.27	1.16	0.99	0.96	0.90	0.56	0.60	0.58	0.43	8.53	9.73	10.43	13.68	14.62	18.22	8.58	7.46	7.38
MgO	2.81	2.72	2.83	10.04	10.10	10.09	7.95	8.08	7.58	0.30	0.31	0.27	0.11	0.09	0.09	0.18	0.09	0.10
CaO	4.16	3.69	3.16	1.34	1.20	1.39	2.58	2.47	2.31	31.63	31.96	32.21	30.42	31.66	31.25	29.69	30.08	30.57
MnO	2.32	2.42	2.43	1.20	1.11	1.10	0.84	0.96	0.96	0.52	0.56	0.58	1.03	0.87	0.83	1.00	1.28	1.20
FeO	31.91	32.45	32.99	25.91	25.91	25.78	27.55	27.50	28.33	4.31	3.79	3.47	4.17	3.04	2.93	6.31	5.76	5.27
Na_2O	0.00	0.00	0.00	0.00	0.00	0.00	0.00	0.00	0.00	0.06	0.11	0.10	0.05	0.14	0.08	0.12	0.15	0.14
Total:	**100.13**	**100.11**	**100.09**	**100.10**	**100.09**	**100.06**	**99.99**	**100.06**	**100.05**	**100.88**	**100.90**	**101.01**	**100.00**	**100.73**	**100.61**	**100.75**	**100.75**	**100.73**
Structural formula (O=12)																		
Si	3.003	3.006	3.000	3.002	3.018	3.015	3.030	3.021	3.028	2.985	2.951	2.939	2.973	2.967	2.898	2.955	2.997	3.000
Fe^{3+}	0.000	0.000	0.000	0.000	0.000	0.000	0.000	0.000	0.000	0.015	0.049	0.061	0.027	0.033	0.102	0.045	0.003	0.000
Al	0.000	0.000	0.000	0.000	0.000	0.000	0.000	0.000	0.000	0.000	0.000	0.000	0.000	0.000	0.000	0.000	0.000	0.000
Tetr. Z:	**3.003**	**3.006**	**3.000**	**3.002**	**3.018**	**3.015**	**3.030**	**3.021**	**3.028**	**3.000**	**3.000**	**3.000**	**3.000**	**3.000**	**3.000**	**3.000**	**3.000**	**3.000**
Ti	0.000	0.000	0.000	0.000	0.000	0.000	0.000	0.000	0.000	0.099	0.081	0.096	0.139	0.138	0.189	0.077	0.078	0.076
Al	1.922	1.925	1.940	1.943	1.937	1.956	1.943	1.950	1.947	1.400	1.383	1.344	1.042	1.000	0.783	1.454	1.472	1.477
Cr	0.000	0.000	0.000	0.001	0.000	0.002	0.002	0.002	0.009	0.002	0.006	0.000	0.002	0.000	0.004	0.000	0.000	0.000
Fe^{3+}	0.077	0.070	0.060	0.056	0.052	0.032	0.035	0.034	0.025	0.482	0.522	0.551	0.796	0.842	1.008	0.460	0.434	0.431
Oct. Y:	**1.998**	**1.996**	**2.000**	**1.999**	**1.988**	**1.990**	**1.980**	**1.986**	**1.981**	**1.985**	**1.992**	**1.992**	**1.980**	**1.979**	**1.983**	**1.992**	**1.984**	**1.984**
Mg	0.337	0.326	0.340	1.148	1.153	1.151	0.917	0.932	0.877	0.035	0.037	0.031	0.013	0.011	0.011	0.021	0.010	0.012
Ca	0.358	0.318	0.273	0.110	0.098	0.114	0.214	0.205	0.192	2.629	2.667	2.691	2.608	2.696	2.709	2.488	2.506	2.543
Mn	0.158	0.165	0.166	0.078	0.072	0.071	0.055	0.063	0.063	0.034	0.037	0.038	0.070	0.059	0.057	0.066	0.084	0.079
Fe^{2+}	2.144	2.184	2.222	1.662	1.659	1.649	1.784	1.779	1.839	0.279	0.247	0.226	0.279	0.202	0.198	0.413	0.374	0.342
Na	0.000	0.000	0.000	0.000	0.000	0.000	0.000	0.000	0.000	0.009	0.016	0.015	0.008	0.021	0.013	0.018	0.023	0.021
X-Pos:	**2.997**	**2.994**	**3.000**	**2.998**	**2.982**	**2.985**	**2.970**	**2.979**	**2.972**	**2.986**	**3.004**	**3.002**	**2.978**	**2.990**	**2.988**	**3.005**	**2.998**	**2.997**
Total:	**7.998**	**7.996**	**8.000**	**7.999**	**7.988**	**7.990**	**7.980**	**7.986**	**7.981**	**7.970**	**7.996**	**7.994**	**7.958**	**7.969**	**7.971**	**7.997**	**7.982**	**7.981**
Endmembers:																		
Uv:	0.0	0.0	0.0	0.0	0.0	0.1	0.1	0.1	0.5	0.1	0.3	0.0	0.1	0.0	0.2	0.0	0.0	0.0
Adr:	3.8	3.5	3.0	2.8	2.6	1.6	1.8	1.7	1.3	29.3	30.3	32.5	47.3	49.5	60.3	27.0	25.8	25.5
Grs:	8.1	7.1	6.1	0.9	0.7	2.1	5.3	5.1	4.7	58.9	58.7	57.6	40.4	41.3	30.5	56.3	58.4	59.9
Alm:	71.6	73.0	74.1	55.4	55.6	55.2	60.1	59.7	61.9	9.4	8.3	7.6	9.4	6.8	6.7	13.8	12.6	11.5
Sps:	5.3	5.5	5.5	2.6	2.4	2.4	1.9	2.1	2.1	1.1	1.2	1.3	2.3	2.0	1.9	2.2	2.8	2.7
Prp:	11.2	10.9	11.3	38.3	38.7	38.5	30.9	31.3	29.5	1.2	1.2	1.0	0.4	0.4	0.4	0.7	0.4	0.4

Table 3.2 Selected microprobe analyses of biotite.

Biotite	ALT-03	ALT-03	ALT-03	BPD-02	BPD-02	BPD-02	K-1	K-1	K-1	YKK-2d	YKK-2d	YKK-2d
	F3 3	F7 2	F7 3	F4 1	F5 4	F5 5	F2 1	F2 4	F2 5	F1 1	F1 5	F2 4
	core	core	core	core	core	core	core	core	core	core	core	core
SiO_2	35.41	35.76	35.58	38.28	37.90	37.75	37.36	37.45	37.39	36.91	37.49	37.46
TiO_2	6.00	6.00	6.27	7.29	8.16	8.32	4.76	5.02	4.35	2.71	1.90	3.17
Al_2O_3	12.78	12.61	12.78	14.45	14.23	14.31	16.33	16.56	16.72	16.57	16.69	16.18
Cr_2O_3	0.00	0.00	0.00	0.13	0.01	0.09	0.00	0.00	0.00	0.04	0.07	0.00
MgO	8.58	9.00	8.86	12.70	12.18	11.94	12.89	12.59	12.72	17.03	18.40	17.54
CaO	0.01	0.02	0.01	0.00	0.00	0.00	0.08	0.00	0.00	0.06	0.01	0.18
MnO	0.07	0.02	0.06	0.09	0.09	0.03	0.19	0.00	0.00	0.05	0.09	0.09
FeO	23.30	22.98	23.06	14.00	14.35	14.58	15.20	15.46	15.66	12.98	11.67	11.79
BaO	0.00	0.00	0.00	0.00	0.00	0.00	0.00	0.00	0.00	0.00	0.00	0.00
Na_2O	0.16	0.07	0.03	0.01	0.03	0.00	0.50	0.00	0.00	0.12	0.13	0.19
K_2O	9.84	9.88	10.04	8.94	8.98	8.92	8.63	8.86	9.11	9.40	9.41	9.24
Total:	**96.15**	**96.34**	**96.69**	**95.90**	**95.93**	**95.94**	**95.94**	**95.94**	**95.95**	**95.87**	**95.87**	**95.84**
Structural formula (O=11):												
Si	2.758	2.773	2.753	2.814	2.794	2.784	2.760	2.764	2.765	2.712	2.734	2.735
Al^{IV}	1.173	1.153	1.165	1.186	1.206	1.216	1.240	1.236	1.235	1.288	1.266	1.265
Tetrahedron	**3.932**	**3.925**	**3.918**	**4.000**	**4.000**	**4.000**	**4.000**	**4.000**	**4.000**	**4.000**	**4.000**	**4.000**
Al^{VI}	0.000	0.000	0.000	0.065	0.029	0.029	0.181	0.204	0.222	0.147	0.169	0.128
Cr	0.000	0.000	0.000	0.008	0.001	0.005	0.000	0.000	0.000	0.002	0.004	0.000
Ti	0.352	0.350	0.365	0.403	0.453	0.461	0.264	0.278	0.242	0.150	0.104	0.174
Fe^{2+}	1.518	1.490	1.492	0.860	0.885	0.899	0.939	0.954	0.968	0.797	0.712	0.720
Mn	0.005	0.002	0.004	0.005	0.005	0.002	0.012	0.000	0.000	0.003	0.006	0.006
Mg	0.996	1.040	1.022	1.392	1.339	1.313	1.420	1.385	1.403	1.865	2.000	1.909
Octahedron	**2.870**	**2.881**	**2.883**	**2.734**	**2.711**	**2.710**	**2.817**	**2.821**	**2.835**	**2.965**	**2.994**	**2.936**
Ba	0.000	0.000	0.000	0.000	0.000	0.000	0.000	0.000	0.000	0.000	0.000	0.000
Ca	0.001	0.002	0.001	0.000	0.000	0.000	0.006	0.000	0.000	0.005	0.001	0.014
Na	0.024	0.011	0.005	0.001	0.004	0.000	0.071	0.000	0.000	0.017	0.019	0.027
K	0.977	0.977	0.991	0.838	0.844	0.840	0.814	0.834	0.859	0.881	0.876	0.861
Interlayer	**1.002**	**0.989**	**0.996**	**0.840**	**0.848**	**0.840**	**0.891**	**0.834**	**0.859**	**0.903**	**0.895**	**0.902**
Total:	**7.804**	**7.795**	**7.797**	**7.573**	**7.560**	**7.549**	**7.708**	**7.655**	**7.694**	**7.869**	**7.889**	**7.838**
X_{Mg}:	0.396	0.411	0.407	0.618	0.602	0.594	0.602	0.592	0.592	0.701	0.738	0.726

Table 3.3 Selected microprobe analyses of clino- and orthopyroxene. Ferric iron in clinopyroxene after Ryburn et al. (1976)

Clinopyroxene	M-25	M-25	M-25	YKK-1a	YKK-1a	YKK-1a	YKK-1c	YKK-1c	YKK-1c	***Clinopyroxene***	YKK-2d	YKK-2d	YKK-2d	***Orthopyroxene***	ALT-03	ALT-03	ALT-03
	F3 6	F3 3	F3 1	F4 1	F2 18	F5 1	F4 0	F4 1	F6 0		F1 1	F3 5	F3 7		F5 12	F5 17	F5 20
Na-rich Cpx	core	intemediate	rim	core	intemediate	rim	core	rim	core	Na-poor Cpx	core	core	rim		core	intermediate	rim
SiO_2	47.64	47.26	46.11	46.50	45.07	44.60	43.80	44.26	44.90	SiO_2	52.55	52.11	52.72	SiO_2	48.96	49.16	49.15
TiO_2	1.03	1.02	1.20	1.13	1.26	1.42	1.82	2.04	1.98	TiO_2	0.47	0.24	0.16	TiO_2	0.19	0.20	0.18
Al_2O_3	6.05	6.31	6.72	5.99	5.43	5.29	8.10	7.62	7.00	Al_2O_3	2.93	3.01	2.90	Al_2O_3	0.64	0.63	0.64
Cr_2O_3	0.00	0.00	0.00	0.00	0.00	0.00	0.00	0.00	0.00	Cr_2O_3	0.00	0.00	0.00	Cr_2O_3	0.00	0.00	0.00
Fe_2O_3	4.62	6.18	4.56	6.39	11.21	10.89	6.61	5.34	4.69	Fe_2O_3	0.09	0.65	0.76	Fe_2O_3	0.00	0.00	0.00
MgO	5.31	5.17	4.98	1.81	1.85	1.70	2.25	2.17	2.25	MgO	14.41	14.07	14.30	MgO	11.06	11.12	11.13
CaO	20.56	20.32	21.25	19.53	18.23	18.69	20.39	20.15	20.26	CaO	21.68	21.98	21.83	CaO	0.55	0.57	0.47
MnO	0.45	0.37	0.22	0.65	0.69	0.66	0.53	0.51	0.54	MnO	0.22	0.19	0.25	MnO	1.02	0.86	0.87
FeO	12.94	11.84	12.11	17.14	14.51	15.32	14.82	16.29	17.14	FeO	8.07	7.27	7.48	FeO	37.59	37.45	37.55
Na_2O	1.88	2.15	1.68	2.28	2.85	2.52	1.85	1.79	1.69	Na_2O	0.33	0.39	0.43	Na_2O	0.00	0.00	0.00
K_2O	0.00	0.00	0.00	0.00	0.00	0.00	0.00	0.00	0.00	K_2O	0.01	0.00	0.00	K_2O	0.00	0.00	0.00
Total:	**100.47**	**100.62**	**98.83**	**101.43**	**101.10**	**101.09**	**100.17**	**100.17**	**100.45**	**Total:**	**100.76**	**99.92**	**100.83**	**Total:**	**100.01**	**99.99**	**99.99**
Structural formula (O=6)										Structural formula (O=6)				Structural formula (O=6)			
T Si	1.836	1.818	1.806	1.821	1.778	1.768	1.729	1.751	1.773	**T** Si	1.934	1.932	1.938	**T** Si	1.975	1.980	1.980
Al	0.164	0.182	0.194	0.179	0.222	0.232	0.271	0.249	0.227	Al	0.066	0.068	0.062	Al	0.025	0.020	0.020
Total T:	**2.000**	**2.000**	**2.000**	**2.000**	**2.000**	**2.000**	**2.000**	**2.000**	**2.000**	**Total T:**	**2.000**	**2.000**	**2.000**	**Total T:**	**2.000**	**2.000**	**2.000**
M1 Al	0.111	0.104	0.116	0.097	0.031	0.015	0.106	0.106	0.099	**M1** Al	0.061	0.064	0.063	**M1** Al	0.006	0.010	0.010
Fe^{3+}	0.134	0.179	0.134	0.188	0.333	0.325	0.197	0.159	0.139	Fe^{3+}	0.003	0.018	0.021	Fe^{3+}	0.000	0.000	0.000
Cr	0.000	0.000	0.000	0.000	0.000	0.000	0.000	0.000	0.000	Cr	0.000	0.000	0.000	Cr	0.000	0.000	0.000
Ti	0.030	0.030	0.035	0.033	0.037	0.042	0.054	0.061	0.059	Ti	0.013	0.007	0.004	Ti	0.006	0.006	0.005
Mg	0.305	0.297	0.291	0.106	0.109	0.100	0.132	0.128	0.132	Mg	0.703	0.706	0.705	Mg	0.340	0.341	0.340
Fe^{2+}	0.417	0.381	0.397	0.561	0.479	0.508	0.489	0.539	0.566	Fe^{2+}	0.221	0.205	0.207	Fe^{2+}	0.648	0.643	0.644
Mn	0.004	0.010	0.007	0.014	0.011	0.009	0.018	0.008	0.004	Mn	0.000	0.000	0.000	Mn	0.000	0.000	0.000
Total M1:	**1.000**	**1.000**	**0.981**	**1.000**	**1.000**	**1.000**	**0.996**	**1.000**	**1.000**	**Total M1:**	**1.000**	**1.000**	**1.000**	**Total M1:**	**1.000**	**1.000**	**1.000**
M2 Mg	0.000	0.000	0.000	0.000	0.000	0.000	0.000	0.000	0.000	**M2** Mg	0.087	0.072	0.079	**M2** Mg	0.325	0.327	0.328
Fe^{2+}	0.000	0.000	0.000	0.000	0.000	0.000	0.000	0.000	0.000	Fe^{2+}	0.027	0.021	0.023	Fe^{2+}	0.620	0.618	0.621
Mn	0.011	0.002	0.000	0.008	0.012	0.013	0.000	0.009	0.014	Mn	0.007	0.006	0.008	Mn	0.035	0.029	0.030
Ca	0.849	0.838	0.892	0.819	0.771	0.794	0.863	0.854	0.857	Ca	0.855	0.873	0.860	Ca	0.024	0.025	0.020
Na	0.140	0.160	0.128	0.173	0.218	0.194	0.142	0.137	0.129	Na	0.024	0.028	0.031	Na	0.000	0.000	0.000
K	0.000	0.000	0.000	0.000	0.000	0.000	0.000	0.000	0.000	K	0.000	0.000	0.000	K	0.000	0.000	0.000
Total M2:	**1.000**	**1.000**	**1.019**	**1.000**	**1.000**	**1.000**	**1.004**	**1.000**	**1.000**	**Total M2:**	**1.000**	**1.000**	**1.000**	**Total M2:**	**1.004**	**0.999**	**0.999**
Endmembers after Morimoto et al. (1988)										Endmembers after Lindsley (1983)				Endmembers after Lindsley (1983)			
Q	84.8	82.5	86.1	81.1	75.7	78.4	84.0	84.7	85.7	Wo:	40.9	41.9	41.4	Wo:	0.9	0.7	0.5
Jd	1.1	1.9	0.8	2.4	7.8	6.2	1.3	1.0	0.9	En:	45.0	45.1	45.3	Fs:	34.1	34.4	34.4
Aeg	14.0	15.6	13.1	16.5	16.5	15.5	14.7	14.2	13.4	Fs:	14.1	13.1	13.3	En:	65.0	64.9	65.1

Table 3.4 Selected analyses of plagioclase.

Plagioclase	ALT-03	ALT-03	ALT-03	BPD-02	BPD-02	BPD-02	K-1	K-1	K-1	YKK-1c	YKK-1c	YKK-1c	YKK-2d	YKK-2d	YKK-2d
	F6 1	F6 2	F6 3	F7 6	F7 8	F7 9	F2 1	F2 6	F2 7	F5 Pl	F7 Pl	F7 Pl1	F1 1	F1 2	F1 3
	rim	intermediate	core	core	intermediate	rim	rim	intermediate	core	core	core	rim	core	intermediate	rim
SiO_2	62.63	62.72	62.69	63.46	63.76	63.85	58.54	58.57	58.75	61.27	61.84	61.69	47.76	47.76	47.15
Al_2O_3	23.44	23.34	23.36	22.98	22.77	22.93	26.31	26.12	26.08	23.27	23.36	23.48	33.14	33.14	32.70
MgO	0.00	0.00	0.00	0.00	0.00	0.00	0.00	0.00	0.00	0.00	0.00	0.00	0.00	0.00	0.00
CaO	5.29	5.25	5.29	4.60	4.39	4.34	8.33	8.32	8.29	4.66	4.78	4.87	17.11	17.11	17.08
MnO	0.00	0.00	0.00	0.00	0.00	0.00	0.00	0.00	0.00	0.00	0.00	0.00	0.00	0.00	0.00
FeO	0.00	0.00	0.00	0.00	0.00	0.00	0.00	0.00	0.00	0.14	0.10	0.10	0.00	0.00	0.00
BaO	0.00	0.00	0.00	0.00	0.00	0.00	0.00	0.00	0.00	0.80	0.60	0.60	0.00	0.00	0.00
Na_2O	8.29	8.24	8.19	8.75	8.81	8.89	6.61	6.63	6.54	8.70	8.66	8.70	1.75	1.75	1.76
K_2O	0.35	0.45	0.47	0.22	0.28	0.00	0.22	0.37	0.33	0.32	0.42	0.42	0.00	0.00	0.00
Total:	**100.00**	**100.00**	**100.00**	**100.01**	**100.01**	**100.01**	**100.01**	**100.01**	**99.99**	**99.16**	**99.76**	**99.86**	**99.76**	**99.76**	**98.69**
Cations (O=8)															
Si	2.774	2.778	2.777	2.803	2.815	2.814	2.615	2.619	2.625	2.758	2.763	2.755	2.194	2.194	2.192
Al	1.224	1.218	1.220	1.196	1.185	1.191	1.385	1.377	1.373	1.234	1.230	1.236	1.794	1.794	1.791
Mg	0.000	0.000	0.000	0.000	0.000	0.000	0.000	0.000	0.000	0.000	0.000	0.000	0.000	0.000	0.000
Ca	0.251	0.249	0.251	0.218	0.208	0.205	0.399	0.399	0.397	0.225	0.229	0.233	0.842	0.842	0.851
Mn	0.000	0.000	0.000	0.000	0.000	0.000	0.000	0.000	0.000	0.000	0.000	0.000	0.000	0.000	0.000
Fe	0.000	0.000	0.000	0.000	0.000	0.000	0.000	0.000	0.000	0.005	0.004	0.004	0.000	0.000	0.000
Ba	0.000	0.000	0.000	0.000	0.000	0.000	0.000	0.000	0.000	0.014	0.011	0.011	0.000	0.000	0.000
Na	0.712	0.708	0.703	0.749	0.754	0.760	0.573	0.575	0.567	0.759	0.750	0.753	0.156	0.156	0.159
K	0.020	0.025	0.027	0.012	0.016	0.000	0.013	0.021	0.019	0.019	0.024	0.024	0.000	0.000	0.000
Total:	**4.980**	**4.979**	**4.978**	**4.979**	**4.977**	**4.970**	**4.985**	**4.990**	**4.981**	**5.014**	**5.010**	**5.016**	**4.987**	**4.987**	**4.992**
Endmembers (mol.-%):															
Kfs:	2.0	2.6	2.7	1.3	1.6	0.0	1.3	2.1	1.9	1.8	2.4	2.3	0.0	0.0	0.0
Ab:	72.4	72.0	71.7	76.5	77.1	78.8	58.2	57.8	57.7	74.7	74.0	73.8	15.6	15.6	15.7
An:	25.5	25.4	25.6	22.2	21.2	21.2	40.5	40.1	40.4	22.1	22.6	22.8	84.4	84.4	84.3
Cel:	0.0	0.0	0.0	0.0	0.0	0.0	0.0	0.0	0.0	1.4	1.0	1.0	0.0	0.0	0.0

Table 3.5 Selected microprobe analyses of K-feldspar.

Orthoclase	ALT-03	ALT-03	ALT-03	BPD-02	BPD-02	BPD-02	K-1	K-1	K-1	M-25	M-25	M-25	YKK-1a	YKK-1a	YKK-1a
	F1 3	F1 6	F1	F3 10	F3 12	F3	F4 13	F4 14	F4	F1 11	F1 15	Kfs	F3 1	F3 11	Kfs
	core	intermediate	avg.	core	rim	avg.	core	intermediate	avg.	core	rim	avg.	core	intermediate	avg.
SiO_2	66.67	66.75	66.47	65.90	65.96	66.09	65.78	65.78	65.77	65.92	65.89	65.85	65.89	65.49	66.09
Al_2O_3	18.65	18.70	18.74	18.82	18.92	18.88	18.70	18.54	18.60	18.73	18.66	18.74	19.03	18.50	18.88
MgO	0.00	0.00	0.00	0.00	0.00	0.00	0.00	0.00	0.00	0.00	0.00	0.00	0.00	0.00	0.00
CaO	0.00	0.00	0.06	0.52	0.58	0.48	0.14	0.18	0.18	0.28	0.25	0.30	0.28	0.28	0.28
MnO	0.00	0.00	0.00	0.03	0.00	0.01	0.00	0.00	0.00	0.00	0.05	0.01	0.00	0.00	0.02
FeO	0.00	0.00	0.00	0.02	0.09	0.03	0.00	0.00	0.00	0.10	0.11	0.06	0.09	0.12	0.12
BaO	0.00	0.00	0.04	0.15	0.05	0.08	0.00	0.00	0.19	0.35	0.45	0.38	0.46	0.43	0.43
Na_2O	3.04	3.69	3.24	3.24	3.40	3.32	1.36	1.20	1.33	2.64	2.39	2.53	3.47	4.61	3.67
K_2O	11.63	10.87	11.45	11.29	10.91	11.08	14.03	14.29	13.93	11.97	12.20	12.13	10.77	10.27	10.51
Total:	**99.99**	**100.01**	**100.00**	**99.97**	**99.91**	**99.97**	**100.01**	**99.99**	**100.00**	**99.99**	**100.00**	**100.00**	**99.99**	**99.70**	**99.98**
Cations (O=8)															
Si	3.019	3.016	3.011	2.994	2.992	2.997	3.006	3.010	3.009	3.002	3.004	3.001	2.991	2.989	2.997
Al	0.995	0.996	1.001	1.008	1.012	1.009	1.007	1.000	1.003	1.005	1.003	1.007	1.018	0.995	1.009
Mg	0.000	0.000	0.000	0.000	0.000	0.000	0.000	0.000	0.000	0.000	0.000	0.000	0.000	0.000	0.000
Ca	0.000	0.000	0.003	0.025	0.028	0.023	0.007	0.009	0.009	0.014	0.012	0.014	0.014	0.014	0.014
Mn	0.000	0.000	0.000	0.001	0.000	0.000	0.000	0.000	0.000	0.000	0.002	0.001	0.000	0.000	0.001
Fe	0.000	0.000	0.000	0.001	0.003	0.001	0.000	0.000	0.000	0.004	0.004	0.002	0.003	0.005	0.005
Ba	0.000	0.000	0.001	0.003	0.001	0.001	0.000	0.000	0.003	0.006	0.008	0.007	0.008	0.008	0.008
Na	0.267	0.323	0.285	0.285	0.299	0.292	0.121	0.106	0.118	0.233	0.211	0.224	0.305	0.408	0.322
K	0.672	0.627	0.661	0.654	0.631	0.641	0.818	0.834	0.813	0.695	0.710	0.705	0.624	0.598	0.608
Total:	**4.953**	**4.961**	**4.962**	**4.972**	**4.967**	**4.965**	**4.959**	**4.960**	**4.955**	**4.960**	**4.955**	**4.960**	**4.964**	**5.016**	**4.963**
Endmembers (mol.-%):															
Kfs:	71.6	66.0	69.6	67.6	65.8	66.9	86.5	87.9	86.2	73.3	75.4	74.2	65.6	58.2	64.0
Ab:	28.4	34.0	30.0	29.5	31.2	30.5	12.7	11.2	12.5	24.6	22.4	23.5	32.1	39.7	33.8
An:	0.0	0.0	0.3	2.6	2.9	2.4	0.7	0.9	1.0	1.4	1.3	1.5	1.4	1.3	1.4
Cel:	0.0	0.0	0.1	0.3	0.1	0.2	0.0	0.0	0.4	0.7	0.9	0.7	0.9	0.7	0.8

Table 3.6 Selected electron microprobe analyses of nepheline.

Nepheline	M_25	M_25	M_25	YKK-1a	YKK-1a	YKK-1a	YKK-1c	YKK-1c	YKK-1c
	F2 15	F5 16	Ne	F4 1	F4 4	Ne	F6 Ne1 4	F4 Ne1 2	Ne
	rim	core	avg.	rim	core	avg.	rim	core	avg.
SiO_2	44.74	43.20	43.75	43.23	43.91	43.91	43.35	43.19	44.16
Al_2O_3	33.33	33.98	33.70	33.07	33.42	33.54	33.65	33.56	33.55
MgO	0.00	0.00	0.00	0.00	0.00	0.00	0.00	0.00	0.00
CaO	1.62	1.55	1.58	0.99	1.02	0.97	1.41	1.47	1.68
MnO	0.00	0.03	0.04	0.00	0.00	0.00	0.00	0.05	0.02
Fe_2O_3	0.51	0.06	0.31	0.33	0.58	0.47	0.40	0.28	0.35
BaO	0.00	0.00	0.00	0.00	0.00	0.00	0.04	0.03	0.04
Na_2O	14.75	15.59	15.44	16.67	16.51	16.48	17.15	17.16	16.16
K_2O	5.11	5.60	5.22	5.33	4.62	4.68	4.65	4.69	4.03
Total	**100.06**	**100.01**	**100.03**	**99.62**	**100.06**	**100.05**	**100.65**	**100.43**	**100.00**
Cations (O=32)									
Si	8.508	8.283	8.361	8.338	8.384	8.382	8.269	8.262	8.407
Al	7.470	7.678	7.591	7.517	7.520	7.545	7.565	7.566	7.527
Mg	0.000	0.000	0.000	0.000	0.000	0.000	0.000	0.000	0.001
Ca	0.330	0.318	0.324	0.205	0.209	0.198	0.288	0.301	0.344
Mn	0.000	0.005	0.007	0.000	0.000	0.000	0.000	0.008	0.003
Fe^{3+}	0.073	0.008	0.044	0.048	0.083	0.067	0.058	0.041	0.050
Ba	0.000	0.000	0.000	0.000	0.000	0.000	0.003	0.002	0.003
Na	5.438	5.795	5.720	6.234	6.112	6.100	6.343	6.364	5.964
K	1.240	1.370	1.272	1.311	1.125	1.140	1.132	1.145	0.979
Total	**23.059**	**23.457**	**23.318**	**23.652**	**23.433**	**23.432**	**23.657**	**23.689**	**23.277**
X_K:	0.177	0.183	0.174	0.169	0.151	0.153	0.146	0.147	0.134

Table 3.7 Selected electron microprobe analyses of clinoamphibole. Ferric iron calculated according to (Leake et al. 1997) using the midpoint method.

Amphibole		YKK-2d	YKK-2d	YKK-2d	YKK-2d	YKK-2d	YKK-2d
		F1 1	F2 1	F2 2	F3 2	F3 3	F4 1
midpoint Fe^{3+}		core	core	rim	core	rim	core
	SiO_2	43.14	42.93	42.99	42.83	43.00	42.98
	TiO_2	1.43	1.45	1.51	1.19	1.24	1.20
	Al_2O_3	13.10	13.37	13.10	13.53	13.69	13.76
	Fe_2O_3	1.47	1.06	1.30	2.11	1.98	2.49
	Cr_2O_3	0.00	0.00	0.00	0.00	0.00	0.00
	MgO	13.47	13.20	13.19	13.50	13.28	13.52
	CaO	11.76	11.68	11.64	11.55	11.47	11.34
	MnO	0.00	0.00	0.00	0.00	0.00	0.00
	FeO	10.27	10.17	10.38	9.59	9.75	9.44
	Na_2O	2.32	2.23	2.22	2.34	2.33	2.47
	K_2O	1.41	1.41	1.45	1.32	1.28	1.32
	Total:	**98.37**	**97.50**	**97.78**	**97.96**	**98.03**	**98.52**
Structural formula (23 O)							
T	Si	6.293	6.304	6.307	6.259	6.274	6.243
	Al	1.707	1.696	1.693	1.741	1.726	1.757
	Total T:	**8.000**	**8.000**	**8.000**	**8.000**	**8.000**	**8.000**
C	Al	0.545	0.618	0.572	0.590	0.629	0.599
	Cr	0.000	0.000	0.000	0.000	0.000	0.000
	Fe^{3+}	0.161	0.117	0.144	0.232	0.218	0.272
	Ti	0.157	0.160	0.167	0.131	0.136	0.131
	Mg	2.929	2.890	2.885	2.941	2.889	2.928
	Fe^{2+}	1.207	1.215	1.233	1.106	1.129	1.070
	Mn	0.000	0.000	0.000	0.000	0.000	0.000
	Total C:	**5.000**	**5.000**	**5.000**	**5.000**	**5.000**	**5.000**
B	Mg	0.000	0.000	0.000	0.000	0.000	0.000
	Fe^{2+}	0.046	0.033	0.041	0.066	0.062	0.077
	Mn	0.000	0.000	0.000	0.000	0.000	0.000
	Ca	1.838	1.838	1.830	1.809	1.793	1.765
	Na	0.116	0.129	0.130	0.126	0.145	0.158
	Total B:	**2.000**	**2.000**	**2.000**	**2.000**	**2.000**	**2.000**
A	Na	0.540	0.506	0.502	0.537	0.514	0.537
	K	0.262	0.264	0.271	0.246	0.238	0.245
	Total A:	**0.802**	**0.770**	**0.773**	**0.783**	**0.752**	**0.782**
	Total:	**15.802**	**15.770**	**15.773**	**15.783**	**15.752**	**15.782**

Table 3.8 Selected electron microprobe analyses of scapolite.

Scapolite	YKK-1c	YKK-1c	YKK-1c
	F3 19	F3 2	Scp
	19	2	avg.
SiO_2	51.86	51.52	51.67
TiO_2	0.00	0.00	0.00
Al_2O_3	24.74	24.23	24.65
CaO	11.73	12.12	11.97
FeO	0.00	0.00	0.00
Na_2O	6.57	6.58	6.54
K_2O	0.50	0.65	0.57
CO_2	2.95	2.84	2.95
SO_3	0.00	0.00	0.00
F-	0.00	0.00	0.00
Cl-	1.61	1.65	1.59
Total:	**99.95**	**99.59**	**99.95**
Total cor.:	**99.58**	**99.22**	**99.59**
Ions (Si+Al=12)			
Si	7.682	7.721	7.682
Al	4.318	4.279	4.318
Total Si+Al:	**12.000**	**12.000**	**12.000**
Ti	0.000	0.000	0.000
Fe^{2+}	0.000	0.000	0.000
Ca	1.861	1.946	1.906
Na	1.886	1.912	1.886
K	0.095	0.125	0.109
Total MeRest:	**3.843**	**3.983**	**3.901**
C	0.596	0.581	0.600
S	0.000	0.000	0.000
F	0.000	0.000	0.000
Cl	0.404	0.419	0.401
Total Vol.:	**1.000**	**1.000**	**1.000**
X_{Me}:	0.497	0.504	0.503

Samples YKK-1a, YKK-1c and YKK-2d originate from different sections of a m-wide mafic layer within a calcsilicate marble succession (Figure 3.4h). The structure of this layer and its appearance within the metasedimentary unit strongly remind of a magmatic dyke. Sample YKK-1a, a medium grained mafic gneiss with patchy felsic sections, originates from the central part of the layer (Figures 3.4e & h) and resembles to the nepheline gneiss M-25 concerning its mineralogy and rock fabric. Based on its mineral assemblage, the rock is a carbonate-bearing garnet-K-feldspar clinopyroxene-nepheline gneiss. Under the microscope, it shows a random orientation of granoblastic nepheline and K-feldspar as well as irregular intergrowths of garnet and clinopyroxene (Figures 3.6c & d). Accessory minerals are calcite, apatite, titanite and magnetite, which is in part mantled by pyrite. Reddish brown garnet grains often show dark brown rim sections, which sometimes display excavated and symplectitic shapes. Electron microprobe analyses testify to rather constant compositions of the central garnet sections with $Alm_{6.8\text{-}10.1}Prp_{0.2\text{-}0.5}Sps_{1.3\text{-}2.4}Uv_{0\text{-}0.3}Grs_{38.1\text{-}42.2}Adr_{47.3\text{-}50.6}$ whereas the rim sections show a distinct decrease of andradite at the expense of grossular ($Alm_{7.3\text{-}7.9}Prp_{0.3\text{-}0.6}Sps_{1.5\text{-}2.0}Uv_{0\text{-}0.3}Grs_{28.6\text{-}32}Adr_{57.6\text{-}61.1}$). As already observed in sample M-25, garnet contains elevated TiO_2 contents of 2.3 wt.-% (core) to 3.1 wt.-% (rim). Green clinoamphibole is virtually unzoned aegirine-rich augite and aegirine-augite (classification after Morimoto et al. 1988) showing slightly variable compositions ($Q_{75.7\text{-}82.5}Aeg_{13.9\text{-}18.2}Jd_{2.4\text{-}7.9}$) from grain to grain. Nepheline yields Si-contents of 8.338-8.413 and X_K-values of 0.147-0.171. Electron microprobe analyses of K-feldspar vary from grain to grain $Or_{53.2\text{-}76.4}Ab_{21.8\text{-}45.2}An_{1.1\text{-}1.5}Cs_{0.5\text{-}1.1}$ and carbonate is almost pure calcite ($CaCO_3$ >99.3 mole-%).

Sample YKK-1c was also part of the central section of the mafic layer and resembles sample YKK-1a. It is an inhomogeneous mafic gneiss with cm-sized leucocratic patches and also does not show any parallel texture (Figures 3.6e & f). Microscopic investigations classify the sample as a carbonate-bearing scapolite-garnet-plagioclase-clinopyroxene-nepheline gneiss. Its melanocratic sections prove to be sieve-like intergrowths of green clinopyroxene and plagioclase with minor poikiloblastic, pinkish brown garnet. In the felsic lenses elongate, irregular nepheline crystals are intergrown with large subhedral plagioclase and sometimes with scapolite and minor carbonate. Accessories are titanite, apatite and pyrite. Electron microprobe analyses of garnet show a composition of $Alm_{11.5\text{-}14.9}Prp_{0.4\text{-}0.7}Sps_{2.1\text{-}3.4}Grs_{57.4\text{-}59.9}Adr_{25.5\text{-}27.4}$ and TiO_2-contents of 1.3-1.7 wt.-%, which strongly resembles the garnet from nepheline gneiss M-25. Clinopyroxene is aegirine-rich augite with a composition of $Q_{80.5\text{-}85.8}Aeg_{13.3\text{-}17.3}Jd_{0.8\text{-}2.84}$, which varies from grain to grain. Nepheline yields Si-contents of 8.191-8.456 p.f.u. and X_K-values of 0.117-0.147. Plagioclase shows slight variations in composition from grain to grain ($Ab_{55.9\text{-}58.3}An_{39.9\text{-}41.9}Or_{1.3\text{-}2.3}$). Electron microprobe

analyses of scapolite prove a composition halfway between Ca-endmember meionite and the Na-endmember marialite (X_{Me} = 0.499-0.51) with Cl-contents of up to 1.67 wt.-% and a lack fluorine and sulfur. Carbonate is almost pure calcite with $CaCO_3$ >98.7 mole-%.

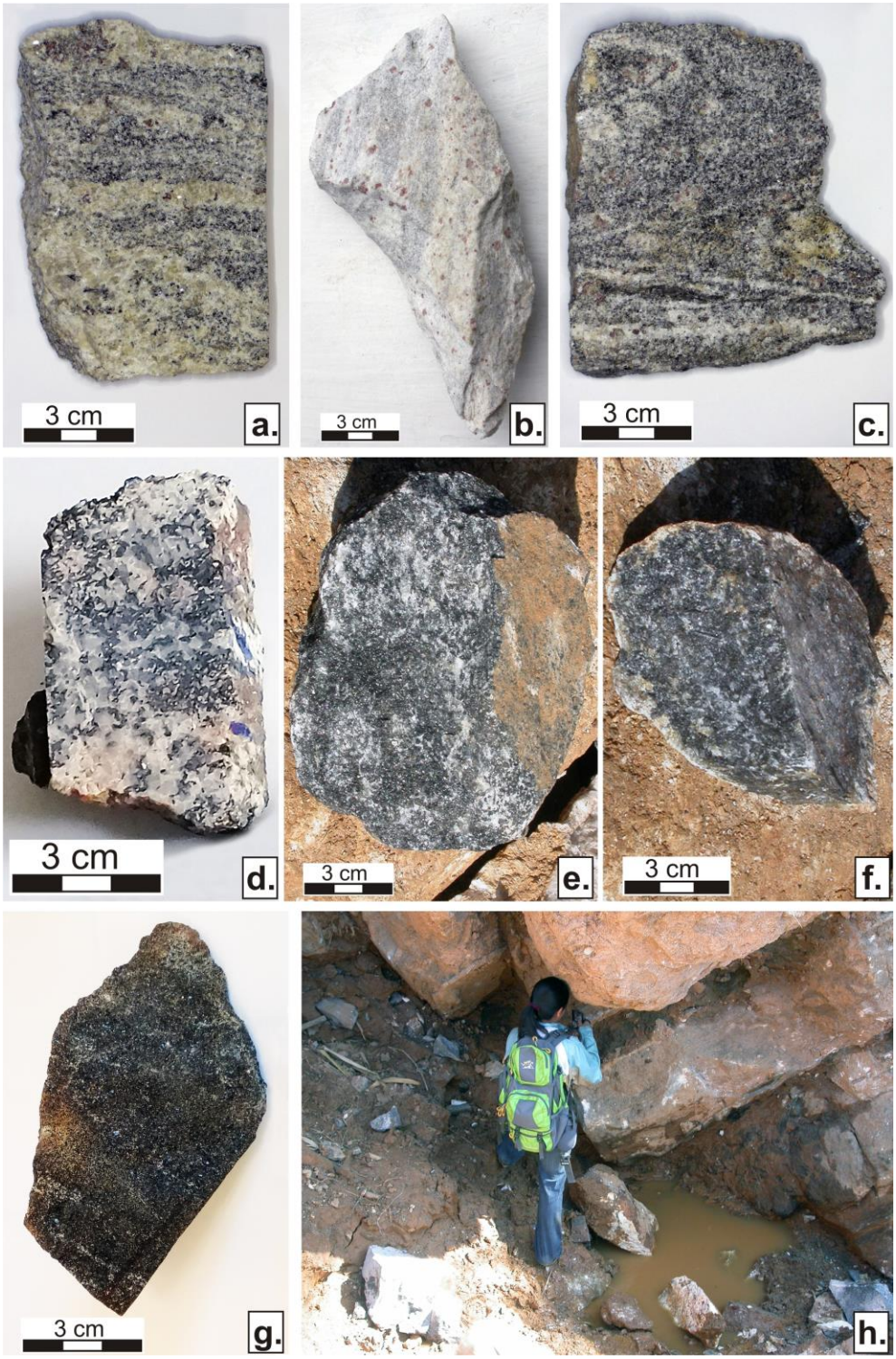

Figure 3.4 Photos of hand specimen of the investigated samples and the outcrop of the metadyke; a.) Sample ALT-03, b.) Sample BPD-02, c.) Sample K-1, d.) Sample M-25, e.) Sample YKK-1a, f.) Sample YKK-1c, g.) Sample YKK-2d, h.) Outcrop of metadyke (lower, dark grey layers) within marble (upper pale brown section) at the location Yadanar Kaday Kadar (YKK).

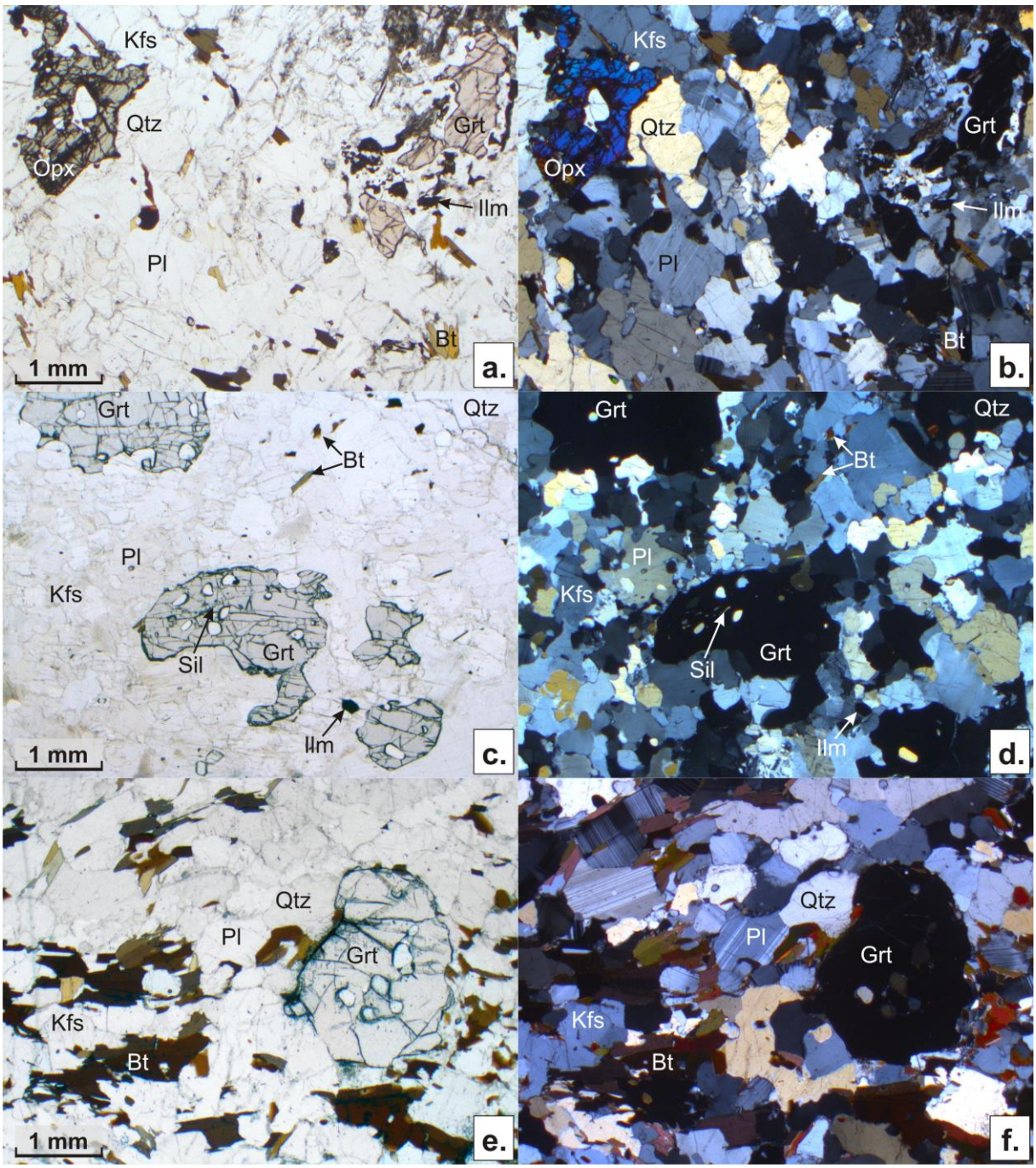

Figure 3.5 Microphotographs of the quartz gneisses: a.) sample ALT-03 with II pol., b.) with X pol.; c.) sample BPD-02 with II pol., d). with X pol.; e.) sample K-1 with II pol., f.) with X pol.

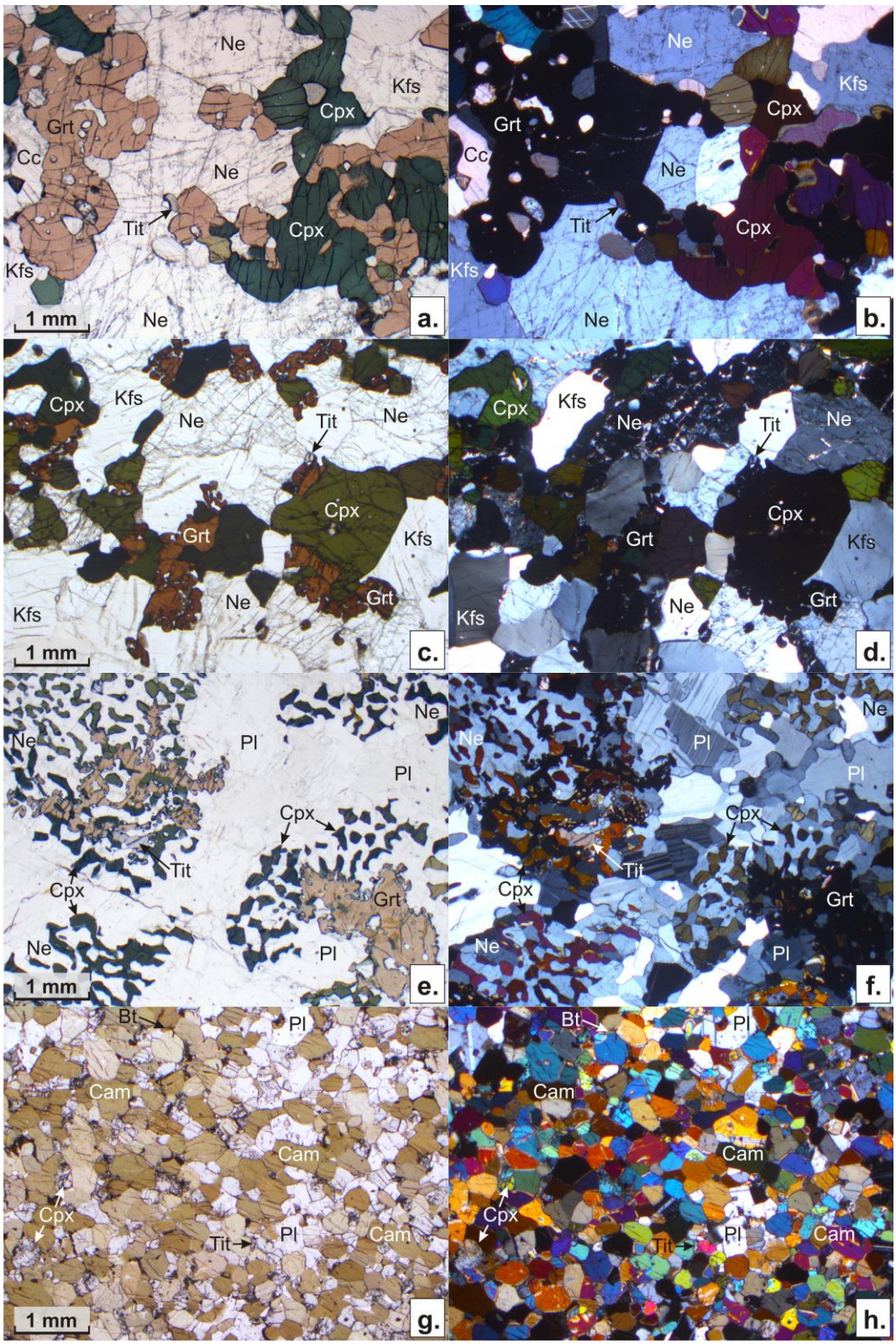

Figure 3.6 Microphotographs of the nepheline gneisses and the clinopyroxyene-clinoamphibole gneiss; a.) sample M-25 with II pol., b.) with X pol.; c.) sample YKK-1a with II pol., d.) with X pol.; e.) sample YKK-1c with II pol., f.) with X pol.; g.) sample YKK-2d with II pol., h.) with X pol.

Table 3.9 Mineral assemblages of garnet-quartz gneisses, garnet-nepheline gneisses and the clinopyroxene-clinoamphibole gneiss from the central and western Mogok area.

Sample	Location	Grt	Bt	Pl	Kfs	Opx	Cpx	Nep	Amp	Scp	Qtz	Ilm	Mag	Py	Zrn	Sil	Cc	Ttn
ALT-03	22°55'32.30"N 96°25'34.54"E	√	√	√	√	√	–	–	–	–	√	√	–	–	√	–	–	–
BPD-02	22°56'5.31"N 96°27'22.16"E	√	√	√	√	–	–	–	–	–	√	√	–	–	√	√	–	–
K-01	22°55'49.06"N 96°19'6.99"E	√	√	√	√	–	–	–	–	–	√	–	–	–	√	–	–	–
M-25	22°56'50.00"N 96°19'22.52"	√	–	–	√	–	√	√	–	–	–	–	√	–	–	–	√	√
YKK-1a	22°54'42.14"N 96°23'17.35"E	√	–	–	√	–	√	√	–	–	–	–	√	√	–	–	√	√
YKK-1c	22°54'42.14"N 96°23'17.35"E	√	–	√	–	–	√	√	–	√	–	–	–	√	√	–	√	√
YKK-2d	22°54'42.14"N 96°23'17.35"E	–	–	√	–	–	√	–	√	–	–	–	–	√	–	–	–	√

Sample YKK-2d originates from the lower part of the mafic layer (Figures 3.4g & h) and is distinctly more melanocratic than the gneisses from its central section. The fine-grained rock is classified as a clinopyroxene-clinoamphibole gneiss, which consists of ultramafic layers formed by brow Ti-hornblende and clinopyroxene while more felsic, plagioclase-bearing layers are subordinate (Figures 3.6g & h). Accessories in this rock are biotite, apatite, titanite and pyrite. Clinopyroxene is augite after the classification of Morimoto et al. (1988) showing a composition of $Wo_{38.2\text{-}41.9}En_{45.0\text{-}47.2}Fs_{13.1\text{-}15.2}$. Remarkably, stoichiometric calculations using the method of Ryburn et al. (1976) yield only low amounts of ferric iron (1-8.3% of total Fe). Clinoamphibole is Ti-rich pargasite following the classification of Hawthorne et al. (2012), yields TiO_2-contents of 1.2-1.5 wt.-% and X_{Mg}-values of 0.70-0.74. Biotite shows somewhat variable TiO_2-contents of 1.9-3.1 wt.-% and X_{Mg}-values of 0.70-0.74. Plagioclase is calcic with small variations from grain to grain ($Ab_{14.7\text{-}17.3}An_{82.7\text{-}85.1}$).

3.6 Geothermobarometry

Geothermobarometric investigations were performed using a combination of conventional methods and the Theriak-Domino program of (De Capitani and Petrakakis 2010; calculation with tcdb55c2 dataset except for sample YKK-2d where tcds62c dataset was applied). For rocks with H_2O-bearing phases (i.e. the quartz-bearing gneisses) the application of these two independent methods does not only determine the metamorphic PT-conditions but also allows to estimate the water

activity during metamorphism. In granulite facies terrains, the water activity is distinctly reduced as otherwise the rock would melt forming migmatites (cf. Bader et al. 2014 and citations within).

3.6.1 Quartz bearing gneisses

In sample ALT-03, the biotite-garnet-orthopyroxene gneiss, the application of the garnet-orthopyroxene-plagioclase quartz geothermobarometer of (Lal 1993) calculates granulite facies conditions of 758°C at 7.3 kbar for the garnet analysis with the highest X_{Mg}-value from the core section of the garnet. Temperatures are well in accord with the Ti-in biotite geothermometer of (Henry et al. 2005), which yields 766-779°C. For the garnet rim section, the geothermobarometer of (Lal 1993) points to PT-conditions of 725°C at 6.1 kbar, which highlight a part of the retrograde PT-path of the rock (Figure 3.8a). For the calculations with the Theriak-Domino program, the bulk composition of the rock around the investigated garnet was determined by point counting and using the respective electron microprobe analyses of the minerals from this section. Equilibrium phase diagram calculations and isopleth intersections for the garnet core composition with the Domino program in the TiCaNaKFMASH system were then performed with H_2O in excess and variable water activities (a_{H2O}) ranging from 0.1 to 1 (cf. Figures. 3.7a-h). At low water activities of 0.1, the stability field of the observed mineral assemblage (Grt-Opx-Bt-Qtz-Pl-Kfs-Ilm) is found at PT-conditions of the lower to middle amphibolite facies and the intersection of the garnet isopleths plots outside the stability field of the observed mineral assemblage at 628°C and 5.7 kbar (Figure 3.7a), i.e. far away from the PT-conditions determined by the conventional method. An increase of the water activity shifts the stability field towards higher PT-conditions and at a_{H2O}=0.2, the garnet isopleths intersect at 676°C and 6.2 kbar and within the stability field of the observed mineral assemblage (Figure 3.7b). At a_{H2O}=0.3, the stability field of the observed mineral assemblage and the garnet isopleth intersection are located at distinctly higher PT-conditions (Figure 3.7c) and at a_{H2O}=0.4, the best fit between the Domino calculations and the conventional geothermobarometry is observed as the garnet isopleths intersect at 743°C and 6.9 kbar (Figure 3.7d). At a_{H2O}=0.55, the field of anatexis is strongly enlarged (Figure 3.7e) and at a_{H2O}=0.60, the stability field of the observed mineral assemblage has become very small (Figure 3.7f). Finally, the stability filed of the observed mineral assemblage has vanished completely at a_{H2O}=0.65 (Figure 3.7g) and calculating the diagram at a_{H2O}=1.0 reveals an extended field of anatexis and an intersection of the garnet isopleths far away from the PT-estimate of the conventional method (Figure 3.7h). Another method to estimate the water activity in the sample is given by the Theriak-Domino program, which calculates the modal

mineral amount of the sample at the intersection point of the garnet isopleths at different a_{H2O}-values. For sample ALT-03, the best fit between the calculated modal amount of minerals and the modal amount determined by point-counting of the thin section is given at a_{H2O}=0.2, which is a bit lower than the estimate using the conventional thermobarometry data.

Sample BPD-02, the sillimanite-bearing biotite garnet, was investigated thermobarometrically using the garnet composition of the rim section with the highest X_{Mg}. The garnet-biotite geothermometer of Holdaway (2000) in combination with the GASP geobarometer of Koziol and Newton (1988) calculate 792°C at 7.6 kbar. As garnet in sample BPD-02 is virtually unzoned, calculation using other garnet analyses yields almost identical results. Temperatures of 819-828°C are gained with the Ti-in-biotite geothermometer of Henry et al. (2005) reproducing the results of the garnet-biotite thermometry within the error of the methods. Calculations with the Theriak-Domino program in an analogous manner as described for sample ALT-03 indicates the closest fit of the phase diagram with the conventional thermobarometry at a water activity of 0.34 with garnet isopleths intersecting at 789°C and 8.4 kbar (Figure 3.8b). The best fit between the modal mineral amount calculated at the garnet intersections by the Theriak-Domino program and the modal mineral amount determined by point-counting is at a_{H2O}=0.4.

In biotite-garnet gneiss sample K-01, a combination of the garnet-biotite geothermometer of Holdaway (2000) with the garnet-biotite-plagioclase-quartz geobarometer of (Wu et al. 2004; Fe-calibration) calculates PT-conditions of 756°C at 7.4 kbar using a garnet analysis from the rim section. Despite of the absence of a Ti-bearing ore phase in this sample, the Ti-in-biotite geothermometer of Henry et al. (2005) supplies very similar temperatures of 758-764°C. Phase diagram calculations using the same approach as in the two foregoing samples yield the closest fit between the Theriak-Domino program and the conventional thermobarometry at a water activity of 0.4 (Figure 3.8c). Remarkably, the garnet isopleths intersect at 766°C and 6.6 kbar in the stability field of the assemblage Grt-Bt-Opx-Kfs-Pl-Qtz. The best fit of the modal mineral amount calculated at the garnet isopleth intersections by the Theriak-Domino program and the one determined by point-counting is at a_{H2O}=0.5 and thus quite close to the water activity derived using the conventional thermobarometric estimates.

3.6.2 Nepheline bearing gneisses and clinopyroxene-clinoamphibole gneiss

Thermobarometric investigations of these unusual rocks are strongly aggravated by their exotic chemical composition, by the lack of reasonable thermodynamic data and mixing models for some of the minerals as well as by the elevated oxygen fugacity of the nepheline gneisses. It will, however, be demonstrated below that despite of these complicacies, a general estimate of their metamorphic conditions is possible.

The carbonate-garnet-K-feldspar-clinopyroxene-nepheline gneiss M-25 shows a tight intergrowth of garnet and clinopyroxene, which should permit the application of the garnet-clinopyroxene geothermometer. Calculations using various calibrations, however, yield widely variable results ranging from 659°C Brey and Köhler (1990) to 1428°C Powell (1985). This is probably due to the very Fe-rich whole rock composition and to the high concentration of ferric iron in both garnet and clinopyroxene, which were not considered by any of the presently available calibrations. The only conventional method, which could be applied to this sample, is the nepheline-K-feldspar thermometry of Powell & Powell (1977). To avoid unmixing or inhomogeneity, both minerals were mapped with an enlarged electron microprobe beam and the average compositions were used for the calculations, which results in temperatures of 709°C. Phase equilibrium calculations with the Theriak-Domino program highlight a stability field for the assemblage calcite - K-feldspar – garnet – clinopyroxene – nepheline – leucite - magnetite at temperatures <680°C and pressures >5kbar (Figure 3.8d). The presence of leucite in the assemblage is due to the occurrence of elevated amounts of K in nepheline and to its oversaturation in Si. A calculation of most prominent garnet isopleths almandine, grossular and andradite was performed but did not display a common intersection. An intersection of the K_D-value of the nepheline-K-feldspar thermometry with the stability of the observed mineral assemblage, however, points to high-grade metamorphic PT-conditions similar to the neighbouring host rocks (taking into account an error in excess of ±50°C for the geothermometer; cf. Powell & Powell 1977).

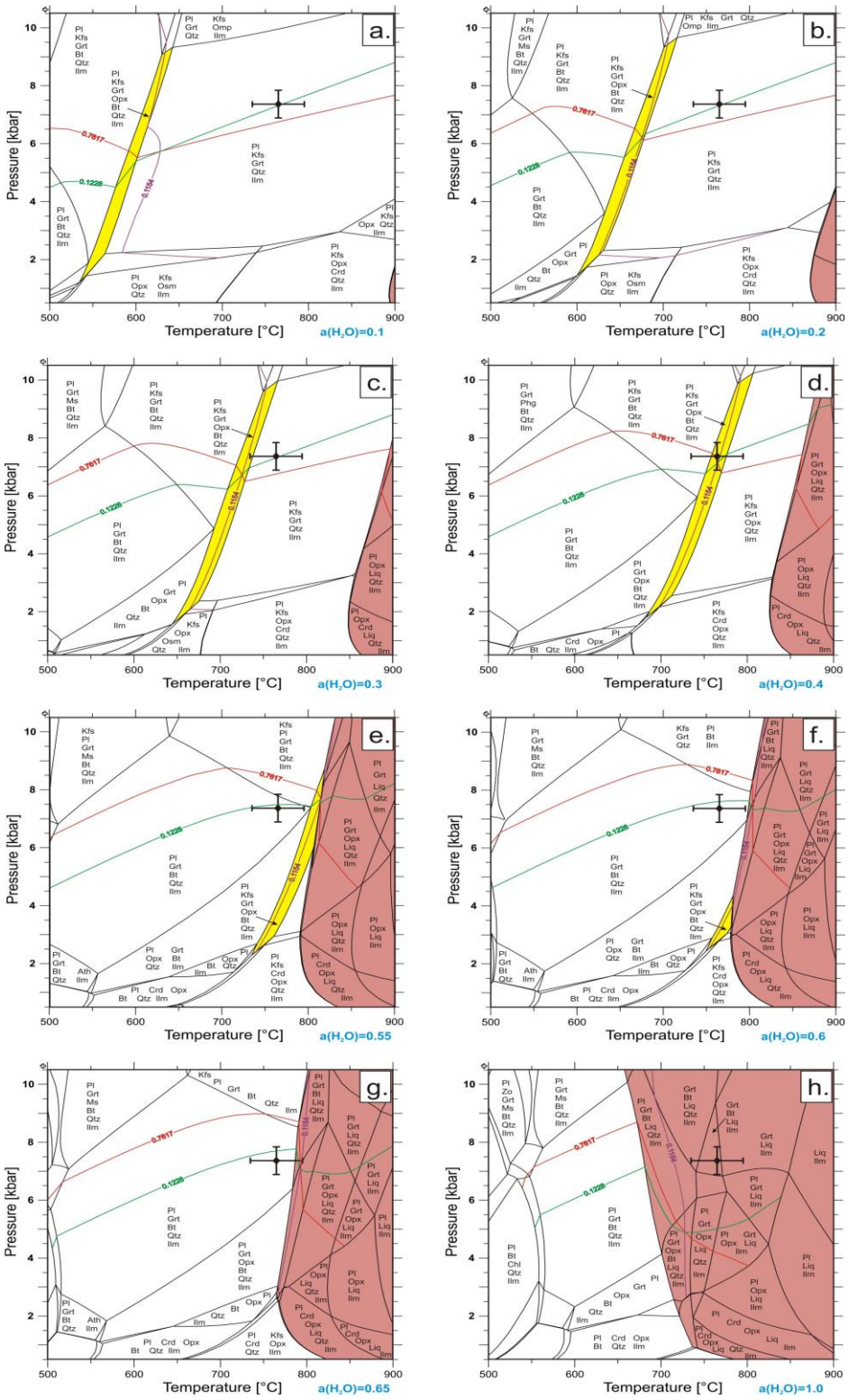

Figure 3.7 Theriak-Domino equilibrium phase diagram modelling of the Bt-Grt-Opx gneiss ALT-03. Bulk = Si(4.525) Ti(0.021) Al(1.137) Fe(0.507) Mg(0.173) Ca(0.167) K(0.217) Na(0.438) H(50) O(?) and water activities are 0.1 (a.), 0.2 (b.), 0.3 (c.), 0.4 (d.), 0.55 (e.), 0.6 (f.), 0.65 (g.) and 1.0 (h.). The stability field of the observed mineral assemblage is marked in yellow and the reddish-brown field indicates anataxis. The garnet isochores are shown as red lines (Alm), green lines (Grs) and purple lines (Prp). The error bar shows the PT-estimate of the conventional geothermobarometry.

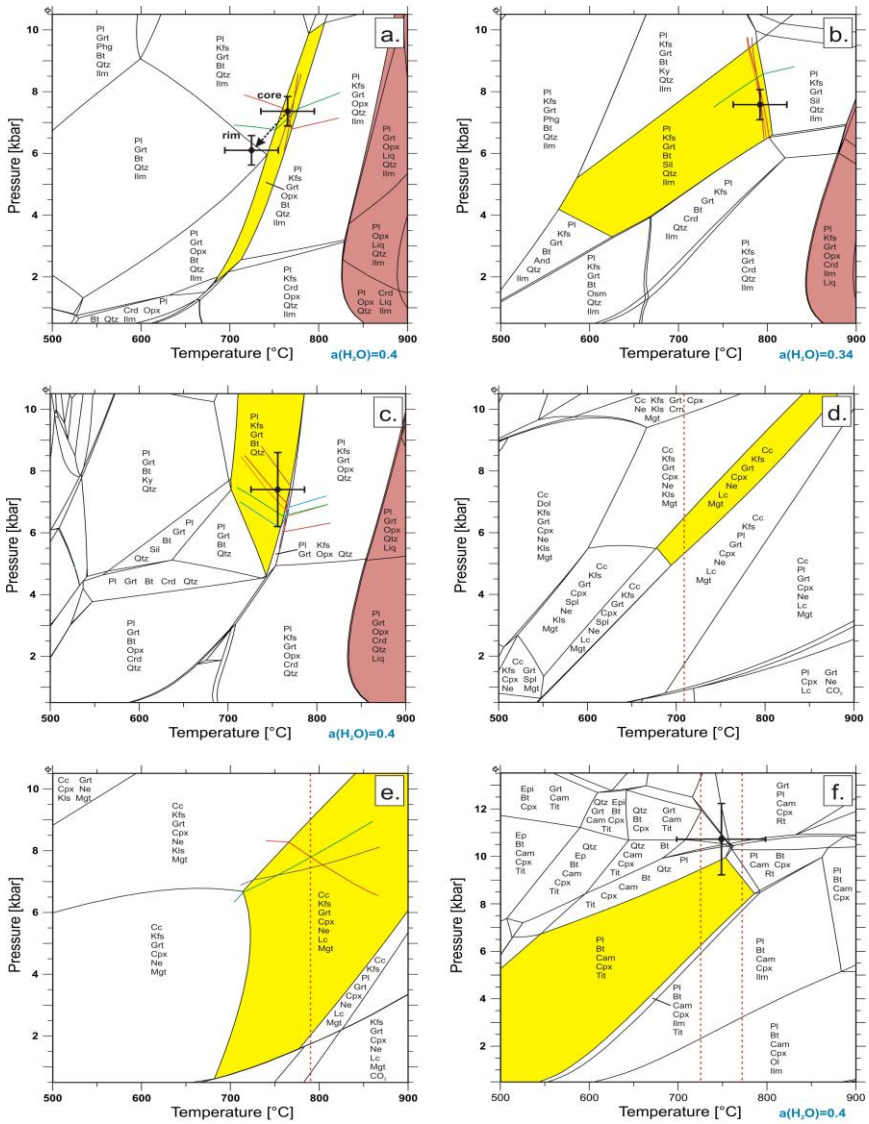

Figure 3.8 Equilibrium phase diagrams of quartz- and nepheline and clinopyroxene-clinoamphibole gneisses; stability fields of the observed mineral assemblage are shown in yellow and fields of anataxis in reddish-brown, error bars indicate the PT-estimates of the conventional thermobarometry (see text); a.) Bt-Grt-Opx gneiss ALT-03 (bulk = Si(4.525) Ti(0.021) Al(1.137) Fe(0.507) Mg(0.173) Ca(0.167) K(0.217) Na(0.438) H(50) O(?)) with isopleths of Alm (red), Grs (green), Prp (violet) and X_{Mg} of Bt (brown) for the peak metamorphic conditions (core); b.) Sil-Bt-Grt gneiss BPD-02 (bulk = Si(4.339) Al(1.413) Ti(0.031) Fe(0.363) Mn(0.014) Mg(0.245) Ca(0.078) K(0.506) Na(0.363) H(50) O(?)) with isopleths of Alm (red), Grs (green), Prp (violet) and Sps (orange); c.) Bt-Grt gneiss K-1 (bulk = Si(4.138) Al(1.336) Fe(0.810) Mg(0.500) Mn(0.026) Ca(0.185) K(0.131) Na(0.161) H(50) O(?)) with isopleths of Alm (red), Grs (green), Prp (violet), Sps (orange) and An-content in Pl (blue); d.) Ne gneiss M-25 (bulk = Si(3.252) Al(1.913) Fe(0.341) Mg(0.149) Ca(0.891) Na(1.223) K(0.360) C(0.167) O(12)) with result of the Ne-Kfs thermometry (dotted red line); e.) Ne gneiss YKK-1a (bulk = Si(3.409) Al(1.656) Fe(0.674) Mg(0.068) Ca(0.898) Na(1.147) K(0.343) C(0.037) O(12)) with isopleths of Alm (red), Grs (green), Adr (violet) and result of Ne-Kfs thermometry (red dotted line); f.) Cam-Cpx gneiss YKK-2d (bulk = Si(3.360) Ti(0.082) Al(1.246) Fe(0.590) Mg(1.309) Ca(1.122) K(0.095) Na(0.280) H(50) O(37)) with range of the Ti-in-Hbl thermometry (red dotted lines). Note that the error bar only displays maximum pressures for the rock.

Sample YKK-1a, the carbonate-bearing garnet-K-feldspar clinopyroxene-nepheline gneiss, displays the same mineral assemblage as sample M-25 and permits the application of the same type of thermobarometry. Garnet-clinopyroxene thermometry again calculates a wide range of temperatures using different calibrations ranging from 758°C (Brey and Köhler 1990) to 1612°C (Powell 1985) for the garnet and clinopyroxene core compositions. For the garnet rim, very similar temperatures were gained. The nepheline-K-feldspar thermometry of Powell & Powell (1977) calculates temperatures of 790°C for the integrated nepheline and K-feldspar analyses. Equilibrium phase diagram calculations with the Theriak-Domino program reveal a wide stability field for the assemblage calcite-K-feldspar-garnet-clinopyroxene-nepheline-leucite-magnetite at high temperatures (Figure 3.8e). Remarkably, the intersections of the garnet isopleths (Alm, Grs & Adr) plot in a PT-range of 784-812°C at 7.8-8.4 kbar, which is quite close to the estimates of the quartz-gneisses from the central part of the Mogok Metamorphic Belt. There was no intersection for the garnet isopleths of the dark brown garnet rim.

Thermobarometry of sample YKK-1c, the carbonate-bearing scapolite-garnet-plagioclase-clinopyroxene-nepheline gneiss, proved to be most problematic. Garnet-clinopyroxene thermometry again shows the wide range (653-1370°C) also observed in the other nepheline gneisses and the application of the thermometry of Powell & Powell (1977) is not possible due to the absence of K-feldspar. Furthermore, the plagioclase-scapolite geothermometer of Goldsmith and Newton (1977) is restricted to Na-poor scapolite and calcic plagioclase. Equilibrium phase diagram calculations with the Theriak-Domino program did not show any stability field of scapolite, which is probably due to the lack of a reasonable solid solution model in the tcdb55c2 dataset. Furthermore, the calculations indicated the presence of K-feldspar over the widest parts of the phase diagram, which results from the lack of a solid solution model for nepheline. Furthermore, an intersection of the garnet isopleths (Alm, Grs, Adr) was not observed, which is probably mainly due to the problematic estimate of ferric iron in garnet and clinopyroxene.

In the clinopyroxene-clinoamphibole gneiss YKK-2d, the application of the Ti-in-amphibole geothermometer of Colombi (1988) on the Ti-rich pargasite leads to temperatures of 729-765°C. This is in accord with the amphibole-plagioclase geothermometer of Holland & Blundy (1994), which calculates 774-784°C. Due to the lack of critical mineral assemblages, a pressure estimate is delicate. A combination of the Ti-in-Hbl geothermometer of Colombi (1988) with the amphibole-plagioclase P1-geobarometer of Bhadra and Bhattacharya (2007) using the average composition of all

clinoamphibole and plagioclase analyses yields 10.7 kbar at 746°C. However, due to the absence of quartz in the rock which, this pressure estimate can only be regarded as maximum value. Equilibrium phase diagram calculations with the Theriak-Domino program and the tcds62c dataset, which supplies a very sophisticated clinoamphibole model, shows a wide stability field for the observed mineral assemblage in the rock (Figure 3.8f). An intersection of the Ti-in Hbl barometry with this stability field indicates PT-conditions of 730-765°C at 6.2-9.5 kbar at aH_2O=0.4, which is in accord with the results from the other samples.

3.7 Geochemistry of the nepheline gneisses and the clinopyroxene-clinoamphibole gneiss

The nepheline and clinopyroxene-clinoamphibole gneisses are high-K calcalkaline (YKK-1c, YKK-2d) and shoshonitic (M25, YKK-1a) rocks (cf. Figure 3.9a). The nepheline bearing rocks are characterized by variable, but low to moderate SiO_2 contents (39.1 to 50.4 wt.-%), relatively low MgO contents (0.62 to 1.39 wt.-%), and high Na_2O+K_2O contents (7.57 to 11.1 wt.-%) and correspond chemically to foidite, phonotephrite, or thephriphonolite (Figure 3.9b). The low contents of the compatible elements Ni and Cr in combination with the low MgO contents indicate that these rocks have experienced significant fractionation. These rocks have high CaO contents that range from 6.96 wt.-% to 19.6 wt.-% (Table 3.10). Alkaline magmatic rocks with these chemical signatures may be obtained by fractionation of clinopyroxene, which reduces the contents of Mg, Ni, and Cr and allows for an increase of SiO_2 and high CaO (Table 3.10). Typical examples for such rocks include leucitites and foidites (e.g., Lustrino et al. 2019; Prelević et al. 2015). The formation of such rocks involved the partial melting of a lithospheric mantle source that first had been depleted by partial melting and then became enriched by fluids and melts derived from subducted sedimentary or crustal material. Partial melting of this source typically occurs during an event separate from metasomatism, as for instance changing slab geometry that results in extension with adiabatic melting of metasomatized domains (e.g. Lustrino et al. 2019; Prelević et al. 2015). Interaction with the hosting carbonates also may increase the CaO (and Sr) and decrease the SiO_2 contents of these alkaline magmatic rocks (e.g. Conte et al. 2009; Elitok 2019).

The clinopyroxene-clinoamphibole gneiss has high MgO (12.5 wt.-%) and relatively low contents of Na_2O+K_2O (2.43 wt.%) and possibly originally was a picrobasalt. This sample has high contents of the compatible elements Co, Ni, and Cr and, therefore, did not experience significant

fractionation. Calculations of the CIPW normative mineralogy (total Fe=Fe^{2+}) show that all the rocks are nepheline-normative while samples YKK-1a and M-25 additionally contain leucite.

In the Nb-Zr-Y triangle of Meschede (1986), a ternary tectonic discrimination diagram, these rocks fall in the fields of volcanic arc basalt/N-MORB (YKK-1a & YKK-2d) and volcanic arc basalt/within plate tholeiite (M-25) whereas sample YKK-1c lies in the N-MORB field (Figure 3.10a). In the Ti-Zr-Y triangle of Pearce & Cann (1973), the nepheline gneisses plot in or close to the calcalkaline basalt field while the clinopyroxene-clinoamphibole-gneiss shows a position in the calcalkaline basalt/island arc tholeiite field (Figure 3.10b). In the TiO_2-MnO-P_2O_5 triangle of Mullen (1983), two nepheline gneisses (YKK-1a and YKK-1c) and the clinopyroxene-clinoamphibole gneiss YKK-2d reveal a position in the island arc tholeiite field whereas nepheline gneiss M-25 plots in the MORB field (Figure 3.10c). In conclusion, all three diagrams demonstrate that the metamorphic dykes from Myanmar have close relations to calcalkaline magmatics and to volcanic arc basalts and therefore probably originate from a subduction-related magmatic setting. The use of tectonic discrimination diagrams, however, may be problematic for the nepheline gneisses, in part as some diagrams originally were defined for basalts and alkali basalts and other diagrams include Ti that may be mobile in systems with CO_2 (e.g. Hynes 1980).

Table 3.10 Geochemical analyses of main and trace elements.

Samples	YKK-1a	YKK-1c	YKK-2d	M-25
	Major element analyses (wt.-%)			
SiO_2	45.69	50.35	43.78	39.11
TiO_2	0.75	0.61	0.93	1.4
Al_2O_3	16.9	24.43	12.6	16.38
Fe_2O_3	12	4.22	11.09	8.12
MnO	0.31	0.1	0.18	0.19
MgO	0.71	0.62	12.5	1.39
CaO	11.95	6.96	13.82	19.55
Na_2O	6.35	9.41	1.56	4.79
K_2O	3.44	1.67	0.87	2.78
P_2O_5	0.34	0.07	0.24	0.71
H_2O	0.34	0.78	1.35	0.34
CO_2	0.57	0.23	0.29	4.6
Total:	99.36	99.45	99.2	99.34
	Trace element analyses (ppm)			
Co	16	6	51	18
Ni	2	3	128	1
Cr	<10	<10	684	<10
V	42	3	311	122
Ga	14	18	13	14
Rb	226	94	9	95
Sr	789	1726	312	386
Y	49	19	22	49
Zr	154	72	48	224
Nb	4	11.9	2.5	11.6
Cs	5.2	2.3	0.2	1
Ba	656	1756	94	392
La	42	18	7.8	44
Ce	90	33	24	93
Pr	11	4.1	3.8	11
Nd	43	15	19	45
Sm	8.5	2.6	4.5	9.5
Eu	2.4	1.2	1.2	2.5
Gd	8.3	2.6	4.6	9.2
Tb	1.3	0.4	0.7	1.4
Dy	8.3	2.9	4.3	9.3
Ho	1.8	0.6	0.8	1.8
Er	5.6	2.1	2.5	5.6
Tm	0.9	0.3	0.4	0.8
Yb	6.2	2.2	2.3	5.2
Lu	0.9	0.3	0.3	0.7
Hf	2.9	2.1	2.2	3.9
Tl	0.7	0.5	0.1	0.5
Pb	6.2	9.2	2.2	5.6
Th	6.5	5.1	0.3	18.5
U	1.8	1.9	0.1	4.4

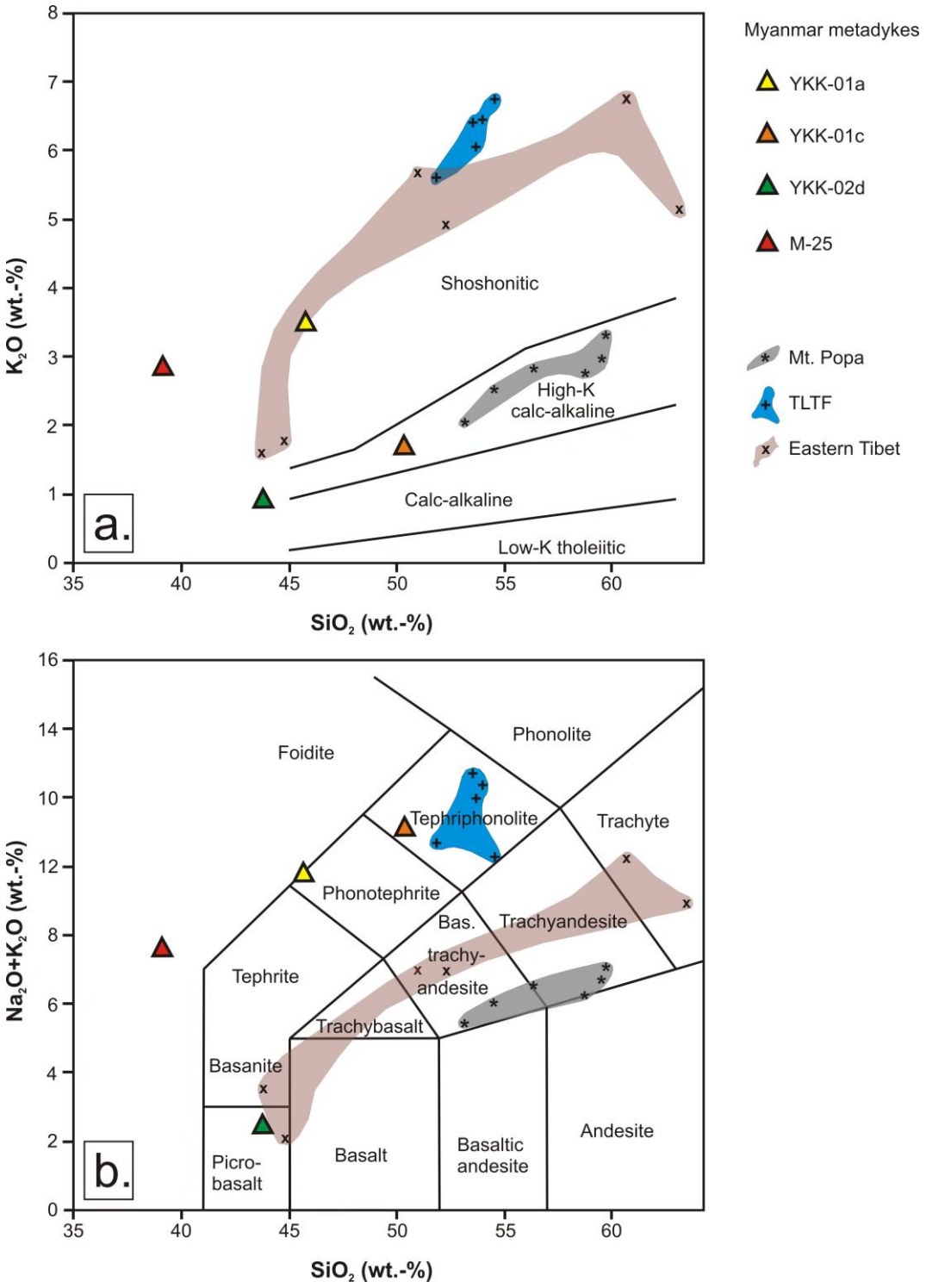

Figure 3.9 (a) K_2O vs. SiO_2-diagram with series boundaries after Rickwood (1989) with the Myanmar metadykes and distribution field of arc volcanics from Mt. Popa in Myanmar (H.-Y. Lee et al. 2016) and Tabar-Lihir-Tanga-Feni islands (TLTF; Horz et al. 2004) as well as shoshonites from Eastern Tibet (Campbell et al. 2013). b.) Total alkali vs. silica diagram after Le Bas et al.(1986).

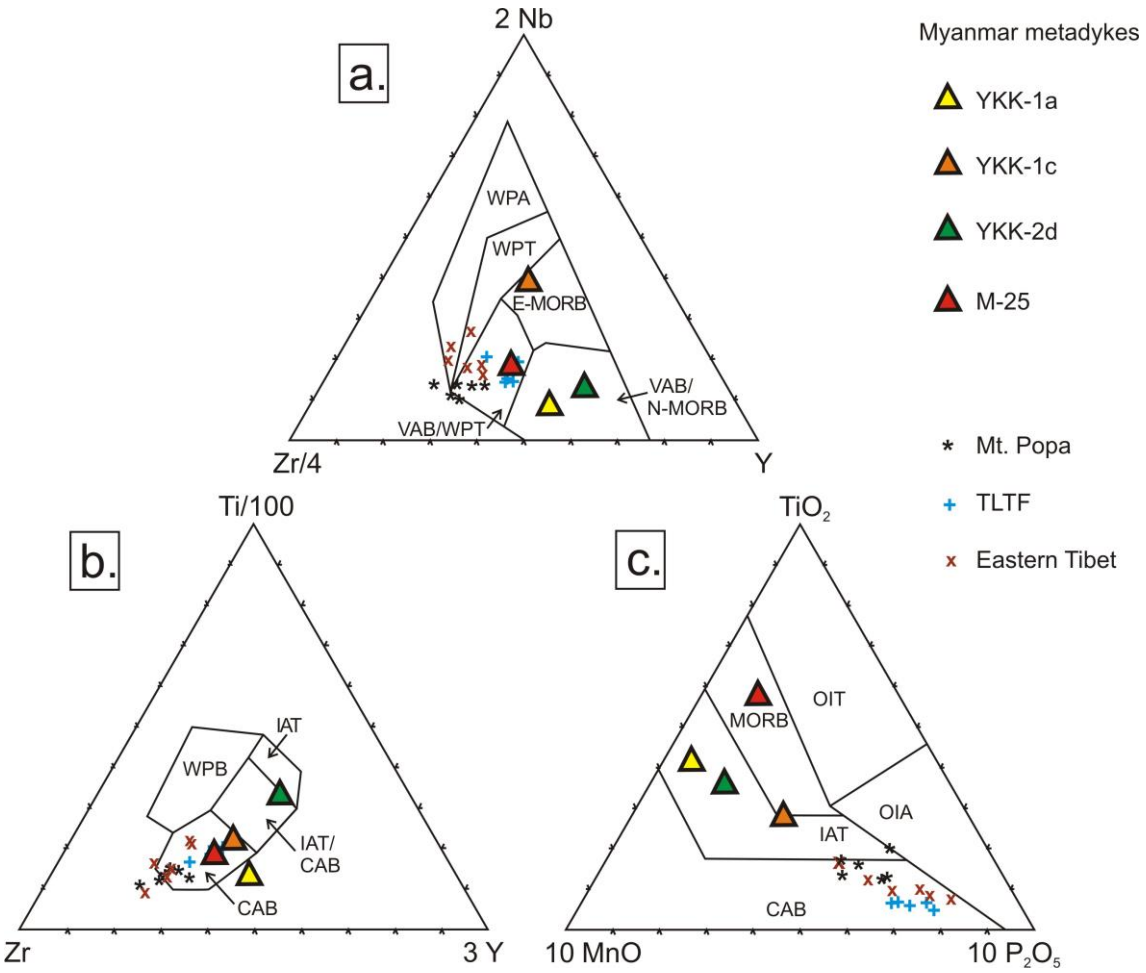

Figure 3.10 Ternary tectonic discrimination diagrams showing the position of Myanmar metadykes and volcanics from similar settings, i.e. Mt. Popa, Tabar-Lihir-Tanga-Feni (TLTF) and Eastern Tibet; (citations see Figure 9) a.) Nb–Zr–Y diagram after Meschede (1986), b.) T-Zr-Y diagram after Pearce and Cann (1973) and c.) TiO_2-MnO-P_2O_5-diagram after Mullen (1983).

For a further comparison, three suits of subduction-related magmatic rocks from different settings and locations were chosen. The first suite incorporates high-calcalkaline trachyandesites and basaltic trachyandesites (see Figure 3.9) from the volcanic arc Mt. Popa (Myanmar), which formed in Mid-Miocene by partial melting of a juvenile mantle wedge during the subduction of the Indian oceanic lithosphere under the Burma plate (Lee et al. 2015). The second suite of magmatics is made up of Late Quaternary shoshonites from the Tabar-Lihir-Tanga-Feni volcanic fore-arc chain (Figure 3.9), which formed in an enriched mantle during the subduction of the Pacific plate underneath the Bismarck microplate in Papua New Guinea (Group A volcanic ashes of Horz et al.

2004). The third suite consists of intrusive shoshonites from Eastern Tibet (Figure 3.9), which formed by melting of Indian crust at mantle depth during the subduction of Indian crust beneath Eurasia in Eocene/Oligocene time (Campbell et al. 2014). In the Nb-Zr-Y triangle of Meschede (1986), most of Mt. Popa and TLTF rocks plot in the volcanic arc field close to sample M-25, while the East Tibetan shoshonites range from the volcanic arc field over the within plate tholeiite field to the within plate andesite field (Figure 3.10a). In the Ti-Zr-Y triangle of Pearce & Cann (1973), most samples from all three magmatic rock suits display a position within or next to the calcalkaline basalt field (Figure 3.10b), close to the samples YKK-1a, YKK-1c and M-25. In the TiO_2-MnO-P_2O_5 triangle of Mullen (1983), the three magmatic rock suits plot in the calcalkaline basalt and the island arc tholeiite field (Figure 3.10c).

The trace element pattern of the various magmatic rocks is little affected by interaction with the carbonates that have low contents for most trace elements. Addition of carbonates would result in a reduction of the trace element contents, with the possible exception of Sr that may reach high contents in some carbonates. The nepheline gneisses have Sr contents of 380 to 1730 ppm. Most notably, sample with the highest Ca content has the lowest Sr content. Thus, the relation between Sr and Ca is likely to be controlled by different processes than interaction with the carbonate wall rocks. The two groups of rocks (nepheline vs. clinopyroxene-clinoamphibole bearing) also have different trace element patterns, reflecting possibly not only different degree of fractionation, but also different magma sources.

To highlight the similarities between the three magmatic rock suites and the metadykes from Myanmar, MORB-normalized spidergrams were compiled. The trace element patterns of the nepheline-bearing rocks are strongly enriched in Cs, Rb, Ba, Th, and U, show positive anomalies in K and Pb and variably negative anomalies for Ti, Nb, and possibly Ta (Figure 3.11a). Although the pattern of the clinopyroxene-clinoamphibole gneiss YKK-2d is similar to the other patterns and also reveals a negative Nb anomaly, it does not have such a steep inclination. The trace element patterns observed in the Myanmar metadykes are typical for rocks derived from the lithospheric mantle that have been modified by the subduction of material from the continental crust, as for instance from volcanic arc rocks, but also shoshonites and orogenic lamprophyres (Lee et al. 2016; Horz et al. 2004; Campbell et al. 2014). Consequently, the trace element patterns of the Myanmar metadykes strongly resemble to the patterns of the arc-volcanics from Mt. Popa (Figure 3.11b), to the fore-arc

volcanics from Tabar-Lihir-Tanga-Feni (Figure 3.11c) and to the shoshonites from Tibet (Figure 3.11d).

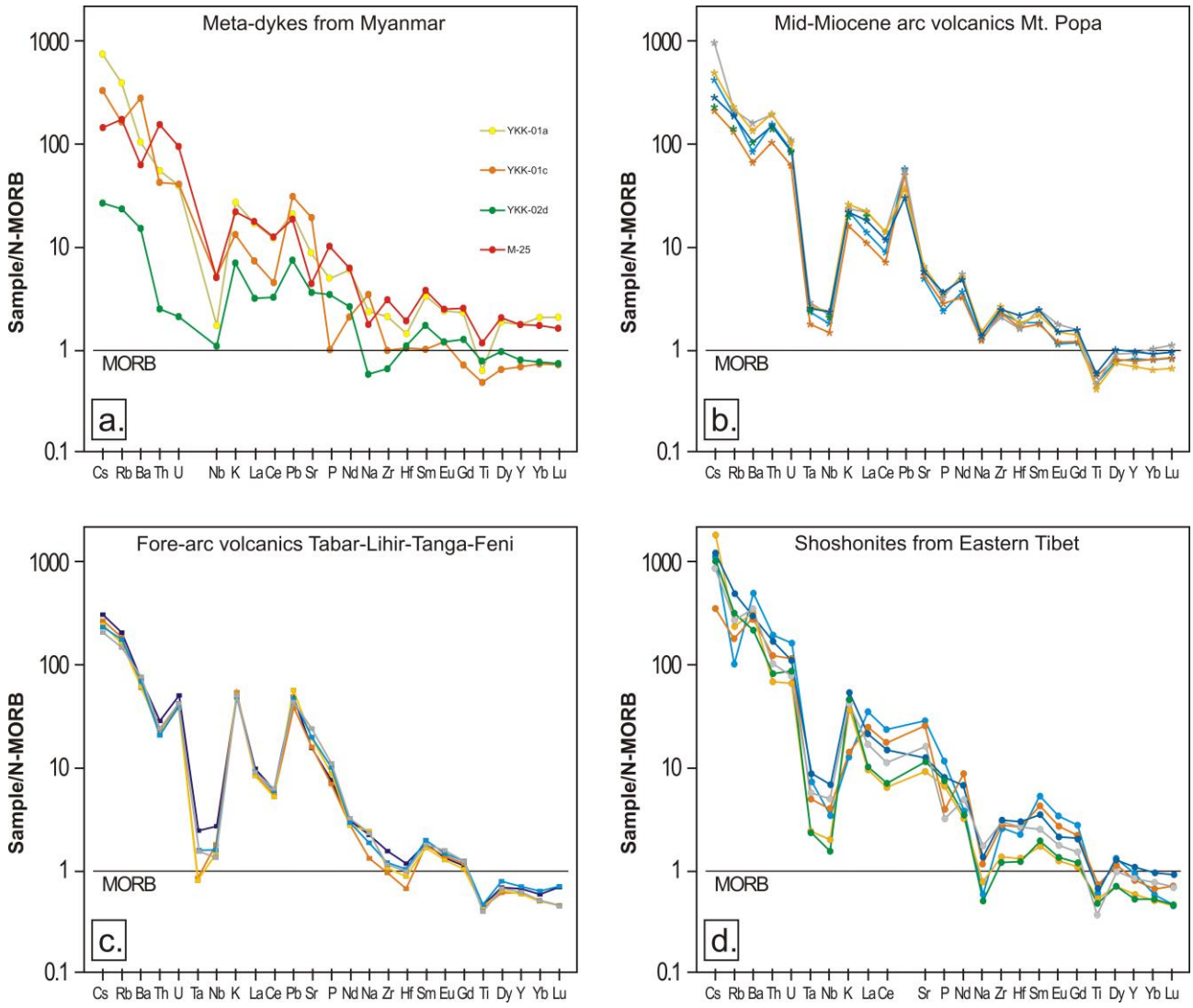

Figure 3.11 MORB-normalized spidergrams with N-MORB values for normalization after Pearce and Parkinson (1993) with a.) Myanmar metadykes; b.) arc volcanics from Mt. Popa (Myanmar; cf. Lee et al. 2016); c.) fore-arc volcanics from the Tabar-Lihir-Tanga-Feni islands (Papua New Guinea; cf. Horz et al. 2004) and d.) subduction-related shoshonites from Eastern Tibet (cf. Campbell et al. 2013).

The subduction signature is not only contained in the Ti-Nb anomaly, but also the slightly enhanced K and Pb contents, and most importantly in the Sr-Nd-Pb isotopic composition (Figures 3.12 & 3.13 and Table 3.11). For instance, the Pb isotopic compositions of all samples fall in a relatively narrow range with $^{206}Pb/^{204}Pb$ values of 18.3 to 19.0 and very high $^{207}Pb/^{204}Pb$ values of 15.71 to 15.76 (Figure 3.12a). Such high $^{207}Pb/^{204}Pb$ values imply derivation of Pb from very old, i.e., Paleoproterozoic or Archean, continental crust. The relatively high $^{208}Pb/^{204}Pb$ values of 38.5 to 39.2 (Figure 3.12b) make these samples fall above typical upper crustal and orogenic Pb growth curves and therefore indicate that this crustal material also includes contribution of material that has experienced high-grade metamorphism in the Neoproterozoic or Archean. The Indian subcontinent may be the source of such Pb and subduction of sediments derived from this continent may have brought this Pb to the lithospheric mantle. As the depleted mantle has low Pb contents, the Pb isotopic composition of rocks derived from the lithospheric mantle will be dominated by the subducted material (e.g., Hofmann 1988; Prelević et al. 2008). In contrast to Pb, the mixtures of material derived from the mantle and subducted sedimentary material derived from the continental crust is clearly visible in isotopic composition of Sr and Nd (Figure 3.13). Typical Neoproterozoic and Archean continental crustal has εNd_0 values around -18 and -30, respectively, which implies that the observed Nd isotopic compositions of the gneisses include 25 to 45 % contribution of crustal Nd, depending on age of the subducted material and the composition of the depleted mantle. Using the isotopic composition of metamorphic rocks of the Himalayas as a proxy for the isotopic composition of the material that was subducted before the collision illustrates that ancient crustal significantly contributed the crustal isotopic and geochemical fingerprint of the magmatic rocks (cf. Figure 3.13).

It should be noted that the crustal rocks of Myanmar have too high εNd_0 values (using the isotopic composition of sedimentary rocks as a proxy) to be the major source of the crustal material in the magmatic rocks. Isotopic data, however, do not exclude that local crustal rocks contributed to the crustal signature of the magmatic rocks. Isotope data just imply that Myanmar was not the major source of the crustal material (cf. Figure 3.13). The Sr isotopic composition is far more variable than the one of Nd, and therefore, similar mass balance estimates are highly uncertain. The radiogenic Sr isotopic composition of 0.7075 to 0.7087, however, is far more radiogenic than depleted mantle. It should be noted that because of the contrasting trace element contents of metasoma and depleted mantle (as for instance in a veined-mantle type source as commonly employed form lamprophyres or shoshonites), these simple mass balance estimates only apply to respective elements, but not to the rock volumes. If the protolith of the clinopyroxene-

clinoamphibole gneiss is derived from a similar source as the nepheline gneisses, the Sr and Nd isotopic data may reflect a lower metasome to ambient mantle ratio, which also accounts for the distinctly lower content of incompatible trace elements, and little or no fractional crystallization contributing to the higher content of compatible elements.

Table 3.11 Whole-rock Sr, Nd, and Pb isotope composition of the nepheline gneisses and the clinopyroxene-clinoamphibole gneiss (Myanmar); initials calculated for 30 Ma.

	Sample [a]	^{87}Sr / ^{86}Sr [b]	$^{87}Sr_{30}$ / ^{86}Sr [c]	^{143}Nd / ^{144}Nd [b]	εNd_{30} [c]	^{206}Pb / ^{204}Pb [d]	^{207}Pb / ^{204}Pb [d]	^{208}Pb / ^{204}Pb [d]	$^{206}Pb^{30}$ / ^{204}Pb [e]	$^{207}Pb^{30}$ / ^{204}Pb [e]	$^{208}Pb_{30}$ / ^{204}Pb [e]
1	M-25	0.710642±5	0.70930	0.512239±2	0.51221	19.211	15.773	39.484	18.97	15.76	39.16
2	YKK-1a	0.709083±5	0.70874	0.512404±3	0.51238	18.956	15.763	39.202	18.87	15.76	39.10
3	YKK-1c	0.707976±4	0.70791	0.512243±2	0.51222	18.379	15.712	38.529	18.32	15.71	38.47
4	YKK-2d	0.706561±5	0.70653	0.512372±4	0.51234	18.604	15.737	39.001	18.59	15.74	38.99

Samples were dissolved with concentrated HF for four days at 160°C on the hot plate. Digested samples were dried, taken up in 2N HNO_3, and slowly dried at 80°C over night. The nitrates were taken up in 6N

[a] HCl and dried. Sr and Nd were separated and purified using ion-exchange chromatography as described in Romer et al. (2005) and Romer & Hahne (2010). Pb was separated using the HBr-HCl ion-exchange procedure described in Romer et al. (2001, 2005).

$^{87}Sr/^{86}Sr$ and $^{143}Nd/^{144}Nd$, normalized to $^{86}Sr/^{88}Sr = 0.1194$ and $^{146}Nd/^{144}Nd = 0.7219$, respectively, were obtained on a Thermo-Triton mass-spectrometer using dynamic multi-collection. Analytical

[b] uncertainties are given at $2\sigma_m$ level. Strontium and Nd reference materials NBS987, La Jolla, and JNdi-1 gave longtime values of =.710258 ± 8 (2SD, n= 11), 0.511854 ± 8 (2SD, n= 10), and 0.512095 ± 18 (2 SD, n=18), respectively.

$^{87}Sr/^{86}Sr_{30}$ and εNd_{30} were calculated for the age of the predominant zircon population, using $\lambda^{87}Rb =$

[c] 1.3972E-11 y^{-1} and $\lambda^{147}Sm = 6.54E\text{-}12\ y^{-1}$, $(^{147}Sm/^{144}Nd)^0_{CHUR} = 0.1967$, and $(^{143}Nd/^{144}Nd)^0_{CHUR} = 0.512638$, respectively, and the concentration data given in Table 3.10.

Lead isotope data were obtained on a Thermo-Triton mass-spectrometer using static multi-collection

[d] and corrected for instrumental mass discrimination with 0.1% / A.M.U. Accuracy at the 2σ level is better than 0.1%.

Lead isotope data recalculated to the age of the predominant zircon population, using contents of Pb,

[e] Th, and U from Table 3.10 and decay constants recommended by the IUGS: $\lambda^{238}U = 1.55125E\text{-}10\ y^{-1}$; $\lambda^{235}U = 9.848E\text{-}10\ y^{-1}$; $\lambda^{232}Th = 4.9475E\text{-}11\ y^{-1}$.

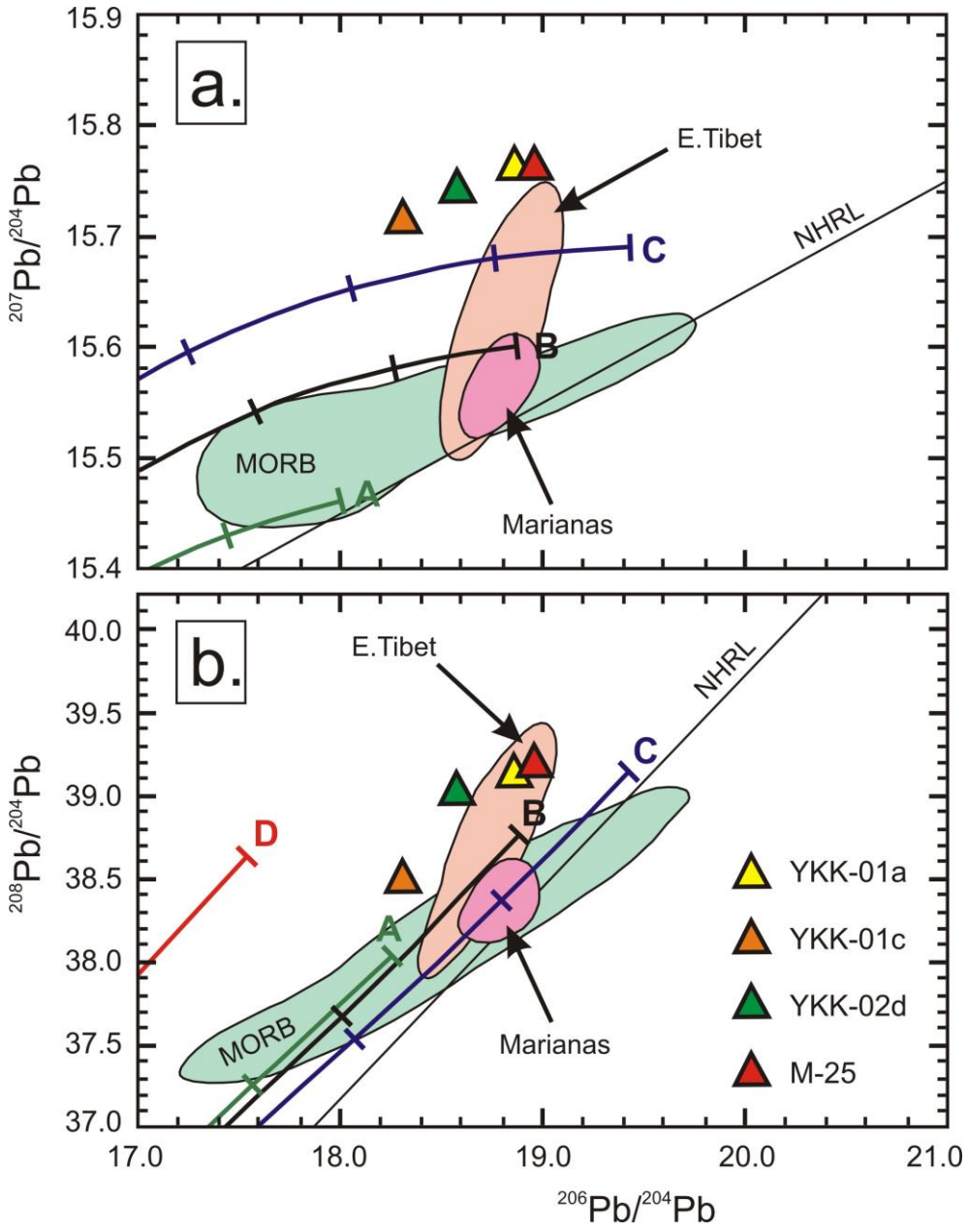

Figure 3.12 (a.) Plot of $^{207}Pb/^{204}Pb$ against $^{206}Pb/^{204}Pb$ and b.) Plot of $^{208}Pb/^{204}Pb$ against $^{206}Pb/^{204}Pb$. Data for MORB, Eastern Tibet, Marianas, NHRL and HIMU from Campbell et al. (2014). Lead-isotope evolution curves for the mantle (A), orogene (B), upper crust contributed to the orogene (C), and lower crust contributed to the orogene (D) by Zartman & Doe (1981). Tig marks along each curve indicate progressively older time in 0.4-b.y. increments.

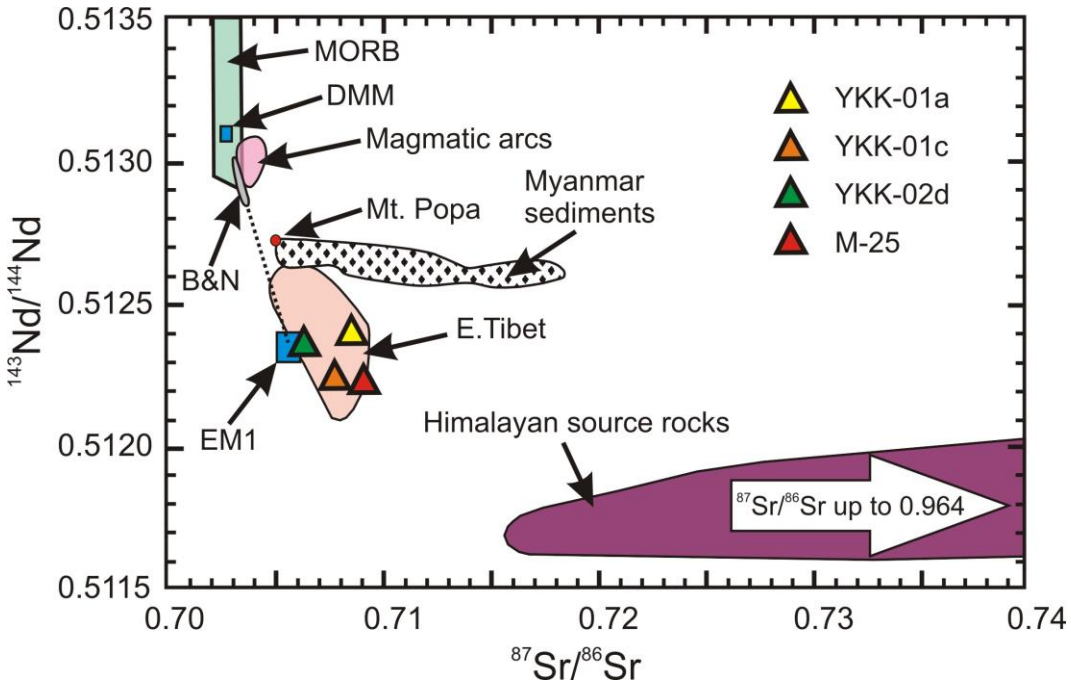

Figure 3.13 Plot of $^{143}Nd/^{144}Nd$ against $^{87}Sr/^{86}Sr$ with the metadykes from Myanmar, MORB and Eastern Tibet shoshonites (Campbell et al. 2014), magmatic arc volcanics from Marianas, New Britain, Aleutians, South Sandwich and Lesser Antilles (Arculus and Powell 1986), arc volcanics from Mt. Popa (red spot; Lee et al. 2016) and Myanmar sediments (Licht et al. 2013). Isotope data of basanites and nephelinites (B&N) with mixing array (dotted line) between enriched mantle (EM1) and depleted mantle (DMM) from Faure (2001; page 314). Himalayan source rocks for subduction from Ahmad et al. (2000), Miller et al. (2001) and Richards et al. (2005).

3.8 Discussion and conclusions

Petrological and conventional thermobarometric investigations reveal granulite facies metamorphic conditions of 756-792°C at 7.4-7.6 kbar for quartz-garnet gneisses from the Mogok area of the MMB. These findings are in accord with earlier investigations (e.g. Thu et al. 2016) of the same area. A combination of equilibrium phase diagram calculations using the Theriak-Domino program and conventional geothermobarometry reproduces these data and reveals water activities of 0.34-0.4 in the investigated samples. Another method to estimate the water activity in the quartz-garnet gneiss sample is given by the modal mineral amount of the sample calculated by the Theriak-Domino program at the intersection point of the garnet isopleths at different a_{H2O}-values. For the three quartz-garnet gneiss samples, the best fit between the calculated mineral amount and the modal mineral amount determined by point-counting of the thin section is given at a_{H2O}=0.2-0.5 and thus in line with the data above. For the calculation of granulite facies conditions, numerous researchers (e.g. Tajčmanová et al. 2006; Xiang et al. 2012) use a fixed but limited amount of H_2O, which implies the absence of a free fluid at certain metamorphic PT-conditions and therefore dry conditions. The worldwide observation of fluid inclusions in granulite facies rocks (e.g. Bader et al. 2014; Newton et al. 1998; Santosh and Omori 2008; Touret 1971; Touret and Huizenga 2012) and the presence of granulite facies, fluid bearing minerals like biotite in the investigated gneisses renders fluid-absence unlikely. Therefore, the Theriak-Domino calculations of this study were performed with H_2O in excess but with controlled water activity. As evident from the equilibrium phase diagram calculations and their analogy with the petrology of the rocks and the conventional geothermobarometry, these a_{H2O}-values appear to model the granulite facies conditions of the Mogok area quite nicely. The calculated water activities are similar to those calculated with the Theriak-Domino program for felsic and mafic granulites from the Tongbai in east-central China (Bader et al. 2014).

The presence of garnet-nepheline gneisses in association with clinopyroxene-clinoamphibole gneiss within spinel- and ruby-bearing marbles and calcsilicate rocks is quite remarkable. Nepheline- and corundum bearing gneisses have been described from several locations worldwide, e.g. from the Haliburton-Bancroft area of Ontario (USA), where they are assumed to have formed by magmatic interaction of granites with calcsilicate rocks and mafic gneisses (Moyd 1949). Nepheline gneisses also occur in the vicinity of the Darkainle nepheline-syenite complex in Somali, where they formed during metasomatic processes in the high-grade, migmatitic host rocks of the syenites (Gellatly & Hornung 1968). In the Ilomba and Ulindi complexes of the North Nyasa

Alkaline Province (Malawi), nepheline gneisses were generated by pre- to syntectonic intrusions of nepheline syenites under upper greenschist- to amphibolite facies conditions (Eby et al. 1998). None of these nepheline gneisses, however, bears any garnet and none of them experienced granulite facies metamorphic conditions, which makes the Mogok nepheline gneisses unique. Despite of their exotic geochemistry, a high-grade metamorphic overprint comparable to the surrounding gneisses can be proved by equilibrium phase diagram calculations and conventional thermometry. Remarkable is also the high oxygen fugacity of these rocks, which resulted in the blastesis of aegirine-rich clinopyroxene and a garnet with a high andradite component.

The petrology of these rocks and their occurrence as dyke-shaped bodies within marble and calcsilicate rocks points to a pre- to syn-tectonic intrusion of foid-bearing, mafic dykes. This is also underlined by the geochemistry of these nepheline gneisses, which classifies their protoliths as high-K calcalkaline and shoshonitic magmatites. The nepheline gneisses show remarkably low X_{Mg}-values as well as low Ni and Cr contents, which is interpreted to result from explicit fractionation processes during ascent. Furthermore, high Ca and Sr contents point to an interaction with the hosting calcsilicate rocks and marbles. In contrast, the clinopyroxene-clinoamphibole gneiss has a distinctly higher X_{Mg}-value and different trace element patterns, which possibly not only reflect a different degree of fractionation, but also a different magma source. Discrimination diagrams demonstrate that the metamorphic dykes from Myanmar have close relations to calcalkaline magmatics and to volcanic arc basalts and therefore have strong affinities to magmatites from a subduction-related magmatic setting. These findings are also supported by MORB-normalized trace element patterns, which show a typical enrichment in Cs, Rb, K, Ba and the light REE, which is decreasing towards T, Zr, Y and V. Furthermore, a typical depletion of Nb (and possibly also Ta) is recorded in the Myanmar metadykes. The subduction signature is also revealed by the Sr-Nd-Pb isotopic composition with the origin of Pb isotopes being probably derived from Neoproterozoic or Archean crust of the Indian subcontinent. In contrast to Pb, mixtures of material derived from the mantle and subducted sedimentary material derived from the continental crust is clearly visible in isotopic composition of Sr and Nd. It is assumed that the magmatic protoliths of the nepheline gneisses may be related to the nepheline and hornblende syenites, which are found in numerous locations in Myanmar (Searle et al. 2007; 2017). These syenites intruded syn- to post-metamorphically and were dated by Barley et al. (2003) at 35-23 Ma. Geochemical data of these rocks, however, are to date not available.

3.9 Acknowledgements

First of all, we would like to thanks for financially supporters: a grant from the Kanton Basel (Stipendienkommission für Nachwuchskräfte aus Entwicklungsländern), a research grant from FAG (Freiwillige Akademische Gesellschaft Basel) and SSEF (Schweizerisches Gemmologisches Institut). Moreover, special thanks to Pascal Tschudin for his kind preparation for all rock sections. Further, special thanks to several mining companies and miners for their fascinating samples and thanks to Ah Ba and Aunty Phyu for their kind encouragement, also thanks to Sebastian Hänsel, U Aung Kyaw Htoon and Ko Ja Mu for their help during the field trip to the Mogok area, Myanmar.

References

Ahmad, T., Harris, N., Bickle, M., Chapman, H., Bunbury, J., & Prince, C. (2000). Isotopic constraints on the structural relationships between the lesser Himalayan series and the high Himalayan crystalline series, Garhwal Himalaya. *Geological Society of America Bulletin*, *112*, 467–477.

Arculus, R. J., & Powell, R. (1986). Source component mixing in the regions of arc magma generation. *Journal of Geophysical Research*, *91*(B6), 5913. doi:10.1029/JB091iB06p05913

Aung, L. L., Zin, E. E., Theingi, P., Elvera, N., Aung, P. P., Han, T. T., et al. (2017). Myanmar Climate Report. *MET report*, (9).

Bader, T., Franz, L., de Capitani, C., & Zhang, L. (2014). The effect of water activity on calculated phase equilibria and garnet isopleth thermobarometry of granulites, with particular reference to Tongbai (east-central China). *European Journal of Mineralogy*, *26*, 5–23.

Bader, T., Franz, L., De Capitani, C., & Zhang, L. (2014). The effect of water activity on calculated phase equilibria and garnet isopleth thermobarometry of granulites, with particular reference to Tongbai (east-central China). *European Journal of Mineralogy*, *26*, 5–23.

Barley, M. E., Pickard, A. L., Zaw, K., Rak, P., & Doyle, M. G. (2003). Jurassic to Miocene magmatism and metamorphism in the Mogok metamorphic belt and the India-Eurasia collision in Myanmar. *Tectonics*, *22*(3), 1–11. doi:10.1029/2002TC001398

BAS, M. J. L., MAITRE, R. W. L., STRECKEISEN, A., & ZANETTIN, B. (1986). A Chemical Classification of Volcanic Rocks Based on the Total Alkali-Silica Diagram. *Journal of Petrology*, *27*(3), 745–750. doi:10.1093/petrology/27.3.745

Bayliss, P., Mazzi, F., Munno, R., & White, T. J. (1989). Mineral nomenclature : zirconolite. *Mineralogical Magazine*, *53*, 565–569.

Bender, F. (1983). *Geology of Burma*.

Bertrand, G., Rangin, C., Maluski, H., & Bellon, H. (2001). Diachronous cooling along the Mogok Metamorphic Belt (Shan Scarp , Myanmar): the trace of the northward migration of India-Indochina oblique convergence since the Oligocene. *Journal of Asian Earth Sciences*, *19*, 649–659. doi:10.1016/S1367-9120(00)00061-4

Bertrand, G., Rangin, C., Maluski, H., Han, T. A., Thein, M., Myint, O., et al. (1999). Cenozoic metamorphism along the Shan scarp (Myanmar): evidences for ductile shear along the Sagaing fault or the northward migration of the eastern Himalayan syntaxis? *Geophysical Research Letters*, *26*(7), 915–918.

Bhadra, S., & Bhattacharya, A. (2007). The barometer tremolite + tschermakite + 2 albite = 2 pargasite + 8 quartz: Constraints from experimental data at unit silica activity, with

application to garnet-free natural assemblages. *American Mineralogist*, *92*, 491–502.

Bieri, W., Grobety, B., Peretti, A., Hametner, K., & Gunther, D. (2010). Chemical composition of apatite inclusions in corundum and spinel determined by LA-ICP-MS and its potential for authentication and provenance determination. *Geochimica et Cosmochimica Acta*, *74*(12), A89–A89.

Black, L. P., Kamo, S. L., Allen, C. M., Aleinikoff, J. N., Davis, D. W., Korsch, R. J., & Foudoulis, C. (2003). TEMORA 1: a new zircon standard for phanerozoic U–Pb geochronology. *Chemical Geology*, *200*, 155–170.

Brey, G. P., & Köhler, T. (1990). Geothermobarometry in four-phase lherzolites. I. New thermobarometers and practical assessment of existing thermobarometers. *Journal of Petrology*, *31*, 1353–1378.

Brook, M., & Snelling, N. J. (1976). K/Ar and Rb/Sr age determinations on rocks and minerals from Burma. *Institute of Geological Sciences, Keyworth, Nottingham, UK, Isotope Geology Unit Report*, *76*(12).

Brown, B., & Judd, J. W. (1896). The Rubies of Burma and Associated Minerals : Their Mode of Occurrence , Origin , and Metamorphoses . A Contribution to the History of Corundum. In *Philosophical Transactions of the Royal Society of London. Series A, Containing Papers of a Mathematical or Physical Character* (Vol. 187, pp. 151–228).

Campbell, I. H., Aleksandr, S., Stepanov, A. S., Liang, H.-Y., Allen, C. M., Norman, M. D., et al. (2013). The origin of shoshonites: new insights from the Tertiary high-potassium intrusions of eastern Tibet. *Contributions to Mineralogy and Petrology*, *167*, 983–1005.

Campbell, I. H., Stepanov, A. S., Liang, H. Y., Allen, C. M., Norman, M. D., Zhang, Y. Q., & Xie, Y. W. (2014). The origin of shoshonites: New insights from the Tertiary high-potassium intrusions of eastern Tibet. *Contributions to Mineralogy and Petrology*, *167*(3), 1–22. doi:10.1007/s00410-014-0983-9

Chhibber, H. L. (1934). *The Geology of Burma*. *Macmillan and Co.,Ltd, St.Martin's Street, London*.

Clegg, E. L. G. (1941). The Cretaceous and associated rocks of Burma. *Memoirs of the Geological Survey of India*, *74*(1), 1–102.

Coenraads, R. R., Lin Sutherland, F., & Kinny, P. D. (1990). The origin of sapphires: U–Pb dating of zircon inclusions sheds new light. *Mineralogical Magazine*, *54*, 113–122. doi:10.1180/minmag.1990.054.374.13

Colombi, A. (1988). *Métamorphisme et géochimie des roches mafiques des Alpes ouest-centrales (Géoprofil Viège-Domodossola-Locarno).*

Conte, A. M., Dolfi, D., Gaeta, M., Misiti, V., Mollo, S., & Perinelli, C. (2009). Experimental constraints on evolution of leucite-basanite magma at 1 and 10− 4 GPa: implications for parental compositions of Roman high-potassium magmas. *European Journal of Mineralogy*, *21*, 763–782.

De Capitani, C., & Petrakakis, K. (2010). The computation of equilibrium assemblage diagrams with Theriak/Domino software. *American Mineralogist*, *95*, 1006–1016.

Deer, W. A., Howie, R. A., & Zussman, M. A. (1992). *An introduction to the rock forming minerals.* Longman, London.

Dewey, J. F., Cande, S., & Pitman, W. C. (1989). Tectonic evolution of the India/Eurasia Collision Zone. *Eclogae Geologicae Helvetiae*, *82*(3), 717–734. doi:10.1177/053331647600900219

Dewey, J. F., Shackleton, R. M., Chengfa., C., & Sun, Y. (1988). The tectonic evolution of the Tibetan Plateau. *Phil. Trans. Roy. Soc. Lond*, *327*, 379–413.

Downs, R. T. (2006). The RRUFF Project: an integrated study of the chemistry, crystallography, Raman and infrared spectroscopy of minerals. In *Program and Abstracts of the 19th General Meeting of the International Mineralogical Association in Kobe, Japan.* (pp. O03-13).

Dzikowski, T. J. (2013). *A Comparative study of the origin of carbonate-hosted gem corundum deposits in Canada*. *unpublished thesis*. Retrieved from http://ir.obihiro.ac.jp/dspace/handle/10322/3933

Dzikowski, T. J., Dipple, G. M., Groat, L. A., Giuliani, G., & Cempírek, J. (2014). Origin of gem corundum in calcite marble: The Revelstoke occurrence in the Canadian Cordillera of British Columbia. *Lithos*, *198–199*, 281–297. doi:10.1016/j.lithos.2014.03.030

Eby, N., Woolley, A. R., Din, V., & Platt, G. (1998). Geochemistry and petrogenesis of nepheline syenites: Kaungu-Chipala, Iloba, and Ulindi nepheline syenites intrusions, North Nyasa alkaline Province, Malawi. *Journal of Petrology*, *39*, 1405–1424.

Elitok, Ö. (2019). Geology and petrology of the potassic and ultrapotassic rocks from the northern part of Senirkent (Isparta-SW Turkey): evidence of magma–carbonate wall-rock interactions. Arabian. *Journal of Geosciences*, *12*, 289–312.

Elmaleh, E., Schmidt, S. T., Karampelas, S., Link, K., Kiefert, L., Süssenberger, A., & Paul, A. (2019). U-Pb ages of zircon inclusions in Sapphires from Ratnapura and Balangoda (Sri Lanka) and Implications for Geographic origin, (May). doi:10.5741/GEMS.55.1.18

Faure, G. (2001). Alkalic Igneous Rocks on the Continents. In H. Springer, Berlin (Ed.), *Origin of Igneous Rocks* (pp. 281–350). Berlin, Heidelberg: Springer Berlin Heidelberg. doi:10.1007/978-3-662-04474-2_6

Fermor, L. L. (1930). *General report for the Geological Survey of India*. *Records of the Geological Survey, India*.

Gardiner, N. J., Robb, L. J., Morley, C. K., Searle, M. P., Cawood, P. A., Whitehouse, M. J., et al. (2016). The tectonic and metallogenic framework of Myanmar: A Tethyan mineral system. *Ore Geology Reviews*, *79*, 26–45. doi:10.1016/j.oregeorev.2016.04.024

Gardiner, N. J., Searle, M. P., Morley, C. K., Whitehouse, M. P., Spencer, C. J., & Robb, L. J. (2016). The closure of Palaeo-Tethys in Eastern Myanmar and Northern Thailand: New insights from zircon U–Pb and Hf isotope data. *Gondwana Research*, *39*, 401–422. doi:10.1016/j.gr.2015.03.001

Garnier, V., Long, P. Van, Fallick, A. E., Maluski, H., Lhomme, T., Giuliani, G., et al. (2008). Marble-hosted ruby deposits from Central and Southeast Asia: Towards a new genetic model. *Ore Geology Reviews*, *34*(1–2), 169–191. doi:10.1016/j.oregeorev.2008.03.003

Garnier, V., Maluski, H., Ohnenstetter, D., Giuliani, G., & Schwarz, D. (2006). Ar-Ar and U-Pb ages of marble-hosted ruby deposits from central and southeast Asia. *Canadian Journal of Earth Sciences*, *43*(4), 509–532. doi:10.1139/e06-005

Garnier, V., Ohnenstetter, D., Giuliani, G., Blanc, P., & Schwarz, D. (2002). Trace-element contents and cathodoluminescence of “trapiche” rubies from Mong Hsu, Myanmar (Burma): Geological significance. *Mineralogy and Petrology*, *76*(3–4), 179–193. doi:10.1007/s007100200040

Garnier, V., Ohnenstetter, D., Giuliani, G., Maluski, H., Deloule, E., Trong, T. P., et al. (2005). Age and significance of ruby-bearing marble from the Red River Shear Zone, Northern Vietnam. *The Canadian Mineralogist*, *43*, 1315–1329.

Gellatly, D. C., & Hornung, G. (1968). Metasomatic nepheline-bearing gneisses from Darkainle Somali Republic. *The Journal of Geology*, *76*, 678–691.

GIAC. (1999). *The Tectonic of Myanmar: Final report GIAC project 1996-1999*.

Giuliani, G., Dubessy, J., Ohnenstetter, D., Banks, D., Branquet, Y., Feneyrol, J., et al. (2018). The role of evaporites in the formation of gems during metamorphism of carbonate platforms: a review. *Mineralium Deposita*, *53*(1). doi:10.1007/s00126-017-0738-4

Giuliani, G., Fallick, A. E., Boyce, A. J., Pardieu, V., & Pham, V. L. (2017). Pink and red spinels in marble: Trace elements, oxygen isotopes, and sources. *The Canadian Mineralogist*, *55*, 743–761. doi:10.3749/canmin.1700009

Giuliani, G., Fallick, A. E., Garnier, V., France-Lanord, C., Ohnenstetter, D., & Schwarz, D. (2005). Oxygen isotope composition as a tracer for the origins of rubies and sapphires. *Geology*, *33*(4), 249–252. doi:10.1130/G21261.1

Giuliani, G., Lhomme, T., Dubessy, J., Ohnenstetter, D., & Banks, D. A. (2015). Fluid inclusions in ruby from Asian marble deposits: genetic implications. *European Journal of Mineralogy*, *27*, 393–404. doi:10.1127/ejm/2015/0027-2442

Goldsmith, J. R., & Newton, R. C. (1977). Scapolite-plagioclase stability relations at high pressures and temperatures in the system NaAlSi3O8-CaAl2Si2O8-CaCO3-CaSO4. *American Mineralogist*, *62*, 1063–1081.

Gübelin, E. J. (1965). The Ruby Mines in Mogok in Burma. *Journal of Gemmology*, *9*(12), 411–426.

Gübelin, E. J., & Koivula, J. I. (1986). *Photoatlas of Inclusions in Gemstones, ABC Edition*.

Gübelin, E. J., & Koivula, J. I. (2005). *Photoatlas of Inclusions in Gemstones, Vol. 2*.

Gübelin, E. J., & Koivula, J. I. (2008). *Photolas of Inclusions in Gemstones, Vol. 3*.

Halford-Watkins, J. F. (1932a). The Ruby Mines of Upper Burma: A Short History of their Working,. *The Gemmologist*, *1*(9), 263–272.

Halford-Watkins, J. F. (1932b). Methods of Ruby Mining in Burma. *The Gemmologist*, *1*(11), 335–342.

Halford-Watkins, J. F. (1932c). Methods of Ruby Mining in Burma. *The Gemmologist*, *1*(12), 367–373.

Harlow, G. E., Sorensen, S. S., & Sisson, V. B. (2007). Jade, in Groat, L.A., ed., The Geology of Gem Deposits: Quebec. *Mineralogical Association of Canada, Short Course Series, 37*, 207–254.

Hawthorne, F. C., Oberti, R., Harlow, G. E., Maresch, W. V., Martin, R. F., Schumacher, J. C., & Welch, M. D. (2012). Nomenclature of the amphibole supergroup. *American Mineralogist*, *97*, 2031–2048.

Henry, D. J., Guidotti, C. V., & Thomson, J. (2005). The Ti-saturation surface for low-to-medium pressure metapelitic biotites: Implications for geothermometry and Ti-substitution mechanisms. *American Mineralogist*, *90*, 316–328.

Hofmann, A. W. (1988). Chemical differentiation of the Earth: the relationship between mantle, continental crust, and oceanic crust. Earth and. *Planetary Science Letters*, *90*, 297–314.

Holdaway, M. J. (2000). Application of new experimental and garnet Margules data to the garnet-biotite geothermometer. *American Mineralogist*, *85*, 881–892.

Holland, T., & Blundy, J. (1994). Non-ideal interactions in calcic amphiboles and their bearing on amphibole-plagioclase thermometry. *Contributions to Mineralogy and Petrology*, *116*, 433–447.

Horz, K. H., Worthington, T. J., Winn, K., & Stoffers, P. (2004). Late Quaternary tephra in the New Ireland Basin, Papua New Guinea. *Journal of Volcanology and Geothermal Research*, *132*(1),

73–95. doi:10.1016/S0377-0273(03)00421-9

Htay, K. N., Aung, L. T., Tajcmanova, L., & Heinrich, C. A. (2017). The Evidances of High Temperature-Medium Pressure, Granulite grade metamorphism in Momeik Area, Mogok Metamorphic Belt, Myanmar. In *Conference Abstract of 1st Myanmar Applied Earth Sciences Associtation*.

Hughes, R. W. (1997). *Ruby & Sapphire*.

Hughes, R. W. (2014). *Ruby & Sapphire—A Collector's Guide*.

Hughes, R. W. (2016). *Ruby & Sapphire: A Gemologists Guide*.

Hynes, A. (1980). Carbonatization and mobility of Ti, Y, and Zr in Ascot Formation metabasalts, SE Quebec. *Contributions to Mineralogy and Petrology*, *75*, 79–87.

Iyer, L. A. N. (1953). *The Geology and Gemstones of the Mogok Stone Tract, Burma*.

Jackson, S. E., Longerich, H. P., Dunning, G. R., & Freyer, B. J. (1992). The application of laser-ablation microprobe; inductively coupled plasma-mass spectrometry (LAM-ICP-MS) to in situ trace-element determinations in minerals. *The Canadian Mineralogist*, *30*(4), 1049–1064. https://doi.org/

Jackson, S. E., Pearson, N. J., Griffin, W. L., & Belousova, E. A. (2004). The application of laser ablation-inductively coupled plasma-mass spectrometry to in situ U-Pb zircon geochronology. *Chemical Geology*, *211*(1–2), 47–69. doi:10.1016/j.chemgeo.2004.06.017

Keller, P. C. (1985). Gemstones and Their Origins. *Terra*, *23*(3–12). doi:10.1007/978-1-4684-6674-4

Koziol, A. M., & Newton, R. C. (1988). Redetermination of the anorthite breakdown reaction and improvement of the plagioclase-garnet-Al2SiO5-quartz geobarometer. *American Mineralogist*, *73*, 216–223.

La Touche, T. H. D. (1913). *Geology of the Northern Shan State*. *Office of the Geological Survey of India, Calcutta, India*.

Lal, R. K. (1993). Internally consistent recalibrations of mineral equilibria for geothermobarometry involving garnet-orthopyroxene-plagioclase-quartz assemblages and their application to the South Indian granulites. *Journal of Metamorphic Geology*, *11*, 855–866.

Leake, B. W., Wooley, A. R., Arps, C. E. S., Birch, W. D., Gilbert, M. C., Grice, J. D., et al. (1997). Nomenclature of amphiboles. Report of the subcommittee on amphiboles of the International Mineralogical Association Commission on new minerals and mineral names. *European Journal of Mineralogy*, *9*, 623–651.

Lee, H.-Y., Sun-Lin Chung, S.-L., & H.-M., H.-M. Y. (2016). Late Cenozoic volcanism in central Myanmar: Geochemical characteristics and geodynamic significance. *Lithos*, *245*, 174–190.

Lee, H. Y., Chung, S. L., & Yang, H. M. (2016). Late Cenozoic volcanism in central Myanmar: Geochemical characteristics and geodynamic significance. *Lithos*, *245*, 174–190. doi:10.1016/j.lithos.2015.09.018

Licht, A., France-Lanord, C., Reisberg, L., Fontaine, C., Soe, A. N., & Jaeger, J.-J. (2013). A paleo Tibet-Myanmar connection? Reconstructing the Later Eocene drainage systems of Central Myanmar using a multi-proxy approach. *J. Geol. Soc. London*, *170*, 929–939.

Link, K. (2015). Age determination of zircon inclusions in faceted sapphires. *J. Gemmol.*, *34*, 692–700.

Link, K. (2016). New age data for blue sapphire from Mogok, Myanmar. *J. Gemmol.*, *35*, 107–109.

Lustrino, M., Fedele, L., Agostini, S., Prelević, D., & Salari, G. (2019). Leucitites within and around the Mediterranean area. *Lithos*, *324–325*, 216–233.

Meschede, M. (1986). A method of discrimination between different types of mid-ocean ridge basalts and continental tholeiites with the Nb–Zr–Y diagram. *Chemical Geology*, *56*, 207–218.

Miller, C., Thoni, M., Frank, W., Grasemann, B., Klotzli, U., Guntli, P., & Draganits, E. (2001). The early Palaeozoic magmatic event in the Northwest Himalaya, India: source, tectonic setting and age of emplacement. *Geol. Mag.*, *138*, 237–251.

Min, M. (2007a). *Chapter 5. Exhumation of the Mogok Belt in central Myanmar:a geochronologic study. In: thermochronology applied to strike-slip zones Central Ameria and Myanmar.*

Min, M. (2007b). *Chapter 5 Exhumation of the Mogok belt in central Myanmar : a geochronologic study*.

Mitchell, A. H. G. (1993). Cretaceous-Cenozoic tectonic events in the western Myanmar (Burma)-Assam region. *Journal of the Geological Society*, *150*, 1089–1102.

Mitchell, A. H. G., Marshall, T. R., Skinner, A. C., Baker, A. D., Amos, B. J., & Bateson, J. H. (1977). Geology and exploration geochemistry of the Yadanartheingi anf Kyaukme-Longtawkno areas, Northern Shan States, Burma. *Overseas Geology and Mineral Resources*, *51*(35).

Mitchell, A. H. G., Oo, T., Win, M. N., Hlaing, T., Htun, K. M., & Htay, M. T. (2006). Rock relationships in the Mogok metamorphic belt, Tatkon to Mandalay, central Myanmar. *Journal of Asian Earth Sciences*, *29*(5–6), 891–910. doi:10.1016/j.jseaes.2006.05.009

Mitchell, A., Oo, T., Lin, T.-H., Hung, C.-H., & Chung, S.-L. (2012). Zircon U–Pb ages in Myanmar: Magmatic–metamorphic events and the closure of a neo-Tethys ocean? *Journal of Asian Earth Sciences*, *56*, 1–23. doi:10.1016/j.jseaes.2012.04.019

Morimoto, N., Fabries, J., Ferguson, A. K., Ginzburg, I. V., Ross, M., Seifert, F. A., et al. (1988). Nomenclature of amphiboles. *Mineralogy and Petrology*, *39*, 55–76.

Moyd, L. (1949). Petrology of the nepheline and corundum rocks of southeastern Ontario. *American Mineralogist*, *34*, 736–750.

Mullen, E. D. (1983). MnO/TiO2/P2O5: a major element discriminant for basaltic rocks of oceanic environments and its implications for petrogenesis. *Earth Planet. Sci. Lett.*, *62*, 53–62.

Newton, R. C., Aranovich, L. Y., Hansen, E. C., & Vandenheuvel, B. A. (1998). Hypersaline fluids in Precambrian deep-crustal metamorphism. *Precambrian Res.*, *91*, 41–63.

Norman, M. D., & Nemchin, A. A. (2014). A 4.2 billion year old impact basin on the Moon: U-Pb dating of zirconolite and apatite in lunar melt rock 67955. *Earth and Planetary Science Letters*, *388*, 387–398. doi:10.1016/j.epsl.2013.11.040

Pearce, J. A., & Cann, J. R. (1973). Tectonic setting of basic volcanic rocks using Ti, Zr and Y. *Earth and Planetary Sciences and Letters*, *19*, 290–300.

Pearce, J. A., & Parkinson, I. J. (1993). Trace element models for mantle melting: application to volcanic arc petrogenesis; in Prichard, H.M., Alabaster, T., Harris, N.B.W., and Neary, C.R., eds., Magmatic Processes and Plate Tectonics,. *Geological Society Special Publications*, *76*, 373–403.

Peretti, A., Peretti, A. K., & Günther, D. (2015). World of Magnificent Spinels Provenance and Identification. *Contributions to Gemology*, *11*(May).

Phyo, M. M., Franz, L., Bieler, E., Balmer, W., & Krzemnicki, M. S. (2019). Spinel from Mogok, Myanmar—A Detailed Inclusion Study by Raman Microspectroscopy and Scanning Electron Microscopy. *The Journal of Gemmology*, *36*(5), 418–435. doi:10.15506/JoG.2019.36.5.418

Powell, M. & Powell, R. (1977). A nepheline-alkali feldspar geothermometer. *Contributions to Mineralogy and Petrology*, *62*, 193–204.

Powell, R. (1985). Regression diagnostics and robust regression in geothermometer/geobarometer calibration: the garnet-clinopyroxene geothermometer revisited. *Journal of Metamorphic Geology*, *3*, 231–243.

Prelević, D., Akal, C., Romer, R. L., Mertz-Kraus, R., & Helvacı, C. (2015). Magmatic response to slab tearing: constraints from the Afyon Alkaline Volcanic Complex, Western Turkey. *Journal of Petrology*, *56*, 527–562.

Prelević, D., Foley, S. F., Romer, R., & Conticelli, S. (2008). Mediterranean Tertiary lamproites derived from multiple source components in postcollisional geodynamics. *Geochimica et Cosmochimica Acta*, *72*, 2125–2156.

Reiners, P. W., Carlson, R. W., Renne, P. R., Coo per, K. M., Granger, D. E., M c Lean, N. M., & Schoene, B. (2018). *Geochronology and Thermochronology.* (J. W. & Sons, Ed.).

RICHARDS, A., ARGLES, T., HARRIS, N., PARRISH, R., AHMAD, T., DARBYSHIRE, F., & DRAGANITS, E. (2005). Himalayan architecture constrained by isotopic tracers from clastic sediments. *Earth and Planetary Science Letters*, *236*(3–4), 773–796. doi:10.1016/j.epsl.2005.05.034

Rickwood, P. C. (1989). Boundary lines within petrologic diagrams which use oxides of major and minor elements. *Lithos*, *22*(4), 247–263. doi:10.1016/0024-4937(89)90028-5

Romer, R. L., & Hahne, K. (2010). Life of the Rheic Ocean: Scrolling through the shale record. *Gondwana Res.*, *17*, 236–253.

Ryburn, R. J., Raheim, A., & Green, D. H. (1976). Determination of P,T paths of natural eclogites; a correction. *Lithos*, *9*, 161–164.

Santosh, M., & Omori, S. (2008). CO2 flushing: a plate tectonic perspective. *Gondwana Res.*, *13*, 86–102.

Schaltegger, U., Schmitt, A. K., & Horstwood, M. S. A. (2015). U-Th-Pb zircon geochronology by ID-TIMS, SIMS, and laser ablation ICP-MS: Recipes, interpretations, and opportunities. *Chemical Geology*, *402*(March), 89–110. doi:10.1016/j.chemgeo.2015.02.028

Searle, D. L., & Haq, B. T. (1964). The Mogok belt of Burma and its relationship to the Himalayan orogeny. In *The international geological congress 22* (pp. 132–161).

Searle, M. P., Noble, S. R., Cottle, J. M., Waters, D. J., Mitchell, A. H. G., Hlaing, T., & Horstwood, M. S. A. (2007). Tectonic evolution of the Mogok metamorphic belt, Burma (Myanmar) constrained by U-Th-Pb dating of metamorphic and magmatic rocks. *Tectonics*, *26*(3). doi:10.1029/2006TC002083

Searle, M. P., Waters, D. J., Morley, C. K., Gardiner, N. J., Htun, U. K., Nu, T. T., & Robb, L. J. (2017). *Chapter 12 Tectonic evolution of the Mogok metamorphic and Jade mines belts and ophiolitic terranes of Burma (Myanmar)*. *Myanmar: Geology, Resources and Tectonics* (Vol. 48). Geological Society Memoir48. doi:10.1029/2006TC002083

Sláma, J., Košler, J., Condon, D. J., Crowley, J. L., Gerdes, A., Hanchar, J. M., et al. (2008). Plešovice zircon — A new natural reference material for U–Pb and Hf isotopic microanalysis. *Chemical Geology*, *249*, 1–35.

Sone, M., & Metcalfe, I. (2008). Parallel Tethyab sutures in mainland Southeast Asia: new insights for Palaeo-Tethys closure and implications for the Indosinian Orogeny. *Comptes Rendus Geoscience*, *340*, 166–179.

Stern, R. J., Tsujimori, T., Harlow, G., & Groat, L. A. (2013). Plate tectonic gemstones. *Geology*, *41*(7), 723–726. doi:10.1130/G34204.1

Stucki, A., Trommsdorff, V., & Gunther, D. (2001). Zirconolite in metarodingites of Penninic

Mesozoic ophiolites, Central Alps. *Schweizerische Mineralogische Und Petrographische Mitteilungen*, *81*(2), 257–265.

Sutherland, F. ., Coenraads, R. ., Hoskin, P. W. ., Bosshart, G., & Fanning, C. . (2002). Sapphire crystallization, age and origin, Ban Huai Sai, Laos: age based on zircon inclusions. *Journal of Asian Earth Sciences*, *20*(7), 841–849. doi:10.1016/s1367-9120(01)00067-0

Sutherland, F. L., Duroc-Danner, J. M., & Meffre, S. (2008). Age and origin of gem corundum and zircon megacrysts from the Mercaderes-Rio Mayo area, South-west Colombia, South America. *Ore Geology Reviews*, *34*(1–2), 155–168. doi:10.1016/j.oregeorev.2008.01.004

Sutherland, F. L., Piilonen, P. C., Zaw, K., Meffre, S., & Thompson, J. (2015). Sapphire within zircon-rich gem deposits , Bo Loei , Ratanakiri Province , Cambodia : trace elements , inclusions , U – Pb dating and genesis. *Australian Journal of Earth Sciences*, *62*, 761–773. doi:10.1080/08120099.2015.1101015

Sutherland, F. L., Zaw, K., Meffre, S., Thompson, J., Goemann, K., Thu, K., et al. (2018). Diversity In Ruby Geochemistry And Its Inclusions, Intra- And Inter Comparisons From Myanmar And East Australia. In *Meeting of the international mineralogical association* (p. 329).

Sutherland, F. L., Zaw, K., Meffre, S., Thompson, J., Goemann, K., Thu, K., et al. (2019). Diversity in Ruby Geochemistry and Its Inclusions: Intra- and Inter- Continental Comparisons from Myanmar and Eastern Australia. *Minerals*, *9*(1), 28. doi:10.3390/min9010028

Sylvester, P. J., & Ghaderi, M. (1997). Trace element analysis of scheelite by excimer laser ablation-inductively coupled plasma-mass spectrometry (ELA-ICP-MS) using a synthetic silicate glass standard. *Chemical Geology*, *141*(1–2), 49–65. doi:10.1016/S0009-2541(97)00057-0

Tajčmanová, L., Konopasek, J., & Schulmann, K. (2006). Thermal evolution of the orogenic lower crust during exhumation within a thickened Moldanubian root of the Variscan belt of central Europe. *Journal of Metamorphic Geol.*, *24*, 119–134.

Thein, M. (1973). A preliminary synthesis of the geological evolution of Burma with reference to the tectonic development of Southeast Asia. *Geological Society of Malaysia*, *6*, 87–116.

Thein, M. (2008). Modes of occurrence and origin of precious gemstone deposits of the Mogok Stone Tract. *Journal of the Myanmar Geosciences Society*, *1*, 75–84.

Thein, M. L., Myint, O., Kyi, S., & P. N. Win. (1990). *Geology and stratigraphy of the metamorphosed Early Paleozoic rocks of the Mogok–Thabeikkyin–Singu–Madaya Areas. Unpublished staff report* (Vol. 98).

Themelis, T. (2008). *Gems and Mines of Mogok*.

Thu, K. (2007). *The Igneous Rocks of the Mogok Stone Tract: Their Distribution, Petrography,*

Petrochemistry, Sequence, Geochronology and Economic Geology. Ph.D. Thesis, University of Yangon, Yangon, Myanmar.

Thu, Y. K., Enami, M., Kato, T., & Tsuboi, M. (2017). Granulite facies paragneisses from the middle segment of the Mogok metamorphic belt, central Myanmar. *Journal of Mineralogical and Petrological Sciences*, *112*(1), 1–19. doi:10.2465/jmps.160526

Thu, Y. K., Win, M. M., Enami, M., & Tsuboi, M. (2016). Ti-rich biotite in spinel and quartz-bearing paragneiss and related rocks from the Mogok metamorphic belt, central Myanmar. Journal of Mineralogical and. *Petrological Sciences*, *111*, 270–282.

Touret, J. L. R. (1971). Le faciés granulite en Norvège Méridionale. II: les inclusions fluides. *Lithos*, *4*, 423–436.

Touret, J. L. R., & Huizenga, J. M. (2012). Fluid-assisted granulite metamorphism: a continental journey. *Gondwana Res.*, *21*, 224–235.

Ulianov, A., Müntener, O., Schaltegger, U., & Bussy, F. (2012). The data treatment dependent variability of U-Pb zircon ages obtained using mono-collector, sector field, laser ablation ICPMS. *Journal of Analytical Atomic Spectrometry*, *27*(4), 663–676. doi:10.1039/c2ja10358c

Vermeesch, P. (2018). IsoplotR: A free and open toolbox for geochronology. *Geoscience Frontiers*, *9*(5), 1479–1493. doi:10.1016/j.gsf.2018.04.001

Waltham, T. (1999). The ruby mines of Mogok. *Geology Today*, *15*, 143–149.

Wang, Y., Sieh, K., Thura, A., Soe, M., Saw, N. K., & Soe, T. T. (2011). Earthquakes and Slip rate of the sounthern Sagaing-fault: insights from an offset ancient fort wall, lower Burma (Myanmar). *Geophysical Journal International*, *185*, 49–64.

Wiedenbeck, M., Alle, P., Corfu, F., Griffin, W. L., Meier, M., F., O., et al. (1995). Three natural zircon standards for U–Th–Pb, Lu–Hf, trace element and REE analyses. *Geostandards Newsletter*, *19*, 1–23.

Win, M. M., Enami, M., & Kato, T. (2016). Metamorphic conditions and CHIME monazite ages of Late Eocene to Late Oligocene high-temperature Mogok metamorphic rocks in central Myanmar. *Journal of Asian Earth Sciences*, *117*, 304–316. doi:10.1016/j.jseaes.2015.11.023

Wu, C.-M., Zhang, J., & Ren, L. D. (2004). Empirical garnet-biotite-plagioclase-quartz (GBPQ) geobarometry in medium-to high-grade metapelites. *Journal of Petrology*, *45*, 1907–1921.

Wu, F. Y., Yang, Y. H., Mitchell, R. H., Bellatreccia, F., Li, Q. L., & Zhao, Z. F. (2010). In situ U-Pb and Nd-Hf-(Sr) isotopic investigations of zirconolite and calzirtite. *Chemical Geology*, *277*(1–2), 178–195. doi:10.1016/j.chemgeo.2010.08.007

Wuhrer, R., Beattie, R., Coenraads, R. R., Abduriyim, A., Giuliani, G., Hoskin, P. W. O., et al. (2015).

Corundum (sapphire) and zircon relationships, Lava Plains gem fields, NE Australia: Integrated mineralogy, geochemistry, age determination, genesis and geographical typing. *Mineralogical Magazine*, *79*(03), 545–581. doi:10.1180/minmag.2015.079.3.04

Xiang, H., Zhang, L., Zhong, Z.-Q., Santosh, M., Zhou, H.-W., Zhang, H.-F., et al. (2012). Ultrahigh-temperature metamorphism and anticlockwise P-T-t path of Paleozoic granulites from north Qinling-Tongbai orogen, Central China. *Gondwana Res.*, *21*, 559–576.

Yang, W. Bin, Niu, H. C., Shan, Q., Sun, W. D., Zhang, H., Li, N. B., et al. (2014). Geochemistry of magmatic and hydrothermal zircon from the highly evolved Baerzhe alkaline granite: Implications for Zr-REE-Nb mineralization. *Mineralium Deposita*, *49*(4), 451–470. doi:10.1007/s00126-013-0504-1

Yonemura, K., OsanaiI, Y., Zaw, T. N., Nakano, N., Charusiri, P., & Adachi, T. (2013). EPMA U-Th-Pb monazite dating of metamorphic rocks from the Mogok Metamorphic Belt, central Myanmar. *Journal of Mineralogical and Petrological Sciences*, *108*(3), 184–188. doi:10.2465/jmps.121019a

Yui, T. F., Zaw, K., & Wu, C. M. (2008). A preliminary stable isotope study on Mogok Ruby, Myanmar. *Ore Geology Reviews*, *34*(1–2), 192–199. doi:10.1016/j.oregeorev.2008.05.001

Zartman, R. E., & Doe, B. R. (1981). Plumbotectonics - the model. *Tectonophysics*, *75*, 135–162.

Zaw, K. (1989). Comments on transcurrent movements in the Myanmar-Andaman sea region. *Geology*, *17*, 93–95.

Zaw, K. (1990). Geological, petrological and geochemical characteristics of granitoid rocks in Burma: with special reference to the associated W-Sn mineralization and their tectonic setting. *Journal of Southeast Asian Earth Sciences*, *4*, 293–335.

Zaw, K. (1998). Geological evolution of selected granitic pegmatites in myanmar (burma): Constraints from regional setting, lithology, and fluid-inclusion studies. *International Geology Review*, *40*(7), 647–662. doi:10.1080/00206819809465229

Zaw, K. (2017). *Overview of mineralization styles and tectonic-metallogenic setting in Myanmar. In Myanmar: Geology, Resources and Tectonics; Chapter 24; Barber, A.J., Zaw, K., Crow, M.J., Eds.; Geological Society London Memoirs*.

Zaw, K., Sutherland, F. L., Graham, I., Meffre, S., & Thu, K. (2010). Dating zircon inclusions in gem corundum deposits and genetic implications, 7.

Zaw, K., Sutherland, L., Yui, T. F., Meffre, S., & Thu, K. (2014). Vanadium-rich ruby and sapphire within Mogok Gemfield, Myanmar: implications for gem color and genesis. *Mineralium Deposita*, *50*(1), 25–39. doi:10.1007/s00126-014-0545-0

Zaw, K., Thu, K., Meffre, S., Yui, T. F., & Sutherland, F. L. (2015). Vanadium-rich ruby and sapphire within Mogok Gemfield, Myanmar: implications for gem color and genesis. *Mineralium Deposita*, *50*(1), 25–39. doi:10.1007/s00126-014-0545-0

Zuleger, E., & Erzinger, J. (1988). Determination of the REE and Y in silicate materials with ICP-AES. *Fresenius' Zeitschrift für Analytische Chemie*, *332*(2), 140–143. doi:10.1007/BF00470631

CHAPTER IV

U-Pb age dating of zircon and zirconolite inclusions in marble hosted gem-quality ruby and spinel from Mogok, Myanmar

Myint Myat Phyo[1], Hao A.O. Wang[2], Marcel Guillong[3], Alfons Berger[4], Leander Franz[1], Walter A. Balmer[2], and, Michael S. Krzemnicki[2]

[1]Mineralogical Petrographic Institute, University of Basel,

[2]Swiss Gemmological Institute SSEF, Basel,

[3]Institute of Geochemistry and Petrology, ETH Zurich,

[4]Geological Institute, University of Bern

Figure 4.1 Faceted ruby and rough ruby crystal within marble from Mogok area, Myanmar.

4.1 Abstract

The Mogok area, Myanmar (Burma) is one of the finest ruby and spinel deposits in the world. The formation age of ruby and spinel from this area is a critical information for the linkage between gemstone generation and magmatic and metamorphic events of that area. In this study, we applied

U-Pb age-dating on zircon and zirconolite inclusions in marble hosted gem-quality ruby, spinel as well as their marble host rocks. In addition, zircon inclusions in neighbouring gneisses (Mogok gneiss from west Mogok and felsic gneiss from central Mogok) were age-dated for complementary information.

The U-Pb ages of zircon inclusions in gem-quality ruby, spinel and their hosting marble revealed Late Cretaceous ~75 Ma in the core and Late Oligocene ~25 Ma in the rim of the grains. In addition, the Mogok gneiss showed significant lead loss conditions and U-Pb age of ranging from Precambrian ~990 Ma to Jurassic ~165 Ma in the core and rim of zircon grain revealed early Oligocene ~30 Ma. The felsic gneiss from central Mogok showed Middle Jurassic age ~169Ma in the core and the rim revealed Early Oligocene ~30 Ma ages. These old zircon cores from Mogok gneiss probably reflect older magmatic events in the area. These U-Pb isotopes age dating results supported to estimate the formation of marble hosted corundum and spinel from the Mogok area. Our age results are not only in agreement those from previous geochronological researches of Mogok as well as along the Mogok Metamorphic Belt (MMB), but also pointed out that the Mogok area has experienced several metamorphic and magmatic events. Based on our data we estimate that the rubies and spinel of gem-quality for which the Mogok area is famous formed during Late Oligocene to Early Miocene.

Keywords: Mogok Metamorphic Belt, geochronology, U-Pb dating, zirconolite

4.2 Introduction

Ruby, the red chromium-bearing variety of corundum Al_2O_3 and red chromium-bearing spinel $MgAl_2O_4$ are among the world's most valued gemstones. The Mogok area in Myanmar is one of the most eminent occurrences for both gemstones, apart from a number of further economically viable deposits producing gem-quality material (such as Mozambique and Tanzania in East-Africa, Madagascar, Sri Lanka, Thailand, Nepal, Pakistan, Tajikistan, and Vietnam, to name a few). In the past, corundum and to a lesser extent spinel, from Mogok has been extensively studied, either in general (Keller 1985; Sutherland et al. 2002; Themelis 2008; Peretti et al. 2015), or focusing specifically on trace elements (Garnier et al. 2006; Bieri et al. 2010; Sutherland et al. 2015, 2019; Zaw et al. 2015), stable isotopes (Tashia J. Dzikowski et al. 2014; Giuliani et al. 2005; Yui et al. 2008; Khin Zaw et al. 2014), solid inclusions(Gübelin and Koivula 1986, 2005, 2008), and fluid inclusions (Tashia Jayne Dzikowski 2013; Giuliani et al. 2015). In addition, a number of geochronology studies

were published, either about minerals related to gemstone formation or inclusions in gemstones (Coenraads et al. 1990; Garnier et al. 2002, 2005, 2006, Sutherland et al. 2008, 2019; Zaw et al. 2010; Wuhrer et al. 2015), as well as about inclusions from faceted gemstones (Link 2015).

In recent years, U-Pb age dating of inclusions (e.g. zircon, titanite, etc.) in gemstones using Laser-Ablation Inductively-Coupled Plasma Mass Spectrometry (LA-ICP-MS) has become more popular due to easier access to instrumentation, minimum sample preparation, smaller laser crater size and improved instrument sensitivity (Sutherland et al. 2008, 2015, 2019; Zaw et al. 2010; Link 2015; Elmaleh et al. 2019). The calculated U-Pb ages of inclusions found in a gemstone indicate the maximum possible formation age of that gemstones. As such, these radiometric ages may provide gemmologocal laboratories with additional evidence when carrying out origin determination, especially in case of rubies and sapphires (Sutherland et al. 2018).

In this study, we will present U-Pb ages of zircon and zirconolite, both as inclusions in ruby and spinel, and as accessory mineral found in marble-host rock and gneisses from the Mogok area. In our study, we applied two different LA-ICP-MS setups; a) Time-Of-Flight MS (TOF-MS) and Sector-Field MS (SF-MS). These two setups were specifically chosen, in order to achieve multi-element data (TOF-MS) and to profit from the small laser spot size (SF-MS) enabling age dating even on narrow growth layers of the analysed inclusions. When combining the results from both instruments setup, we observed a wide range of radiometric ages on our zircon and zirconolite grains which corresponds to multiple magmatic and metamorphic events that happened along the Mogok Metamorphic Belt (MMB). Our research intends to contribute to the knowledge about geological formation in the studied area by adding new geochronological results from multiple inclusions in gem-quality ruby and spinel as well as from host rocks.

4.3 Geological Setting

The Mogok Metamorphic Belt (MMB) named by La Touche (1913) and further described in early studies (Chhibber 1934; Fermor 1930; Iyer 1953), is a large sickle-shaped belt of regionally metamorphised rocks (A. H. G. Mitchell et al. 2006) strechting N-S from central to upper Myanmar as the southern continuation of the Himalayan Syntaxis (see Figure 4.2). It forms the western margin of the Shan-Thai Block (Sibumasu Block) and is adjacent to the north-south trending right-lateral strike-slip Sagaing Fault, related to the youngest Cenozoic metamorphism (Bertrand et al. 1999) . It is also known as the Mogok-Mandalay-Mergui Belt, as it extends to the south of Myanmar until

Mergui area (Bender 1983; K. Zaw 1990; K. Zaw et al. 2015; K Zaw 2017). In the so-called Mogok Stone Tract (Chhibber 1934), located at the northeastern end of the MMB, there is an accumulation of world-class gem deposits, namely for rubies, sapphires, and spinel (Hughes 1997; Iyer 1953; Themelis 2008). The formation of those gemstones is related to late-stage metamorphic events (Cenozoic) within this geological unit (Bertrand et al. 1999; Gardiner, Robb, et al. 2016; H. Y. Lee et al. 2016). The Mogok area mainly consists of high-grade metamorphic rocks (upper amphibolite to granulite facies), such as marbles, schists and gneisses. From these, the so-called Mogok gneisses (La Touche 1913) in the southern part of the Mogok area are regarded as the oldest rock units in the area Myanmar . Gem-quality rubies and spinels are found in the Mogok area in both, primary deposits in marbles and secondary deposits in alluvial and eluvial placers, as well as accumulated placers in karstic sinkholes and caverns (M. Thein 2008)

The MMB has been extensively studied with a main focus on regional geology, geochemistry and geochronology (Barley et al. 2003; Bertrand et al. 1999; Brook and Snelling 1976; Gardiner, Searle, et al. 2016; Min 2007a). In terms of geochronology, the ruby and spinel bearing marbles from the Mogok area are interpreted as metamorphosed limestones of Precambrian age (Chhibber 1934; Iyer 1953). Contrasting to this, Searle & Haq (1964) considered the Mogok metasediments originally to be Precambrian to Jurassic rocks of the Shan Plateau, whereas Clegg (1941) described them as mid-Cretaceous limestones and Jurassic sediments. Form Precambrian to Cenozoic, the MMB has experienced several magmatic and metamorphic events, which are commonly subsumed as Precambrian to Paleozoic regional metamorphism (Barley et al. 2003; A. Mitchell et al. 2012; A. H. G. Mitchell et al. 1977; K. Thu 2007; Wang et al. 2011). Moreover, geochronological dating analysis on radiometric mineral inclusions from gemstones such as ruby, sapphire as well as Ar/Ar and/or K/Ar dating on hosting marble were also carried out from Mogok area (Gardiner, Searle, et al. 2016; Sutherland et al. 2019; K Zaw et al. 2010). Although several data had been done already on Mogok area, more data analyses on geochronological study of it and its surrounding is still needed to assume and built a model for the formation of gesmtones from that area. In our research, we mainly focused on the U-Pb geochronological dating of zircon inclusions from gemstones (ruby and spinel) as well as host rocks.

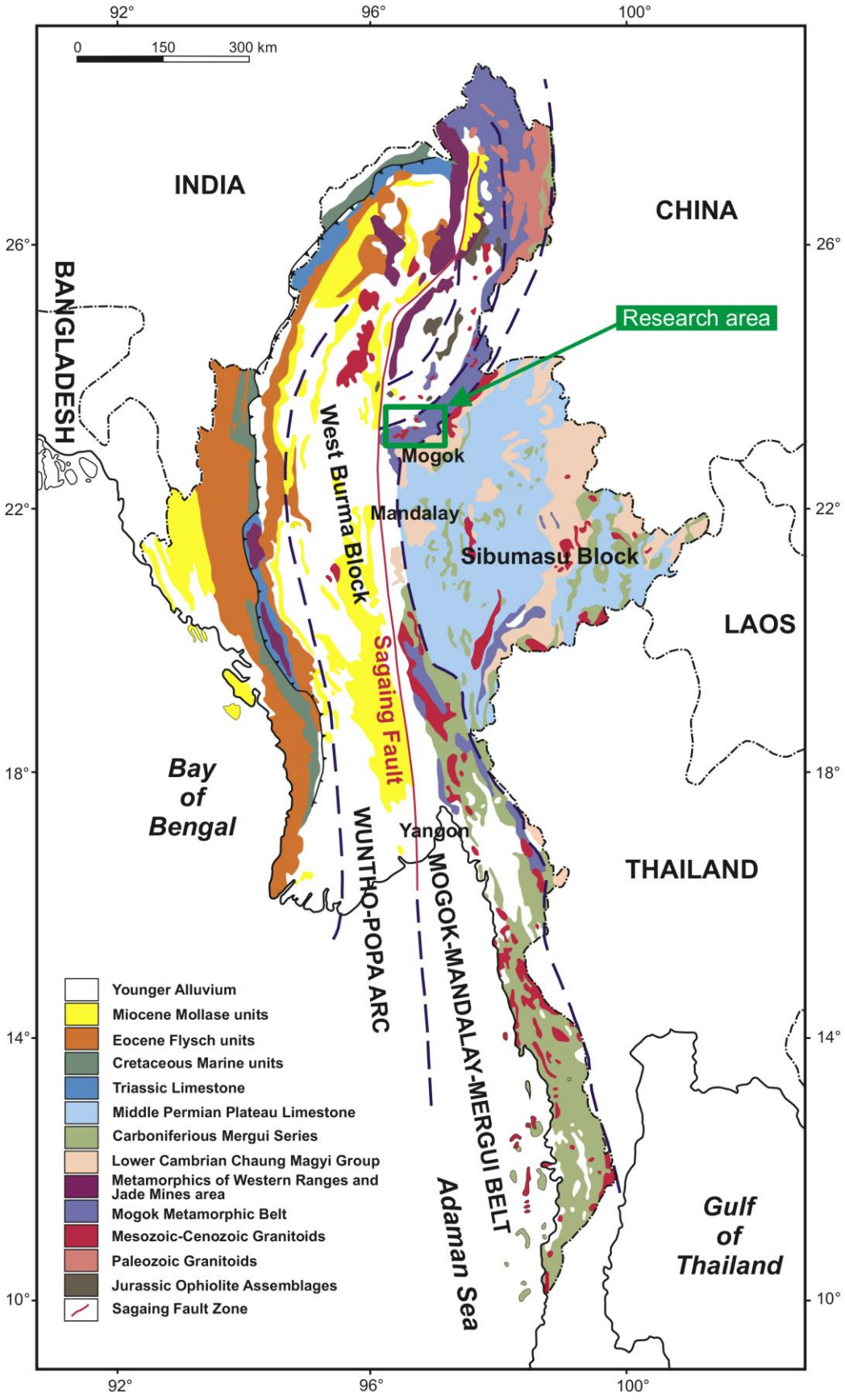

Figure 4.2 The research area (Mogok) is highlighted (green rectangle) in the regional geological map of Myanmar. (modified after Sone & Metcalfe, 2008)

4.4 Material and Methods

For this geochronological study, radiometric U-Pb dating was carried out on zircon and zirconolite inclusions in six gem-quality rubies and three spinels as well as in three rock samples (one ruby- and spinel- bearing marble from Bawlongyi, one biotite-garnet gneiss from Kinn in western Mogok and one biotite-garnet-orthopyroxene gneiss from Aunglan Taung in central Mogok; cf. Chapter 3 of this study). All samples were collected directly from various mining sites in the Mogok area (see Figure 4.3). Generally, zircon and zirconolite inclusions are rarely found in gem-quality rubies and spinels (also see in Chapter 2, Figure 2.17). We observed only 15 zircon and 5 zirconolite inclusions in nearly 300 of ruby and spinel samples. Especially zircon seems to be more abundant in the host rocks; we counted 101 zircon grains in the hosting marble and gneiss samples. Additionally, zirconolite occurred as rim and as inclusions in 15 grains of zircon from the hosting marble. A detailed list of the studied samples and their occurrence is given in Table 4.1.

All zircon inclusions in the gem-quality ruby and spinel as well as host rock samples were identified by microscopy (Cambridge gemmological microscope: StereoZoom®7 and binocular: Leica DMLSP), Raman microspectroscopy (Renishaw inVia using an argon-ion laser at 514.5 nm, and Bruker Senterra using a frequency doubled Nd-YAG laser at 532 nm) and scanning electron microscopy equipped with an energy-dispersive spectrometer (FEI Nova Nano SEM 230). For more details see also also(Phyo et al. 2019).

Zircon grains often show complex zonation patterns, which may strongly influence radiometric dating if an analysis is conducted across growth zones of different age (Reiners et al. 2018; Schaltegger et al. 2015). In order to visualize such zonation in our samples and to determine the location where to carry out age dating, we additionally registered VPSE images (Variable Pressure Secondary Electron imaging) of zircons using a ZEISS EVO 50 scanning electron microscope.

For the radiometric U-Pb dating of the zircon and zirconolite inclusions we used two setups to benefit from advantages each of these systems offers, a) a Laser Ablation-Inductively Coupled Plasma-Time-Of-Flight-Mass Spectrometer (LA-ICP-TOF-MS) and b) a Sector-Field Mass Spectrometer (LA-ICP-SF-MS), both equipped with a 193 nm ArF excimer laser for ablation. Details of both setups and measurement parameters can be found in Table 4.2. Laser spot size of SF-MS was adjusted based on the grain size of the inclusion. These two setups were chosen because single detector SF-MS excels in sensitivity, hence smaller laser spot size provides sufficient sensitivity to quantify parent and daughter isotopes from U-Pb radioactive decay, whereas TOF-mass

spectrometry offers simultaneous acquisition of the full mass spectrum ranging from Li to U. Thus, by LA-ICP-TOF-MS, it was possible to constantly monitor variations in the elemental composition (e.g. when passing from one mineral to another), especially when laser drilling into small inclusions. However, a drawback of this method is its relatively low sensitivity (thus requiring larger laser spots), especially challenging when analysing very small zircon and zirconolite grains or in case of those inclusions showing thin or complex growth zoning patterns. Therefore, we applied LA-ICP-SF-MS to analyse small and complex zoned zircon grains using smaller spot size (13 to 19 µm) and zirconolite (found as thin rim in zircon grain). In this way, we are able to measure both core and rim of zircon grains separately. In sequential analysis of SF-MS, we used integration times of 10 ms (^{202}Hg, ^{208}Pb, ^{232}Th, ^{235}U, ^{238}U), 20 ms (^{204}Pb), 75 ms (^{207}Pb), and 90 ms (^{206}Pb), resulting in a total sweep time of 0.243 seconds for the selected isotopes of interest. Contrasting to this, TOF-MS acquires full mass spectrum (Li to U) simultaneously in every 33 µs, then 5000 full mass spectra were averaged and reported in one output data point (integration time 0.151 s). We applied 35 µm laser spot size for all TOF-MS measurement. For both TOF- and SF-MS instrument parameters are listed in Table 4.2.

For LA-ICP-SF-MS, we used zircon GJ-1 (609 ± 5 Ma) as primary age dating standard, with additionally zircon secondary standards Plesovice (339 ± 3.2 Ma), Temora (418 ± 5.3 Ma), Zircon 91500 (1065 ± 12.3 Ma) (Black et al. 2003; Jackson et al. 2004; Sláma et al. 2008; Wiedenbeck et al. 1995). Data processing was carried out using the software packages Iolite (V2.5) and VizualAge (Version 201302) for age calculation and uncertainty propagation. Further, we corrected element fractionation using Laser Induced Element Fractionation (LIEF), which assumes that the reference material and the samples behave identically. Except whereas mentioned, calculated ages are quoted as two times standard error (2SE), propagation is by quadratic addition. Reproducibility and age uncertainty of reference material are propagated where appropriate.

For TOF-MS, we used an in-house developed zircon single crystal SSEF87244 as primary standard, (523 ± 10 Ma, measured by SF-MS), characterised by a high uranium concentration (^{238}U 2076 mg/kg) and no detectable amount of common lead (^{204}Pb), and Zircon 91500 (1065 ± 12.3 Ma) as secondary standard (Wiedenbeck et al. 1995). For data processing, we used an in-house developed calculation script based on MATLAB R2018b. Benefiting from the full mass spectrum analysis in TOF-MS, it is possible to recheck the whole measurements were done on targeted inclusions or moved into host materials (ruby, spinel, marble, etc.) by using transient signal as well as other isotopes in TofDaq software (V1.2.97). Furthermore, raw transient signals were carefully checked for common Pb interference based on isotopes ^{204}Pb. In most of our samples, ^{204}Pb signal

was below the detection limit. Therefore, no common Pb correction and disequilibrium correction were applied. However, there may be still a small amount of common Pb present in our samples due to the low natural abundance of ^{204}Pb isotope. Intensity ratio of U-Pb isotopes were monitored in TofDaq software to select appropriate sections in transient signal for age dating calculation. The radiometric ages based on ^{206}Pb/^{238}U and ^{207}Pb/^{235}U ratios were calculated using gas blank corrected signals. The radiometric ages were calculated in ratio of the mean method and errors (2SE) were propagated following the procedures suggested by Ulianov et al. (2012). All age dating results were plotted on *IsoplotR* (Vermeesch 2018).

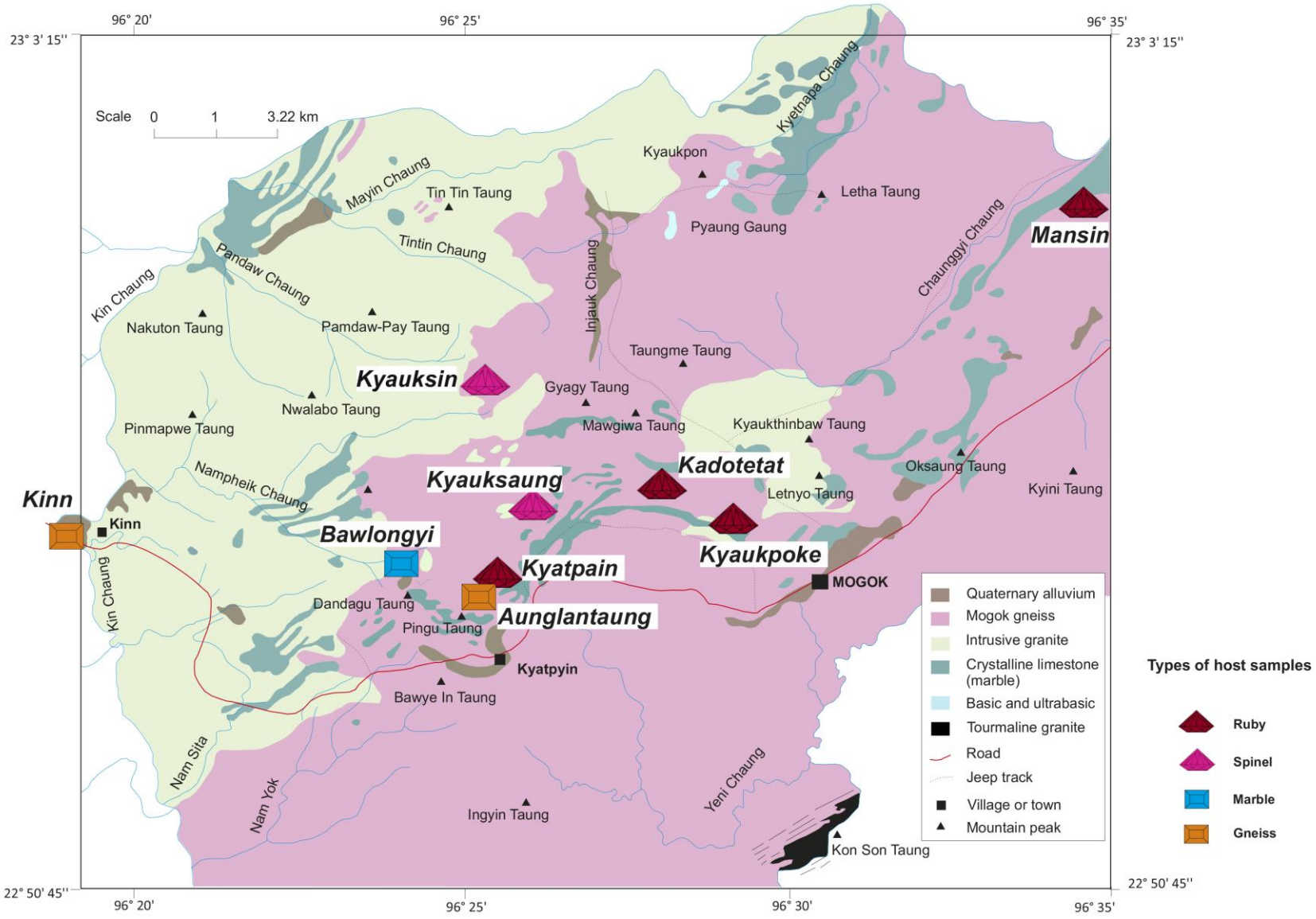

Figure 4.3 Sample location plotted on the geological map of the Mogok area (after Iyer 1953).

Table 4.1 List of the samples (ruby, spinel and host rocks) from Mogok area containing zircon and zirconolite inclusions which were analysed in this study for U-Pb age dating.

Sample Number	Locality	Types of host	Analysed Material	Weight (ct)	Sample Photo
SSEF96667A	Kyatpyin	Ruby	Zircon	1.615	
SSEF96666A	Kadotetat			2.431	
SSEF96666B				1.270	
SSEF96668A	Kyaukpoke			0.268	
SSEF96668B				0.323	
SSEF96663A	Mansin		Zircon & zirconolite	2.411	
SSEF92725D	Kyauksin	Spinel	Zircon	0.673	
SSEF92725E				0.940	
SSEF92720D	Kyauksaung			0.405	
BLG-12	Bawlongyi	Ruby and spinel bearing marble	Zircon & zirconolite		
ALT-03	Aunglantaung	Gneiss	Zircon		
K-01	Kinn				

Table 4.2 LA-ICP-MS Instrument Operating Parameters

Parameters	LA-ICP-Sector-Field-MS	LA-ICP-Time-Of-Flight-MS
Laser model and type	Resolution S155 ASI (Resonetics)	NWR 193 UC Elemental Scientific Lasers
Laser wavelength (nm)	193	193
Fluence (J cm^{-2})	~2	~4
Repetition rate (Hz)	5	10
Ablation duration (s)	40	30
Spot diameter (µm)	13 / 19	35
Carrier gas flow (He, L min^{-1})	0.5 - 0.7	0.8
Mass spectrometer model and type	Thermo Element XR, Sector-field single collector ICP-MS	*icp*TOF from TOFWERK, modified from iCAP Qc, ThermoFisher Scientific
RF power (W)	1350 - 1550	1300
Make-up gas flow (Ar, L min^{-1})	0.90 - 1.07 (tuned daily)	0.65 - 0.68 (tuned daily)
Masses measured (amu)	202, 204, 206, 207, 208, 232, 235, 238	full mass spectrum (7 to 238)
Total integration time per output data point (s)	0.243	0.151

4.5 Results

We observed nine zircon inclusions in four different ruby mining sites from Mogok area - Kyatpyin, Kadotetat, Kyaukpoke and Mansin (see Figure 4.3). Six zircon grains are found in spinel from Kyauksin and Kyauksaung area, 41 zircon grains in ALT-03 gneiss, 25 zircons in K-01 gneiss and 35 zircons in BLG-12 marble. However, we observed zirconolite in Mansin ruby as solitary tabular crystals, zirconolite in marble from Bawlongyi area occurred as rim of zircons and as inclusions in zircon grains. We applied TOF-MS and SF-MS methods on both zircons and zirconolites. The results of U-Pb age dating results of both instruments set up are shown in Appendix A.

4.5.1 Zircon and zirconolite in ruby and spinel

Zircon grains from gem-quality ruby are approximately ranging from 50 to 300 µm in size. Zircon from spinel are quite small and maximum 50 µm in size, some grains are as small as 10 µm. Although zircon grains from spinel did not show any apparent zoning under VPSE images, zircons from Kyatpyin ruby showed nicely zoned core and rim nature (Figures 4.4a & b) while zircon grains from Mansin area showed aggregated textures in the core and homogeneous rim sections (Figure 4.4i). All zircons and zirconolites were analysed with TOF- and/or the SF-Mass Spectrometers depending on their size and core and rim nature.

We analysed both core and rim of zircon grains and U-Pb isotopes dating ages based on $^{206}Pb/^{238}U$ and $^{207}Pb/^{235}U$ isotopes of zircon cores from gem-quality rubies and spinels that revealed a wide range of ages ranging from Cretaceous to Eocene period (Figure 4.5a). Similar ages on zircon from Mogok were already recorded in previous investigations of (Thu 2007; Zaw et al. 2010), as well as from titanite inclusion in ruby from Mogok (Sutherland et al. 2019), from zircons of Kabaing granite (Gardiner, Robb, et al. 2016) and furthermore on biotite from Mogok metamorphic rocks of (GIAC project 1999). The U-Pb ages of zircon rims revealed Oligocene ages of ~33 Ma to 23 Ma and the youngest ages are concordant at 22.26 ± 0.36 Ma (ruby) and 22.88 ± 0.72 Ma (spinel) are shown in Figure 4.7a & b. This concordia age is quite similar to the age dating result of zircon inclusions in Mogok sapphire (Link 2016) and in Mong Hsu ruby (Sutherland et al. 2019). It is a bit younger than the age dating result on titanite inclusion in ruby from Thurein Taung (Sutherland et al. 2019). Our U-Pb geochronology dating results of zircon rims from gemstones fall within the similar age range of Oligocene to Early Miocene.

Additionally, we observed tabular zirconolite crystals in Mansin ruby, which have a grain size of 60 to 100 µm (Figures 4.4c & d). No Raman characteristic peaks have been observed in these zirconolite grains. However, based on the shape of the inclusion, we postulate that zirconolite may crystalize in orthorhombic, monoclinic or trigonal system, as also suggested in previous study (Bayliss et al. 1989). The zirconolite from Mansin didn't show zoning in VPSE nor BSE images. For age dating analyses of zirconolite, we applied the same set of zircon standards (SSEF87244, 523 ± 10 Ma and 91500, 1065 ± 12.3 Ma, measured by SF-MS). Interestingly, the U-Pb ages measured by TOF-MS and SF-MS were not consistent (Figure 4.5b). TOF-MS analyses measured in the center of grain revealed a younger concordia age of 18.06 ± 0.36 Ma (Figure 4.7e) whereas the SF-MS analysis measured adjacent to the TOF-MS measurements revealed an older concordia age at 29.78 ± 0.38

Ma (Figure 4.7d). These different results of zirconolite measured by TOF and SF might be due to the application of non-matrix matched satandard (zircon), which induces various fractionation behaviour (Jackson et al. 1992; Sylvester and Ghaderi 1997) with different instrument operating parameters and fractionation correction. Both ages are within the range previously reported in literature, using other mineral inclusions (Bertrand et al. 2001; Brook and Snelling 1976; Min 2007b; M. P. Searle et al. 2007). Further analyses, on the cause of the discrepancy and the method to limitate the difference in order to obtain a more accurate ages using zirconolite is ongoing.

Trace element analyses (LA-ICP-TOF-MS) in zircons from ruby, spinel and the hosting marble show relatively low concentrations in LREE, which often fall below the detection limit. Towards the HREE, concentrations continuously increase up to 480 ppm. Figure 4.8a shows REE pattern in a chondrite-normalized spider diagram. Whereas Chrondrite-normalized spidergrams of zirconolites show negative anomalies in La and Eu, relatively constant in trend (Figure 4.8d).

4.5.2 Zircon and zirconolite in Bawlongyi marble

Intrestingly, we recognized ruby, spinel, zircon and zirconolite as accessory minerals in our Bawlongyi marble sample. We observed 35 zircon grains and in these zircon grains, we also found zirconolite both as a rims around zircon and as inclusions in zircons. These minerals were identified by SEM-EDS analyses. No characteristic Raman peaks were detected in zirconolite grains. Both zircon and zirconolite from Bawlongyi marble did not show any distinct growth zoning (Figure 4.4e-h).

The calculated U-Pb ages of zircons from the Bawlongyi marble cover a wide range from Cretaceous to Early Miocene. This is similarly found for zircon inclusions in gemstones (Figure 4.5c). The youngest concordia age of zircon is at 17.11 ± 0.22 Ma (see Figure. 4.7c). Zirconolite from Bawlongyi marble reveals concordia ages at 20.30 ± 0.30 Ma for TOF-MS (Figure 4.7g) and 23.61 ± 0.36 Ma for SF-MS (Figure 4.7f). These U-Pb age dating results are well in accordance with our dating results of zircon rims from gem-quality rubies and spinels and are comparable with ages gained on several different minerals from the Mogok area (Bertrand et al. 2001; Brook and Snelling 1976; Virginie Garnier et al. 2008; Min 2007b; D. L. Searle and Haq 1964; M. P. Searle et al. 2007; K. Thu 2007).

The chondrite-normalized REE pattern of zircons within marble is similar in trend to that of zircons within gem-quality ruby and spinel (Figure 4.8b). Moreover, the REE pattern of zirconolite from both, gemstones and marble, show similar negative anomalies for La and Eu, which is similar to the REE pattern of zirconolite from lunar melt rock 67955 of Norman and Nemchin (2014), but differs distinctly from the REE pattern of zirconolite reported in gabbro (Gana Rossa) from the Central Alps in Switzerland (Stucki et al. 2001) and alluvial zirconolite grains from Afrikanda, Kovdor (Russia), Phalaborwa (South Africa) and Jacupiranga (Brazil) reported by Wu et al. (2010). To our knowledge, our study provides the first analysis of the full range of REEs in zirconolite from Mogok.

4.5.3 Zircon in gneisses from Aunglan Taung and Kinn

We analysed 41 zircon grains from a biotite-garnet-orthopyroxene gneiss from Aunglan Taung (see Figure 4.3). These zircons show three different types of zoning: (1) zoning with bright core sectionsand darker rims (Figure 4.4j), (2) zoning with dark grey zircon core sections and bighter rims (Figure 4.4k) and (3) irregular zoning.

The U-Pb dating of zircon core from Aunglan Taung yields two age groups ranging from Middle Jurassic (~180 Ma to ~140 Ma) to Early Cretaceous (~110 Ma to ~90 Ma) as shown in Figure 4.6b. Middle Jurassice zircon ages were previously recorded in granite from the Mogok area (K. Thu 2007) and in orthogneiss of Kyanigan Hills close to the Mogok area (Barley et al. 2003). Early Cretaceous ages were also mentioned in (Mitchell 1993). The U-Pb isotopes ages of zircon rim are concordant at 31.98 ± 0.30 Ma (Figure 4.7h). These rim ages are similar to those of previous investigations within the Mogok area (cf. Searle et al. 2007; Thu 2007; Zaw et al. 2010).

The biotite -garnet gneiss from Kinn area is also known as Mogok gneiss (Chhibber 1934) and is supposed to be part of the oldest rock unit of the Mogok area (La Touche 1913). This granulite facies gneiss (see chapter 3 of this study) yields small zircon grains of 10 to 20 µm. In these zircon crystals, we observed very thin darker rim under VPSE-images (Figure 4.4j). U-Pb ages of zircon grains from Kinn showed Pb-loss condition and we assumed that U-Pb isotope data of this gneiss reveal an upper intersect in the Middle Proterozoic (~1047Ma; cf Figure 4.6a). These age results are well in accordance with the former investigation of Mogok gneisses and metasedimentary rocks (Chhibber 1934). The U-Pb isotope data for the zircon rim reveal a lower intersect at ~38 Ma. Two zircon rim measurements are concordant at 26.39 ± 1.24 Ma (Figure 4.7i). These rim ages are also

well accordance with the zircons rims ages of gemstones from this research and previous record on monazite dating of leucogranite from the Mogok Metamorphic Belt (Searle et al. 2007).

Chondrite-normalized trace element patterns for zircons of both gneisses from Aunglan Taung and Kinn are similar to the patterns of zircon inclusions in ruby, spinel and the hosting marble (Bawlongyi). But they additionally indicate negative anomalies of Pr, Nd and Eu (Figure 4.8c). Quite similar REE patterns were reported for magmatic zircon from granite of the Baerzhe pluton in northeastern China (Yang et al. 2014).

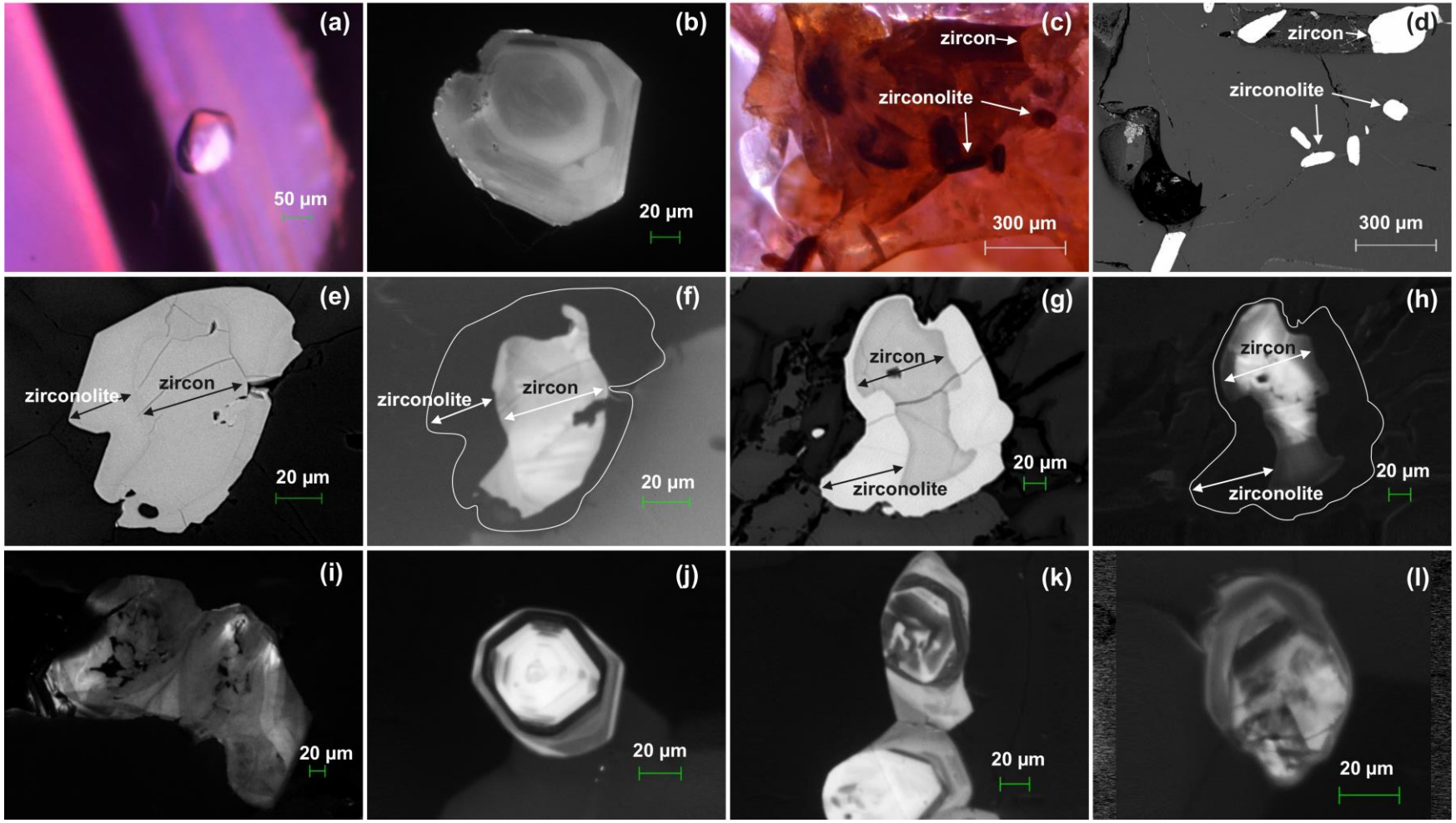

Figure 4.4 (a) Microphotograph of zircon inclusion from Kyatpyin ruby (b) showing distinct zoning under VPSE-image (c) Microphotograph of zircon and zirconolite inclusions in Mansin ruby and (d) their BSE-image (e) BSE-image of zircon and zirconolite (zirconolite occur as rim of zircon grain) in Bawlongyi marble and (f) their VPSE-image (g) BSE-image of zircon and zirconolite found in Bawlongyi marble and (h) their VPSE-image (i) zircon in Mansin ruby, displaying an aggregated core and a homogeneous rim under VPSE- image. (j) & (k) VPSE images of zircon in Aunglan Taung gneiss. (l) Complex irregular zoning in zircon from Kinn.

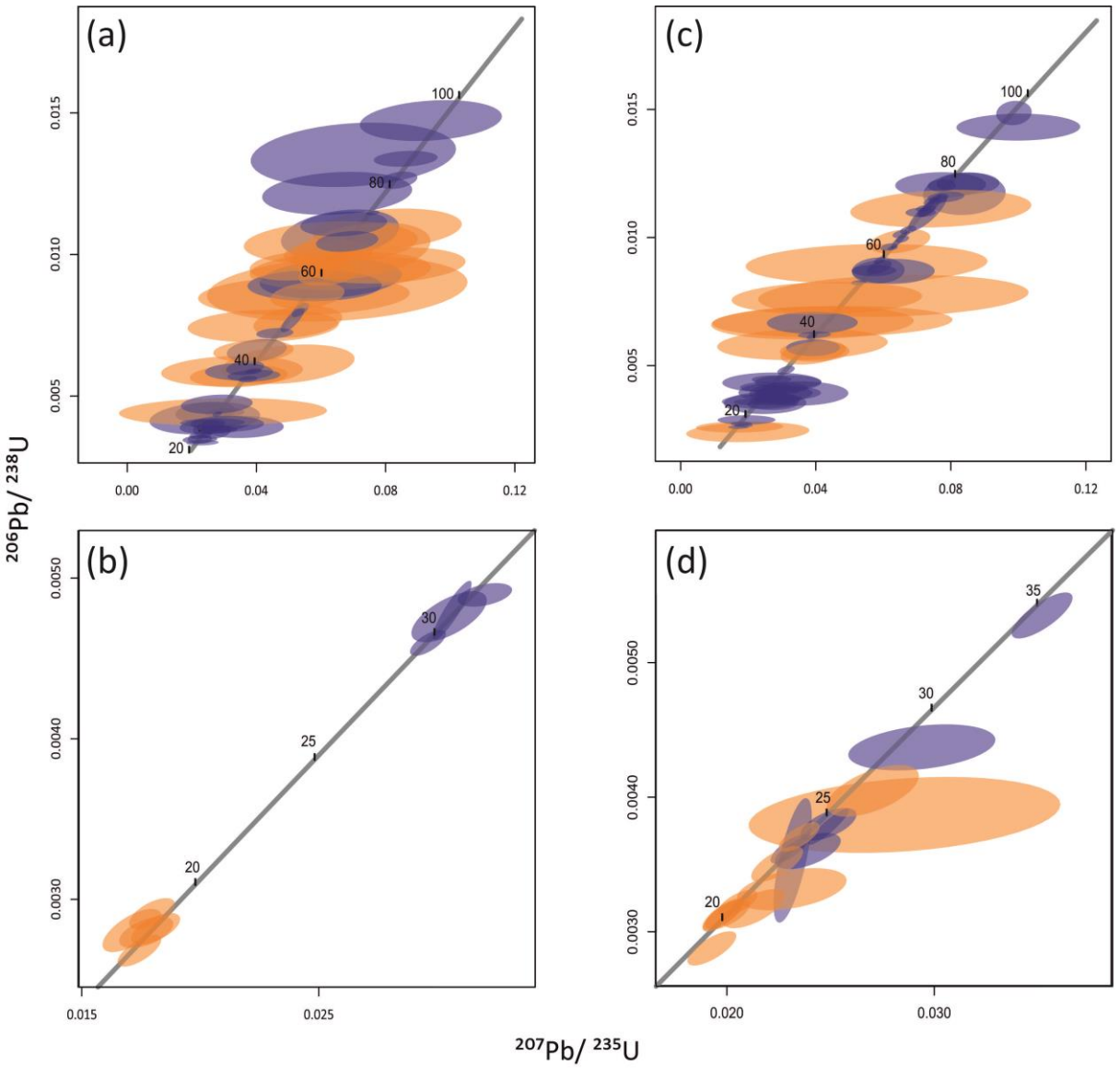

Figure 4.5 (a) Summarising our data shows a wide range of U-Pb ages for the zircon inclusions from gemstones. The Late Cretaceous to Eocene age resulted from zircon cores, whereas the Tertiary ages (~25 Ma) were measured at the rim of zircon grains. (b) U-Pb ages of zirconolites. (c) A wide range of U-Pb ages of zircon from the studied Bawlongyi marble (Note: Zircon occurred as core or center and zirconolite was present as rim on zircons or as single inclusions). (d) U-Pb ages of zirconolite from Bawlongyi marble.

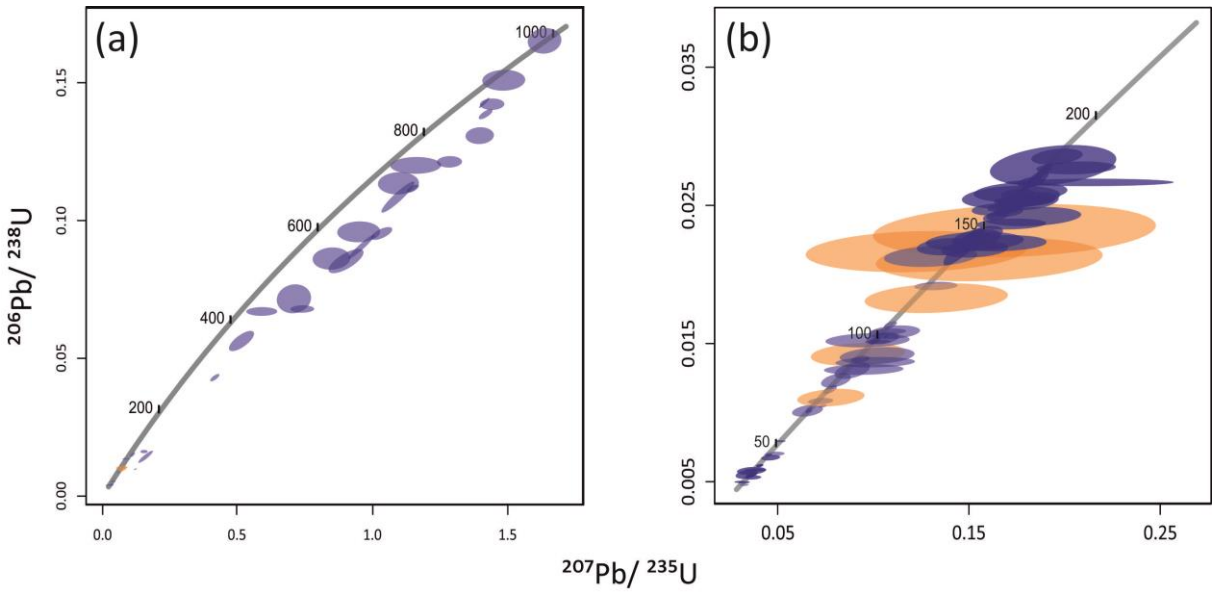

Figure 4.6 (a) U-Pb ages of zircons from the Kinn gneiss shows Pb-loss conditions. (b) U-Pb ages of zircons from the Aunglan Taung gneiss yield core ages ranging from Middle Jurassic (~180-140 Ma) to Early Cretaceous (~100-70 Ma) whereas rim ages plot in Tertiary time (~30-35 Ma).

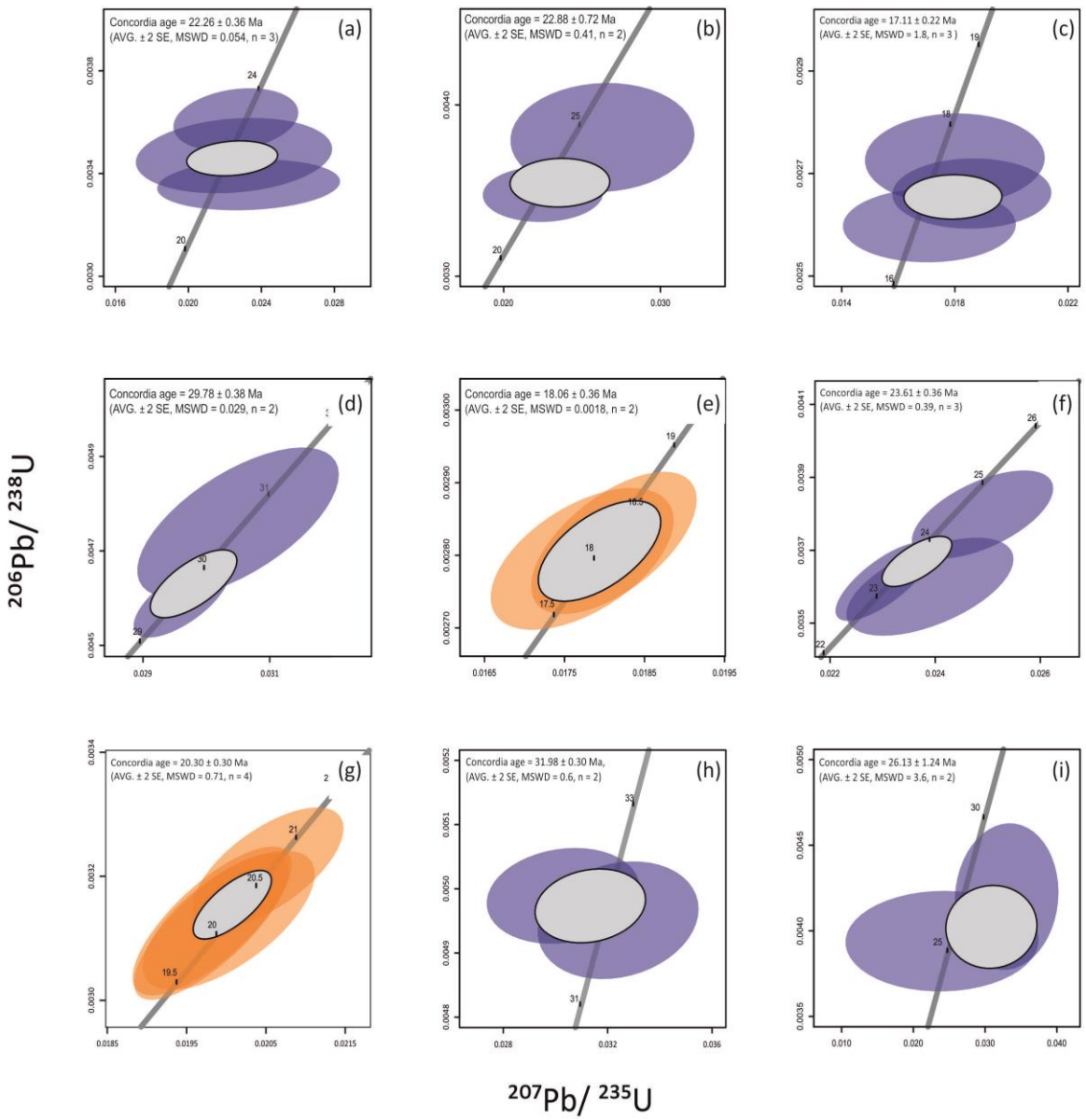

Figure 4.7 Concordia age of zircon from (a) ruby, 22.26 ± 0.36 Ma, MSWD = 0.54, probability of concordance = 0.86 (b) spinel, 22.88 ± 0.72 Ma, MSWD = 0.41, probability of concordance = 0.52 (c) marble, 17.11 ± 0.22 Ma, MSWD = 1.8, probability of concordance = 0.18 (d) zirconolite from gemstones, 29.78 ± 0.38 Ma, MSWD = 0.029, probability of concordance =0.86 (SF-MS) (e) 18.06 ± 0.36 Ma, MSWD = 0.0006, probability of concordance =0.98 (TOF-MS) (f) zirconolite from marble, 23.61 ± 0.36 Ma, MSWD = 0.029, probability of concordance =0.86 (SF-MS) (g) 20.44 ± 0.30 Ma, MSWD = 1.3, probability of concordance = 0.26 (TOF-MS), (h) zircon from Aunglan Taung, 31.98 ± 0.30 Ma, MSWD = 0.6, probability of concordance = 0.44 and (i) zircon from Kinn, 26.39 ± 1.24 Ma, MSWD = 2.7, probability of concordance = 0.1.

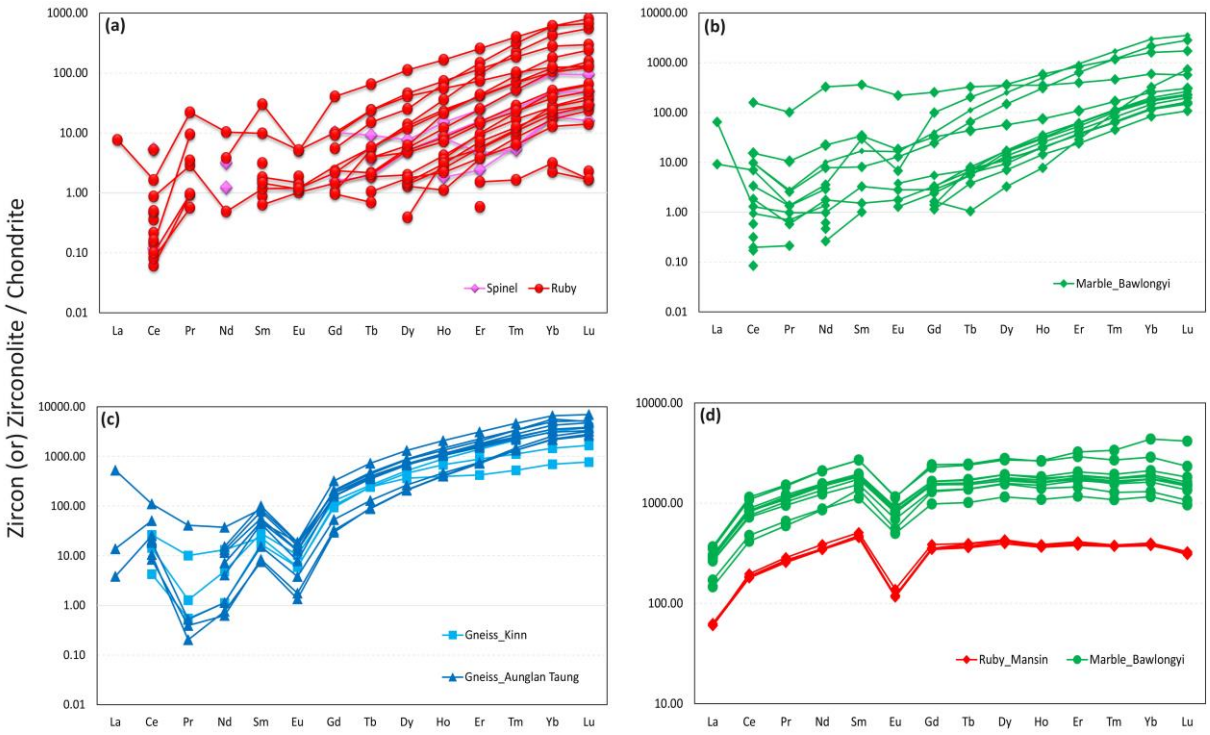

Figure 4.8 REE patterns of zircon from (a) gemstones (b) marble (c) gneisses and (d) zirconolite from ruby and marble normalized to chondrite value of McDonough & Sun (1995).

4.6 Discussion and Conclusions

The U-Pb ages of zircons from gemstones and ruby- and spinel-bearing marble from the research area revealed consistent radiometric ages over a wide range from Late Cretaceous to Late Oligocene period. Moreover, we observed in the cores of accessory zircons from the Aunglan Taung gneiss (Kyatpyin, central Mogok) two age groups: a) middle Jurassic and b) early Cretaceous. The old zircon core ages we calculated from zircons in gemstones, marbles and Aunglan Taung gneiss are similar to the age dating results of Late Cretaceous (83±4 Ma) reported from leucogranite (associated with ruby in leucogranite matrix) in the Wet-Loo area (Thu 2007), and monzonite and hornblende syenite from Mandalay Hill (Pickard et al. 1996, Barley et al. 2003 & Barber et al. 2017). The analysed zircons from the Mogok gneiss, reported as the oldest rock unit in the study area, showed Pb loss conditions and their Pb loss ages yield an upper intersect at ~ 1000 Ma and a lower intersect at ~ 30 Ma. The oldest U-Pb ages were found in the core of the analysed zircon grains and we thus assume that these zircon cores are detrital grains. These old zircon core ages are assumed to mirror multiple magmatic and metamorphic events in the Mogok area.

Younger ages (Late Oligocene) were found in the rim of zircon grains as well as in zirconolite inclusions in ruby and spinel, and in ruby- and spinel-bearing marble. In our study, we were focussing in the formation of marble-hosted ruby and spinel of gem quality. Based on our data, we therefore assume that the U-Pb ages calculated in the rim of zircon grains and from zirconolite indicate a late metamorphic event and are related to the formation of the marble-hosted ruby and spinel in the Mogok area. As youngest concordia ages of zircon rims from gemstones we calculated 22.26 ± 0.18 Ma, 1 SE (ruby) and 22.88 ± 0.36 Ma, 1 SE (spinel). Zircon grains from marbles were found to be even younger with 17.11 ± 0.11 Ma, 1 SE. Zirconolite from ruby revealed U-Pb ages of 18.06 ± 0.09 Ma using TOF-MS (larger laser spot: 35 µm) and 29.78 ± 0.19 Ma, 1 SE using SF-MS (small laser spots: 13 & 19 µm). Zirconolite from ruby- and spinel- bearing marble showed very similar U-Pb ages of 20.43± 0.07 Ma, 1 SE (TOF) and 23.61 ± 0.18 Ma, 1 SE (SF). Additionally, the youngest zircon rim ages from Aunglan Taung gneiss revealed a concordia age at 31.98 ± 0.15 Ma, 1 SE, whereas zircons (Pb loss) from the Mogok gneiss were concordant at 26.39 ± 0.13 Ma, 1 SE.

Both, ruby and spinel revealed similar ages of the analysed zircon rims. Therefore, we presume that ruby and spinel both formed in Late Oligocene to Early Miocene as a result of post-tectonic events of the collision of the Indian and Eurosian plate, and that they formed more or less at the same metamorphic conditions. Finally, our U-Pb age-dating results on zircon and zirconolite found as inclusions in ruby and spinel, and as accessory minerals in marble (host rock) and adjacent

granulite facies gneisses do well fit with data collected in Mogok and its surrounding area and reported in literature (Barley et al. 2003; Bertrand et al. 2001; Brook and Snelling 1976; Virginie Garnier et al. 2008; GIAC 1999; Min 2007a; A. Mitchell et al. 2012; D. L. Searle and Haq 1964; M. P. Searle et al. 2007; K. Thu 2007; K Zaw et al. 2010).

4.7 Acknowledgements

I would like to thank to Ma Mie Mie (Silken East Co., Ltd, Thailand), Ko Chu (Kyauksaung mine, Mogok) and local mine owners. I am appreciated and really thanks Ko Kyaw Swar, Ko Nay, Sebastian Hänsel, U Aung Kyaw Htun, Ko Ja Mu, Ah Ba, Anty Phyu and all local people for their great help during the field trip to Mogok in 2016. Finally, special thanks to Pascal Tschudin for his kind preparation of thin sections and all colleagues from University of Basel and Swiss Gemmological Institute (SSEF).

References

Ahmad, T., Harris, N., Bickle, M., Chapman, H., Bunbury, J., & Prince, C. (2000). Isotopic constraints on the structural relationships between the lesser Himalayan series and the high Himalayan crystalline series, Garhwal Himalaya. *Geological Society of America Bulletin*, *112*, 467–477.

Arculus, R. J., & Powell, R. (1986). Source component mixing in the regions of arc magma generation. *Journal of Geophysical Research*, *91*(B6), 5913. doi:10.1029/JB091iB06p05913

Aung, L. L., Zin, E. E., Theingi, P., Elvera, N., Aung, P. P., Han, T. T., et al. (2017). Myanmar Climate Report. *MET report*, (9).

Bader, T., Franz, L., de Capitani, C., & Zhang, L. (2014). The effect of water activity on calculated phase equilibria and garnet isopleth thermobarometry of granulites, with particular reference to Tongbai (east-central China). *European Journal of Mineralogy*, *26*, 5–23.

Bader, T., Franz, L., De Capitani, C., & Zhang, L. (2014). The effect of water activity on calculated phase equilibria and garnet isopleth thermobarometry of granulites, with particular reference to Tongbai (east-central China). *European Journal of Mineralogy*, *26*, 5–23.

Barley, M. E., Pickard, A. L., Zaw, K., Rak, P., & Doyle, M. G. (2003). Jurassic to Miocene magmatism and metamorphism in the Mogok metamorphic belt and the India-Eurasia collision in Myanmar. *Tectonics*, *22*(3), 1–11. doi:10.1029/2002TC001398

BAS, M. J. L., MAITRE, R. W. L., STRECKEISEN, A., & ZANETTIN, B. (1986). A Chemical Classification of Volcanic Rocks Based on the Total Alkali-Silica Diagram. *Journal of Petrology*, *27*(3), 745–750. doi:10.1093/petrology/27.3.745

Bayliss, P., Mazzi, F., Munno, R., & White, T. J. (1989). Mineral nomenclature : zirconolite. *Mineralogical Magazine*, *53*, 565–569.

Bender, F. (1983). *Geology of Burma*.

Bertrand, G., Rangin, C., Maluski, H., & Bellon, H. (2001). Diachronous cooling along the Mogok Metamorphic Belt (Shan Scarp , Myanmar): the trace of the northward migration of India-Indochina oblique convergence since the Oligocene. *Journal of Asian Earth Sciences*, *19*, 649–659. doi:10.1016/S1367-9120(00)00061-4

Bertrand, G., Rangin, C., Maluski, H., Han, T. A., Thein, M., Myint, O., et al. (1999). Cenozoic metamorphism along the Shan scarp (Myanmar): evidences for ductile shear along the

Sagaing fault or the northward migration of the eastern Himalayan syntaxis? *Geophysical Research Letters*, *26*(7), 915–918.

Bhadra, S., & Bhattacharya, A. (2007). The barometer tremolite + tschermakite + 2 albite = 2 pargasite + 8 quartz: Constraints from experimental data at unit silica activity, with application to garnet-free natural assemblages. *American Mineralogist*, *92*, 491–502.

Bieri, W., Grobety, B., Peretti, A., Hametner, K., & Gunther, D. (2010). Chemical composition of apatite inclusions in corundum and spinel determined by LA-ICP-MS and its potential for authentication and provenance determination. *Geochimica et Cosmochimica Acta*, *74*(12), A89–A89.

Black, L. P., Kamo, S. L., Allen, C. M., Aleinikoff, J. N., Davis, D. W., Korsch, R. J., & Foudoulis, C. (2003). TEMORA 1: a new zircon standard for phanerozoic U–Pb geochronology. *Chemical Geology*, *200*, 155–170.

Brey, G. P., & Köhler, T. (1990). Geothermobarometry in four-phase lherzolites. I. New thermobarometers and practical assessment of existing thermobarometers. *Journal of Petrology*, *31*, 1353–1378.

Brook, M., & Snelling, N. J. (1976). K/Ar and Rb/Sr age determinations on rocks and minerals from Burma. *Institute of Geological Sciences, Keyworth, Nottingham, UK, Isotope Geology Unit Report*, *76*(12).

Brown, B., & Judd, J. W. (1896). The Rubies of Burma and Associated Minerals : Their Mode of Occurrence , Origin , and Metamorphoses . A Contribution to the History of Corundum. In *Philosophical Transactions of the Royal Society of London. Series A, Containing Papers of a Mathematical or Physical Character* (Vol. 187, pp. 151–228).

Campbell, I. H., Aleksandr, S., Stepanov, A. S., Liang, H.-Y., Allen, C. M., Norman, M. D., et al. (2013). The origin of shoshonites: new insights from the Tertiary high-potassium intrusions of eastern Tibet. *Contributions to Mineralogy and Petrology*, *167*, 983–1005.

Campbell, I. H., Stepanov, A. S., Liang, H. Y., Allen, C. M., Norman, M. D., Zhang, Y. Q., & Xie, Y. W. (2014). The origin of shoshonites: New insights from the Tertiary high-potassium intrusions of eastern Tibet. *Contributions to Mineralogy and Petrology*, *167*(3), 1–22. doi:10.1007/s00410-014-0983-9

Chhibber, H. L. (1934). *The Geology of Burma*. *Macmillan and Co.,Ltd, St.Martin's Street, London*.

Clegg, E. L. G. (1941). The Cretaceous and associated rocks of Burma. *Memoirs of the Geological Survey of India*, *74*(1), 1–102.

Coenraads, R. R., Lin Sutherland, F., & Kinny, P. D. (1990). The origin of sapphires: U–Pb dating of zircon inclusions sheds new light. *Mineralogical Magazine*, *54*, 113–122. doi:10.1180/minmag.1990.054.374.13

Colombi, A. (1988). *Métamorphisme et géochimie des roches mafiques des Alpes ouest-centrales (Géoprofil Viège-Domodossola-Locarno).*

Conte, A. M., Dolfi, D., Gaeta, M., Misiti, V., Mollo, S., & Perinelli, C. (2009). Experimental constraints on evolution of leucite-basanite magma at 1 and 10− 4 GPa: implications for parental compositions of Roman high-potassium magmas. *European Journal of Mineralogy*, *21*, 763–782.

De Capitani, C., & Petrakakis, K. (2010). The computation of equilibrium assemblage diagrams with Theriak/Domino software. *American Mineralogist*, *95*, 1006–1016.

Deer, W. A., Howie, R. A., & Zussman, M. A. (1992). *An introduction to the rock forming minerals.* Longman, London.

Dewey, J. F., Cande, S., & Pitman, W. C. (1989). Tectonic evolution of the India/Eurasia Collision Zone. *Eclogae Geologicae Helvetiae*, *82*(3), 717–734. doi:10.1177/053331647600900219

Dewey, J. F., Shackleton, R. M., Chengfa., C., & Sun, Y. (1988). The tectonic evolution of the Tibetan Plateau. *Phil. Trans. Roy. Soc. Lond*, *327*, 379–413.

Downs, R. T. (2006). The RRUFF Project: an integrated study of the chemistry, crystallography, Raman and infrared spectroscopy of minerals. In *Program and Abstracts of the 19th General Meeting of the International Mineralogical Association in Kobe, Japan.* (pp. O03-13).

Dzikowski, T. J. (2013). *A Comparative study of the origin of carbonate-hosted gem corundum deposits in Canada*. *unpublished thesis*. Retrieved from http://ir.obihiro.ac.jp/dspace/handle/10322/3933

Dzikowski, T. J., Dipple, G. M., Groat, L. A., Giuliani, G., & Cempírek, J. (2014). Origin of gem corundum in calcite marble: The Revelstoke occurrence in the Canadian Cordillera of British Columbia. *Lithos*, *198–199*, 281–297. doi:10.1016/j.lithos.2014.03.030

Eby, N., Woolley, A. R., Din, V., & Platt, G. (1998). Geochemistry and petrogenesis of nepheline syenites: Kaungu-Chipala, Iloba, and Ulindi nepheline syenites intrusions, North Nyasa alkaline Province, Malawi. *Journal of Petrology*, *39*, 1405–1424.

Elitok, Ö. (2019). Geology and petrology of the potassic and ultrapotassic rocks from the northern part of Senirkent (Isparta-SW Turkey): evidence of magma–carbonate wall-rock interactions. Arabian. *Journal of Geosciences*, *12*, 289–312.

Elmaleh, E., Schmidt, S. T., Karampelas, S., Link, K., Kiefert, L., Süssenberger, A., & Paul, A. (2019). U-Pb ages of zircon inclusions in Sapphires from Ratnapura and Balangoda (Sri Lanka) and Implications for Geographic origin, (May). doi:10.5741/GEMS.55.1.18

Faure, G. (2001). Alkalic Igneous Rocks on the Continents. In H. Springer, Berlin (Ed.), *Origin of Igneous Rocks* (pp. 281–350). Berlin, Heidelberg: Springer Berlin Heidelberg. doi:10.1007/978-3-662-04474-2_6

Fermor, L. L. (1930). *General report for the Geological Survey of India*. *Records of the Geological Survey, India*.

Gardiner, N. J., Robb, L. J., Morley, C. K., Searle, M. P., Cawood, P. A., Whitehouse, M. J., et al. (2016). The tectonic and metallogenic framework of Myanmar: A Tethyan mineral system. *Ore Geology Reviews*, *79*, 26–45. doi:10.1016/j.oregeorev.2016.04.024

Gardiner, N. J., Searle, M. P., Morley, C. K., Whitehouse, M. P., Spencer, C. J., & Robb, L. J. (2016). The closure of Palaeo-Tethys in Eastern Myanmar and Northern Thailand: New insights from zircon U–Pb and Hf isotope data. *Gondwana Research*, *39*, 401–422. doi:10.1016/j.gr.2015.03.001

Garnier, V., Long, P. Van, Fallick, A. E., Maluski, H., Lhomme, T., Giuliani, G., et al. (2008). Marble-hosted ruby deposits from Central and Southeast Asia: Towards a new genetic model. *Ore Geology Reviews*, *34*(1–2), 169–191. doi:10.1016/j.oregeorev.2008.03.003

Garnier, V., Maluski, H., Ohnenstetter, D., Giuliani, G., & Schwarz, D. (2006). Ar-Ar and U-Pb ages of marble-hosted ruby deposits from central and southeast Asia. *Canadian Journal of Earth Sciences*, *43*(4), 509–532. doi:10.1139/e06-005

Garnier, V., Ohnenstetter, D., Giuliani, G., Blanc, P., & Schwarz, D. (2002). Trace-element contents and cathodoluminescence of “trapiche” rubies from Mong Hsu, Myanmar (Burma): Geological

significance. *Mineralogy and Petrology*, *76*(3–4), 179–193. doi:10.1007/s007100200040

Garnier, V., Ohnenstetter, D., Giuliani, G., Maluski, H., Deloule, E., Trong, T. P., et al. (2005). Age and significance of ruby-bearing marble from the Red River Shear Zone, Northern Vietnam. *The Canadian Mineralogist*, *43*, 1315–1329.

Gellatly, D. C., & Hornung, G. (1968). Metasomatic nepheline-bearing gneisses from Darkainle Somali Republic. *The Journal of Geology*, *76*, 678–691.

GIAC. (1999). *The Tectonic of Myanmar: Final report GIAC project 1996-1999*.

Giuliani, G., Dubessy, J., Ohnenstetter, D., Banks, D., Branquet, Y., Feneyrol, J., et al. (2018). The role of evaporites in the formation of gems during metamorphism of carbonate platforms: a review. *Mineralium Deposita*, *53*(1). doi:10.1007/s00126-017-0738-4

Giuliani, G., Fallick, A. E., Boyce, A. J., Pardieu, V., & Pham, V. L. (2017). Pink and red spinels in marble: Trace elements, oxygen isotopes, and sources. *The Canadian Mineralogist*, *55*, 743–761. doi:10.3749/canmin.1700009

Giuliani, G., Fallick, A. E., Garnier, V., France-Lanord, C., Ohnenstetter, D., & Schwarz, D. (2005). Oxygen isotope composition as a tracer for the origins of rubies and sapphires. *Geology*, *33*(4), 249–252. doi:10.1130/G21261.1

Giuliani, G., Lhomme, T., Dubessy, J., Ohnenstetter, D., & Banks, D. A. (2015). Fluid inclusions in ruby from Asian marble deposits: genetic implications. *European Journal of Mineralogy*, *27*, 393–404. doi:10.1127/ejm/2015/0027-2442

Goldsmith, J. R., & Newton, R. C. (1977). Scapolite-plagioclase stability relations at high pressures and temperatures in the system NaAlSi3O8-CaAl2Si2O8-CaCO3-CaSO4. *American Mineralogist*, *62*, 1063–1081.

Gübelin, E. J. (1965). The Ruby Mines in Mogok in Burma. *Journal of Gemmology*, *9*(12), 411–426.

Gübelin, E. J., & Koivula, J. I. (1986). *Photoatlas of Inclusions in Gemstones, ABC Edition*.

Gübelin, E. J., & Koivula, J. I. (2005). *Photoatlas of Inclusions in Gemstones, Vol. 2*.

Gübelin, E. J., & Koivula, J. I. (2008). *Photolas of Inclusions in Gemstones, Vol. 3*.

Halford-Watkins, J. F. (1932a). The Ruby Mines of Upper Burma: A Short History of their Working,. *The Gemmologist*, *1*(9), 263–272.

Halford-Watkins, J. F. (1932b). Methods of Ruby Mining in Burma. *The Gemmologist*, *1*(11), 335–342.

Halford-Watkins, J. F. (1932c). Methods of Ruby Mining in Burma. *The Gemmologist*, *1*(12), 367–373.

Harlow, G. E., Sorensen, S. S., & Sisson, V. B. (2007). Jade, in Groat, L.A., ed., The Geology of Gem Deposits: Quebec. *Mineralogical Association of Canada, Short Course Series, 37*, 207–254.

Hawthorne, F. C., Oberti, R., Harlow, G. E., Maresch, W. V., Martin, R. F., Schumacher, J. C., & Welch, M. D. (2012). Nomenclature of the amphibole supergroup. *American Mineralogist*, *97*, 2031–2048.

Henry, D. J., Guidotti, C. V., & Thomson, J. (2005). The Ti-saturation surface for low-to-medium pressure metapelitic biotites: Implications for geothermometry and Ti-substitution mechanisms. *American Mineralogist*, *90*, 316–328.

Hofmann, A. W. (1988). Chemical differentiation of the Earth: the relationship between mantle, continental crust, and oceanic crust. Earth and. *Planetary Science Letters*, *90*, 297–314.

Holdaway, M. J. (2000). Application of new experimental and garnet Margules data to the garnet-biotite geothermometer. *American Mineralogist*, *85*, 881–892.

Holland, T., & Blundy, J. (1994). Non-ideal interactions in calcic amphiboles and their bearing on amphibole-plagioclase thermometry. *Contributions to Mineralogy and Petrology*, *116*, 433–447.

Horz, K. H., Worthington, T. J., Winn, K., & Stoffers, P. (2004). Late Quaternary tephra in the New Ireland Basin, Papua New Guinea. *Journal of Volcanology and Geothermal Research*, *132*(1), 73–95. doi:10.1016/S0377-0273(03)00421-9

Htay, K. N., Aung, L. T., Tajcmanova, L., & Heinrich, C. A. (2017). The Evidances of High Temperature-Medium Pressure, Granulite grade metamorphism in Momeik Area, Mogok Metamorphic Belt, Myanmar. In *Conference Abstract of 1st Myanmar Applied Earth Sciences Associtation*.

Hughes, R. W. (1997). *Ruby & Sapphire*.

Hughes, R. W. (2014). *Ruby & Sapphire—A Collector's Guide*.

Hughes, R. W. (2016). *Ruby & Sapphire: A Gemologists Guide*.

Hynes, A. (1980). Carbonatization and mobility of Ti, Y, and Zr in Ascot Formation metabasalts, SE Quebec. *Contributions to Mineralogy and Petrology*, *75*, 79–87.

Iyer, L. A. N. (1953). *The Geology and Gemstones of the Mogok Stone Tract, Burma*.

Jackson, S. E., Longerich, H. P., Dunning, G. R., & Freyer, B. J. (1992). The application of laser-ablation microprobe; inductively coupled plasma-mass spectrometry (LAM-ICP-MS) to in situ trace-element determinations in minerals. *The Canadian Mineralogist*, *30*(4), 1049–1064. https://doi.org/

Jackson, S. E., Pearson, N. J., Griffin, W. L., & Belousova, E. A. (2004). The application of laser ablation-inductively coupled plasma-mass spectrometry to in situ U-Pb zircon geochronology. *Chemical Geology*, *211*(1–2), 47–69. doi:10.1016/j.chemgeo.2004.06.017

Keller, P. C. (1985). Gemstones and Their Origins. *Terra*, *23*(3–12). doi:10.1007/978-1-4684-6674-4

Koziol, A. M., & Newton, R. C. (1988). Redetermination of the anorthite breakdown reaction and improvement of the plagioclase-garnet-Al2SiO5-quartz geobarometer. *American Mineralogist*, *73*, 216–223.

La Touche, T. H. D. (1913). *Geology of the Northern Shan State*. *Office of the Geological Survey of India, Calcutta, India*.

Lal, R. K. (1993). Internally consistent recalibrations of mineral equilibria for geothermobarometry involving garnet-orthopyroxene-plagioclase-quartz assemblages and their application to the South Indian granulites. *Journal of Metamorphic Geology*, *11*, 855–866.

Leake, B. W., Wooley, A. R., Arps, C. E. S., Birch, W. D., Gilbert, M. C., Grice, J. D., et al. (1997). Nomenclature of amphiboles. Report of the subcommittee on amphiboles of the International Mineralogical Association Commission on new minerals and mineral names. *European Journal of Mineralogy*, *9*, 623–651.

Lee, H.-Y., Sun-Lin Chung, S.-L., & H.-M., H.-M. Y. (2016). Late Cenozoic volcanism in central Myanmar: Geochemical characteristics and geodynamic significance. *Lithos*, *245*, 174–190.

Lee, H. Y., Chung, S. L., & Yang, H. M. (2016). Late Cenozoic volcanism in central Myanmar: Geochemical characteristics and geodynamic significance. *Lithos*, *245*, 174–190. doi:10.1016/j.lithos.2015.09.018

Licht, A., France-Lanord, C., Reisberg, L., Fontaine, C., Soe, A. N., & Jaeger, J.-J. (2013). A paleo Tibet-Myanmar connection? Reconstructing the Later Eocene drainage systems of Central Myanmar using a multi-proxy approach. *J. Geol. Soc. London*, *170*, 929–939.

Link, K. (2015). Age determination of zircon inclusions in faceted sapphires. *J. Gemmol.*, *34*, 692–700.

Link, K. (2016). New age data for blue sapphire from Mogok, Myanmar. *J. Gemmol.*, *35*, 107–109.

Lustrino, M., Fedele, L., Agostini, S., Prelević, D., & Salari, G. (2019). Leucitites within and around the Mediterranean area. *Lithos*, *324–325*, 216–233.

Meschede, M. (1986). A method of discrimination between different types of mid-ocean ridge basalts and continental tholeiites with the Nb–Zr–Y diagram. *Chemical Geology*, *56*, 207–218.

Miller, C., Thoni, M., Frank, W., Grasemann, B., Klotzli, U., Guntli, P., & Draganits, E. (2001). The early Palaeozoic magmatic event in the Northwest Himalaya, India: source, tectonic setting and age of emplacement. *Geol. Mag.*, *138*, 237–251.

Min, M. (2007a). *Chapter 5. Exhumation of the Mogok Belt in central Myanmar:a geochronologic study. In: thermochronology applied to strike-slip zones Central Ameria and Myanmar.*

Min, M. (2007b). *Chapter 5 Exhumation of the Mogok belt in central Myanmar : a geochronologic study*.

Mitchell, A. H. G. (1993). Cretaceous-Cenozoic tectonic events in the western Myanmar (Burma)-Assam region. *Journal of the Geological Society*, *150*, 1089–1102.

Mitchell, A. H. G., Marshall, T. R., Skinner, A. C., Baker, A. D., Amos, B. J., & Bateson, J. H. (1977). Geology and exploration geochemistry of the Yadanartheingi anf Kyaukme-Longtawkno areas, Northern Shan States, Burma. *Overseas Geology and Mineral Resources*, *51*(35).

Mitchell, A. H. G., Oo, T., Win, M. N., Hlaing, T., Htun, K. M., & Htay, M. T. (2006). Rock relationships in the Mogok metamorphic belt, Tatkon to Mandalay, central Myanmar. *Journal of Asian Earth Sciences*, *29*(5–6), 891–910. doi:10.1016/j.jseaes.2006.05.009

Mitchell, A., Oo, T., Lin, T.-H., Hung, C.-H., & Chung, S.-L. (2012). Zircon U–Pb ages in Myanmar: Magmatic–metamorphic events and the closure of a neo-Tethys ocean? *Journal of Asian Earth Sciences*, *56*, 1–23. doi:10.1016/j.jseaes.2012.04.019

Morimoto, N., Fabries, J., Ferguson, A. K., Ginzburg, I. V., Ross, M., Seifert, F. A., et al. (1988). Nomenclature of amphiboles. *Mineralogy and Petrology*, *39*, 55–76.

Moyd, L. (1949). Petrology of the nepheline and corundum rocks of southeastern Ontario. *American Mineralogist*, *34*, 736–750.

Mullen, E. D. (1983). MnO/TiO2/P2O5: a major element discriminant for basaltic rocks of oceanic environments and its implications for petrogenesis. *Earth Planet. Sci. Lett.*, *62*, 53–62.

Newton, R. C., Aranovich, L. Y., Hansen, E. C., & Vandenheuvel, B. A. (1998). Hypersaline fluids in Precambrian deep-crustal metamorphism. *Precambrian Res.*, *91*, 41–63.

Norman, M. D., & Nemchin, A. A. (2014). A 4.2 billion year old impact basin on the Moon: U-Pb dating of zirconolite and apatite in lunar melt rock 67955. *Earth and Planetary Science Letters*, *388*, 387–398. doi:10.1016/j.epsl.2013.11.040

Pearce, J. A., & Cann, J. R. (1973). Tectonic setting of basic volcanic rocks using Ti, Zr and Y. *Earth and Planetary Sciences and Letters*, *19*, 290–300.

Pearce, J. A., & Parkinson, I. J. (1993). Trace element models for mantle melting: application to volcanic arc petrogenesis; in Prichard, H.M., Alabaster, T., Harris, N.B.W., and Neary, C.R., eds., Magmatic Processes and Plate Tectonics,. *Geological Society Special Publications*, *76*, 373–403.

Peretti, A., Peretti, A. K., & Günther, D. (2015). World of Magnificent Spinels Provenance and Identification. *Contributions to Gemology*, *11*(May).

Phyo, M. M., Franz, L., Bieler, E., Balmer, W., & Krzemnicki, M. S. (2019). Spinel from Mogok, Myanmar—A Detailed Inclusion Study by Raman Microspectroscopy and Scanning Electron Microscopy. *The Journal of Gemmology*, *36*(5), 418–435. doi:10.15506/JoG.2019.36.5.418

Powell, M. & Powell, R. (1977). A nepheline-alkali feldspar geothermometer. *Contributions to Mineralogy and Petrology*, *62*, 193–204.

Powell, R. (1985). Regression diagnostics and robust regression in geothermometer/geobarometer calibration: the garnet-clinopyroxene geothermometer revisited. *Journal of Metamorphic Geology*, *3*, 231–243.

Prelević, D., Akal, C., Romer, R. L., Mertz-Kraus, R., & Helvacı, C. (2015). Magmatic response to slab tearing: constraints from the Afyon Alkaline Volcanic Complex, Western Turkey. *Journal of*

Petrology, *56*, 527–562.

Prelević, D., Foley, S. F., Romer, R., & Conticelli, S. (2008). Mediterranean Tertiary lamproites derived from multiple source components in postcollisional geodynamics. *Geochimica et Cosmochimica Acta*, *72*, 2125–2156.

Reiners, P. W., Carlson, R. W., Renne, P. R., Coo per, K. M., Granger, D. E., M c Lean, N. M., & Schoene, B. (2018). *Geochronology and Thermochronology.* (J. W. & Sons, Ed.).

RICHARDS, A., ARGLES, T., HARRIS, N., PARRISH, R., AHMAD, T., DARBYSHIRE, F., & DRAGANITS, E. (2005). Himalayan architecture constrained by isotopic tracers from clastic sediments. *Earth and Planetary Science Letters*, *236*(3–4), 773–796. doi:10.1016/j.epsl.2005.05.034

Rickwood, P. C. (1989). Boundary lines within petrologic diagrams which use oxides of major and minor elements. *Lithos*, *22*(4), 247–263. doi:10.1016/0024-4937(89)90028-5

Romer, R. L., & Hahne, K. (2010). Life of the Rheic Ocean: Scrolling through the shale record. *Gondwana Res.*, *17*, 236–253.

Ryburn, R. J., Raheim, A., & Green, D. H. (1976). Determination of P,T paths of natural eclogites; a correction. *Lithos*, *9*, 161–164.

Santosh, M., & Omori, S. (2008). CO2 flushing: a plate tectonic perspective. *Gondwana Res.*, *13*, 86–102.

Schaltegger, U., Schmitt, A. K., & Horstwood, M. S. A. (2015). U-Th-Pb zircon geochronology by ID-TIMS, SIMS, and laser ablation ICP-MS: Recipes, interpretations, and opportunities. *Chemical Geology*, *402*(March), 89–110. doi:10.1016/j.chemgeo.2015.02.028

Searle, D. L., & Haq, B. T. (1964). The Mogok belt of Burma and its relationship to the Himalayan orogeny. In *The international geological congress 22* (pp. 132–161).

Searle, M. P., Noble, S. R., Cottle, J. M., Waters, D. J., Mitchell, A. H. G., Hlaing, T., & Horstwood, M. S. A. (2007). Tectonic evolution of the Mogok metamorphic belt, Burma (Myanmar) constrained by U-Th-Pb dating of metamorphic and magmatic rocks. *Tectonics*, *26*(3). doi:10.1029/2006TC002083

Searle, M. P., Waters, D. J., Morley, C. K., Gardiner, N. J., Htun, U. K., Nu, T. T., & Robb, L. J. (2017). *Chapter 12 Tectonic evolution of the Mogok metamorphic and Jade mines belts and ophiolitic terranes of Burma (Myanmar)*. *Myanmar: Geology, Resources and Tectonics* (Vol. 48).

Geological Society Memoir48. doi:10.1029/2006TC002083

Sláma, J., Košler, J., Condon, D. J., Crowley, J. L., Gerdes, A., Hanchar, J. M., et al. (2008). Plešovice zircon — A new natural reference material for U–Pb and Hf isotopic microanalysis. *Chemical Geology*, *249*, 1–35.

Sone, M., & Metcalfe, I. (2008). Parallel Tethyab sutures in mainland Southeast Asia: new insights for Palaeo-Tethys closure and implications for the Indosinian Orogeny. *Comptes Rendus Geoscience*, *340*, 166–179.

Stern, R. J., Tsujimori, T., Harlow, G., & Groat, L. A. (2013). Plate tectonic gemstones. *Geology*, *41*(7), 723–726. doi:10.1130/G34204.1

Stucki, A., Trommsdorff, V., & Gunther, D. (2001). Zirconolite in metarodingites of Penninic Mesozoic ophiolites, Central Alps. *Schweizerische Mineralogische Und Petrographische Mitteilungen*, *81*(2), 257–265.

Sutherland, F. ., Coenraads, R. ., Hoskin, P. W. ., Bosshart, G., & Fanning, C. . (2002). Sapphire crystallization, age and origin, Ban Huai Sai, Laos: age based on zircon inclusions. *Journal of Asian Earth Sciences*, *20*(7), 841–849. doi:10.1016/s1367-9120(01)00067-0

Sutherland, F. L., Duroc-Danner, J. M., & Meffre, S. (2008). Age and origin of gem corundum and zircon megacrysts from the Mercaderes-Rio Mayo area, South-west Colombia, South America. *Ore Geology Reviews*, *34*(1–2), 155–168. doi:10.1016/j.oregeorev.2008.01.004

Sutherland, F. L., Piilonen, P. C., Zaw, K., Meffre, S., & Thompson, J. (2015). Sapphire within zircon-rich gem deposits , Bo Loei , Ratanakiri Province , Cambodia : trace elements , inclusions , U – Pb dating and genesis. *Australian Journal of Earth Sciences*, *62*, 761–773. doi:10.1080/08120099.2015.1101015

Sutherland, F. L., Zaw, K., Meffre, S., Thompson, J., Goemann, K., Thu, K., et al. (2018). Diversity In Ruby Geochemistry And Its Inclusions, Intra- And Inter Comparisons From Myanmar And East Australia. In *Meeting of the international mineralogical association* (p. 329).

Sutherland, F. L., Zaw, K., Meffre, S., Thompson, J., Goemann, K., Thu, K., et al. (2019). Diversity in Ruby Geochemistry and Its Inclusions: Intra- and Inter- Continental Comparisons from Myanmar and Eastern Australia. *Minerals*, *9*(1), 28. doi:10.3390/min9010028

Sylvester, P. J., & Ghaderi, M. (1997). Trace element analysis of scheelite by excimer laser ablation-

inductively coupled plasma-mass spectrometry (ELA-ICP-MS) using a synthetic silicate glass standard. *Chemical Geology*, *141*(1–2), 49–65. doi:10.1016/S0009-2541(97)00057-0

Tajčmanová, L., Konopasek, J., & Schulmann, K. (2006). Thermal evolution of the orogenic lower crust during exhumation within a thickened Moldanubian root of the Variscan belt of central Europe. *Journal of Metamorphic Geol.*, *24*, 119–134.

Thein, M. (1973). A preliminary synthesis of the geological evolution of Burma with reference to the tectonic development of Southeast Asia. *Geological Society of Malaysia*, *6*, 87–116.

Thein, M. (2008). Modes of occurrence and origin of precious gemstone deposits of the Mogok Stone Tract. *Journal of the Myanmar Geosciences Society*, *1*, 75–84.

Thein, M. L., Myint, O., Kyi, S., & P. N. Win. (1990). *Geology and stratigraphy of the metamorphosed Early Paleozoic rocks of the Mogok–Thabeikkyin–Singu–Madaya Areas. Unpublished staff report* (Vol. 98).

Themelis, T. (2008). *Gems and Mines of Mogok*.

Thu, K. (2007). *The Igneous Rocks of the Mogok Stone Tract: Their Distribution, Petrography, Petrochemistry, Sequence, Geochronology and Economic Geology. Ph.D. Thesis, University of Yangon, Yangon, Myanmar*.

Thu, Y. K., Enami, M., Kato, T., & Tsuboi, M. (2017). Granulite facies paragneisses from the middle segment of the Mogok metamorphic belt, central Myanmar. *Journal of Mineralogical and Petrological Sciences*, *112*(1), 1–19. doi:10.2465/jmps.160526

Thu, Y. K., Win, M. M., Enami, M., & Tsuboi, M. (2016). Ti-rich biotite in spinel and quartz-bearing paragneiss and related rocks from the Mogok metamorphic belt, central Myanmar. Journal of Mineralogical and. *Petrological Sciences*, *111*, 270–282.

Touret, J. L. R. (1971). Le faciés granulite en Norvège Méridionale. II: les inclusions fluides. *Lithos*, *4*, 423–436.

Touret, J. L. R., & Huizenga, J. M. (2012). Fluid-assisted granulite metamorphism: a continental journey. *Gondwana Res.*, *21*, 224–235.

Ulianov, A., Müntener, O., Schaltegger, U., & Bussy, F. (2012). The data treatment dependent variability of U-Pb zircon ages obtained using mono-collector, sector field, laser ablation ICPMS. *Journal of Analytical Atomic Spectrometry*, *27*(4), 663–676. doi:10.1039/c2ja10358c

Vermeesch, P. (2018). IsoplotR: A free and open toolbox for geochronology. *Geoscience Frontiers*, *9*(5), 1479–1493. doi:10.1016/j.gsf.2018.04.001

Waltham, T. (1999). The ruby mines of Mogok. *Geology Today*, *15*, 143–149.

Wang, Y., Sieh, K., Thura, A., Soe, M., Saw, N. K., & Soe, T. T. (2011). Earthquakes and Slip rate of the sounthern Sagaing-fault: insights from an offset ancient fort wall, lower Burma (Myanmar). *Geophysical Journal International*, *185*, 49–64.

Wiedenbeck, M., Alle, P., Corfu, F., Griffin, W. L., Meier, M., F., O., et al. (1995). Three natural zircon standards for U–Th–Pb, Lu–Hf, trace element and REE analyses. *Geostandards Newsletter*, *19*, 1–23.

Win, M. M., Enami, M., & Kato, T. (2016). Metamorphic conditions and CHIME monazite ages of Late Eocene to Late Oligocene high-temperature Mogok metamorphic rocks in central Myanmar. *Journal of Asian Earth Sciences*, *117*, 304–316. doi:10.1016/j.jseaes.2015.11.023

Wu, C.-M., Zhang, J., & Ren, L. D. (2004). Empirical garnet-biotite-plagioclase-quartz (GBPQ) geobarometry in medium-to high-grade metapelites. *Journal of Petrology*, *45*, 1907–1921.

Wu, F. Y., Yang, Y. H., Mitchell, R. H., Bellatreccia, F., Li, Q. L., & Zhao, Z. F. (2010). In situ U-Pb and Nd-Hf-(Sr) isotopic investigations of zirconolite and calzirtite. *Chemical Geology*, *277*(1–2), 178–195. doi:10.1016/j.chemgeo.2010.08.007

Wuhrer, R., Beattie, R., Coenraads, R. R., Abduriyim, A., Giuliani, G., Hoskin, P. W. O., et al. (2015). Corundum (sapphire) and zircon relationships, Lava Plains gem fields, NE Australia: Integrated mineralogy, geochemistry, age determination, genesis and geographical typing. *Mineralogical Magazine*, *79*(03), 545–581. doi:10.1180/minmag.2015.079.3.04

Xiang, H., Zhang, L., Zhong, Z.-Q., Santosh, M., Zhou, H.-W., Zhang, H.-F., et al. (2012). Ultrahigh-temperature metamorphism and anticlockwise P-T-t path of Paleozoic granulites from north Qinling-Tongbai orogen, Central China. *Gondwana Res.*, *21*, 559–576.

Yang, W. Bin, Niu, H. C., Shan, Q., Sun, W. D., Zhang, H., Li, N. B., et al. (2014). Geochemistry of magmatic and hydrothermal zircon from the highly evolved Baerzhe alkaline granite: Implications for Zr-REE-Nb mineralization. *Mineralium Deposita*, *49*(4), 451–470. doi:10.1007/s00126-013-0504-1

Yonemura, K., OsanaiI, Y., Zaw, T. N., Nakano, N., Charusiri, P., & Adachi, T. (2013). EPMA U-Th-Pb

monazite dating of metamorphic rocks from the Mogok Metamorphic Belt, central Myanmar. *Journal of Mineralogical and Petrological Sciences*, *108*(3), 184–188. doi:10.2465/jmps.121019a

Yui, T. F., Zaw, K., & Wu, C. M. (2008). A preliminary stable isotope study on Mogok Ruby, Myanmar. *Ore Geology Reviews*, *34*(1–2), 192–199. doi:10.1016/j.oregeorev.2008.05.001

Zartman, R. E., & Doe, B. R. (1981). Plumbotectonics - the model. *Tectonophysics*, *75*, 135–162.

Zaw, K. (1989). Comments on transcurrent movements in the Myanmar-Andaman sea region. *Geology*, *17*, 93–95.

Zaw, K. (1990). Geological, petrological and geochemical characteristics of granitoid rocks in Burma: with special reference to the associated W-Sn mineralization and their tectonic setting. *Journal of Southeast Asian Earth Sciences*, *4*, 293–335.

Zaw, K. (1998). Geological evolution of selected granitic pegmatites in myanmar (burma): Constraints from regional setting, lithology, and fluid-inclusion studies. *International Geology Review*, *40*(7), 647–662. doi:10.1080/00206819809465229

Zaw, K. (2017). *Overview of mineralization styles and tectonic-metallogenic setting in Myanmar. In Myanmar: Geology, Resources and Tectonics; Chapter 24; Barber, A.J., Zaw, K., Crow, M.J., Eds.; Geological Society London Memoirs*.

Zaw, K., Sutherland, F. L., Graham, I., Meffre, S., & Thu, K. (2010). Dating zircon inclusions in gem corundum deposits and genetic implications, 7.

Zaw, K., Sutherland, L., Yui, T. F., Meffre, S., & Thu, K. (2014). Vanadium-rich ruby and sapphire within Mogok Gemfield, Myanmar: implications for gem color and genesis. *Mineralium Deposita*, *50*(1), 25–39. doi:10.1007/s00126-014-0545-0

Zaw, K., Thu, K., Meffre, S., Yui, T. F., & Sutherland, F. L. (2015). Vanadium-rich ruby and sapphire within Mogok Gemfield, Myanmar: implications for gem color and genesis. *Mineralium Deposita*, *50*(1), 25–39. doi:10.1007/s00126-014-0545-0

Zuleger, E., & Erzinger, J. (1988). Determination of the REE and Y in silicate materials with ICP-AES. *Fresenius' Zeitschrift für Analytische Chemie*, *332*(2), 140–143. doi:10.1007/BF00470631

CHAPTER V

Summary and Conclusions

In my thesis, I have focused on the formation of the gemstones ruby and spinel from the Mogok Stone Tract combining mineralogical, gemmological, geochronological and petrological investigations. In my thesis, I present my results in three parts, a published paper about inclusions in spinels from Mogok, and two paper drafts to be submitted about the petrology and geochronology of the mineralisations in the Mogok area.

Summarising the first part, I could document 16 new mineral inclusions in gem-quality spinel from Mogok, so far not described in gemmological literature. These include mineral inclusions such as pargasite, anatase, baddeleyite, boehmite, brucite, chlorite, clinohumite, clinopyroxene, diaspore, geikielite, goethite, halite, marcasite, molybdenite, periclase and pyrrhotite. Moreover, I could confirm the presence of numerous inclusions already described in spinel from Mogok, such as anhydrite, apatite, carbonates (calcite, dolomite and magnesite), chondrodite, elemental sulphur, graphite, iron oxides or iron hydroxides, forsterite, phlogopite and zircon. The presence of the high-grade inclusions anatase, clinopyroxene, chondrodite, olivine and periclase in Mogok spinel highlights granulite facies metamorphism while the presence of sulphur and graphite inclusions point to a highly reducing environment.

For the second part (petrology), I investigated selected samples of quartz gneiss, nepheline gneiss and clinopyroxene-clinoamphibole gneiss collected in the vicinity of gemstones bearing marbles of the Mogok area. Conventional geothermobarometry and phase equilibrium calculations using the Theriak-Domino software revealed granulite facies conditions of 756-792°C at 7-8 kbar and water activities of 0.3-0.4 in the quartz gneiss. Similar metamorphic conditions could also be estimated for the nepheline gneiss and the clinopyroxene-clinoamphibole gneiss, whose metamorphic overprint and field relations characterise them as pre- to syn-tectonic metadykes. Geochemical studies of the nepheline gneiss and the clinopyroxene-clinoamphibole gneiss classified them as foidite, phonotephrite, tephriphonolite and picrobasalt. Discrimination diagrams, trace element patterns and isotopic data highlight a strong magmatic fractionation of these rocks pointing to a generation during subduction-related magmatic processes. Especially the magmatic protoliths of the nepheline gneisses are assumed to be genetically linked to foid-bearing syenites, which intruded the Mogok Metamorphic Belt 35-23 Ma ago.

For the third part (geochronology), I analysed selected zircon and zirconolite inclusions from gemstones as well as host rocks (marble and gneisses) from the Mogok area in Myanmar. A wide range U-Pb ages were calculated in the core of zircon grains found in gemstones and host rocks, thus suggesting that Mogok area had experienced several magmatic and metamorphic events during Middle Phanerozoic. U-Pb age dating results of zircon rims and zirconolite reveal Concordia ages between Oligocene to Early Miocene (around ~32 Ma to ~20 Ma).

In conclusions, I postulate that the formation of the marble-hosted ruby and spinel in the Mogok are took place at granulite facies conditions between Oligocene to Early Miocene (~32 Ma to ~20 Ma) and was related to syn- and post-tectonic events during the collisions of the Indian plate with the Eurasian plate.

These findings are in accordance with recent literature within the Mogok area and its adjacent area (Bertrand et al. 2001; Brook and Snelling 1976; Gardiner, Robb, et al. 2016; V Garnier et al. 2006; Min 2007b; A. Mitchell et al. 2012; M. P. Searle et al. 2007; Sutherland et al. 2019; K. Thu 2007) and offer numerous perspectives for further research on the petrology, geochronology and gemmology in the Mogok area and similar settings in Myanmar. Raman microspectroscopy on gem-quality ruby and spinel from other mines as well as phase diagram calculations (T vs XCO_2 analysis) of ruby- and spinel- bearing marble from Mogok could provide effective tools for the identification of their origin, both locally and genetically. The finding of such peculiar rocks as the nepheline gneisses raises the question whether such calc-alkaline to shoshonitic magmatites occur in other parts of Myanmar. Furthermore, a thorough geochemical and geochronological study of Paleogene nepheline syenites from Myanmar should enable us to interpret their genetic relation to the nepheline gneisses and exhaustively characterize their geotectonic setting. Finally, a combination of all these data could lead to a completely new and innovative model for the generation of the Mogok gemstone deposits.

References

Ahmad, T., Harris, N., Bickle, M., Chapman, H., Bunbury, J., & Prince, C. (2000). Isotopic constraints on the structural relationships between the lesser Himalayan series and the high Himalayan crystalline series, Garhwal Himalaya. *Geological Society of America Bulletin*, *112*, 467–477.

Arculus, R. J., & Powell, R. (1986). Source component mixing in the regions of arc magma generation. *Journal of Geophysical Research*, *91*(B6), 5913. doi:10.1029/JB091iB06p05913

Aung, L. L., Zin, E. E., Theingi, P., Elvera, N., Aung, P. P., Han, T. T., et al. (2017). Myanmar Climate Report. *MET report*, (9).

Bader, T., Franz, L., de Capitani, C., & Zhang, L. (2014). The effect of water activity on calculated phase equilibria and garnet isopleth thermobarometry of granulites, with particular reference to Tongbai (east-central China). *European Journal of Mineralogy*, *26*, 5–23.

Bader, T., Franz, L., De Capitani, C., & Zhang, L. (2014). The effect of water activity on calculated phase equilibria and garnet isopleth thermobarometry of granulites, with particular reference to Tongbai (east-central China). *European Journal of Mineralogy*, *26*, 5–23.

Barley, M. E., Pickard, A. L., Zaw, K., Rak, P., & Doyle, M. G. (2003). Jurassic to Miocene magmatism and metamorphism in the Mogok metamorphic belt and the India-Eurasia collision in Myanmar. *Tectonics*, *22*(3), 1–11. doi:10.1029/2002TC001398

BAS, M. J. L., MAITRE, R. W. L., STRECKEISEN, A., & ZANETTIN, B. (1986). A Chemical Classification of Volcanic Rocks Based on the Total Alkali-Silica Diagram. *Journal of Petrology*, *27*(3), 745–750. doi:10.1093/petrology/27.3.745

Bayliss, P., Mazzi, F., Munno, R., & White, T. J. (1989). Mineral nomenclature : zirconolite. *Mineralogical Magazine*, *53*, 565–569.

Bender, F. (1983). *Geology of Burma*.

Bertrand, G., Rangin, C., Maluski, H., & Bellon, H. (2001). Diachronous cooling along the Mogok Metamorphic Belt (Shan Scarp , Myanmar): the trace of the northward migration of India-Indochina oblique convergence since the Oligocene. *Journal of Asian Earth Sciences*, *19*, 649–659. doi:10.1016/S1367-9120(00)00061-4

Bertrand, G., Rangin, C., Maluski, H., Han, T. A., Thein, M., Myint, O., et al. (1999). Cenozoic metamorphism along the Shan scarp (Myanmar): evidences for ductile shear along the

Sagaing fault or the northward migration of the eastern Himalayan syntaxis? *Geophysical Research Letters*, *26*(7), 915–918.

Bhadra, S., & Bhattacharya, A. (2007). The barometer tremolite + tschermakite + 2 albite = 2 pargasite + 8 quartz: Constraints from experimental data at unit silica activity, with application to garnet-free natural assemblages. *American Mineralogist*, *92*, 491–502.

Bieri, W., Grobety, B., Peretti, A., Hametner, K., & Gunther, D. (2010). Chemical composition of apatite inclusions in corundum and spinel determined by LA-ICP-MS and its potential for authentication and provenance determination. *Geochimica et Cosmochimica Acta*, *74*(12), A89–A89.

Black, L. P., Kamo, S. L., Allen, C. M., Aleinikoff, J. N., Davis, D. W., Korsch, R. J., & Foudoulis, C. (2003). TEMORA 1: a new zircon standard for phanerozoic U–Pb geochronology. *Chemical Geology*, *200*, 155–170.

Brey, G. P., & Köhler, T. (1990). Geothermobarometry in four-phase lherzolites. I. New thermobarometers and practical assessment of existing thermobarometers. *Journal of Petrology*, *31*, 1353–1378.

Brook, M., & Snelling, N. J. (1976). K/Ar and Rb/Sr age determinations on rocks and minerals from Burma. *Institute of Geological Sciences, Keyworth, Nottingham, UK, Isotope Geology Unit Report*, *76*(12).

Brown, B., & Judd, J. W. (1896). The Rubies of Burma and Associated Minerals : Their Mode of Occurrence , Origin , and Metamorphoses . A Contribution to the History of Corundum. In *Philosophical Transactions of the Royal Society of London. Series A, Containing Papers of a Mathematical or Physical Character* (Vol. 187, pp. 151–228).

Campbell, I. H., Aleksandr, S., Stepanov, A. S., Liang, H.-Y., Allen, C. M., Norman, M. D., et al. (2013). The origin of shoshonites: new insights from the Tertiary high-potassium intrusions of eastern Tibet. *Contributions to Mineralogy and Petrology*, *167*, 983–1005.

Campbell, I. H., Stepanov, A. S., Liang, H. Y., Allen, C. M., Norman, M. D., Zhang, Y. Q., & Xie, Y. W. (2014). The origin of shoshonites: New insights from the Tertiary high-potassium intrusions of eastern Tibet. *Contributions to Mineralogy and Petrology*, *167*(3), 1–22. doi:10.1007/s00410-014-0983-9

Chhibber, H. L. (1934). *The Geology of Burma*. *Macmillan and Co.,Ltd, St.Martin's Street, London*.

Clegg, E. L. G. (1941). The Cretaceous and associated rocks of Burma. *Memoirs of the Geological Survey of India*, *74*(1), 1–102.

Coenraads, R. R., Lin Sutherland, F., & Kinny, P. D. (1990). The origin of sapphires: U–Pb dating of zircon inclusions sheds new light. *Mineralogical Magazine*, *54*, 113–122. doi:10.1180/minmag.1990.054.374.13

Colombi, A. (1988). *Métamorphisme et géochimie des roches mafiques des Alpes ouest-centrales (Géoprofil Viège-Domodossola-Locarno).*

Conte, A. M., Dolfi, D., Gaeta, M., Misiti, V., Mollo, S., & Perinelli, C. (2009). Experimental constraints on evolution of leucite-basanite magma at 1 and 10− 4 GPa: implications for parental compositions of Roman high-potassium magmas. *European Journal of Mineralogy*, *21*, 763–782.

De Capitani, C., & Petrakakis, K. (2010). The computation of equilibrium assemblage diagrams with Theriak/Domino software. *American Mineralogist*, *95*, 1006–1016.

Deer, W. A., Howie, R. A., & Zussman, M. A. (1992). *An introduction to the rock forming minerals.* Longman, London.

Dewey, J. F., Cande, S., & Pitman, W. C. (1989). Tectonic evolution of the India/Eurasia Collision Zone. *Eclogae Geologicae Helvetiae*, *82*(3), 717–734. doi:10.1177/053331647600900219

Dewey, J. F., Shackleton, R. M., Chengfa., C., & Sun, Y. (1988). The tectonic evolution of the Tibetan Plateau. *Phil. Trans. Roy. Soc. Lond*, *327*, 379–413.

Downs, R. T. (2006). The RRUFF Project: an integrated study of the chemistry, crystallography, Raman and infrared spectroscopy of minerals. In *Program and Abstracts of the 19th General Meeting of the International Mineralogical Association in Kobe, Japan.* (pp. O03-13).

Dzikowski, T. J. (2013). *A Comparative study of the origin of carbonate-hosted gem corundum deposits in Canada*. *unpublished thesis*. Retrieved from http://ir.obihiro.ac.jp/dspace/handle/10322/3933

Dzikowski, T. J., Dipple, G. M., Groat, L. A., Giuliani, G., & Cempírek, J. (2014). Origin of gem corundum in calcite marble: The Revelstoke occurrence in the Canadian Cordillera of British Columbia. *Lithos*, *198–199*, 281–297. doi:10.1016/j.lithos.2014.03.030

Eby, N., Woolley, A. R., Din, V., & Platt, G. (1998). Geochemistry and petrogenesis of nepheline syenites: Kaungu-Chipala, Iloba, and Ulindi nepheline syenites intrusions, North Nyasa alkaline Province, Malawi. *Journal of Petrology*, *39*, 1405–1424.

Elitok, Ö. (2019). Geology and petrology of the potassic and ultrapotassic rocks from the northern part of Senirkent (Isparta-SW Turkey): evidence of magma–carbonate wall-rock interactions. Arabian. *Journal of Geosciences*, *12*, 289–312.

Elmaleh, E., Schmidt, S. T., Karampelas, S., Link, K., Kiefert, L., Süssenberger, A., & Paul, A. (2019). U-Pb ages of zircon inclusions in Sapphires from Ratnapura and Balangoda (Sri Lanka) and Implications for Geographic origin, (May). doi:10.5741/GEMS.55.1.18

Faure, G. (2001). Alkalic Igneous Rocks on the Continents. In H. Springer, Berlin (Ed.), *Origin of Igneous Rocks* (pp. 281–350). Berlin, Heidelberg: Springer Berlin Heidelberg. doi:10.1007/978-3-662-04474-2_6

Fermor, L. L. (1930). *General report for the Geological Survey of India*. *Records of the Geological Survey, India*.

Gardiner, N. J., Robb, L. J., Morley, C. K., Searle, M. P., Cawood, P. A., Whitehouse, M. J., et al. (2016). The tectonic and metallogenic framework of Myanmar: A Tethyan mineral system. *Ore Geology Reviews*, *79*, 26–45. doi:10.1016/j.oregeorev.2016.04.024

Gardiner, N. J., Searle, M. P., Morley, C. K., Whitehouse, M. P., Spencer, C. J., & Robb, L. J. (2016). The closure of Palaeo-Tethys in Eastern Myanmar and Northern Thailand: New insights from zircon U–Pb and Hf isotope data. *Gondwana Research*, *39*, 401–422. doi:10.1016/j.gr.2015.03.001

Garnier, V., Long, P. Van, Fallick, A. E., Maluski, H., Lhomme, T., Giuliani, G., et al. (2008). Marble-hosted ruby deposits from Central and Southeast Asia: Towards a new genetic model. *Ore Geology Reviews*, *34*(1–2), 169–191. doi:10.1016/j.oregeorev.2008.03.003

Garnier, V., Maluski, H., Ohnenstetter, D., Giuliani, G., & Schwarz, D. (2006). Ar-Ar and U-Pb ages of marble-hosted ruby deposits from central and southeast Asia. *Canadian Journal of Earth Sciences*, *43*(4), 509–532. doi:10.1139/e06-005

Garnier, V., Ohnenstetter, D., Giuliani, G., Blanc, P., & Schwarz, D. (2002). Trace-element contents and cathodoluminescence of “trapiche” rubies from Mong Hsu, Myanmar (Burma): Geological

significance. *Mineralogy and Petrology*, *76*(3–4), 179–193. doi:10.1007/s007100200040

Garnier, V., Ohnenstetter, D., Giuliani, G., Maluski, H., Deloule, E., Trong, T. P., et al. (2005). Age and significance of ruby-bearing marble from the Red River Shear Zone, Northern Vietnam. *The Canadian Mineralogist*, *43*, 1315–1329.

Gellatly, D. C., & Hornung, G. (1968). Metasomatic nepheline-bearing gneisses from Darkainle Somali Republic. *The Journal of Geology*, *76*, 678–691.

GIAC. (1999). *The Tectonic of Myanmar: Final report GIAC project 1996-1999*.

Giuliani, G., Dubessy, J., Ohnenstetter, D., Banks, D., Branquet, Y., Feneyrol, J., et al. (2018). The role of evaporites in the formation of gems during metamorphism of carbonate platforms: a review. *Mineralium Deposita*, *53*(1). doi:10.1007/s00126-017-0738-4

Giuliani, G., Fallick, A. E., Boyce, A. J., Pardieu, V., & Pham, V. L. (2017). Pink and red spinels in marble: Trace elements, oxygen isotopes, and sources. *The Canadian Mineralogist*, *55*, 743–761. doi:10.3749/canmin.1700009

Giuliani, G., Fallick, A. E., Garnier, V., France-Lanord, C., Ohnenstetter, D., & Schwarz, D. (2005). Oxygen isotope composition as a tracer for the origins of rubies and sapphires. *Geology*, *33*(4), 249–252. doi:10.1130/G21261.1

Giuliani, G., Lhomme, T., Dubessy, J., Ohnenstetter, D., & Banks, D. A. (2015). Fluid inclusions in ruby from Asian marble deposits: genetic implications. *European Journal of Mineralogy*, *27*, 393–404. doi:10.1127/ejm/2015/0027-2442

Goldsmith, J. R., & Newton, R. C. (1977). Scapolite-plagioclase stability relations at high pressures and temperatures in the system NaAlSi3O8-CaAl2Si2O8-CaCO3-CaSO4. *American Mineralogist*, *62*, 1063–1081.

Gübelin, E. J. (1965). The Ruby Mines in Mogok in Burma. *Journal of Gemmology*, *9*(12), 411–426.

Gübelin, E. J., & Koivula, J. I. (1986). *Photoatlas of Inclusions in Gemstones, ABC Edition*.

Gübelin, E. J., & Koivula, J. I. (2005). *Photoatlas of Inclusions in Gemstones, Vol. 2*.

Gübelin, E. J., & Koivula, J. I. (2008). *Photolas of Inclusions in Gemstones, Vol. 3*.

Halford-Watkins, J. F. (1932a). The Ruby Mines of Upper Burma: A Short History of their Working,. *The Gemmologist*, *1*(9), 263–272.

Halford-Watkins, J. F. (1932b). Methods of Ruby Mining in Burma. *The Gemmologist*, *1*(11), 335–342.

Halford-Watkins, J. F. (1932c). Methods of Ruby Mining in Burma. *The Gemmologist*, *1*(12), 367–373.

Harlow, G. E., Sorensen, S. S., & Sisson, V. B. (2007). Jade, in Groat, L.A., ed., The Geology of Gem Deposits: Quebec. *Mineralogical Association of Canada, Short Course Series, 37*, 207–254.

Hawthorne, F. C., Oberti, R., Harlow, G. E., Maresch, W. V., Martin, R. F., Schumacher, J. C., & Welch, M. D. (2012). Nomenclature of the amphibole supergroup. *American Mineralogist*, *97*, 2031–2048.

Henry, D. J., Guidotti, C. V., & Thomson, J. (2005). The Ti-saturation surface for low-to-medium pressure metapelitic biotites: Implications for geothermometry and Ti-substitution mechanisms. *American Mineralogist*, *90*, 316–328.

Hofmann, A. W. (1988). Chemical differentiation of the Earth: the relationship between mantle, continental crust, and oceanic crust. Earth and. *Planetary Science Letters*, *90*, 297–314.

Holdaway, M. J. (2000). Application of new experimental and garnet Margules data to the garnet-biotite geothermometer. *American Mineralogist*, *85*, 881–892.

Holland, T., & Blundy, J. (1994). Non-ideal interactions in calcic amphiboles and their bearing on amphibole-plagioclase thermometry. *Contributions to Mineralogy and Petrology*, *116*, 433–447.

Horz, K. H., Worthington, T. J., Winn, K., & Stoffers, P. (2004). Late Quaternary tephra in the New Ireland Basin, Papua New Guinea. *Journal of Volcanology and Geothermal Research*, *132*(1), 73–95. doi:10.1016/S0377-0273(03)00421-9

Htay, K. N., Aung, L. T., Tajcmanova, L., & Heinrich, C. A. (2017). The Evidances of High Temperature-Medium Pressure, Granulite grade metamorphism in Momeik Area, Mogok Metamorphic Belt, Myanmar. In *Conference Abstract of 1st Myanmar Applied Earth Sciences Associtation*.

Hughes, R. W. (1997). *Ruby & Sapphire*.

Hughes, R. W. (2014). *Ruby & Sapphire—A Collector's Guide*.

Hughes, R. W. (2016). *Ruby & Sapphire: A Gemologists Guide*.

Hynes, A. (1980). Carbonatization and mobility of Ti, Y, and Zr in Ascot Formation metabasalts, SE Quebec. *Contributions to Mineralogy and Petrology*, *75*, 79–87.

Iyer, L. A. N. (1953). *The Geology and Gemstones of the Mogok Stone Tract, Burma*.

Jackson, S. E., Longerich, H. P., Dunning, G. R., & Freyer, B. J. (1992). The application of laser-ablation microprobe; inductively coupled plasma-mass spectrometry (LAM-ICP-MS) to in situ trace-element determinations in minerals. *The Canadian Mineralogist*, *30*(4), 1049–1064. https://doi.org/

Jackson, S. E., Pearson, N. J., Griffin, W. L., & Belousova, E. A. (2004). The application of laser ablation-inductively coupled plasma-mass spectrometry to in situ U-Pb zircon geochronology. *Chemical Geology*, *211*(1–2), 47–69. doi:10.1016/j.chemgeo.2004.06.017

Keller, P. C. (1985). Gemstones and Their Origins. *Terra*, *23*(3–12). doi:10.1007/978-1-4684-6674-4

Koziol, A. M., & Newton, R. C. (1988). Redetermination of the anorthite breakdown reaction and improvement of the plagioclase-garnet-Al2SiO5-quartz geobarometer. *American Mineralogist*, *73*, 216–223.

La Touche, T. H. D. (1913). *Geology of the Northern Shan State*. *Office of the Geological Survey of India, Calcutta, India*.

Lal, R. K. (1993). Internally consistent recalibrations of mineral equilibria for geothermobarometry involving garnet-orthopyroxene-plagioclase-quartz assemblages and their application to the South Indian granulites. *Journal of Metamorphic Geology*, *11*, 855–866.

Leake, B. W., Wooley, A. R., Arps, C. E. S., Birch, W. D., Gilbert, M. C., Grice, J. D., et al. (1997). Nomenclature of amphiboles. Report of the subcommittee on amphiboles of the International Mineralogical Association Commission on new minerals and mineral names. *European Journal of Mineralogy*, *9*, 623–651.

Lee, H.-Y., Sun-Lin Chung, S.-L., & H.-M., H.-M. Y. (2016). Late Cenozoic volcanism in central Myanmar: Geochemical characteristics and geodynamic significance. *Lithos*, *245*, 174–190.

Lee, H. Y., Chung, S. L., & Yang, H. M. (2016). Late Cenozoic volcanism in central Myanmar: Geochemical characteristics and geodynamic significance. *Lithos*, *245*, 174–190. doi:10.1016/j.lithos.2015.09.018

Licht, A., France-Lanord, C., Reisberg, L., Fontaine, C., Soe, A. N., & Jaeger, J.-J. (2013). A paleo Tibet-Myanmar connection? Reconstructing the Later Eocene drainage systems of Central Myanmar using a multi-proxy approach. *J. Geol. Soc. London*, *170*, 929–939.

Link, K. (2015). Age determination of zircon inclusions in faceted sapphires. *J. Gemmol.*, *34*, 692–700.

Link, K. (2016). New age data for blue sapphire from Mogok, Myanmar. *J. Gemmol.*, *35*, 107–109.

Lustrino, M., Fedele, L., Agostini, S., Prelević, D., & Salari, G. (2019). Leucitites within and around the Mediterranean area. *Lithos*, *324–325*, 216–233.

Meschede, M. (1986). A method of discrimination between different types of mid-ocean ridge basalts and continental tholeiites with the Nb–Zr–Y diagram. *Chemical Geology*, *56*, 207–218.

Miller, C., Thoni, M., Frank, W., Grasemann, B., Klotzli, U., Guntli, P., & Draganits, E. (2001). The early Palaeozoic magmatic event in the Northwest Himalaya, India: source, tectonic setting and age of emplacement. *Geol. Mag.*, *138*, 237–251.

Min, M. (2007a). *Chapter 5. Exhumation of the Mogok Belt in central Myanmar:a geochronologic study. In: thermochronology applied to strike-slip zones Central Ameria and Myanmar.*

Min, M. (2007b). *Chapter 5 Exhumation of the Mogok belt in central Myanmar : a geochronologic study*.

Mitchell, A. H. G. (1993). Cretaceous-Cenozoic tectonic events in the western Myanmar (Burma)-Assam region. *Journal of the Geological Society*, *150*, 1089–1102.

Mitchell, A. H. G., Marshall, T. R., Skinner, A. C., Baker, A. D., Amos, B. J., & Bateson, J. H. (1977). Geology and exploration geochemistry of the Yadanartheingi anf Kyaukme-Longtawkno areas, Northern Shan States, Burma. *Overseas Geology and Mineral Resources*, *51*(35).

Mitchell, A. H. G., Oo, T., Win, M. N., Hlaing, T., Htun, K. M., & Htay, M. T. (2006). Rock relationships in the Mogok metamorphic belt, Tatkon to Mandalay, central Myanmar. *Journal of Asian Earth Sciences*, *29*(5–6), 891–910. doi:10.1016/j.jseaes.2006.05.009

Mitchell, A., Oo, T., Lin, T.-H., Hung, C.-H., & Chung, S.-L. (2012). Zircon U–Pb ages in Myanmar: Magmatic–metamorphic events and the closure of a neo-Tethys ocean? *Journal of Asian Earth Sciences*, *56*, 1–23. doi:10.1016/j.jseaes.2012.04.019

Morimoto, N., Fabries, J., Ferguson, A. K., Ginzburg, I. V., Ross, M., Seifert, F. A., et al. (1988). Nomenclature of amphiboles. *Mineralogy and Petrology*, *39*, 55–76.

Moyd, L. (1949). Petrology of the nepheline and corundum rocks of southeastern Ontario. *American Mineralogist*, *34*, 736–750.

Mullen, E. D. (1983). MnO/TiO2/P2O5: a major element discriminant for basaltic rocks of oceanic environments and its implications for petrogenesis. *Earth Planet. Sci. Lett.*, *62*, 53–62.

Newton, R. C., Aranovich, L. Y., Hansen, E. C., & Vandenheuvel, B. A. (1998). Hypersaline fluids in Precambrian deep-crustal metamorphism. *Precambrian Res.*, *91*, 41–63.

Norman, M. D., & Nemchin, A. A. (2014). A 4.2 billion year old impact basin on the Moon: U-Pb dating of zirconolite and apatite in lunar melt rock 67955. *Earth and Planetary Science Letters*, *388*, 387–398. doi:10.1016/j.epsl.2013.11.040

Pearce, J. A., & Cann, J. R. (1973). Tectonic setting of basic volcanic rocks using Ti, Zr and Y. *Earth and Planetary Sciences and Letters*, *19*, 290–300.

Pearce, J. A., & Parkinson, I. J. (1993). Trace element models for mantle melting: application to volcanic arc petrogenesis; in Prichard, H.M., Alabaster, T., Harris, N.B.W., and Neary, C.R., eds., Magmatic Processes and Plate Tectonics,. *Geological Society Special Publications*, *76*, 373–403.

Peretti, A., Peretti, A. K., & Günther, D. (2015). World of Magnificent Spinels Provenance and Identification. *Contributions to Gemology*, *11*(May).

Phyo, M. M., Franz, L., Bieler, E., Balmer, W., & Krzemnicki, M. S. (2019). Spinel from Mogok, Myanmar—A Detailed Inclusion Study by Raman Microspectroscopy and Scanning Electron Microscopy. *The Journal of Gemmology*, *36*(5), 418–435. doi:10.15506/JoG.2019.36.5.418

Powell, M. & Powell, R. (1977). A nepheline-alkali feldspar geothermometer. *Contributions to Mineralogy and Petrology*, *62*, 193–204.

Powell, R. (1985). Regression diagnostics and robust regression in geothermometer/geobarometer calibration: the garnet-clinopyroxene geothermometer revisited. *Journal of Metamorphic Geology*, *3*, 231–243.

Prelević, D., Akal, C., Romer, R. L., Mertz-Kraus, R., & Helvacı, C. (2015). Magmatic response to slab tearing: constraints from the Afyon Alkaline Volcanic Complex, Western Turkey. *Journal of*

Petrology, *56*, 527–562.

Prelević, D., Foley, S. F., Romer, R., & Conticelli, S. (2008). Mediterranean Tertiary lamproites derived from multiple source components in postcollisional geodynamics. *Geochimica et Cosmochimica Acta*, *72*, 2125–2156.

Reiners, P. W., Carlson, R. W., Renne, P. R., Coo per, K. M., Granger, D. E., M c Lean, N. M., & Schoene, B. (2018). *Geochronology and Thermochronology.* (J. W. & Sons, Ed.).

RICHARDS, A., ARGLES, T., HARRIS, N., PARRISH, R., AHMAD, T., DARBYSHIRE, F., & DRAGANITS, E. (2005). Himalayan architecture constrained by isotopic tracers from clastic sediments. *Earth and Planetary Science Letters*, *236*(3–4), 773–796. doi:10.1016/j.epsl.2005.05.034

Rickwood, P. C. (1989). Boundary lines within petrologic diagrams which use oxides of major and minor elements. *Lithos*, *22*(4), 247–263. doi:10.1016/0024-4937(89)90028-5

Romer, R. L., & Hahne, K. (2010). Life of the Rheic Ocean: Scrolling through the shale record. *Gondwana Res.*, *17*, 236–253.

Ryburn, R. J., Raheim, A., & Green, D. H. (1976). Determination of P,T paths of natural eclogites; a correction. *Lithos*, *9*, 161–164.

Santosh, M., & Omori, S. (2008). CO2 flushing: a plate tectonic perspective. *Gondwana Res.*, *13*, 86–102.

Schaltegger, U., Schmitt, A. K., & Horstwood, M. S. A. (2015). U-Th-Pb zircon geochronology by ID-TIMS, SIMS, and laser ablation ICP-MS: Recipes, interpretations, and opportunities. *Chemical Geology*, *402*(March), 89–110. doi:10.1016/j.chemgeo.2015.02.028

Searle, D. L., & Haq, B. T. (1964). The Mogok belt of Burma and its relationship to the Himalayan orogeny. In *The international geological congress 22* (pp. 132–161).

Searle, M. P., Noble, S. R., Cottle, J. M., Waters, D. J., Mitchell, A. H. G., Hlaing, T., & Horstwood, M. S. A. (2007). Tectonic evolution of the Mogok metamorphic belt, Burma (Myanmar) constrained by U-Th-Pb dating of metamorphic and magmatic rocks. *Tectonics*, *26*(3). doi:10.1029/2006TC002083

Searle, M. P., Waters, D. J., Morley, C. K., Gardiner, N. J., Htun, U. K., Nu, T. T., & Robb, L. J. (2017). *Chapter 12 Tectonic evolution of the Mogok metamorphic and Jade mines belts and ophiolitic terranes of Burma (Myanmar)*. *Myanmar: Geology, Resources and Tectonics* (Vol. 48).

Geological Society Memoir48. doi:10.1029/2006TC002083

Sláma, J., Košler, J., Condon, D. J., Crowley, J. L., Gerdes, A., Hanchar, J. M., et al. (2008). Plešovice zircon — A new natural reference material for U–Pb and Hf isotopic microanalysis. *Chemical Geology*, *249*, 1–35.

Sone, M., & Metcalfe, I. (2008). Parallel Tethyab sutures in mainland Southeast Asia: new insights for Palaeo-Tethys closure and implications for the Indosinian Orogeny. *Comptes Rendus Geoscience*, *340*, 166–179.

Stern, R. J., Tsujimori, T., Harlow, G., & Groat, L. A. (2013). Plate tectonic gemstones. *Geology*, *41*(7), 723–726. doi:10.1130/G34204.1

Stucki, A., Trommsdorff, V., & Gunther, D. (2001). Zirconolite in metarodingites of Penninic Mesozoic ophiolites, Central Alps. *Schweizerische Mineralogische Und Petrographische Mitteilungen*, *81*(2), 257–265.

Sutherland, F. ., Coenraads, R. ., Hoskin, P. W. ., Bosshart, G., & Fanning, C. . (2002). Sapphire crystallization, age and origin, Ban Huai Sai, Laos: age based on zircon inclusions. *Journal of Asian Earth Sciences*, *20*(7), 841–849. doi:10.1016/s1367-9120(01)00067-0

Sutherland, F. L., Duroc-Danner, J. M., & Meffre, S. (2008). Age and origin of gem corundum and zircon megacrysts from the Mercaderes-Rio Mayo area, South-west Colombia, South America. *Ore Geology Reviews*, *34*(1–2), 155–168. doi:10.1016/j.oregeorev.2008.01.004

Sutherland, F. L., Piilonen, P. C., Zaw, K., Meffre, S., & Thompson, J. (2015). Sapphire within zircon-rich gem deposits , Bo Loei , Ratanakiri Province , Cambodia : trace elements , inclusions , U – Pb dating and genesis. *Australian Journal of Earth Sciences*, *62*, 761–773. doi:10.1080/08120099.2015.1101015

Sutherland, F. L., Zaw, K., Meffre, S., Thompson, J., Goemann, K., Thu, K., et al. (2018). Diversity In Ruby Geochemistry And Its Inclusions, Intra- And Inter Comparisons From Myanmar And East Australia. In *Meeting of the international mineralogical association* (p. 329).

Sutherland, F. L., Zaw, K., Meffre, S., Thompson, J., Goemann, K., Thu, K., et al. (2019). Diversity in Ruby Geochemistry and Its Inclusions: Intra- and Inter- Continental Comparisons from Myanmar and Eastern Australia. *Minerals*, *9*(1), 28. doi:10.3390/min9010028

Sylvester, P. J., & Ghaderi, M. (1997). Trace element analysis of scheelite by excimer laser ablation-

inductively coupled plasma-mass spectrometry (ELA-ICP-MS) using a synthetic silicate glass standard. *Chemical Geology*, *141*(1–2), 49–65. doi:10.1016/S0009-2541(97)00057-0

Tajčmanová, L., Konopasek, J., & Schulmann, K. (2006). Thermal evolution of the orogenic lower crust during exhumation within a thickened Moldanubian root of the Variscan belt of central Europe. *Journal of Metamorphic Geol.*, *24*, 119–134.

Thein, M. (1973). A preliminary synthesis of the geological evolution of Burma with reference to the tectonic development of Southeast Asia. *Geological Society of Malaysia*, *6*, 87–116.

Thein, M. (2008). Modes of occurrence and origin of precious gemstone deposits of the Mogok Stone Tract. *Journal of the Myanmar Geosciences Society*, *1*, 75–84.

Thein, M. L., Myint, O., Kyi, S., & P. N. Win. (1990). *Geology and stratigraphy of the metamorphosed Early Paleozoic rocks of the Mogok–Thabeikkyin–Singu–Madaya Areas. Unpublished staff report* (Vol. 98).

Themelis, T. (2008). *Gems and Mines of Mogok*.

Thu, K. (2007). *The Igneous Rocks of the Mogok Stone Tract: Their Distribution, Petrography, Petrochemistry, Sequence, Geochronology and Economic Geology. Ph.D. Thesis, University of Yangon, Yangon, Myanmar*.

Thu, Y. K., Enami, M., Kato, T., & Tsuboi, M. (2017). Granulite facies paragneisses from the middle segment of the Mogok metamorphic belt, central Myanmar. *Journal of Mineralogical and Petrological Sciences*, *112*(1), 1–19. doi:10.2465/jmps.160526

Thu, Y. K., Win, M. M., Enami, M., & Tsuboi, M. (2016). Ti-rich biotite in spinel and quartz-bearing paragneiss and related rocks from the Mogok metamorphic belt, central Myanmar. Journal of Mineralogical and. *Petrological Sciences*, *111*, 270–282.

Touret, J. L. R. (1971). Le faciés granulite en Norvège Méridionale. II: les inclusions fluides. *Lithos*, *4*, 423–436.

Touret, J. L. R., & Huizenga, J. M. (2012). Fluid-assisted granulite metamorphism: a continental journey. *Gondwana Res.*, *21*, 224–235.

Ulianov, A., Müntener, O., Schaltegger, U., & Bussy, F. (2012). The data treatment dependent variability of U-Pb zircon ages obtained using mono-collector, sector field, laser ablation ICPMS. *Journal of Analytical Atomic Spectrometry*, *27*(4), 663–676. doi:10.1039/c2ja10358c

Vermeesch, P. (2018). IsoplotR: A free and open toolbox for geochronology. *Geoscience Frontiers*, *9*(5), 1479–1493. doi:10.1016/j.gsf.2018.04.001

Waltham, T. (1999). The ruby mines of Mogok. *Geology Today*, *15*, 143–149.

Wang, Y., Sieh, K., Thura, A., Soe, M., Saw, N. K., & Soe, T. T. (2011). Earthquakes and Slip rate of the sounthern Sagaing-fault: insights from an offset ancient fort wall, lower Burma (Myanmar). *Geophysical Journal International*, *185*, 49–64.

Wiedenbeck, M., Alle, P., Corfu, F., Griffin, W. L., Meier, M., F., O., et al. (1995). Three natural zircon standards for U–Th–Pb, Lu–Hf, trace element and REE analyses. *Geostandards Newsletter*, *19*, 1–23.

Win, M. M., Enami, M., & Kato, T. (2016). Metamorphic conditions and CHIME monazite ages of Late Eocene to Late Oligocene high-temperature Mogok metamorphic rocks in central Myanmar. *Journal of Asian Earth Sciences*, *117*, 304–316. doi:10.1016/j.jseaes.2015.11.023

Wu, C.-M., Zhang, J., & Ren, L. D. (2004). Empirical garnet-biotite-plagioclase-quartz (GBPQ) geobarometry in medium-to high-grade metapelites. *Journal of Petrology*, *45*, 1907–1921.

Wu, F. Y., Yang, Y. H., Mitchell, R. H., Bellatreccia, F., Li, Q. L., & Zhao, Z. F. (2010). In situ U-Pb and Nd-Hf-(Sr) isotopic investigations of zirconolite and calzirtite. *Chemical Geology*, *277*(1–2), 178–195. doi:10.1016/j.chemgeo.2010.08.007

Wuhrer, R., Beattie, R., Coenraads, R. R., Abduriyim, A., Giuliani, G., Hoskin, P. W. O., et al. (2015). Corundum (sapphire) and zircon relationships, Lava Plains gem fields, NE Australia: Integrated mineralogy, geochemistry, age determination, genesis and geographical typing. *Mineralogical Magazine*, *79*(03), 545–581. doi:10.1180/minmag.2015.079.3.04

Xiang, H., Zhang, L., Zhong, Z.-Q., Santosh, M., Zhou, H.-W., Zhang, H.-F., et al. (2012). Ultrahigh-temperature metamorphism and anticlockwise P-T-t path of Paleozoic granulites from north Qinling-Tongbai orogen, Central China. *Gondwana Res.*, *21*, 559–576.

Yang, W. Bin, Niu, H. C., Shan, Q., Sun, W. D., Zhang, H., Li, N. B., et al. (2014). Geochemistry of magmatic and hydrothermal zircon from the highly evolved Baerzhe alkaline granite: Implications for Zr-REE-Nb mineralization. *Mineralium Deposita*, *49*(4), 451–470. doi:10.1007/s00126-013-0504-1

Yonemura, K., OsanaiI, Y., Zaw, T. N., Nakano, N., Charusiri, P., & Adachi, T. (2013). EPMA U-Th-Pb

monazite dating of metamorphic rocks from the Mogok Metamorphic Belt, central Myanmar. *Journal of Mineralogical and Petrological Sciences*, *108*(3), 184–188. doi:10.2465/jmps.121019a

Yui, T. F., Zaw, K., & Wu, C. M. (2008). A preliminary stable isotope study on Mogok Ruby, Myanmar. *Ore Geology Reviews*, *34*(1–2), 192–199. doi:10.1016/j.oregeorev.2008.05.001

Zartman, R. E., & Doe, B. R. (1981). Plumbotectonics - the model. *Tectonophysics*, *75*, 135–162.

Zaw, K. (1989). Comments on transcurrent movements in the Myanmar-Andaman sea region. *Geology*, *17*, 93–95.

Zaw, K. (1990). Geological, petrological and geochemical characteristics of granitoid rocks in Burma: with special reference to the associated W-Sn mineralization and their tectonic setting. *Journal of Southeast Asian Earth Sciences*, *4*, 293–335.

Zaw, K. (1998). Geological evolution of selected granitic pegmatites in myanmar (burma): Constraints from regional setting, lithology, and fluid-inclusion studies. *International Geology Review*, *40*(7), 647–662. doi:10.1080/00206819809465229

Zaw, K. (2017). *Overview of mineralization styles and tectonic-metallogenic setting in Myanmar. In Myanmar: Geology, Resources and Tectonics; Chapter 24; Barber, A.J., Zaw, K., Crow, M.J., Eds.; Geological Society London Memoirs*.

Zaw, K., Sutherland, F. L., Graham, I., Meffre, S., & Thu, K. (2010). Dating zircon inclusions in gem corundum deposits and genetic implications, 7.

Zaw, K., Sutherland, L., Yui, T. F., Meffre, S., & Thu, K. (2014). Vanadium-rich ruby and sapphire within Mogok Gemfield, Myanmar: implications for gem color and genesis. *Mineralium Deposita*, *50*(1), 25–39. doi:10.1007/s00126-014-0545-0

Zaw, K., Thu, K., Meffre, S., Yui, T. F., & Sutherland, F. L. (2015). Vanadium-rich ruby and sapphire within Mogok Gemfield, Myanmar: implications for gem color and genesis. *Mineralium Deposita*, *50*(1), 25–39. doi:10.1007/s00126-014-0545-0

Zuleger, E., & Erzinger, J. (1988). Determination of the REE and Y in silicate materials with ICP-AES. *Fresenius' Zeitschrift für Analytische Chemie*, *332*(2), 140–143. doi:10.1007/BF00470631

Table 4.3. U-Pb isotopes ratios and ages of zircon and zirconolite measured by TOF- and SF-MS.

No.	Measurement	Sample Type	Location	Area	Spot	Method	207Pb/235U	2σ	206Pb/238U	2σ	Rho	207Pb/235U	2 SE	206Pb/238U	2 SE
1	ALT_03a_13_ZrnInGneiss_2	Zircon In Gneiss	AungLan Taung	rim	19 µm	SF	0.032400	0.002000	0.004770	0.000067	0.227547	32.38	0.98	30.68	0.21
2	ALT_03a_4_ZrnInGneiss_2	Zircon In Gneiss	Aunglan Taung	rim	19 µm	SF	0.032400	0.002500	0.004951	0.000074	0.193706	32.38	1.23	31.84	0.24
3	ALT_03b_1_ZrnInGneiss_1	Zircon In Gneiss	Aunglan Taung	core	19 µm	SF	0.030300	0.002400	0.004989	0.000061	0.154365	30.31	1.18	32.08	0.2
4	ALT_03c_5_ZrnInGneiss_1	Zircon In Gneiss	AungLan Taung	core	19 µm	SF	0.037000	0.003600	0.005300	0.000120	0.232704	36.89	1.76	34.08	0.38
5	ALT_03d_7_ZrnInGneiss_2	zircon-black-rim	Aunglan Taung	rim	13 µm	SF	0.035700	0.001200	0.005440	0.000070	0.382813	35.62	0.59	34.97	0.22
6	ALT_03c_8_ZrnInGneiss_3	Zircon In Gneiss	AungLan Taung	rim	19 µm	SF	0.036100	0.002100	0.005470	0.000150	0.471402	36.01	1.03	35.17	0.48
7	ALT_03a_4_ZrnInGneiss_3	Zircon In Gneiss	Aunglan Taung	core	19 µm	SF	0.033800	0.004700	0.005530	0.000260	0.338117	33.75	2.31	35.55	0.83
8	ALT_03a_5_ZrnInGneiss_4	Zircon In Gneiss	AungLan Taung	rim	19 µm	SF	0.036300	0.006200	0.005790	0.000230	0.232576	36.21	3.04	37.22	0.74
9	ALT_03d_3 _ZrnInGneiss_1	Zircon In Gneiss	AungLan Taung	rim	19 µm	SF	0.038400	0.004700	0.005845	0.000096	0.134190	38.26	2.3	37.57	0.31
10	ALT_03c_6_ZrnInGneiss_1	Zircon In Gneiss	AungLan Taung	core	19 µm	SF	0.040600	0.001600	0.006165	0.000094	0.386902	40.41	0.78	39.62	0.3
11	ALT_03d_11_ZrnInGneiss_2	zircon-rim-black	Aunglan Taung	rim	13 µm	SF	0.040600	0.001500	0.006169	0.000089	0.390490	40.41	0.73	39.65	0.29
12	ALT_03d_7_ZrnInGneiss_1	Zircon In Gneiss	AungLan Taung	core	19 µm	SF	0.046300	0.004100	0.006730	0.000160	0.268474	45.96	1.99	43.24	0.51
13	ALT_03c_11_ZrnInGneiss_1	Zircon In Gneiss	AungLan Taung	core	19 µm	SF	0.045200	0.001500	0.006924	0.000074	0.322049	44.89	0.73	44.48	0.24
14	ALT_03c_10_ZrnInGneiss_1	Zircon In Gneiss	AungLan Taung	core	19 µm	SF	0.048500	0.004200	0.007010	0.000130	0.214150	48.09	2.03	45.03	0.42
15	ALT_03b_5_ZrnInGneiss_1	Zircon In Gneiss	Aunglan Taung	core	19 µm	SF	0.051300	0.002300	0.007925	0.000062	0.174495	50.8	1.11	50.89	0.2
16	ALT_03d_10_ZrnInGneiss_6	Zircon In Gneiss	Aunglan Taung	mixed	13 µm	SF	0.066200	0.001500	0.010070	0.000110	0.482092	65.09	0.71	64.59	0.35
17	ALT_03b_4_ZrnInGneiss_3	Zircon In Gneiss	Aunglan Taung	core	19 µm	SF	0.065600	0.006600	0.010130	0.000350	0.343414	64.52	3.14	64.97	1.12
18	ALT_03d_10_ZrnInGneiss_5	Zircon In Gneiss	Aunglan Taung	mixed	13 µm	SF	0.066500	0.001400	0.010240	0.000140	0.649414	65.37	0.67	65.68	0.45
19	ALT_03c_9_ZrnInGneiss_1	Zircon In Gneiss	AungLan Taung	core	19 µm	SF	0.073500	0.001800	0.010482	0.000090	0.350601	72.02	0.85	67.22	0.29
20	ALT_03a_4_ZrnInGneiss_4	Zircon In Gneiss	Aunglan Taung	core	19 µm	SF	0.072400	0.005400	0.010830	0.000190	0.235218	70.97	2.56	69.44	0.61
21	ALT_03a_6_ZrnInGneiss_4	Zircon In Gneiss	AungLanTaung	core	35 µm	TOF	0.077840	0.014407	0.011083	0.000524	0.255599	76.11	6.79	71.05	1.67
22	ALT_03d_10_ZrnInGneiss_2	Zircon In Gneiss	Aunglan Taung	core	13 µm	SF	0.077400	0.002900	0.011670	0.000270	0.617498	75.7	1.37	74.79	0.86
23	ALT_03d_13_ZrnInGneiss_2	Zircon In Gneiss	AungLan Taung	mixed	19 µm	SF	0.080500	0.006400	0.012330	0.000420	0.428452	78.61	3.01	79	1.34
24	ALT_03d_4_ZrnInGneiss_1	Zircon In Gneiss	AungLan Taung	core	19 µm	SF	0.089000	0.007600	0.013050	0.000500	0.448679	86.57	3.54	83.58	1.59
25	ALT_03b_2_ZrnInGneiss_1	Zircon In Gneiss	Aunglan Taung	core	19 µm	SF	0.095000	0.017000	0.013120	0.000320	0.136298	92.15	7.88	84.03	1.02
26	ALT_03c_2_ZrnInGneiss_1	Zircon In Gneiss	AungLan Taung	mixed	19 µm	SF	0.101000	0.017000	0.013650	0.000310	0.134928	97.7	7.84	87.4	0.99
27	ALT_03d_10_ZrnInGneiss_4	Zircon In Gneiss	Aunglan Taung	mixed	13 µm	SF	0.093200	0.004100	0.013870	0.000200	0.327782	90.48	1.9	88.8	0.64
28	ALT_03b_3_ZrnInGneiss_2	Zircon In Gneiss	Aunglan Taung	core	19 µm	SF	0.102000	0.016000	0.014120	0.000510	0.230258	98.62	7.37	90.39	1.62
29	ALT_03a_1_ZrnInGneiss_2	Zircon In Gneiss	AungLanTaung	core	35 µm	TOF	0.091947	0.020140	0.014215	0.000684	0.219758	89.32	9.36	90.99	2.17
30	ALT_03b_2_ZrnInGneiss_3	Zircon In Gneiss	Aunglan Taung	core	19 µm	SF	0.102300	0.005500	0.015120	0.000130	0.159921	98.9	2.53	96.74	0.41
31	ALT_03d_2 _ZrnInGneiss_2	Zircon In Gneiss	AungLan Taung	core	19 µm	SF	0.100900	0.002500	0.015200	0.000230	0.610711	97.61	1.15	97.25	0.73
32	ALT_03b_2_ZrnInGneiss_4	Zircon In Gneiss	Aunglan Taung	core	19 µm	SF	0.097000	0.018000	0.015230	0.000420	0.148610	94	8.33	97.44	1.33

Table 4.3. U-Pb isotopes ratios and ages of zircon and zirconolite measured by TOF- and SF-MS. Contd.

No.	Measurement	Sample Type	Location	Area	Spot	Method	207Pb/235U	2σ	206Pb/238U	2σ	Rho	207Pb/235U	2 SE	206Pb/238U	2 SE
33	ALT_03d_2 _ZrnInGneiss_1	Zircon In Gneiss	AungLan Taung	core	19 µm	SF	0.105000	0.007100	0.015380	0.000350	0.336545	101.38	3.26	98.39	1.11
34	ALT_03d_6_ZrnInGneiss_1	Zircon In Gneiss	AungLan Taung	core	19 µm	SF	0.106600	0.001100	0.015520	0.000110	0.686856	102.85	0.5	99.28	0.35
35	ALT_03c_1_ZrnInGneiss_1	Zircon In Gneiss	AungLan Taung	core	19 µm	SF	0.111000	0.011000	0.015820	0.000400	0.255143	106.88	5.03	101.18	1.27
36	ALT_03a_9_ZrnInGneiss_2	Zircon In Gneiss	Aunglan Taung	core	19 µm	SF	0.108100	0.007500	0.015870	0.000180	0.163478	104.23	3.44	101.5	0.57
37	ALT_03c_3_ZrnInGneiss_2	Zircon In Gneiss	AungLan Taung	core	19 µm	SF	0.108900	0.002800	0.016340	0.000230	0.547451	104.96	1.28	104.48	0.73
38	ALT_03a_6_ZrnInGneiss_3	Zircon In Gneiss	AungLanTaung	core	35 µm	TOF	0.132931	0.030626	0.018282	0.000879	0.208635	126.7	13.7	116.79	2.78
39	ALT_03a_8_ZrnInGneiss_2	Zircon In Gneiss	Aunglan Taung	core	19 µm	SF	0.132700	0.009300	0.019160	0.000250	0.186180	126.52	4.17	122.34	0.79
40	ALT_03a_11_ZrnInGneiss_1	Zircon In Gneiss	AungLanTaung	core	35 µm	TOF	0.160614	0.048486	0.021082	0.001290	0.202730	151.2	21.2	134.49	4.07
41	ALT_03b_1_ZrnInGneiss_5	Zircon In Gneiss	Aunglan Taung	core	19 µm	SF	0.130000	0.020000	0.021300	0.000620	0.189202	124.1	8.99	135.87	1.96
42	ALT_03b_6_ZrnInGneiss_1	Zircon In Gneiss	AungLanTaung	core	35 µm	TOF	0.122656	0.047241	0.021681	0.001221	0.146187	117.5	21.4	138.27	3.85
43	ALT_03a_5_ZrnInGneiss_2	Zircon In Gneiss	Aunglan Taung	core	19 µm	SF	0.153000	0.014000	0.021820	0.000450	0.225383	144.56	6.16	139.15	1.42
44	ALT_03c_8_ZrnInGneiss_1	Zircon In Gneiss	AungLan Taung	mixed	19 µm	SF	0.147200	0.008600	0.022000	0.001100	0.855814	139.44	3.81	140.28	3.47
45	ALT_03b_2_ZrnInGneiss_2	Zircon In Gneiss	Aunglan Taung	core	19 µm	SF	0.139000	0.013000	0.022010	0.000470	0.228323	132.15	5.79	140.35	1.48
46	ALT_03a_8_ZrnInGneiss_3	Zircon In Gneiss	Aunglan Taung	core	19 µm	SF	0.147900	0.004700	0.022080	0.000280	0.399052	140.06	2.08	140.79	0.88
47	ALT_03a_4_ZrnInGneiss_6	Zircon In Gneiss	Aunglan Taung	core	19 µm	SF	0.167000	0.019000	0.022260	0.000440	0.173736	156.81	8.27	141.92	1.39
48	ALT_03b_1_ZrnInGneiss_2	Zircon In Gneiss	Aunglan Taung	core	19 µm	SF	0.153000	0.021000	0.022390	0.000570	0.185478	144.56	9.25	142.74	1.8
49	ALT_03d_12_ZrnInGneiss_1	Zircon In Gneiss	AungLan Taung	core	19 µm	SF	0.154000	0.010000	0.022600	0.000530	0.361150	145.44	4.4	144.07	1.67
50	ALT_03c_3_ZrnInGneiss_1	Zircon In Gneiss	AungLan Taung	core	19 µm	SF	0.156500	0.003700	0.022760	0.000140	0.260177	147.63	1.62	145.08	0.44
51	ALT_03d_13_ZrnInGneiss_1	Zircon In Gneiss	AungLan Taung	core	19 µm	SF	0.158100	0.007600	0.022900	0.000470	0.426954	149.04	3.33	145.96	1.48
52	ALT_03a_5_ZrnInGneiss_1	Zircon In Gneiss	AungLanTaung	core	35 µm	TOF	0.173788	0.060507	0.023165	0.001579	0.195831	162.7	26.2	147.63	4.98
53	ALT_03b_5_ZrnInGneiss_2	Zircon In Gneiss	Aunglan Taung	core	19 µm	SF	0.172000	0.015000	0.023650	0.000320	0.155152	161.15	6.5	150.68	1.01
54	ALT_03b_3_ZrnInGneiss_3	Zircon In Gneiss	Aunglan Taung	core	19 µm	SF	0.183000	0.021000	0.024190	0.000570	0.205339	170.64	9.01	154.08	1.79
55	ALT_03a_2_ZrnInGneiss_1	Zircon In Gneiss	Aunglan Taung	core	19 µm	SF	0.164800	0.004400	0.024230	0.000220	0.340074	154.9	1.92	154.33	0.69
56	ALT_03b_5_ZrnInGneiss_3	Zircon In Gneiss	Aunglan Taung	core	19 µm	SF	0.170700	0.006000	0.024560	0.000270	0.312765	160.03	2.6	156.41	0.85
57	ALT_03a_7_ZrnInGneiss_1	Zircon In Gneiss	Aunglan Taung	core	19 µm	SF	0.163800	0.009800	0.024700	0.000320	0.216541	154.02	4.28	157.29	1.01
58	ALT_03b_4_ZrnInGneiss_1	Zircon In Gneiss	Aunglan Taung	core	19 µm	SF	0.169300	0.007600	0.024840	0.000250	0.224198	158.81	3.3	158.17	0.79
59	ALT_03b_4_ZrnInGneiss_2	Zircon In Gneiss	Aunglan Taung	core	19 µm	SF	0.175500	0.008400	0.025210	0.000270	0.223763	164.18	3.63	160.5	0.85
60	ALT_03b_4_ZrnInGneiss_4	Zircon In Gneiss	Aunglan Taung	core	19 µm	SF	0.181000	0.013000	0.025300	0.000530	0.291669	168.92	5.59	161.07	1.67
61	ALT_03a_1_ZrnInGneiss_1	Zircon In Gneiss	Aunglan Taung	core	19 µm	SF	0.179000	0.013000	0.025320	0.000340	0.184895	167.2	5.6	161.19	1.07
62	ALT_03c_8_ZrnInGneiss_2	Zircon In Gneiss	AungLan Taung	mixed	19 µm	SF	0.173100	0.004100	0.025350	0.000200	0.333093	162.11	1.77	161.38	0.63
63	ALT_03a_8_ZrnInGneiss_4	Zircon In Gneiss	Aunglan Taung	core	19 µm	SF	0.182000	0.010000	0.025390	0.000280	0.200709	169.78	4.3	161.63	0.88
64	ALT_03c_12_ZrnInGneiss_1	Zircon In Gneiss	AungLan Taung	core	19 µm	SF	0.176200	0.005500	0.025460	0.000230	0.289409	164.79	2.37	162.07	0.72

Table 4.3. U-Pb isotopes ratios and ages of zircon and zirconolite measured by TOF- and SF-MS. Contd.

No.	Measurement	Sample Type	Location	Area	Spot	Method	207Pb/235U	2σ	206Pb/238U	2σ	Rho	207Pb/235U	2 SE	206Pb/238U	2 SE
65	ALT_03d_9_ZrnInGneiss_1	Zircon In Gneiss	AungLan Taung	core	19 µm	SF	0.174600	0.005200	0.025500	0.000660	0.869050	163.4	2.25	162.32	2.07
66	ALT_03b_1_ZrnInGneiss_3	Zircon In Gneiss	Aunglan Taung	core	19 µm	SF	0.172000	0.021000	0.025590	0.000680	0.217645	161.15	9.1	162.89	2.14
67	ALT_03a_9_ZrnInGneiss_1	Zircon In Gneiss	Aunglan Taung	core	19 µm	SF	0.175300	0.006800	0.025780	0.000300	0.299993	164.01	2.94	164.08	0.94
68	ALT_03a_4_ZrnInGneiss_5	Zircon In Gneiss	Aunglan Taung	rim	19 µm	SF	0.177000	0.020000	0.025960	0.000600	0.204545	165.48	8.63	165.21	1.88
69	ALT_03d_10_ZrnInGneiss_1	Zircon In Gneiss	AungLan Taung	core	19 µm	SF	0.182200	0.002700	0.026560	0.000160	0.406515	169.95	1.16	168.98	0.5
70	ALT_03c_7_ZrnInGneiss_1	Zircon In Gneiss	AungLan Taung	mixed	19 µm	SF	0.213000	0.036000	0.026660	0.000220	0.048825	196.1	15.1	169.61	0.69
71	ALT_03a_5_ZrnInGneiss_3	Zircon In Gneiss	Aunglan Taung	core	19 µm	SF	0.182500	0.005400	0.026670	0.000280	0.354817	170.21	2.32	169.67	0.88
72	ALT_03d_4_ZrnInGneiss_2	Zircon In Gneiss	AungLan Taung	core	19 µm	SF	0.183900	0.003000	0.026790	0.000380	0.869504	171.41	1.29	170.43	1.19
73	ALT_03d_8_ZrnInGneiss_1	Zircon In Gneiss	AungLan Taung	core	19 µm	SF	0.186200	0.004200	0.026960	0.000410	0.674209	173.38	1.8	171.49	1.29
74	ALT_03a_9_ZrnInGneiss_3	Zircon In Gneiss	AungLan Taung	core	19 µm	SF	0.189200	0.003700	0.027490	0.000450	0.837061	175.95	1.58	174.82	1.41
75	ALT_03b_3_ZrnInGneiss_1	Zircon In Gneiss	Aunglan Taung	core	19 µm	SF	0.206000	0.017000	0.027710	0.000380	0.166175	190.19	7.16	176.2	1.19
76	ALT_03b_1_ZrnInGneiss_4	Zircon In Gneiss	Aunglan Taung	rim	19 µm	SF	0.194000	0.027000	0.027900	0.001200	0.309040	180	11.5	177.39	3.76
77	ALT_03a_8_ZrnInGneiss_1	Zircon In Gneiss	Aunglan Taung	core	19 µm	SF	0.196000	0.011000	0.028530	0.000470	0.293535	181.74	4.67	181.34	1.47
78	BLG_12a_6_ZrnInMarble_6	Zircon In Marble	Bawlongyi	core	35 µm	TOF	0.019886	0.014913	0.002406	0.000321	0.177814	19.99	7.42	15.49	1.03
79	BLG_12a_6_ZrnInMarble_3	Zircon In Marble	Bawlongyi	rim	13 µm	SF	0.017100	0.002500	0.002599	0.000059	0.023600	17.22	1.25	16.73	0.19
80	BLG_12a_6_ZrnInMarble_5	Zircon In Marble	Bawlongyi	rim	35 µm	TOF	0.017461	0.010561	0.002606	0.000180	0.114278	17.58	5.27	16.78	0.58
81	BLG_12a_6_ZrnInMarble_2	Zircon In Marble	Bawlongyi	rim	13 µm	SF	0.018600	0.002300	0.002661	0.000056	0.024348	18.71	1.15	17.13	0.18
82	BLG_12a_6_ZrnInMarble_1	Zircon In Marble	Bawlongyi	rim	13 µm	SF	0.018000	0.002600	0.002728	0.000073	0.028077	18.11	1.3	17.56	0.23
83	BLG_12a_6_ZrnInMarble_4	Zircon In Marble	Bawlongyi	rim	13 µm	SF	0.019500	0.007000	0.002880	0.000150	0.021429	19.61	3.49	18.54	0.48
84	BLG_12b_1_ZrnInMarble_1	Zircon In Marble	Bawlongyi	rim	13 µm	SF	0.027200	0.006100	0.003500	0.000190	0.031148	27.25	3.01	22.52	0.61
85	BLG_12a_3_ZrnInMarble_1	Zircon In Marble	Bawlongyi	rim	13 µm	SF	0.025000	0.010000	0.003540	0.000350	0.035000	25.07	4.95	22.78	1.12
86	BLG_12a_5_ZrnInMarble_2	Zircon In Marble	Bawlongyi	rim	13 µm	SF	0.020500	0.003900	0.003580	0.000100	0.025641	20.6	1.94	23.04	0.32
87	BLG_12b_3_ZrnInMarble_1	Zircon In Marble	Bawlongyi	rim	13 µm	SF	0.023700	0.009400	0.003600	0.000230	0.024468	23.78	4.66	23.17	0.74
88	BLG_12a_4_ZrnInMarble_6	Zircon In Marble	Bawlongyi	rim	13 µm	SF	0.027300	0.005600	0.003630	0.000150	0.026786	27.35	2.77	23.36	0.48
89	BLG_12b_1_ZrnInMarble_2	Zircon In Marble	Bawlongyi	rim	13 µm	SF	0.028600	0.006000	0.003700	0.000140	0.023333	28.63	2.96	23.81	0.45
90	BLG_12a_4_ZrnInMarble_5	Zircon In Marble	Bawlongyi	rim	13 µm	SF	0.028000	0.004700	0.003760	0.000140	0.029787	28.04	2.32	24.19	0.45
91	BLG_12a_4_ZrnInMarble_7	Zircon In Marble	Bawlongyi	rim	13 µm	SF	0.035000	0.012000	0.003910	0.000390	0.032500	34.93	5.89	25.16	1.25
92	BLG_12a_2_ZrnInMarble_3	Zircon In Marble	Bawlongyi	rim	13 µm	SF	0.030400	0.007100	0.003920	0.000240	0.033803	30.41	3.5	25.22	0.77
93	BLG_12b_2_ZrnInMarble_1	Zircon In Marble	Bawlongyi	mixed	13 µm	SF	0.031900	0.007900	0.003930	0.000220	0.027848	31.88	3.89	25.28	0.71
94	BLG_12a_4_ZrnInMarble_2	Zircon In Marble	Bawlongyi	mixed	13 µm	SF	0.024200	0.005800	0.003960	0.000260	0.044828	24.28	2.88	25.48	0.83
95	BLG_12a_3_ZrnInMarble_3	Zircon In Marble	Bawlongyi	mixed	13 µm	SF	0.028900	0.005100	0.004000	0.000130	0.025490	28.93	2.52	25.73	0.42
96	BLG_12a_1_ZrnInMarble_2	Zircon In Marble	Bawlongyi	mixed	13 µm	SF	0.030700	0.005700	0.004130	0.000170	0.029825	30.7	2.81	26.57	0.55

Table 4.3. U-Pb isotopes ratios and ages of zircon and zirconolite measured by TOF- and SF-MS. Contd.

No.	Measurement	Sample Type	Location	Area	Spot	Method	207Pb/235U	2σ	206Pb/238U	2σ	Rho	207Pb/235U	2 SE	206Pb/238U	2 SE
97	BLG_12b_3_ZrnInMarble_2	Zircon In Marble	Bawlongyi	rim	13 µm	SF	0.025000	0.006100	0.004160	0.000160	0.026230	25.07	3.02	26.76	0.51
98	BLG_12b_4_ZrnInMarble_1	Zircon In Marble	Bawlongyi	zircon	13 µm	SF	0.027000	0.012000	0.004340	0.000320	0.026667	27.05	5.93	27.92	1.03
99	BLG_12b_3_ZrnInMarble_3	Zircon In Marble	Bawlongyi	zircon	13 µm	SF	0.031800	0.008100	0.004360	0.000220	0.027160	31.79	3.99	28.05	0.71
100	BLG_12b_1_ZrnInMarble_3	Zircon In Marble	Bawlongyi	rim	13 µm	SF	0.026900	0.004800	0.004460	0.000130	0.027083	26.95	2.37	28.69	0.42
101	BLG_12d_19_ZrnInMarble_1	Zircon In Marble	Bawlongyi	mixed	19 µm	SF	0.031200	0.002100	0.004820	0.000140	0.431535	31.2	1.03	31	0.45
102	BLG_12a_1_ZrnInMarble_3	Zircon In Marble	Bawlongyi	mixed	35 µm	TOF	0.039243	0.007910	0.005505	0.000378	0.341093	39.08	3.86	35.39	1.21
103	BLG_12a_2_ZrnInMarble_2	Zircon In Marble	Bawlongyi	mixed	13 µm	SF	0.039700	0.008400	0.005560	0.000330	0.039286	39.53	4.1	35.74	1.06
104	BLG_12a_4_ZrnInMarble_1	Zircon In Marble	Bawlongyi	mixed	13 µm	SF	0.039200	0.006500	0.005700	0.000270	0.041538	39.04	3.18	36.64	0.87
105	BLG_12a_4_ZrnInMarble_8	Zircon In Marble	Bawlongyi	mixed	35 µm	TOF	0.036075	0.020665	0.005830	0.000503	0.150461	36	10.1	37.47	1.61
106	BLG_12d_8_ZrnInMarble_1	Zircon In Marble	Bawlongyi	mixed	19 µm	SF	0.038900	0.001300	0.006150	0.000100	0.486554	38.75	0.64	39.52	0.32
107	BLG_12d_1_ZrnInMarble_1	Zircon In Marble	Bawlongyi	core	19 µm	SF	0.039600	0.004000	0.006200	0.000110	0.175645	39.43	1.95	39.84	0.35
108	BLG_12a_3_ZrnInMarble_2	Zircon In Marble	Bawlongyi	core	13 µm	SF	0.039000	0.011000	0.006670	0.000350	0.031818	38.85	5.37	42.85	1.12
109	BLG_12a_3_ZrnInMarble_6	Zircon In Marble	Bawlongyi	mixed	35 µm	TOF	0.039013	0.024544	0.006671	0.000531	0.126577	38.9	12	42.86	1.7
110	BLG_12a_4_ZrnInMarble_9	Zircon In Marble	Bawlongyi	rim	35 µm	TOF	0.044906	0.029109	0.006721	0.000499	0.114468	44.6	14.1	43.18	1.59
111	BLG_12a_2_ZrnInMarble_5	Zircon In Marble	Bawlongyi	mixed	35 µm	TOF	0.043292	0.023070	0.007634	0.000516	0.126856	43	11.2	49.03	1.65
112	BLG_12a_3_ZrnInMarble_5	Zircon In Marble	Bawlongyi	mixed	35 µm	TOF	0.062973	0.032764	0.007722	0.000667	0.165935	62	15.6	49.59	2.13
113	BLG_12d_2_ZrnInMarble_2	Zircon In Marble	Bawlongyi	core	19 µm	SF	0.052700	0.001900	0.008241	0.000079	0.265891	52.15	0.92	52.91	0.25
114	BLG_12a_5_ZrnInMarble_1	Zircon In Marble	Bawlongyi	core	13 µm	SF	0.063000	0.010000	0.008680	0.000400	0.040000	62.03	4.78	55.71	1.28
115	BLG_12a_1_ZrnInMarble_1	Zircon In Marble	Bawlongyi	core	13 µm	SF	0.058500	0.006400	0.008710	0.000420	0.065625	57.73	3.07	55.91	1.34
116	BLG_12a_2_ZrnInMarble_1	Zircon In Marble	Bawlongyi	core	13 µm	SF	0.057200	0.005400	0.008710	0.000180	0.033333	56.48	2.59	55.91	0.58
117	BLG_12c_7_ZrnInMarble_1	Zircon In Marble	Bawlongyi	core	19 µm	SF	0.058800	0.003000	0.008840	0.000220	0.487783	58.02	1.44	56.74	0.7
118	BLG_12a_2_ZrnInMarble_6	Zircon In Marble	Bawlongyi	mixed	35 µm	TOF	0.055059	0.029292	0.008976	0.000632	0.132294	54.4	14.1	57.6	2.02
119	BLG_12d_9_ZrnInMarble_1	Zircon In Marble	Bawlongyi	core	19 µm	SF	0.058900	0.001400	0.009110	0.000120	0.554179	58.11	0.67	58.46	0.38
120	BLG_12d_16_ZrnInMarble_1	Zircon In Marble	Bawlongyi	core	19 µm	SF	0.062800	0.001200	0.009591	0.000074	0.403781	61.84	0.57	61.53	0.24
121	BLG_12d_6_ZrnInMarble_1	Zircon In Marble	Bawlongyi	core	19 µm	SF	0.061700	0.002100	0.009630	0.000120	0.366118	60.79	1	61.78	0.38
122	BLG_12d_4_ZrnInMarble_1	Zircon In Marble	Bawlongyi	core	35 µm	TOF	0.064879	0.007408	0.009853	0.000389	0.346135	63.83	3.53	63.21	1.24
123	BLG_12d_17_ZrnInMarble_1	Zircon In Marble	Bawlongyi	core	19 µm	SF	0.064700	0.002000	0.009900	0.000270	0.882273	63.66	0.95	63.51	0.86
124	BLG_12c_1_ZrnInMarble_1	zircon In Marble	Bawlongyi	core	19 µm	SF	0.065700	0.001600	0.009930	0.000110	0.454872	64.61	0.76	63.7	0.35
125	BLG_12d_10_ZrnInMarble_1	Zircon In Marble	Bawlongyi	core	19 µm	SF	0.065300	0.002100	0.010140	0.000130	0.398657	64.23	1	65.04	0.41
126	BLG_12d_2_ZrnInMarble_1	Zircon In Marble	Bawlongyi	core	19 µm	SF	0.067400	0.002000	0.010300	0.000130	0.425340	66.23	0.95	66.06	0.41
127	BLG_12d_03_ZrnIInMarble_1	Zircon In Marble	Bawlongyi	zircon	13 µm	SF	0.073100	0.004700	0.010950	0.000580	0.823822	71.64	2.22	70.2	1.85
128	BLG_12b_5_ZrnInMarble_2	Zircon In Marble	Bawlongyi	core	13 µm	SF	0.071100	0.003700	0.010980	0.000150	0.040541	69.74	1.75	70.4	0.48

Table 4.3. U-Pb isotopes ratios and ages of zircon and zirconolite measured by TOF- and SF-MS. Contd.

No.	Measurement	Sample Type	Location	Area	Spot	Method	207Pb/235U	2σ	206Pb/238U	2σ	Rho	207Pb/235U	2 SE	206Pb/238U	2 SE
129	BLG_12d_18_ZrnInMarble_1	Zircon In Marble	Bawlongyi	core	19 µm	SF	0.072800	0.002300	0.011050	0.000190	0.544246	71.35	1.09	70.84	0.61
130	BLG_12d_3_ZrnInMarble_1	Zircon In Marble	Bawlongyi	core	35 µm	TOF	0.077042	0.021927	0.011128	0.000601	0.189791	75.4	10.3	71.34	1.92
131	BLG_12d_12_ZrnInMarble_1	Zircon In Marble	Bawlongyi	core	19 µm	SF	0.072100	0.002000	0.011140	0.000110	0.355969	70.69	0.95	71.42	0.35
132	BLG_12d_05_ZrnIInMarble_2	Zircon In Marble	Bawlongyi	zircon	13 µm	SF	0.073700	0.002700	0.011180	0.000320	0.781289	72.2	1.28	71.67	1.02
133	BLG_12d_11_ZrnInMarble_1	Zircon In Marble	Bawlongyi	core	19 µm	SF	0.074000	0.001700	0.011420	0.000130	0.495519	72.49	0.8	73.2	0.41
134	BLG_12d_14_ZrnInMarble_1	Zircon In Marble	Bawlongyi	core	19 µm	SF	0.076400	0.002400	0.011500	0.000180	0.498261	74.75	1.13	73.71	0.57
135	BLG_12c_8_ZrnInMarble_1	Zircon In Marble	Bawlongyi	core	19 µm	SF	0.078500	0.004500	0.011580	0.000170	0.256093	76.73	2.12	74.22	0.54
136	BLG_12d_15_ZrnInMarble_1	Zircon In Marble	Bawlongyi	core	19 µm	SF	0.076210	0.000840	0.011592	0.000093	0.727876	74.58	0.4	74.3	0.3
137	BLG_12a_3_ZrnInMarble_4	Zircon In Marble	Bawlongyi	core	13 µm	SF	0.084000	0.010000	0.011710	0.000680	0.068000	81.9	4.68	75.05	2.17
138	BLG_12b_4_ZrnInMarble_3	Zircon In Marble	Bawlongyi	core	13 µm	SF	0.077300	0.003400	0.012030	0.000200	0.058824	75.6	1.6	77.09	0.64
139	BLG_12a_4_ZrnInMarble_4	Zircon In Marble	Bawlongyi	core	13 µm	SF	0.077000	0.011000	0.012050	0.000410	0.037273	75.32	5.19	77.21	1.31
140	BLG_12b_5_ZrnInMarble_1	Zircon In Marble	Bawlongyi	core	13 µm	SF	0.085100	0.007600	0.012110	0.000350	0.046053	82.93	3.56	77.6	1.11
141	BLG_12a_4_ZrnInMarble_3	Zircon In Marble	Bawlongyi	core	13 µm	SF	0.100000	0.015000	0.014310	0.000430	0.028667	96.78	6.92	91.59	1.37
142	BLG_12b_4_ZrnInMarble_2	Zircon In Marble	Bawlongyi	core	13 µm	SF	0.098700	0.004300	0.014860	0.000390	0.090698	95.58	1.99	95.09	1.24
143	K_01b_2_ZrnInGneiss_3	Zircon In Gneiss	Kinn	zircon	13 µm	SF	0.024000	0.011000	0.003940	0.000240	0.021818	24.08	5.45	25.35	0.77
144	K_01d_6_ZrnInGneiss_1	Zircon In Gneiss	Kinn	zircon	19 µm	SF	0.027300	0.001700	0.004104	0.000041	0.160432	27.35	0.84	26.4	0.13
145	K_01b_3_ZrnInGneiss_1	Zircon In Gneiss	Kinn	zircon	13 µm	SF	0.033000	0.005900	0.004200	0.000350	0.059322	32.97	2.9	27.02	1.12
146	K_01d_2_ZrnInGneiss_1	Zircon In Gneiss	Kinn	rim	13 µm	SF	0.039200	0.007500	0.005300	0.000230	0.226818	39.04	3.66	34.08	0.74
147	K_01c_3_ZrnInGneiss_1	Zircon In Gneiss	Kinn	zircon	19 µm	SF	0.037100	0.002100	0.005620	0.000210	0.660142	36.99	1.03	36.13	0.67
148	K_01a_2_ZrnInGneiss_1	Zircon In Gneiss	Kinn	zircon	13 µm	SF	0.058700	0.004500	0.008750	0.000180	0.268343	57.92	2.16	56.16	0.58
149	K_01d_6_ZrnInGneiss_2	Zircon In Gneiss	Kinn	zircon	13 µm	SF	0.120900	0.004800	0.009810	0.000190	0.487831	115.89	2.17	62.93	0.61
150	K_01a_1_ZrnInGneiss_2	Zircon In Gneiss	Kinn	core	35 µm	TOF	0.074665	0.011228	0.009855	0.000766	0.516799	73.12	5.3	63.22	2.44
151	K_01b_6_ZrnInGneiss_1	Zircon In Gneiss	Kinn	core	35 µm	TOF	0.070581	0.017281	0.010309	0.000553	0.219170	69.25	8.19	66.12	1.77
152	K_01b_9_ZrnInGneiss_1	Zircon In Gneiss	Kinn	zircon	13 µm	SF	0.087000	0.011000	0.013550	0.000250	0.145924	84.7	5.14	86.76	0.8
153	K_01d_5_ZrnInGneiss_1	Zircon In Gneiss	Kinn	core	19 µm	SF	0.159000	0.022000	0.014300	0.001800	0.909727	149.83	9.64	91.53	5.72
154	K_01d_8_ZrnInGneiss_2	Zircon In Gneiss	Kinn	zircon	13 µm	SF	0.110300	0.007500	0.015070	0.000710	0.692882	106.24	3.43	96.42	2.25
155	K_01b_2_ZrnInGneiss_2	Zircon In Gneiss	Kinn	zircon	13 µm	SF	0.153000	0.011000	0.016180	0.000490	0.044545	144.56	4.84	103.47	1.55
156	K_01d_2_ZrnInGneiss_2	Zircon In Gneiss	Kinn	core	13 µm	SF	0.415000	0.014000	0.043000	0.001100	0.758306	352.47	5.02	271.4	3.4
157	K_01b_7_ZrnInGneiss_2	Zircon In Gneiss	Kinn	zircon	13 µm	SF	0.514000	0.038000	0.056300	0.003000	0.720763	421.1	12.7	353.08	9.15
158	K_01b_12_ZrnInGneiss_1	Zircon In Gneiss	Kinn	zircon	13 µm	SF	0.589000	0.047000	0.067000	0.001300	0.027660	470.2	15	418.06	3.93
159	K_01b_2_ZrnInGneiss_1	Zircon In Gneiss	Kinn	zircon	13 µm	SF	0.739000	0.036000	0.067900	0.001100	0.030556	561.8	10.5	423.49	3.32
160	K_01b_4_ZrnInGneiss_1	Zircon In Gneiss	Kinn	zircon	13 µm	SF	0.708000	0.052000	0.071600	0.004300	0.082692	543.6	15.5	445.8	12.9

Table 4.3. U-Pb isotopes ratios and ages of zircon and zirconolite measured by TOF- and SF-MS. Contd.

No.	Measurement	Sample Type	Location	Area	Spot	Method	207Pb/235U	2σ	206Pb/238U	2σ	Rho	207Pb/235U	2 SE	206Pb/238U	2 SE
161	K_01d_8_ZrnInGneiss_1	Zircon In Gneiss	Kinn	core	13 µm	SF	0.901000	0.053000	0.085300	0.003600	0.717468	652.3	14.2	527.7	10.7
162	K_01b_8_ZrnInGneiss_1	Zircon In Gneiss	Kinn	zircon	13 µm	SF	0.847000	0.057000	0.086200	0.003300	0.057895	623	15.7	533.02	9.79
163	K_01d_4_ZrnInGneiss_1	Zircon In Gneiss	Kinn	core	19 µm	SF	0.958000	0.040000	0.090500	0.003600	0.952707	682.3	10.4	558.5	10.6
164	K_01c_1_ZrnInGneiss_1	Zircon In Gneiss	Kinn	core	19 µm	SF	1.033000	0.032000	0.095300	0.001900	0.643593	720.43	7.99	586.81	5.59
165	K_01b_11_ZrnInGneiss_1	Zircon In Gneiss	Kinn	zircon	13 µm	SF	0.948000	0.065000	0.095900	0.003100	0.047692	677.1	16.9	590.34	9.12
166	K_01b_8_ZrnInGneiss_2	Zircon In Gneiss	Kinn	zircon	13 µm	SF	1.093000	0.050000	0.108500	0.004600	0.926783	750	12.1	664	13.4
167	K_01d_4_ZrnInGneiss_2	Zircon In Gneiss	Kinn	core	13 µm	SF	1.149000	0.018000	0.111600	0.001200	0.686380	776.77	4.25	682.03	3.48
168	K_01b_10_ZrnInGneiss_1	Zircon In Gneiss	Kinn	zircon	13 µm	SF	1.095000	0.062000	0.113500	0.003300	0.053226	750.9	15	693.04	9.55
169	K_01b_10_ZrnInGneiss_2	Zircon In Gneiss	Kinn	zircon	13 µm	SF	1.159000	0.077000	0.120000	0.002500	0.032468	781.5	18.1	730.56	7.19
170	K_01b_5_ZrnInGneiss_1	Zircon In Gneiss	Kinn	zircon	13 µm	SF	1.284000	0.038000	0.121300	0.001700	0.044737	838.63	8.45	738.04	4.89
171	K_01b_5_ZrnInGneiss_2	Zircon In Gneiss	Kinn	zircon	13 µm	SF	1.396000	0.043000	0.130800	0.002500	0.058140	887.24	9.11	792.43	7.13
172	K_01d_7_ZrnInGneiss_1	Zircon In Gneiss	Kinn	core	19 µm	SF	1.418000	0.021000	0.138600	0.001500	0.730777	896.52	4.41	836.74	4.25
173	K_01b_13_ZrnInGneiss_1	Zircon In Gneiss	Kinn	zircon	13 µm	SF	1.442000	0.037000	0.142200	0.001700	0.045946	906.55	7.69	857.09	4.8
174	K_01c_2_ZrnInGneiss_1	Zircon In Gneiss	Kinn	core	19 µm	SF	1.413000	0.016000	0.142700	0.001500	0.928302	894.42	3.37	859.91	4.23
175	K_01b_6_ZrnInGneiss_1	Zircon In Gneiss	Kinn	zircon	13 µm	SF	1.485000	0.065000	0.150900	0.003100	0.047692	924.3	13.3	906.01	8.68
176	K_01b_7_ZrnInGneiss_1	Zircon In Gneiss	Kinn	zircon	13 µm	SF	1.636000	0.051000	0.165200	0.003800	0.074510	984.17	9.82	985.6	10.5
177	SSEF96663_A_2_ZrnInRuby_12	Zircon In Ruby	Mansin	rim	19 µm	SF	0.023300	0.004100	0.003356	0.000081	0.137162	23.39	2.03	21.6	0.26
178	SSEF96667_A_1_ZrnInRuby_8	Zircon In Ruby	Kyatpyin	rim	19 µm	SF	0.022500	0.004400	0.003470	0.000120	0.176840	22.59	2.18	22.33	0.39
179	SSEF96663_A_2_ZrnInRuby_11	Zircon In Ruby	Mansin	mixed	19 µm	SF	0.022600	0.002800	0.003610	0.000100	0.223585	22.69	1.39	23.23	0.32
180	SSEF96666_A_1_ZrnInRuby_4	Zircon In Ruby	Kadote Tet	rim	19 µm	SF	0.024700	0.001400	0.003676	0.000048	0.230375	24.78	0.69	23.65	0.15
181	SSEF96667_A_1_ZrnInRuby_2	Zircon In Ruby	Kyatpyin	rim	19 µm	SF	0.028100	0.004900	0.003800	0.000110	0.166004	28.14	2.42	24.45	0.35
182	SSEF96663_A_2_ZrnInRuby_10	Zircon In Ruby	Mansin	mixed	19 µm	SF	0.025600	0.002000	0.003800	0.000120	0.404211	25.67	0.99	24.45	0.39
183	SSEF96663_A_2_ZrnInRuby_7	Zircon In Ruby	Mansin	rim	19 µm	SF	0.022700	0.005300	0.003930	0.000200	0.217965	22.79	2.63	25.28	0.64
184	SSEF96666_A_1_ZrnInRuby_6	Zircon In Ruby	Kadote Tet	mixed	19 µm	SF	0.026100	0.003500	0.003960	0.000180	0.338961	26.16	1.73	25.48	0.58
185	SSEF96667_A_1_ZrnInRuby_4	Zircon In Ruby	Kyatpyin	core	13µm	SF	0.031000	0.009300	0.004020	0.000230	0.024731	31	4.58	25.86	0.74
186	SSEF96667_A_1_ZrnInRuby_7	Zircon In Ruby	Kyatpyin	mixed	13 µm	SF	0.026400	0.008200	0.004060	0.000130	0.103088	26.46	4.06	26.12	0.42
187	SSEF96667_A_1_ZrnInRuby_6	Zircon In Ruby	Kyatpyin	mixed	13µm	SF	0.024000	0.014000	0.004220	0.000470	0.190928	24.08	6.94	27.15	1.51
188	SSEF96663_A_1_ZrnInRuby_9	Zircon In Ruby	Mansin	rim	19 µm	SF	0.027900	0.001200	0.004368	0.000080	0.425824	27.94	0.59	28.1	0.26
189	SSEF96666_A_1_ZrnInRuby_3	Zircon In Ruby	Kadote Tet	mixed	19 µm	SF	0.030200	0.005000	0.004410	0.000140	0.191746	30.21	2.46	28.37	0.45
190	SSEF96663_A_3_ZrnInRuby_9	Zircon In Ruby	Mansin	rim	19 µm	SF	0.024200	0.007600	0.004430	0.000300	0.215635	24.28	3.77	28.49	0.96
191	SSEF96663_A_3_ZrnInRuby_4	Zircon In Ruby	Mansin	rim	35 µm	TOF	0.029627	0.026337	0.004441	0.000402	0.101905	29.6	13	28.57	1.29
192	SSEF96666_A_1_ZrnInRuby_8	Zircon In Ruby	Kadote Tet	mixed	19 µm	SF	0.037400	0.002400	0.005595	0.000095	0.264596	37.28	1.17	35.97	0.3

Table 4.3. U-Pb isotopes ratios and ages of zircon and zirconolite measured by TOF- and SF-MS. Contd.

No.	Measurement	Sample Type	Location	Area	Spot	Method	207Pb/235U	2σ	206Pb/238U	2σ	Rho	207Pb/235U	2 SE	206Pb/238U	2 SE
193	SSEF96664_B_1_ZrnInRuby_1	Zircon In Ruby	Kadote tat	core	35 µm	TOF	0.034512	0.012383	0.005716	0.000328	0.159830	34.45	6.08	36.74	1.05
194	SSEF96667_A_1_ZrnInRuby_3	Zircon In Ruby	Kyatpyin	core	19 µm	SF	0.039200	0.006700	0.005720	0.000170	0.173886	39.04	3.27	36.77	0.54
195	SSEF96667_A_1_ZrnInRuby_5	Zircon In Ruby	Kyatpyin	core	13µm	SF	0.034600	0.008600	0.005860	0.000250	0.029070	34.54	4.22	37.67	0.8
196	SSEF96667_A_1_ZrnInRuby_7	Zircon In Ruby	Kyatpyin	rim	19 µm	SF	0.039100	0.002100	0.005877	0.000084	0.266122	38.94	1.03	37.77	0.27
197	SSEF96666_A_1_ZrnInRuby_1	Zircon In Ruby	Kadote tat	mixed	35 µm	TOF	0.032443	0.017960	0.005878	0.000442	0.135754	32.42	8.83	37.78	1.42
198	SSEF96663_A_2_ZrnInRuby_6	Zircon In Ruby	Mansin	rim	19 µm	SF	0.036500	0.004800	0.006000	0.000210	0.266146	36.4	2.35	38.56	0.67
199	SSEF96664_C_1_ZrnInRuby_1	Zircon In Ruby	Kadote tat	core	35 µm	TOF	0.039097	0.010184	0.006592	0.000317	0.184633	38.94	4.98	42.36	1.02
200	SSEF96663_A_2_ZrnInRuby_5	Zircon In Ruby	Mansin	rim	19 µm	SF	0.040100	0.007600	0.006610	0.000330	0.263417	39.92	3.71	42.47	1.06
201	SSEF96666_A_1_ZrnInRuby_7	Zircon In Ruby	Kadote Tet	rim	19 µm	SF	0.045700	0.004700	0.007220	0.000150	0.202010	45.37	2.28	46.38	0.48
202	SSEF96663_A_2_ZrnInRuby_2	Zircon In Ruby	Mansin	mixed	35 µm	TOF	0.042070	0.019131	0.007477	0.000472	0.138938	41.84	9.32	48.02	1.51
203	SSEF96663_A_3_ZrnInRuby_3	Zircon In Ruby	Mansin	mixed	35 µm	TOF	0.052820	0.011238	0.007623	0.000461	0.283944	52.26	5.42	48.95	1.47
204	SSEF96666_A_1_ZrnInRuby_5	Zircon In Ruby	Kadote Tet	rim	19 µm	SF	0.051200	0.003000	0.007690	0.000360	0.798960	50.7	1.45	49.38	1.15
205	SSEF96666_B_1_ZrnInRuby_2	Zircon In Ruby	Kadote Tet	rim	19 µm	SF	0.053600	0.002200	0.008040	0.000210	0.636364	53.02	1.06	51.62	0.67
206	SSEF96663_A_3_ZrnInRuby_2	Zircon In Ruby	Mansin	mixed	35 µm	TOF	0.054688	0.026808	0.008548	0.000572	0.136444	54.1	12.9	54.87	1.83
207	SSEF96663_A_2_ZrnInRuby_1	Zircon In Ruby	Mansin	mixed	35 µm	TOF	0.055805	0.009382	0.008561	0.000386	0.268160	55.14	4.51	54.95	1.23
208	SSEF96663_A_1_ZrnInRuby_6	Zircon In Ruby	Mansin	mixed	19 µm	SF	0.065000	0.033000	0.008780	0.000940	0.210879	63.9	15.7	56.35	3
209	SSEF96663_A_3_ZrnInRuby_7	Zircon In Ruby	Mansin	core	19 µm	SF	0.063000	0.018000	0.009140	0.000570	0.218271	62.03	8.6	58.65	1.82
210	SSEF96663_A_2_ZrnInRuby_4	Zircon In Ruby	Mansin	core	35 µm	TOF	0.062174	0.007499	0.009291	0.000325	0.290284	61.25	3.58	59.62	1.04
211	SSEF96666_A_1_ZrnInRuby_2	Zircon In Ruby	Kadote tat	core	35 µm	TOF	0.066038	0.022984	0.009423	0.000558	0.170024	64.9	10.9	60.46	1.78
212	SSEF96663_A_1_ZrnInRuby_3	Zircon In Ruby	Mansin	core	35 µm	TOF	0.052120	0.011640	0.009585	0.000414	0.193186	51.59	5.62	61.49	1.32
213	SSEF96663_A_1_ZrnInRuby_2	Zircon In Ruby	Mansin	mixed	35 µm	TOF	0.065572	0.003746	0.009975	0.000317	0.555968	64.49	1.78	63.98	1.01
214	SSEF96663_A_1_ZrnInRuby_1	Zircon In Ruby	Mansin	mixed	35 µm	TOF	0.062359	0.011393	0.010056	0.000385	0.209482	61.42	5.44	64.5	1.23
215	SSEF96668_A_1_ZrnInRuby_1	Zircon In Ruby	Kyaukpoke	core	35 µm	TOF	0.072249	0.017695	0.010128	0.000821	0.331097	70.83	8.38	64.96	2.62
216	SSEF96663_A_1_ZrnInRuby_8	Zircon In Ruby	Mansin	rim	19 µm	SF	0.063000	0.022000	0.010420	0.000620	0.170389	62	10.5	66.82	1.98
217	SSEF96666_B_1_ZrnInRuby_1	Zircon In Ruby	Kadote tat	core	35 µm	TOF	0.065899	0.014961	0.010723	0.000711	0.291979	64.8	7.13	68.76	2.26
218	SSEF96663_A_3_ZrnInRuby_1	Zircon In Ruby	Mansin	mixed	35 µm	TOF	0.080499	0.018867	0.010907	0.000586	0.229396	78.61	8.87	69.93	1.87
219	SSEF96663_A_4_ZrnInRuby_2	Zircon In Ruby	Mansin	core	19 µm	SF	0.067000	0.011000	0.011080	0.000360	0.197900	65.85	5.23	71.03	1.15
220	SSEF96663_A_1_ZrnInRuby_5	Zircon In Ruby	Mansin	mixed	19 µm	SF	0.076000	0.001700	0.011470	0.000069	0.268937	74.38	0.8	73.52	0.22
221	SSEF96663_A_3_ZrnInRuby_10	Zircon In Ruby	Mansin	rim	19 µm	SF	0.065000	0.019000	0.012160	0.000620	0.174429	63.94	9.06	77.92	1.97
222	SSEF96663_A_3_ZrnInRuby_8	Zircon In Ruby	Mansin	core	19 µm	SF	0.083700	0.005000	0.012620	0.000250	0.331616	81.62	2.34	80.84	0.8
223	SSEF96663_A_1_ZrnInRuby_7	Zircon In Ruby	Mansin	rim	19 µm	SF	0.086200	0.008100	0.013380	0.000230	0.182934	83.96	3.79	85.68	0.73
224	SSEF96663_A_4_ZrnInRuby_4	Zircon In Ruby	Mansin	rim	19 µm	SF	0.070000	0.026000	0.013520	0.000930	0.185196	68.7	12.3	86.57	2.96

Table 4.3. U-Pb isotopes ratios and ages of zircon and zirconolite measured by TOF- and SF-MS. Contd.

No.	Measurement	Sample Type	Location	Area	Spot	Method	207Pb/235U	2σ	206Pb/238U	2σ	Rho	207Pb/235U	2 SE	206Pb/238U	2 SE
225	SSEF96663_A_4_ZrnInRuby_3	Zircon In Ruby	Mansin	core	19 µm	SF	0.094000	0.018000	0.014730	0.000590	0.209173	91.22	8.35	94.26	1.87
226	SSEF92725_E_1_ZrnInSpinel_5	Zircon In Spinel	Kyauksin	rim	13µm	SF	0.022500	0.003100	0.003480	0.000130	0.041935	22.59	1.54	22.39	0.42
227	SSEF92725_E_1_ZrnInSpinel_3	Zircon In Spinel	Kyauksin	rim	13µm	SF	0.026300	0.004800	0.003810	0.000260	0.054167	26.36	2.37	24.51	0.83
228	SSEF92725_E_1_ZrnInSpinel_4	Zircon In Spinel	Kyauksin	mixed	13µm	SF	0.035000	0.011000	0.003910	0.000320	0.029091	34.93	5.4	25.16	1.03
229	SSEF92725_D_2_ZrnInSpinel_1	Zircon In Spinel	Kyauksin	rim	19 µm	SF	0.027700	0.009100	0.004710	0.000280	0.180957	27.74	4.5	30.29	0.9
230	SSEF92725_E_1_ZrnInSpinel_2	Zircon In Spinel	Kyauksin	core	35 µm	TOF	0.049860	0.016801	0.006126	0.000569	0.275542	49.41	8.13	39.37	1.82
231	SSEF92720_D_2_ZrnInSpinel_2	Zircon In Spinel	Kyauksaung	core	13µm	SF	0.058000	0.017000	0.008900	0.000450	0.026471	57.25	8.16	57.12	1.44
232	SSEF92720_D_1_ZrnInSpinel_2	Zircon In Spinel	Kyauksaung	core	35 µm	TOF	0.080058	0.020192	0.009615	0.000524	0.215927	78.2	9.49	61.69	1.67
233	SSEF92720_D_2_ZrnInSpinel_1	Zircon In Spinel	Kyauksaung	core	19 µm	SF	0.068100	0.007900	0.010460	0.000300	0.247235	66.89	3.76	67.08	0.96
234	BLG_12c_04_ZirconoliteInMarble_1	Zirconolite In Marble	Bawlongyi	rim	35 µm	TOF	0.01927	0.00096	0.00288	0.00010	0.72329	19.39	0.48	18.51	0.33
235	BLG_12d_10_ZirconoliteInMarble_1	Zirconolite In Marble	Bawlongyi	rim	35 µm	TOF	0.01981	0.00080	0.00312	0.00010	0.77045	19.92	0.4	20.08	0.31
236	BLG_12d_06_ZirconoliteInMarble_1	Zirconolite In Marble	Bawlongyi	rim	35 µm	TOF	0.01982	0.00082	0.00313	0.00010	0.75793	19.93	0.41	20.13	0.32
237	BLG_12c_01_ZirconoliteInMarble_3	Zirconolite In Marble	Bawlongyi	rim	35 µm	TOF	0.02003	0.00089	0.00313	0.00009	0.66339	20.14	0.44	20.14	0.29
238	BLG_12c_01_ZirconoliteInMarble_1	Zirconolite In Marble	Bawlongyi	rim	35 µm	TOF	0.02130	0.00122	0.00317	0.00012	0.65763	21.4	0.61	20.41	0.38
239	BLG_12c_03_ZirconoliteInMarble_1	Zirconolite In Marble	Bawlongyi	rim	35 µm	TOF	0.02053	0.00078	0.00321	0.00008	0.65308	20.63	0.39	20.69	0.26
240	BLG_12a_05_ZirconoliteInMarble_4	Zirconolite In Marble	Bawlongyi	rim	35 µm	TOF	0.02313	0.00216	0.00332	0.00013	0.41235	23.22	1.07	21.34	0.41
241	BLG_12c_02_ZirconoliteInMarble_1	Zirconolite In Marble	Bawlongyi	rim	35 µm	TOF	0.02242	0.00102	0.00350	0.00011	0.68196	22.52	0.51	22.54	0.35
242	BLG_12c_03_ZirconoliteInMarble_1	Zirconolite In Marble	Bawlongyi	rim	19 µm	SF	0.02317	0.00072	0.00353	0.00019	1.73210	23.26	0.36	22.72	0.61
243	BLG_12c_01_ZirconoliteInMarble_1	Zirconolite In Marble	Bawlongyi	rim	19 µm	SF	0.02390	0.00130	0.00360	0.00011	0.56175	23.98	0.64	23.17	0.35
244	BLG_12d_13_ZirconoliteInMarble_1	Zirconolite In Marble	Bawlongyi	rim	19 µm	SF	0.02302	0.00075	0.00361	0.00009	0.74738	23.11	0.37	23.26	0.28
245	BLG_12c_01_ZirconoliteInMarble_4	Zirconolite In Marble	Bawlongyi	rim	35 µm	TOF	0.02348	0.00081	0.00370	0.00009	0.70348	23.57	0.4	23.83	0.29
246	BLG_12c_04_ZirconoliteInMarble_1	Zirconolite In Marble	Bawlongyi	rim	19 µm	SF	0.02490	0.00080	0.00378	0.00011	0.90575	24.97	0.4	24.32	0.35
247	BLG_12d_05_ZirconoliteInMarble_1	Zirconolite In Marble	Bawlongyi	rim	13 µm	SF	0.02490	0.00110	0.00380	0.00010	0.59005	24.97	0.54	24.44	0.32
248	BLG_12a_05_ZirconoliteInMarble_3	Zirconolite In Marble	Bawlongyi	rim	35 µm	TOF	0.02856	0.00615	0.00387	0.00023	0.27718	28.6	3.03	24.89	0.74
249	BLG_12c_01_ZirconoliteInMarble_2	Zirconolite In Marble	Bawlongyi	rim	35 µm	TOF	0.02704	0.00181	0.00405	0.00016	0.57710	27.09	0.9	26.04	0.5
250	BLG_12a_05_ZirconoliteInMarble_2	Zirconolite In Marble	Bawlongyi	rim	13 µm	SF	0.02940	0.00290	0.00437	0.00014	0.32478	29.42	1.43	28.11	0.45
251	BLG_12a_05_ZirconoliteInMarble_1	Zirconolite In Marble	Bawlongyi	rim	13 µm	SF	0.03520	0.00120	0.00535	0.00014	0.76760	35.13	0.59	34.4	0.45
252	SSEF96663_A_09_ZirconoliteInRuby_1	Zirconolite In Ruby	Mansin	core	35 µm	TOF	0.01743	0.00075	0.00268	0.00008	0.69528	17.55	0.38	17.25	0.26
253	SSEF96663_A_10_ZirconoliteInRuby_1	Zirconolite In Ruby	Mansin	core	35 µm	TOF	0.01772	0.00094	0.00280	0.00008	0.54170	17.84	0.47	17.99	0.26
254	SSEF96663_A_06_ZirconoliteInRuby_1	Zirconolite In Ruby	Mansin	core	35 µm	TOF	0.01712	0.00102	0.00281	0.00011	0.65888	17.24	0.51	18.06	0.35
255	SSEF96663_A_08_ZirconoliteInRuby_1	Zirconolite In Ruby	Mansin	core	35 µm	TOF	0.01812	0.00085	0.00282	0.00008	0.60909	18.23	0.42	18.13	0.26
256	SSEF96663_A_07_ZirconoliteInRuby_1	Zirconolite In Ruby	Mansin	core	35 µm	TOF	0.01796	0.00079	0.00291	0.00008	0.61621	18.08	0.39	18.74	0.25

Table 4.3. U-Pb isotopes ratios and ages of zircon and zirconolite measured by TOF- and SF-MS. Contd.

No.	Measurement	Sample Type	Location	Area	Spot	Method	207Pb/235U	2σ	206Pb/238U	2σ	Rho	207Pb/235U	2 SE	206Pb/238U	2 SE
257	SSEF96663_A_07_ZirconoliteInRuby_2	Zirconolite In Ruby	Mansin	rim	19 µm	SF	0.02961	0.00062	0.00460	0.00007	0.68567	29.63	0.31	29.57	0.21
258	SSEF96663_A_06_ZirconoliteInRuby_2	Zirconolite In Ruby	Mansin	rim	19 µm	SF	0.03050	0.00130	0.00476	0.00013	0.64076	30.51	0.64	30.61	0.42
259	SSEF96663_A_08_ZirconoliteInRuby_2	Zirconolite In Ruby	Mansin	rim	19 µm	SF	0.03063	0.00067	0.00480	0.00012	1.14291	30.63	0.33	30.87	0.38
260	SSEF96663_A_10_ZirconoliteInRuby_2	Zirconolite In Ruby	Mansin	rim	19 µm	SF	0.03201	0.00094	0.00490	0.00006	0.41732	31.99	0.46	31.48	0.19